Assessment of Real-Time Emissions and Fuel Consumption of Light-Duty Vehicles Using Artificial Neural Network Technique: for Addis Ababa Urban Road Conditions

Amanuel Gebisa Aga

A Dissertation Submitted to

The Department of Mechanical Engineering

School of Mechanical, Chemical and Materials Engineering

Presented in Fulfillment of the Requirement for the Degree of Doctor of Philosophy in Automotive Engineering

Office of Graduate Studies

Adama Science and Technology University

August, 2024

Adama, Ethiopia

Assessment of Real-Time Emissions and Fuel Consumption of Light-Duty Vehicles Using Artificial Neural Network Technique: for Addis Ababa Urban Road Conditions

Amanuel Gebisa Aga

Supervisor: Professor Girma Gebresenbet

Co Supervisors: Professor Rajendiran Gopal and

Dr. Ramesh Babu Nallamothu (Asso. Prof.)

A Dissertation Submitted to

The Department of Mechanical Engineering

School of Mechanical, Chemical and Materials Engineering

Presented in Fulfillment of the Requirement for the Degree of Doctor of Philosophy in Automotive Engineering

Office of Graduate Studies

Adama Science and Technology University

August, 2024

Adama, Ethiopia

DECLARATION

I hereby declare that this Dissertation entitled **"Assessment of Real-Time Emissions and Fuel Consumption of Light-Duty Vehicles Using Artificial Neural Network Technique: for Addis Ababa Urban Road Conditions"** is my original work. That is, it has not been submitted for the award of any academic degree, diploma or certificate in any other university. All sources of materials used for this thesis have been duly acknowledged through appropriate citations.

Amanuel Gebisa	______________________	__________
Name of student	Signature	Date

RECOMMENDATION

We, the supervisors of this dissertation, hereby certify that we have read and revised the dissertation which is entitled **"Assessment of Real-Time Emissions and Fuel Consumption of Light-Duty Vehicles Using Artificial Neural Network Technique: for Addis Ababa Urban Road Conditions"** prepared under our guidance by **Amanuel Gebisa Aga** submitted in fulfillment of the requirements for the degree of Doctor of Philosophy in **Automotive Engineering**. Therefore, we recommend the submission of the dissertation to the department for further review and defense.

Professor Girma Gebresenbet Main Supervisor	______________ Signature	________ Date
Professor Rajendiran Gopal Co-supervisor 1	______________ Signature	________ Date
Dr. Ramesh Babu Nallamothu (Asso. Prof.) Co-supervisor 2	______________ Signature	________ Date

APPROVAL SHEET

We hereby certify that the recommendations and suggestions made by the board of examiners are appropriately incorporated into the final version of the dissertation entitled **"Assessment of Real-Time Emissions and Fuel Consumption of Light-Duty Vehicles Using Artificial Neural Network Technique: for Addis Ababa Urban Road Conditions"** by **Amanuel Gebisa**.

Professor Girma Gebresenbet	______	______
Main Supervisor	Signature	Date
Professor Rajendiran Gopal	______	______
Co-supervisor 1	Signature	Date
Dr. Ramesh Babu Nallamothu (Asso. Prof.)	______	______
Co-supervisor 2	Signature	Date

We, the undersigned, members of the Board of Examiners of the final open defense by **Amanuel Gebisa Aga** have read and evaluated the dissertation entitled **"Assessment of Real-Time Emissions and Fuel Consumption of Light-Duty Vehicles Using Artificial Neural Network Technique: for Addis Ababa Urban Road Conditions**" and examined the candidate during open defense. This is, therefore, to certify that the dissertation has been accepted in fulfillment of the requirement of the degree of Doctor of Philosophy in Automotive Engineering.

Dr. Esmael Adem (Ass. Prof.)	______	______
Chairperson	Signature	Date
Dr. Addisu Bekele (Associate Prof.)	______	______
Internal Examiner	Signature	Date
Prof. Venkata Ramayya	______	______
External Examiner 1	Signature	Date
Dr. Aklilu Tesfamichael (Associate Prof.)	______	______
External Examiner 2	Signature	Date

Finally, approval and acceptance of the dissertation is contingent upon submission of its final copy to the office of postgraduate studies (OPGS) through the candidate's department graduate council (DGC) and school graduate committee (SGC).

______	______	______
Department Head	Signature	Date
______	______	______
School Dean	Signature	Date
______	______	______
Office of Postgraduate studies, Dean	Signature	Date

ACKNOWLEDGEMENTS

I am deeply grateful to the All-mighty God for all of his support. Next, it is my pleasure to thank Professor Girma Gebresenbet for providing me with the opportunity to conduct experiments at the Swedish University of Agricultural Science, Uppsala, Sweden. Furthermore, he sent me the portable emissions analyser from Swedish University of Agricultural Science for on-road vehicle emissions testing in Addis Ababa, Ethiopia. Additional, during my stay in Sweden he facilitated me an accommodation fee. Over the past few years, he has provided persistent support and encouragement, as well as positively challenged my results. As a result of his guidance, I have grown professionally and personally. Also, I would like to express my deepest gratitude to my co-supervisors, Dr. Rajendiran Gopal and Dr. Ramesh Babu, for their tremendous assistance, guidance, and technical support. For me, working under them was a pleasant and valuable learning experience.

I express my gratitude to every member of the doctorial committee for their insightful feedback on the progress reports. Furthermore, I would like to thank the Examiners of this dissertation for their thoughtful feedback and recommendations that helped me finalise this study. I would like to thank Dr. Keredin Abatamam, Mr. Temesgen Debeleta, Mr. Bijiga Fikadu, Mr. Adane Abdeta, Chali Petros and staff members of Energy and Technology department at Swedish University of Agricultural Science for their support with data collection.

My sincerest gratitude goes out to Dr. Alemayehu Wakjira, Dr. Getinet, Dr. Teshome Abdo, Dr. Legesse Tulu, Dr. Demissie, and Dr. Yadessa Chimdessa for their kind support and encouragement.

Thanks to Mr. Hadish Teklehaimanot, Mr. Tatek Mamo, Mr. Yared Seifu, Mr. Habtamu Deresso, and Mr. Samuel Tamirat for supporting me in software's study, and answering my technical questions. Lastly, I am grateful to my wife and children who gave their time to bring me up to this level. Additionally, I feel blessed to have wonderful friends and family members.

TABLE OF CONTENTS

Contents **Page**

LIST OF TABLES

LIST OF FIGURES

LIST OF ABBREVIATIONS

AA	Addis Ababa
AADC	Addis Ababa driving cycle including Addis-Adama Expressway
AAE	Addis-Adama Expressway
ANN	Artificial neural network
CD	Chassis dynamometer
CLTC-P	China light-duty vehicle test cycle for passenger cars
COPERT	Computer Program to Estimate Emissions from Road Transport
CO_2	Carbon dioxide
CP	Characteristics parameters
CSE	Center for science and environment
CUEDC	Composite urban Emission drive cycle
CVS	Constant volume sampler
DC	Drive Cycle
DFA	Desirability function analysis
DM	Drive mode
DT	Drive time
ECU	Engine control unit
ELT	Extra-long trips
EPA	Environmental protection agency
FC	Fuel consumption
FNR	False negative rates
FPR	False positive rate
GIS	Geographical information system
IT	Idle time
LDV	Light-duty vehicles
LT	Long trips
MAW	Moving average window
MSE	Mean square error
MT	Micro Trip
NEDC	New European driving cycle

NN	Neural network
NO_X	Nitrogen Oxides
NS	Number of stops
OBD	On-board diagnosis
PB	Power binning
PC	Passenger car
PCA	Principal Component Analysis
PEMS	Portable emission measurement system
PKE	Positive kinetic energy
PM	Particulate matter
PRoPS	Powertrain road performance simulator
PV	Passenger vehicle
RBEI	Route-based emissions inventories
RD	Relative difference
RDE	Real driving emission
RNN	Recurrent neural network
ROC	Receiver operating characteristics
RPA	Relative positive acceleration
RPM	Revolutions per minute
SAFD	Speed-acceleration frequency distribution
SFC	Specific fuel consumption
SI	Spark ignition
SSD	Sum squared difference
ST	Short trips
TPR	True positive rates
TWFA	Toronto Waterfront Area
VOC	Volatile organic compounds
VSP	Vehicle specific power
WHO	World health organization
WLTC	Worldwide harmonized light vehicles test cycle

ABSTRACT

Urbanization and rising vehicle ownership contribute to traffic congestion and negatively impact the environment. Since 2017, Europe has used portable systems for real-time vehicles emissions testing, but these systems are cumbersome, expensive, and inconsistent, making them unsuitable for real-time monitoring in resource-limited countries like Ethiopia. Furthermore, existing emissions models do not account for how varying drive cycle (DC) characteristics affect vehicle emissions. This study aims to develop artificial neural network (ANN) models for real-time assessment of exhaust emissions and fuel consumption (FC) of light-duty vehicles, tailored to the road conditions of Addis Ababa (AA) including the Addis-Adama Expressway. Initially, a representative DC was developed using a neural network (NN) and principal component analysis, reflecting the traffic flow characteristics of the study area. Real-time driving data from five vehicles were collected using GPS devices, and two vehicles were tested for emissions and FC on a chassis dynamometer setup in Uppsala, Sweden. Next, emissions of five primary gases (CO, CO_2, NO_X, PM, and VOC) and FC were determined using the COPERT model for the DC's developed in this study and the Worldwide Harmonized Light Vehicles Test Cycle (WLTC). To reduce CO_2, HC, and CO emissions concurrently, a full factorial design and desirability function analysis (DFA) were employed to assess the effects of vehicle speed and road slope on emissions, with data gathered from two vehicles in AA using a portable emissions analyzer. Finally, an ANN simulation model was developed in Matlab to simulate real-time vehicle exhaust emissions. The model, trained with Bayesian regularization and back-propagation, predicted velocities for individual route segments with an overall R-value of 0.99. Compared to collected data, the NN-derived DCs exhibited a relative difference of 0.056, while the micro trip methods showed a relative difference of 0.111. The findings of this study reveal that driving in the congested urban areas of AA contributes to 56.25% of CO, 37.28% of CO_2, 38.19% of NO_X, 58.25% of VOC, and 29% of both PM2.5 and PM10 emissions, as well as 37.29% of the FC from the overall amount. Utilizing DFA, was found that the most effective speed for the concurrent reduction of CO, HC, and CO_2 emissions was 40 km/h on a level road and 30 km/h on a road with a 2° road slope, achieving composite desirability indexes of 0.83 and 0.72, respectively. The findings revealed that the DC developed in this study resulted in significantly higher levels of emissions and FC compared to the WLTC. The trained ANN model was effective in predicting HC, CO, NO_X, and PM emissions (MSE $<2.438x10^{-5}$, R^2 of 92-99.9%). Except for the number of stops, the predictors used as input to the ANN model proved to be essential in predicting real-time exhaust emissions. The ANN model outperformed the COPERT model and experimental chassis dynamometer in estimating CO, NO_X, and FC. The findings of this study shall be used to develop effective strategies for reducing vehicular emissions and FC in AA.

Keywords: Artificial Neural Network; Drive Cycle; Emissions, Light-Duty Vehicle, Real-Time

CHAPTER ONE

INTRODUCTION

1.1. Background of the study

With more than 1.4 billion vehicles on the road, road transport is essential to the expansion and prosperity of the world economy, but it also greatly increases air pollution rates (Ghaffarpasand & Pope, 2024). This causes the Earth's atmosphere to deteriorate due to vehicular emissions such as carbon monoxide (CO), hydrocarbons (HC), oxides of nitrogen (NO_X), particulate matter (PM), and so on (Abdulraheem et al., 2023; Marques et al., 2021). There is growing concern about poor urban environment quality caused by road transport vehicles (Shepelev et al., 2023), which poses health hazards to humans and animals (Nandi et al., 2023). Vehicles are one of the main contributors to air contamination in urban areas, primarily due to the combustion of fuels (Sati & Dare, 2022). Air quality is deteriorating over time as new vehicles are added to the road (Šarkan et al., 2022), leading to traffic congestion in cities, with negative impacts on the environment, society, and the economy (Shepelev et al., 2023). Various factors impact the vehicle emissions and fuel consumption (FC) (Liu et al., 2019). Therefore, determining and evaluating vehicle emissions is crucial for the management of air pollution (Busho & Alemayehu, 2020).

The restrictions imposed by law limiting air pollutants emitted into the atmosphere are called emission standards (Rahman et al., 2021). In response to the decline in the quality of the local air, the State of California, USA, implemented the first vehicle emission standards in history in 1966 (He & Jin, 2017). Subsequently, in order to regulate tailpipe emissions in their states, the EU, Australia, and Japan began establishing automobile emission standards in the 1970s and 1972, respectively (Singh et al., 2023). The history of the emission regulations for passenger cars (PCs) in the USA, EU, China, and Japan is depicted in Figure 1.1. European regulations on vehicle emissions are progressively introducing ever-stricter limits (Donateo & Filomena, 2020). These limits must be met under transient test conditions and vehicle emissions must be minimized (Chen et al., 2023). Road transport contributed to 21% of global CO_2 emissions in 2016, accounting to 7.9 million tonnes worldwide, and 28% of NOx emissions in European countries in 2018 (Ghaffarpasand & Pope, 2024). The transport sector on the road was responsible for 21% of the EU's total CO_2 in 2017 (Singh et al., 2023). Projections suggest that by 2040, over 50% of the African population will reside in polluted urban areas, with outdoor air pollution accountable for over 210,000 premature deaths on the continent (Roychowdhury et al., 2016).

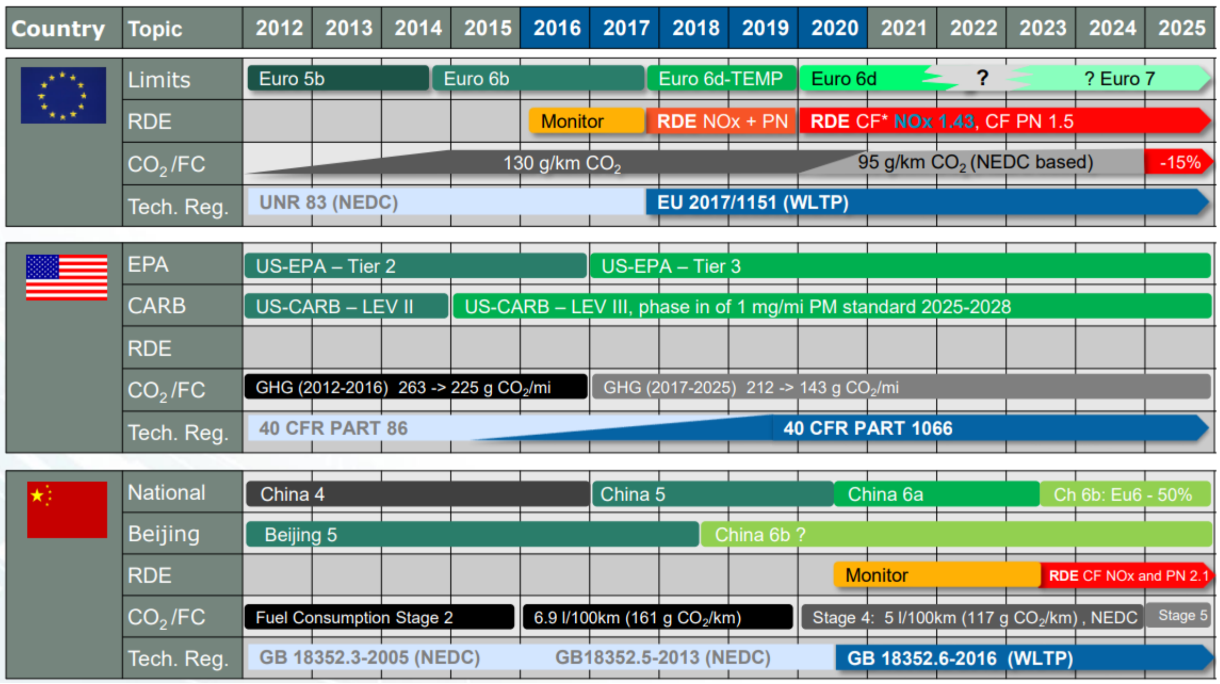

Figure 1.1: Timeline of global emissions regulations for PVs (Kurt, 2018)

Vehicle emissions can be determined in three ways: the first is using a chassis dynamometer (CD) and constant volume sampler (CVS) in the laboratory (Yang et al., 2018); the second is using emissions software such as Computer Program to Estimate Emissions from Road Transport (COPERT) (Ntziachristos et al., 2009), MOVIES, or IVE (Viteri et al., 2023); and the third is on-road emissions test, using portable emissions measurement systems (PMES) (Ricardo et al., 2019). Emissions are generally monitored using the CD testing method, but more comprehensive data from real-time emissions test can be used to identify emissions in the real world resulting from small-scale events that have a significant impact on overall emissions (Meena & Singh, 2022). To determine FC and emissions from vehicles, each of these methods requires a driving cycle (DC).

DC is a graphical representation that depicts the correlation between time and vehicle speed, serving as a means to evaluate the performance, emissions, and FC of a vehicle (Teoh et al., 2019). Various standard DCs such as the worldwide harmonized light vehicles test cycle (WLTC), the Federal Test Procedure (FTP) 75, and JC08 have been created. The UNECE established the WLTC (Figure 1.2) in September 2017 to replace the NEDC for type approval testing of light-duty vehicles following the switch to the Euro 6c emission standard (Grüner & Marker, 2016; Khalfan, 2016). Until the end of 2008, there were multiple modifications made to the DC created by the US environmental protection agency (EPA). It consists of four segments: urban driving (FTP-75), illustrated in Figure 1.2, highway driving (HWFET), aggressive driving (SFTP US06), and the operational air conditioning test (SFTP SC03). The certification of PCs and light-duty trucks requires a weighted composite emissions value consisting of 35% FTP-75, 28% US06, and 37% SC03 (Giakoumis, 2017). For FC, the weighting of the HWFET test is 45% and that of the FTP75 test is 55% (Chappell, 2015). The US DCs closely reflect actual driving behavior (Divakarla et al., 2014), with deviations in FCs between certified and on-road vehicles (Berry, 2010). Since 2011, the Japanese JC08, depicted in Figure 1.2, has been used for PC and light-duty truck emission certification (Kühlwein et al., 2014). The China Light-Duty Vehicle Test Cycle (CLTC-P) reflects real-world conditions, but differs from standard DCs (Liu et al., 2021), due to fleet compositions, driving behaviors, and road conditions (Tsanakas et al., 2020).

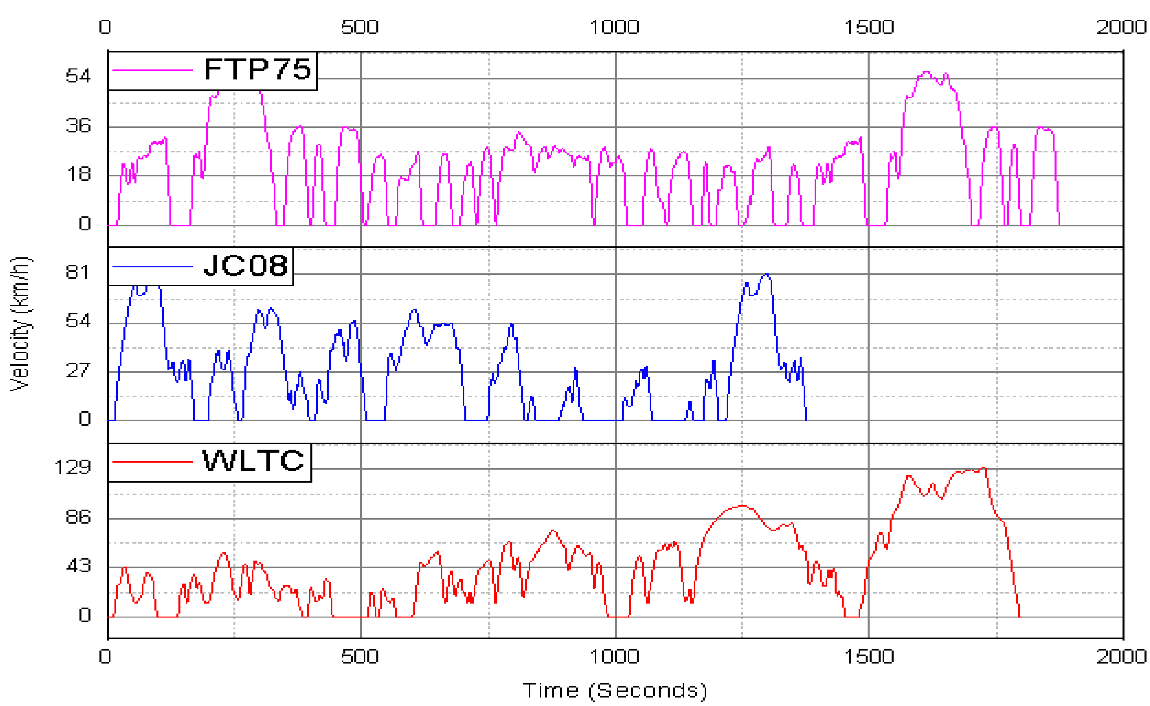

Figure 1.2: FTP75, JC08, and WLTC for class 3a vehicles (DieselNet, 2020)

For DCs used in emissions and FC determination, the micro-trip (MT) method is the typical approach for DC development (Zhao et al., 2021; Guo et al., 2020). In this approach, researchers often determine the DC duration based on their past experiences and previous DC durations. For instance, (Zhao et al., 2021) created two DCs with durations of 1216 and 1261 seconds after initially deciding on a duration between 1200 and 1300 seconds. In the study by (Peng et al., 2015), the duration of the designed DC was set at 1200 seconds to develop the DC for hybrid buses in the Zhengzhou, China. Similarly, (Guo et al., 2020) also chose a duration of 1200 seconds. Researchers have utilized principal component analysis (PCA) with the k-means clustering technique to classify kinematic segments during DC formation into heterogonous groups based on statistical features, as demonstrated by various studies (Guo et al., 2020; Ji et al., 2018; Liu et al., 2021; Liu et al., 2020; Zhao et al., 2021). The study by (Peng et al., 2019), used PCA to condense 15 characteristic parameters into three-factor scores, (Ji et al., 2018) reduced 15 kinematic characteristic values to four principal components, and (Zhou et al., 2017) reduced eight driving parameters to three principal components. Machine learning is the most robust theoretical foundation for deep learning-based DC prediction (Wu et al., 2020). Researchers have used convolutional NN (Chen et al., 2020), recurrent neural networks (RNN) (Qiu et al., 2018), and deep reinforcement learning (Zhao et al., 2018) to develop DCs.

The primary tools used to measure car emission levels in the laboratory are the CD and CVS. Recently, researchers have discovered significant discrepancies in emissions reported using the aforementioned approach. To measure emissions from vehicles on a CD, a car must pass through a predetermined DC (Mahayadin et al., 2017), using a driver's aid to provide signals on how to drive the vehicle around the desired speed trace (Chappell, 2015). The exhaust gas is collected using a CVS system after being diluted with ambient air, and then examined for its contents and concentrations (Yang et al., 2018).

The sector's emissions need an inventory to evaluate their impact, the impact of existing regulations, and the urgency of addressing environmental goals (Singh et al., 2020). Emission inventories provide a scientific foundation for management plans and offer a comprehensive understanding of pollution source emission levels over time, making them valuable tools for investigating pollution characteristics (Abdulraheem et al., 2023; Álvarez et al., 2023; Fan et al., 2023). Emission models like COPERT and HBEFA are widely used in Europe and other countries to estimate urban air pollution from vehicles (Boveroux et al., 2021; Lozhkina & Lozhkin, 2015; Tsanakas et al., 2020). These models are based on average vehicle velocity, (Kousoulidou et al., 2010; Lejri et al., 2018; Tim Murrells, 2017) but MOVES and IVE require engine specifications, vehicle class, instantaneous speed, and vehicle technology (Lin et al., 2019) and IVE (Pour & Tavakoli, 2013; Viteri et al., 2023). Authors such as (Abdulraheem et al., 2023; Arti et al., 2022; Li et al., 2023; Marques et al., 2021; Zhu et al., 2023) have recently conducted emission inventories. European regulations on vehicle emissions are progressively introducing ever-stricter limits (Donateo & Filomena, 2020). These limits must be met under transient test conditions or on-roads (Chen et al., 2023). Real-time emissions monitoring offers extensive data for detecting real-world emissions from micro-scale events, significantly impacting overall emissions, unlike CD testing methods (Meena & Singh, 2022).

Developing an accurate vehicle emissions model is difficult due to varied vehicle catagories, driving situations, driver attitudes, and operating limitations. Currently, researchers such as (Aydin et al., 2018; Chen et al., 2023; Donateo & Filomena, 2020; Hassine et al., 2021; Howlader et al., 2023; Predić et al., 2016; Seo et al., 2022; Shams et al., 2020), have applied NNs for predicting exhaust emissions from vehicles, leveraging the ability of NNs to recognize complex relationships between inputs and outputs. In comparison to conventional emission prediction techniques, (Moradi et al., 2022) obtained superior results using random forest, and Artificial Neural Network (ANN). A study by (Jaikumar et al., 2017) used an ANN to model real-time emissions from a PC. Through parametric studies, those authors identified variables that could be effective inputs (speed, acceleration, VSP) for ANNs to predict vehicle emissions. A study by (Seo et al., 2022) developed a cold-start CO, HC and NO_X emissions model for diesel vehicles using an ANN trained on real-world driving data and input variables such as vehicle speed, VSP, engine RPM, torque, and coolant temperature. Authors in (Arsie et al., 2010) developed a NN to simulate NO_X emissions in SI engines, achieving a less than 4% estimation error compared to real system dynamics. Using a self-learning NN (Shepelev et al., 2023) utilized historical emissions data to predict vehicle-related PM concentrations. According to a review by (Nandi et al., 2023), ANN and deep learning are expected to be utilized in a cross-functional manner in the future.

Ethiopia is actively promoting and implementing a green economic growth strategy. However, testing for emissions, and FC was not yet applied before a car could be imported due to lack of standards, local DC and test facilities. Therefore, extensive research on vehicular emissions and FC was crucial to encourage the Ethiopian government to set emissions standards before air pollution in AA worsened beyond current levels. Additionally, there has been no research estimating vehicle-related air pollution under AA's road conditions including the Addis-Adama Expressway (AAE) using local DC. This study addressed the gap in real-time modeling of exhaust emissions and FC for light-duty vehicles by developing ANN models based on two distinct road types: urban roads within AA and the AAE, which connects AA to the neighboring city of Adama. After developing a representative DC using ANN method, this study assessed emissions and FC for both urban roads in AA and the AAE using experimental CD setups and simulation models.

1.2. Justifications

The exhaust systems of internal combustion (IC) engines emit toxic gases that lead to contamination of the environment, damage to the liver, cancer, and heart problems. In AA, Ethiopia, despite being a major metropolitan city and the seat of the African Union, vehicles are not tested for real-time emissions and FC due to the lack of standards and facilities. Additionally, previous studies in AA relied on European DCs for estimating vehicular emissions and FC due to the absence of a specific DC for the city and Ethiopia. The AA Transport Authority reported 627,460 registered cars in the city in 2021, with their distribution shown in Figure 1.3. The city of AA, has seen a significant increase in the number of vehicles in recent years. This rise in vehicle population has led to a concerning increase in air pollution levels, with higher concentrations of harmful pollutants such as CO, NOx, HC, and PM (Bikis & Pandey, 2021; Jida et al., 2020; Tefera et al., 2020). The growing number of vehicles in Ethiopia as a whole has also had a direct impact on the country's FC. Figure 1.4 presents the annual fuel usage in Ethiopia from 2001 to 2021, which shows a drastic increase in fuel imports over the past two decades.

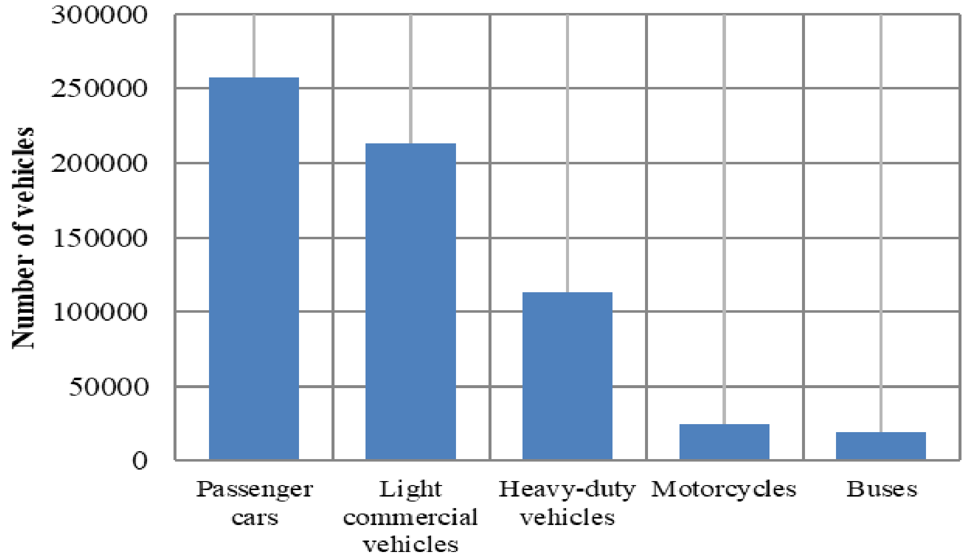

Figure 1.3: Distribution of vehicles category in 2021 (AA Transport Authority, 2021)

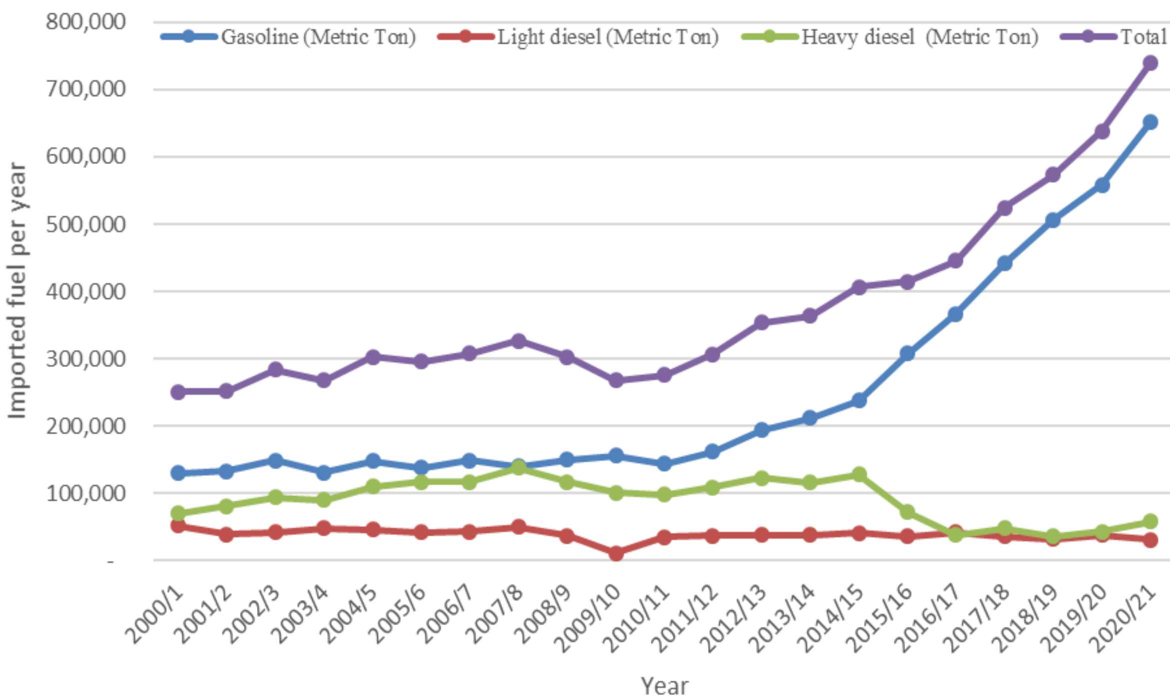

Figure 1.4: Imported fuel per year (Ethiopian Petroleum Enterprise, 2022)

The combination of increased air pollution and rising FC underscores the importance of developing effective strategies to assess and mitigate the environmental impact of vehicles in AA and Ethiopia. This study aims to address this pressing issue by creating representative DCs and simulation models to assess the emissions and FC of light-duty vehicles in the specific driving conditions of AA urban road including the AAE.

1.3. Statement of the problem

In Ethiopia, a representative DC tailored to local conditions is currently absent. Utilizing standard DCs established in other contexts may not accurately characterize local conditions, potentially resulting in erroneous emission levels. To accurately assess FC and vehicle emissions, it's essential to employ a DC that mirrors the typical conditions of the specific area being studied. This cycle should accurately reflect the actual driving patterns and styles, as well as consider the specific environmental factors.

According to the MT method, DC duration is determined by several researchers based on previously published DC durations. In the DC constructing process, random MTs are selected and chained till the required DC duration is obtained. This step is repeated numerous times until candidate cycle are obtained. These DCs, however, cannot be repeated, and the length of the cycle does not reflect real conditions. Moreover, the DC duration affects the estimation of emissions and FC. Therefore, using a real-time data-based methodology for DC length can be more presentative than using the traditional DC durations that have been published in the literature. This study proposes a trip-based method of DC development to resolve these issues. Additionally, previously no evaluation has been conducted on which clustering method is best suited to PCA. In this study, MATLAB was used to apply a machine classification learner to discover the best clustering method.

Previous studies estimated vehicular emissions and FC in AA using European DCs because an AA-specific driving cycle did not exist. This approach has led to lower accuracy in the estimation of vehicle emissions and FC, as the driving characteristics in AA are likely to differ significantly from those in Europe. Furthermore, the AAE, an expressway connecting AA to the nearby city of Adama, has been identified as an integral part of the road network frequently used by vehicles registered in AA. The driving patterns on this expressway, which involve high-speed driving for extended periods without stops, are unique and distinctly different from the driving characteristics on the urban roads within AA. Therefore, it was crucial to include the driving characteristics of the AAE in the development of the DC, as it plays a significant role in the overall emissions and FC profile of vehicles operating in the AA region. Also, the annual Bolo renewal (annual vehicle inspection) in Ethiopia involves vehicle emissions testing, but due to the lack of a CD facility and PEMS, these tests are conducted under static conditions.

Additionally, existing emission inventory methods have primarily relied on vehicle classification, while overlooking the variations in road types. To address these gaps, this study aims to develop representative DC for the urban roads in AA and the AAE. To enable a more accurate and comprehensive assessment of exhaust emissions and FC for light-duty vehicles operating under the specific driving conditions of the AA region including the AAE.

Since 2017, developed countries have been employing portable emission measurement systems (PEMS) to measure on-road emissions for vehicle registration. Nevertheless, PEMS devices are bulky, expensive, and have unrepeatable results due to dynamic nature of the environmental and traffic conditions, and making it unsuitable for monitoring emissions in real-time in developing countries like Ethiopia. As a result, alternative methods to estimate emissions from vehicles have to be developed. Furthermore, in previous studies except for vehicle speed, acceleration, and drive modes related variables, a variety of DC characteristics, such as the slope of the road, the number of stops, the route type, positive kinetic energy (PKE), and relative positive acceleration (RPA) have not been investigated for their importance on DC development utilized for vehicle emissions and FC estimation. To better estimate vehicular emissions that express distinct emission trends on various road types, it is necessary to establish an emissions inventory that also considers the route type as a key factor.

This study aimed to address the lack of representative DC and emissions testing capabilities in AA, Ethiopia. The key steps undertaken included; developing a representative DC using an ANN and PCA, considering the unique traffic flow characteristics of urban roads in AA including the AAE; proposing a route-based emissions inventory method to better capture the distinct emission trends across different road types, which also takes vehicle classification into consideration; applying DFA to identify the optimal driving range for urban routes that can effectively reduce vehicle emissions; developing an ANN-based simulation model to compute real-time vehicle exhaust emissions on a second-by-second basis, reflecting the specific driving conditions in the AA region including the AEE. By following these methodical steps, this study aimed to address the gaps in research and testing capabilities related to vehicular emissions and FC in AA and its surrounding expressway network. The developed tools and models provide a more accurate and comprehensive assessment of the environmental impact of light-duty vehicles operating in this region.

1.4. Objectives

1.4.1. General objective

The main aim of this study was to assess the real-time exhaust emissions and fuel consumption of light-duty vehicles under Addis Ababa's urban road conditions including the Addis-Adama Expressway using an artificial neural network method after developing a representative drive cycle for the study area.

1.4.2. Specific objectives

The following specific objectives were set in order to fulfil the study's purpose:

1. Develop a representative drive cycle for Addis Ababa's road conditions including the Addis-Adama expressway employing principal component analysis and neural networks;
2. Develop inventory models for emissions and fuel consumption for passenger vehicles;
3. Assess the impacts of vehicle speed and road slope on tailpipe emissions using desirability function analysis; and
4. Develop a simulation model to predict real-time exhaust emissions from passenger vehicles using an artificial neural network method.

1.5. Significance of the study

The implication of this study lies in its potential impact on addressing the critical issue of exhaust gas emissions from vehicles in AA, Ethiopia. Vehicle emissions are a major hindrance to the growth and sustainability of any country, and this study provides valuable insights and tools to tackle this problem effectively.

One of the key significances of this study was the establishment of a representative DC for the AA region, including the AAE. This locally-developed DC will assist researchers and the Environmental Protection Authority (EPA) in accurately determining the vehicular emissions and FC of light-duty vehicles. This is a significant step forward, as previous studies had to rely on DCs from other regions, leading to inaccurate estimates. Furthermore, the study will provide the EPA, the AA city administration, and the Ministry of Transport and Logistics (MoTL) with a means of information and data to better understand the extent to which vehicle exhaust emissions are contributing to the air quality issues in AA and the AAE. This evidence-based understanding is crucial for policymakers to develop effective emission control strategies and implement appropriate technology-based solutions.

The study's findings will also be instrumental in determining future emission policies, fuel efficiency standards, and technology plans for light-duty vehicles in study area. Policymakers and vehicle manufacturers will gain valuable insights into the trends and patterns of vehicle emissions, enabling them to make informed decisions regarding emissions regulations, fuel economy targets, and the development of cleaner and more efficient vehicle technologies.

The findings of on-road emissions tests will highlight any differences between laboratory and on-road test results, which is crucial information for legislators and automakers looking at establishing pollution reduction plans.

For academics and researchers interested in the fields of traffic engineering, environmental engineering, health, automotive engineering, and transportation planning, this will be a helpful resource that offers a theoretical foundation. The purpose of this study is to present information regarding potential reductions in vehicle emissions and fuel savings. This information is intended for the Ethiopian government, local stakeholders, and any interested foreign audience.

Overall, the AA city governments, the EPA, the MoTL, researchers, the vehicle manufacturers, and the local community would all benefit from the study's findings.

1.6. Scope of the study

Only light duty vehicles, such as taxis, minibuses, and private PCs in AA, were the focus of this study. ANNs and micro-trip-based construction techniques were the DC construction approaches used in this study, based on data collected from five vehicles. Data collection for DC development was bounded to AA and the AAE. To establish a DC, vehicles utilized for data collection in this study must have been manufactured after 2005. The study considered both the peak and off-peak hours for traffic congestion. The exhaust emissions of CO_2, CO, HC, and NO_X from two PVs (one gasoline and one diesel vehicle) were evaluated using the developed DC in this study utilizing a CD setup under laboratory condition. Additionally, on-road emissions of CO_2, CO, and HC were tested for two PVs (one gasoline and one diesel vehicle) on AA roads. In this study, for on-road emissions testing, vehicles used for data collection must have been manufactured after 2015. Evaporative emissions from vehicles and particulate matter (PM) were not included in this study. The following road classification schemes was used: congested, extra-urban, rural, ring road and expressway. This study fully focused on asphalt roads.

1.7. Limitations

This study was limited to evaluating emissions and FC of light duty vehicles. Additionally, due to the lack of CD facilities in AA, vehicle exhaust emissions were measured in a laboratory abroad, at altitudes different from those in AA. The exhaust emissions measured on CD were only included CO, CO_2, NOx and FC. Additionally, during on road exhaust emissions tests conducted in AA roads, NO_X and PM were not tested due to the lack of test equipment for these emissions, because the portable emissions tester browed from Swedish University of Agricultural Science can only capable of testing CO_2, CO, HC, and H_2S emissions. Furthermore, this study did not cover bulk vehicles because the methodology developed under this study was based on emissions estimation of individual vehicles. This study was slowed by COVID-19 lockdowns and a lack of testing facilities for CDs and PEMS in ASTU and Ethiopia.

1.8. Organization of the Dissertation

There are five chapters in this dissertation, each covering a different topics. A review of previous studies on the DCs for computing vehicle exhaust emission levels and FC is presented in the chapter two. Additionally, a description of the research gap was provided as well. In chapter three, the materials, methodology and details of gathering and analyzing the data were all outlined. A discussion and evaluation of the results are presented in chapter four, where data were gathered from on road, laboratory and simulations. The conclusion and recommendations in chapter five summarize the study’s finding and suggest further research directions.

CHAPTER TWO

LITERATURE REVIEW

2.1. Overview of vehicular emissions and FC

IC engines, commonly used in industrial and transportation applications, are major sources of air pollution and GHG emissions. The mid-20th century saw an increase in energy consumption, leading to a rise in cars on the road (Ashok et al., 2021). The incomplete combustion, oxygen scarcity, and heterogeneity in the air-fuel mixture all contribute to the formation of toxic gases from vehicles (Adeyanju & Manohar, 2017). High temperatures from complete combustion also generate NOx, as diatomic nitrogen in the air rises (Ashok et al., 2021). Figure 2.1 illustrates the diverse hazardous pollutants produced by CI and SI engines. Vehicle emissions such as CO_2, NOx, CO, PM, and HC contribute to climate change and pose risks to human health and air quality (Fan et al., 2018). Understanding fuel combustion trends is crucial for achieving energy efficiency and optimizing engine performance.

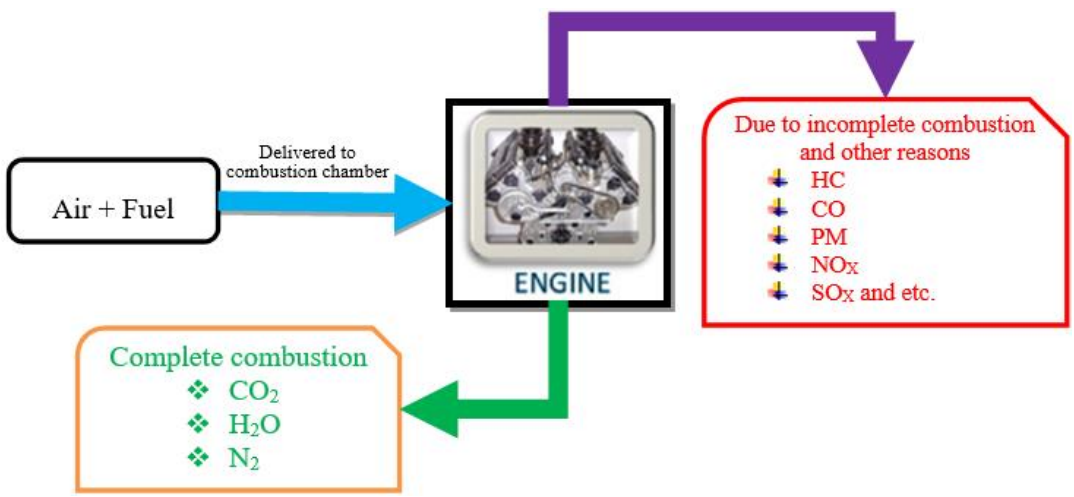

Figure 2.1: Emissions produced from IC engines (Ashok et al., 2021)

Estimating vehicle emissions is crucial for environmental assessment and sustainable transportation planning, as the global population growth leads to increased demand for transportation, affecting air quality and climate change (Wang et al., 2018). Estimating pollutants released by vehicles, such as CO_2, CO, NOx, PM, and HC, helps in understanding the environmental impact of transport systems, creating efficient air quality management plans, and creating legislation to reduce environmental and public health impacts. Emission estimates are used by academics, decision-makers, and urban planners to evaluate emissions standard, reduce emissions, and create environmentally friendly transportation infrastructure (Cedillo et al., 2023). The accuracy of these estimations has improved with real-world data, modelling, and simulation approaches.

This literature review sets the foundation for exploring the methodologies, challenges, and implications associated with estimating vehicle emissions and FC. It underscores the critical importance of accurate assessment in making well-informed decisions in the pursuit of more sustainable and cleaner transportation networks. Additionally, it gives an in-depth analysis of the literature review on DC development and a comparison of emissions data collected in laboratories and on the road.

2.2. Vehicular emissions estimation

2.2.1. Formation of exhaust emissions in IC vehicles

Moving vehicles emit a multitude of harmful chemicals, such as aromatics in petroleum based fuel, each possessing individual harm or carcinogenic potential. Acute health reactions associated with air pollution include asthma attacks, angina attacks, strokes, and early mortality (Ramprasanna et al., 2020). The majority of hazardous emissions stem from engines that operate inefficiently. Most issues are associated with incomplete combustion, influenced by factors like volumetric, thermal, mechanical, and frictional efficiency of engines (Ashok et al., 2021). As combustion occurs, both rich mixtures and insufficient air contribute to CO and HC formation (Lairenlakpam et al., 2018). NOx is generated by high combustion chamber temperatures and rapid cooling of exhaust gases during combustion (Triantafyllopoulos et al., 2019).

Both petrol and diesel engines emit CO, but the composition of this gas varies depending on the system. In comparison to petrol engines, diesel engines produce a significantly lower quantity of CO (Ashok et al., 2021). Complete combustion is nearly always achievable in diesel engines due to high oxygen circulation. However, in petrol systems, the fuel's heterogeneity shifts as the combustion reaction progresses towards lower conversion (Adeyanju & Manohar, 2017). Additionally, vital factor in CO creation in petrol engines is the combustion chamber design. Certain regions with low oxygen levels encourage partial fuel oxidation (Ashok et al., 2021).

Conversely, due to the engine's acceleration, drivers' demands can lead to an oxygen shortage (Adeyanju & Manohar, 2017). Since the aforementioned elements are fundamentally connected to the air to fuel ratio, it follows that this relationship becomes more complex during transient activities, which include shifting gears, acceleration, and deceleration (Yakın & Behçet, 2021). Additionally, in the initial few minutes after starting a cold engine, the mixture may lack sufficient oxygen, leading to the formation of CO (Wu et al., 2022). There are three primary causes of inefficient combustion that result in CO emissions of gasoline engines (Ashok et al., 2021). The first cause for the failure to reach equilibrium is a residence period that is too short. The second cause is inadequate fuel/air mixing, leading to rich localized zones with high equilibrium CO and oxygen deficiency in the burning mixing zone. The third cause is that heat extraction from the cold walls extinguishes the flame before combustion reaches equilibrium. Diesel engines often exhibit a high oxygen content, leading to minimal CO emissions. However, due to the uneven charge distribution, some CO is still generated in small regions of the combustion chamber where there is a lack of oxygen.

The formation of HC particles is correlated with the air-fuel ratio, impacting the combustion process (Mei et al., 2021). Primary combustion releases a substantial amount of HCs, which can undergo oxidation during the exhaust stroke and the expansion of the gaseous mixture, facilitated by desorption from hot oil or crevices. The emission of HCs in the exhaust manifold depends on operational parameters such as temperature. Gasoline engines release short carbon chain and low-density hydrocarbons due to defects in fuel-fed seals (Ashok et al., 2021). These emissions can be categorized as diurnal emissions, hot soak emissions, and running emissions during engine start (Kawsar et al., 2023). Additional sources of HC emissions include crevices, the quench-layer, porous deposits, absorption by oil, bulk quenching, late burning, and the injector effect (Ashok et al., 2021).

NOx, also known as NO and NO_2, is a toxic gas created in internal combustion engines when nitrogen and oxygen mix in a high-temperature chain reaction (Wang et al., 2021). NOx is produced both within the flame and behind it; early burning combinations generate more NOx than late burning mixtures (Ren et al., 2014). Exposure to NO can lead to increased acute respiratory infections, particularly in children and infants (Ashok et al., 2021). NOx is hazardous because it induces fatty acid oxidation, resulting in reactive free radicals that can alter structural proteins and affect membrane characteristics (Jonson et al., 2017). Additionally, the combination of NO and NO_2 with hemoglobin decreases the blood's ability to carry oxygen (Mei et al., 2021). Individuals, both adults, and children regularly exposed to high levels of NO_2 may develop respiratory illnesses. Ground-level ozone, perilous due to its adverse impact on lung function, is primarily formed by NOx. Nitric acid production in the atmosphere by NOx contributes to the formation of acid rain. Besides serving as a secondary greenhouse gas, NOx also plays a role in generating ozone, it is a gas 2000 times more potent than CO_2 (Ashok et al., 2021).

The term "greenhouse effect" was initially coined in the 19th century by Arrhenius, who also anticipated that depleting fossil fuels would elevate CO_2 levels, consequently leading to global warming (Wang et al., 2018). The overarching definition of global warming is a rise in the Earth's average temperature. For the EU states to achieve their goals in mitigating climate change and fulfil their commitments to reduce GHG emissions, it is crucial to reduce both CO_2 emissions and FC in the road transport sector (Tsokolis et al., 2020). Since 2017, the EU has been implementing laws and other measures with the goal of reducing CO_2 emissions from light-duty vehicles (Fontaras & Ciuffo, 2017).

2.2.2. Approaches for assessing vehicle emissions

Continuous monitoring is crucial for tracking emissions and atmospheric fluctuations. Vehicle emissions are acknowledged for their detrimental impact on the environment and public health, especially in cities where a significant portion of main air pollutants originate from vehicle emissions. Exposure to vehicle exhaust pollution is linked to an increased risk of cardiac and respiratory illnesses as well as mortality (Crosignani et al., 2021). The widespread use of fossil fuel-burning vehicles has positioned them as the primary sources of hazardous chemical emissions in urban and residential areas, making the population more vulnerable to pollution from vehicular emissions (Tarekegn & Gulilat, 2018). Vehicle emissions are estimated using various techniques, each providing a unique approach to capture the numerous relationships and variables influencing emissions, common methods include:

Chassis Dynamometer: utilizes a chassis dynamometer (CD) to measure vehicle emissions in a controlled laboratory environment (Adamiak et al., 2023).

Emission Models: integrates mathematical models with traffic flow data, vehicle activity, and emission parameters to simulate and predict emissions in specific regions or road networks (Fan et al., 2018).

On-Road Emissions Test: provides more precise and practical data by directly measuring emissions from vehicles while they are in operation (Karimipour et al., 2021). Portable emissions measuring instruments are employed for this purpose. Moreover, it is also possible to conduct roadside measurements of exhaust emissions from vehicles operating on public roadways using remote sensing equipment (Shi et al., 2023).

Which approach to use depend on the goals of the study, the resources at hand, and the degree of precision needed for emission estimation. The overall accuracy of vehicle emissions estimations can be improved by combining several approaches.

2.3. Driving cycle development process

The DC is defined as a set of data points that depict speed against time, incorporating factors like speed, gear selection over time, speed versus distance within a specific region, or a segment of a road (Galgamuwa et al., 2015). Amirjamshidi, 2015 described DC as a speed-time profile for a study area within which a vehicle can be idling, accelerating, decelerating, or cruising. A DC serves as a representation of a speed-time-sequenced profile tailored to a particular area or city (Khumla et al., 2010). It is a tool for representing, measuring, and regulating exhaust gas emissions, as well as monitoring FC, developed specifically for a certain type of vehicles in a particular environment and driving pattern. The development of vehicle DCs has undergone six conventional major milestones, as depicted in Figure 2.2.

Figure 2.2: Drive cycle development process

2.3.1. Route selection

Traffic congestion in an urban setting is anticipated to vary based on the route and time, with increased congestion expected during regular weekdays and peak hours compared to weekends, public holidays, and off-peak hours (Azman et al., 2018). In selecting representative routes from the actual road network in the study area, considerations should be given to traffic flow conditions influenced by factors such as road type, topography, intersections, population density, gradient, and weather conditions (Romero et al., 2017). The process of route selection requires the identification and confirmation of real-world situations occurring along each route (Mahayadin et al., 2017). Essential features for the chosen routes include high traffic volume, connections to major population centers, elevated emissions along the transit route, presence of various squares and intersections, and accessibility to public transport systems (Amin et al., 2018).

The process of selecting routes is a crucial step in developing DC. Typically, researchers rely on their local knowledge and understanding to choose sample routes (Zhang et al., 2014). However, this approach may introduce selection bias if relevant factors are not taken into account. For instance, (Peng et al., 2019) collected driving data from seven vehicles without pre-planned routes for 20 weeks in Fuzhou city. Similarly, (Anida et al., 2019) simply chosen the five most frequently used routes. In creating the Mashhad DC, two major routes were selected, both 15 km in length, with Azadi Square and Barq Square as the starting point and destination. These routes were chosen because Azadi and Barq squares connect East-West and North-South Mashhad, experiencing the highest traffic volume (Amin et al., 2018). For the development of the MUDC, five routes were chosen based on observations. The tests were conducted on weekdays excluding public holidays, from Monday to Friday, during peak hours from 07:30 to 11:30. This approach covered a mix of congested traffic, slow traffic, smooth traffic, and highway driving within the study area (Azman et al., 2018).

Certain researchers have devised methodologies or approaches to select the most representative routes. For example, (Zhao et al., 2018) utilized ArcGIS software to analyze the overall topological structure of urban roads in Xi'an. They established monitoring points on various types of selected sample roads, investigated traffic flow to determine peak and off-peak times, and then determined the length of each test route. In another instance, (Galgamuwa et al., 2016) employed an economic approach to gather speed-time data in Colombo, Sri Lanka. This involved considering vehicle travel activity patterns throughout the city using origin-destination survey data. The selected routes were subdivided into links using nodes or physical junctions to minimize segment length. They were then categorized into five groups based on daily traffic to assign appropriate weightage. To avoid underestimation, traffic flow variation throughout a typical day was divided into seven segments with noticeable variations. Ultimately, a route with the highest daily traffic within each group was selected as a point estimator to represent that specific group.

In the data collection for the Ljubljana DC development, the paths of vehicles were not predetermined, allowing them to travel randomly in line with the needs of users. A geographical information system (GIS) was employed by the study authors to locate data in the study area. Out of a total of 6,825,444 collected records, GIS analysis identified 416,471 records as the data within the study area, forming the database for subsequent processes (Lipar et al., 2016).

For the Delhi DC, the authors categorized traffic conditions as congested, semi-urban, urban, and extra-urban (Chugh et al., 2012). In the CLTC, traffic conditions were classified based on the vehicle speed phase: low, medium, and high-speed phases, with thresholds of 60, 80, and 120 km/h, respectively. These thresholds were determined based on weighting factors for different speed phases. Finally, the obtained values for the low, medium, and high-speed phases were 674, 693, and 433 seconds, respectively (Liu et al., 2020).

The typical procedures involved in selecting a representative route include:

i. Identifying the peak hour's peak ratio
ii. Establishing criteria to categorize routes as urban, rural, or highway
iii. Evaluating routes based on the level of service (LOS)
iv. Choosing and specifying the sample route length for urban, rural, and highways.

2.3.2. Driving data collection

From the vehicles within the study area, it is essential to choose representative vehicles and equip them with instruments capable of collecting and storing driving activity data from the selected routes. Typically, three methods have been commonly employed for collecting driving data (Azman et al., 2018; Amin et al., 2018):

1. **The chase-car method: i**n this method, a vehicle equipped with a data collection device follows the target vehicle. The target vehicle is randomly selected, and its operations are then replicated at a distance. If the chosen vehicle moves out of the study area, the

pursuing vehicle promptly selects a new one to follow. At the end of each route, the logged data are briefly reviewed to ensure accuracy before proceeding to the next route (Azman et al., 2018). This data collection approach can capture only specific segments of the driver's trip (Nouri & Morency, 2017), may omit details of the entire journey, and is suitable for areas with minimal and smooth traffic flows (Galgamuwa et al., 2016). Two methods are available for collecting data from target vehicles using this technique: laser technology and unlock data (Nouri & Morency, 2017).

2. **The on-board measurement approach:** involves installing instruments on target vehicles to capture speed data while they traverse predetermined routes. This method is suitable for use in areas characterized by high and aggressive traffic flow (Galgamuwa et al., 2016).
3. **The hybrid technique:** is a blend of on-board measurement and circular driving. In this method, a test vehicle equipped with instruments travels along the chosen routes multiple times during both peak and off-peak hours (Zhao et al., 2018).

To accurately develop DCs, a substantial sample of representative driving data is essential (Lipar et al., 2016). Among the prevalent technologies, GPS and an on-board diagnostics (OBD) interface stand out as the most common instruments for collecting driving data.

The GPS: provides information on a vehicle's velocity, time, date, latitude, longitude, and altitude. In the study area, (Galgamuwa et al., 2016) utilized the on-board measurement method with five GPS devices for data collection, gathering data from 78 trips at one-second intervals. The advantages of GPS-based data collection include its compact and easily portable nature, the installation and operation of the device not affecting the vehicle's operation, reliable signal reception, extensive data storage capacity, and a high frequency in the data acquisition system (Wang et al., 2013). A similar approach was adopted by (Yang et al., 2019; Anida et al., 2019; Trobradovic et al., 2020; Nguyen et al., 2019; Yugendar et al., 2020) for data collection using GPS.

The OBD interface: furnishes data on engine RPM and load, vehicle speed, and fuel flow rate. It offers superior data quality and greater accuracy compared to speed data derived from GPS (Ho et al., 2014). Various devices can connect to the OBD II port, including car chip devices (Al-samari, 2017), and ELM TM Bluetooth devices (Romero et al., 2017).

(Zhao et al., 2018) employed a hybrid method, recording driving data with speed-time data captured by OBD to enhance irregular GPS data. (Lipar et al., 2016) utilized an on-board measurement technique that incorporated an OBD II interface, a GPRS/GMS module, and a GPS to record driving data. (Liu et al., 2021) utilized data acquisition equipment, sampling vehicle and engine speeds from the OBD interface, while longitude and latitude were obtained using GPS devices.

As outlined in Table 2.1, a single vehicle was utilized for data collection in the development of DCs for locations such as Mashhad, Baqubah, and Basra. In contrast, for the development of the CLTC, an extensive dataset of 32 million km raw data was collected from 3767 vehicles, with 34% of them being hybrid and electric vehicles. Notably, CLTC combined the driving data of both traditional and electric vehicles, which is one of its weaknesses. Several researchers have addressed this limitation by developing separate DCs specifically tailored for hybrid and electric vehicles. For optimal representativeness, it is advisable to consider various driving scenarios, including peak, off-peak, and weekend situations during data collection. To assess the representativeness of the collected sample size for local DCs, this study introduced the percentage of the developed cycle duration relative to the size of the raw data collected. The data collection duration exhibited significant variation among the compared DCs, ranging from three days to one year. CLTC, with the largest and most comprehensive data collection in the history of DC development. The percentage of local DCs was between 0.19 and 10.93 except for CLTC, which is very high compared with WLTC and CLTC at $3.03*10^{-3}$ and $4.5*10^{-5}$ respectively. This stark difference clearly indicates that local DCs are less representative. The observed trend in local DCs suggests that the collection of a limited amount of driving data with a few vehicles and predetermined route selection is often driven by the objective of minimizing the budget required for data collection.

Table 2.1: Comparison of raw data gathered for developed DCs and WLTC

Driving cycle	No. of Vehicles	Data collection duration	Pathway selection	Route type/LOS	Collected raw data coverage	Duration of DC	% of cycle duration to raw data
LJURBAN (Lipar et al., 2016)	19	6 months	Not predetermined	-	416,471sec	1587sec	0.38
Mashhad (Amin et al., 2018)	1	2 weeks	Predetermined	Two major routes	25,500 sec	1020 sec	4
MURDC (Mahayadin et al., 2018)	1	-	Predetermined	Normal and highway	224 MTs	16MTs 1500sec	7.14
Baqubah (Al-samari, 2017)	1	7 days	Predetermined	From different routes in the city	33512 sec 200km	1052 sec 6.33km	3.14/3.16
Basrah DC (Najem et al., 2018)	1	5 weeks	Predetermined (4 paths)	light and peak traffic conditions	20912 sec	1041sec 6.273km	4.98
CLTC (Liu et al., 2020)	3767	1 year	Not predetermined	Urban, rural and motorway	32 million km	14.48 km 1800 sec	$4.5*10^{-5}$
Tianjin (Liu et al., 2021)	5	2 months	Predetermined	Main, secondary, branch roads and Expressways	165166 sec	1800	1.09
Zhengzhou (Peng et al., 2020)	-	2 weeks	Predetermined (2 routes)	All level of roads	600000sec	1184	0.2
Nanjing (Yang et al., 2019)	1	1 month	Predetermined 5 major routes	Considered also expressways	46569 sec 77.1km	1172	2.52
TMC (Huertas et al., 2019)	15	8 months	Predetermined	Urban, extra urban and mixed extra urban and urban in flat road	54867 sec 72km	6000 sec	10.93
Bangalore (Kiran & Verma, 2018)	1	3 weekdays	Predetermined	6 routes	18hrs 250km	2088 sec 9.4km	3.22/3.76
MUDC (Azman et al., 2018)	1	-	Predetermined	5 routes	367 MTs	1138 sec	
Colombo (Galgamuwa et al., 2016)	5	-	Predetermined	Both trip type	175hr	1200 sec	0.19
WLTC (Tutuianu et al., 2014)			Not predetermined	Urban, rural and motorway	765000km	23.21km 1800 sec	$3.03*10^{-3}$

2.3.3. Raw data filtration

Errors are inherent in the collected data samples from GPS, necessitating a data filtration process (Qiu et al., 2018; Lairenlakpam et al., 2018). Despite this requirement, many researchers, as observed in the reviewed papers, have skipped this crucial step. However, a few researchers have proposed and applied GPS data filtration processes.

Nguyen & Bui, 2020 introduced a comprehensive GPS filtering process comprising nine steps. They developed a MATLAB code to identify and rectify errors in GPS data. In the final steps of the filtration process, a modified Kalman filter was employed to de-noise and smooth the resulting signals. (Duran & Earleywine, 2018) utilized seven logic-based filters in their filtration process. These filters were designed to remove duplicated records and negative differential time steps, replace outlying high/low-speed values, eliminate zero-speed signal drift when the vehicle stopped, replace false zero-speed records, address gaps in data, rectify outlying acceleration or deceleration values, and denoise and smooth the final signals using the Savitzky-Golay filter technique. (Huertas et al., 2018) opted to disregard trip data that lacked typical values, with the criterion of less than 90% of available data. Instead of correcting missing values, they chose to exclude such data from consideration.

2.3.4. Data clustering

The filtered data underwent a clustering process, categorizing them into distinct groups, each intended to represent different driving characteristics and levels of congestion. Clustering is employed to gather micro-trips with similar speed-acceleration values (Huertas et al., 2018). This approach is suitable for consolidating a large number of micro-trips into a smaller set, and the candidate DC is formed by connecting micro-trips within an individual cluster (Chauhan et al., 2020).

Among clustering algorithms, K-means clustering stands out as the simplest and most widely used for grouping extensive datasets (Chauhan et al., 2020; Romero et al., 2017). The K-means algorithm has been utilized by (Anida et al., 2019; Chauhan et al., 2020; Yugendar et al., 2020) for clustering micro-trips. Additionally, (He et al., 2020) applied the mean shift clustering method to address the challenges associated with K-means clustering.

The traffic congestion level was typically represented by three clusters: low, medium, and high speed. In creating the Kuala Terengganu city DC, data were grouped into three clusters reflecting clear traffic conditions, medium traffic conditions, and congested traffic conditions (Anida et al., 2019). In the development of Beijing's DC, the task of DC classification was accomplished using a recurrent neural network (RNN). An RNN comprises a variable number of interconnected identical RNN cells, where each cell utilizes the state generated by the previous one (Qiu et al., 2018).

Driving modes

The prevalent driving modes typically include idle, cruising, acceleration, and deceleration (Lairenlakpam et al., 2018). In the context of the RDE regulation, acceleration is specifically defined as ‘a > 0.1 m/s^2’ However, there were slight variations in the specific values used by different researchers to categorize driving modes, as indicated in Table 2.2.

Table 2.2: Driving mode classification

Reference	Driving modes			
	Idle	Cruising	Acceleration	Deceleration
Lairenlakpam et al. (2018)	V < 1.389 m/s and -0.1389 < a < 0.1389 m/s^2	V ≥ 1.389 m/s and -0.1389 < a < 0.1389 m/s^2	a ≥ 0.1389 m/s^2	a ≤ -0.1389 m/s^2
Yang et al. (2019)	V<0.278 m/s and - 0.14< a <0.14 m/s^2	V ≥ 0.278 m/s and -0.14 < a < 0.14 m/s^2	a > 0.14 m/s^2	a < -0.14 m/s^2
Chauhan et al. (2020)	V < 1.389 m/s and -0.1 m/s^2 < a < 0.1 m/s^2	-	a >0.1 m/s^2	a < -0.1 m/s^2
Liu et al. (2020)	V < 0.1389 m/s and a < 0.15 m/s^2	V ≥ 0.1389 m/s and a < 0.15 m/s^2	a ≥0.15 m/s^2	a ≤ -0.15 m/s^2

2.3.5. Decide DC length

The length of a DC plays a crucial role in ensuring proper representativeness and accurate measurement of emission levels and FC testing in a controlled environment. It is important that the DC testing does not excessively prolong or become overly intricate. There needs to be alignment between the representative DC and its suitability for testing in the controlled environment (Chugh et al., 2012).

In the case of the CLTC, its length was determined based on the duration of the low, medium, and high-speed phases, derived from the weighting factors assigned to these speed phases. Specifically, the low, medium, and high-speed phases were assigned values of 674, 693, and

433 seconds, respectively (Liu et al., 2020). For Delhi's DC, the duration was set at 1500 seconds, taking into account the patterns of legislative DCs (Chugh et al., 2012). Similarly, Malaysia's urban road cycle was designed to last for 1500 seconds, with the authors noting that this duration was adequate for experimental work in the controlled environment laboratory test (Mahayadin et al., 2018).

2.3.6. Driving cycle formation

The process of forming a DC varies depending on the intended use of the DC, which can include estimating emission inventories, FC, or serving traffic engineering purposes (Galgamuwa et al., 2015b). Four major methods have been employed for DC formation: micro-trip-based, segment-based, pattern classification, and modal cycle formation (Chindamo & Gadola, 2018; Peng et al., 2019; Duarte et al., 2016). More recently, (Huertas et al., 2018) introduced a novel approach termed the fuel-based method. Each method possesses distinctive features tailored to represent its intended purpose.

2.3.6.1. Micro-trip based cycle construction

The time interval between the initiation of one idling period and the subsequent occurrence of idling is defined as a micro-trip (MT) (Peng et al., 2019), encompassing the initial idling period as well (Galgamuwa et al., 2015). In this approach, the cycle is constructed by categorizing driving data into different bins based on average speeds when target population parameters are met. Subsequently, a set of MTs is chosen and concatenated to create a candidate DC (Galgamuwa et al., 2015). The two prevalent methods for this combination are quasi-random selection (Huertas et al., 2018) and the best incremental method (Noralm, 2018). However, Chi-squared analysis was used by (Mahayadin et al., 2018) to assess the difference between the chosen MT combination and the entire database when combining MTs, and the combination with the lowest Chi-squared value was ultimately chosen.

The DCs for Vadodara (Chauhan et al., 2020), Ludhiana (Yugendar et al., 2020), Bangkok (Tamsanya & Chungpaibulpatana, 2009), Hong Kong (Hung et al., 2007), Pune (Kamble et al., 2009), and CLTC (Liu et al., 2020) were developed using the MT-based cycle construction method. Table 2.3 presents both the advantages and limitations of the MT approaches. The trip segment method was developed by (Kiran & Verma, 2018) as a novel approach to address the shortcomings of the MT method. The method also includes an algorithm for extracting these units from the provided data..

2.3.6.2. Segment based cycle formation

In this method, the consideration of route type or Level of Service (LOS) is essential when selecting a trip segment, as opposed to choosing adjacent stops (Zégé et al., 2020). Consequently, the selected trip segment can accurately depict the actual traffic conditions and characteristics of the road based on LOS (Amirjamshidi, 2015; Huertas et al., 2019). Hence, in the process of linking trip segments to form the DC, it becomes crucial to ensure a match in speed and acceleration between two consecutive connecting points (Pathak et al., 2016). This method proves to be well-suited for creating a DC designed for traffic engineering purposes and expressways, particularly in scenarios where there are no adjacent stops between the origin and destination (Galgamuwa et al., 2015). The Australian Composite Urban Emission Drive Cycle (CUEDC) was developed utilizing this method (Shi et al., 2016).

2.3.6.3. Pattern classification

This approach involves creating DCs through a statistical method that randomly selects kinematic sequences from segmented activity classes, taking into account the likelihood and occurrences of these sequences (Andre, 2004). ARTEMIS driving cycles were formulated using this technique (Galgamuwa et al., 2015).

2.3.6.4. Modal/Markov chain approach

In this approach, actual driving data patterns are segmented into acceleration, deceleration, cruising, and idling components using the Markov chain theory. This theory assumes that the probability of a specific modal event is dependent solely on the preceding modal event (Galgamuwa et al., 2015). The "wavelet theory" is employed to analyze various frequency components of driving data, specifically in assessing velocity components and decomposing cycle formation into multiple signals with distinct frequencies (Shi et al., 2016). The modal cycle construction method, utilizing the Markov chain approach, has been adopted by researchers such as (Galgamuwa et al., 2016; Nguyen et al., 2019; Puchalski et al., 2020; Peng et al., 2020).

Table 2.3: Advantages and disadvantages of DC construction methods

Method	Advantages	Disadvantages
Micro-trip	A good representation of FC and emissions (Puchalski et al., 2020). Covers each stop-go condition that happens due to traffic congestion (Galgamuwa et al., 2015). A cycle is generated based on real driving data (Galgamuwa et al., 2015). Considered LOS (Zégé et al., 2020).	The starts and ends of MTs are specific speed, acceleration and duration (Zégé et al., 2020). Not possible to differentiate MTs by different types of levels of services (LOS) (Galgamuwa et al., 2015). It is repeatable but not reproducible because it is stochastic in nature (I. Huertas et al., 2019).
Segment based	The cycle starts and ends at any speed (Amirjamshidi, 2015). Suitable for traffic engineering purposes (Galgamuwa et al., 2015). Suitable for express-ways (Galgamuwa et al., 2015).	Matching the speed and acceleration between two successive connecting points is necessary in order to chain the trip segments into a DC (Amirjamshidi, 2015; Romero et al., 2017). Unsuitable for estimating emissions and FC (Galgamuwa et al., 2015).
Pattern based		Not directly related to emissions-related DC, highly statistics-based, requires more information to divide collected data into kinematics sequences and to classify the route (Dai et al., 2008).
Markov chain	Driving patterns are divided into four driving modes. Since chaining the modal bins exploits the chance of each mode occurring on the road, it accurately depicts the actual traffic situation (Galgamuwa et al., 2015).	If the road's traffic behaviour is smooth, the modal event's duration may be significantly greater than the cycle's overall time (Galgamuwa et al., 2015).
Fuel-based	Fuel-based DCs and measured FC on level roads are nearly identical (Huertas et al., 2018). It can be reproduced and repeated (Kumar et al., 2016; Andre, 2004)	Researcher cannot control the length of the chosen DC (Kumar et al., 2016; Andre, 2004).

2.3.6.5. Fuel-based approach

The immediate fuel flow rate of the vehicle is assessed through the engine control unit (ECU), offering the possibility to formulate a DC based on the FC principle. In this method, the average specific fuel consumption (SFC) is calculated for the sampled trips. Subsequently, the trip with the SFC closest to the average SFC is chosen as a representative DC (Duran & Earleywine, 2018; Zhu, 2014). A study by (Huertas et al., 2018) proposed a technique for developing a local DC with FC as a criterion. They gathered data from a fleet of 15 vehicles with similar technology, utilizing the OBD interface provided by the engine manufacturer. This interface facilitated the reading, reporting, and storage of instantaneous engine FC at a 1 Hz sampling period. Additionally, GPS data were employed to track the position, altitude, and speed of the vehicles over time during eight months of regular operation in four regions characterized by diverse topography and roads featuring different LOS. The outcomes of the study confirmed that the characteristic parameters and Speed-Averaged Power Density (SAPD) of the fuel-based DCs closely resembled the measured FC on flat roads.

2.3.7. Conformity assessment

Various potential cycles can be derived from diverse sets of similar raw driving data. Consequently, it becomes necessary to identify the most representative candidate cycle that best aligns with real-world driving data. The assessment of the conformity of candidate cycles with actual driving data is conducted through an analysis that considers:

- speed acceleration frequency distribution (SAFD): the smallest $SAFD_{diff}$ value is selected as the best DC (Chauhan et al., 2020; Trobradović et al., 2020).
- performance value (PV) (Yugendar et al., 2020)
- sum squared difference (SSD) (Yugendar et al., 2020)
- correlation factor (CF): CF value close to one can be selected as the representative DC of the route (Romero et al., 2017)
- Chi-squared: the combination of short trips with the smallest chi-squared value was selected for CLTC (Liu et al., 2020)
- Euclidean distance: the smallest Euclidean distance for each DC derived should be chosen (Najem et al., 2018).

- relative error: an error of 5 % is considered acceptable for each parameter. If the error is more than 5 %, develop a DC again by a random combination of micro-trips, continuing the process until the error rate is less than 5 % (Chauhan et al., 2020).

2.3.8. Assessment of the developed DC

The assessment of the generated DC is essential to verify its alignment with the on-road data gathered and to enable a comparison with the standard DC, specifying any deviations. Characteristics parameters play a crucial role in this evaluation process, ensuring that the developed cycle accurately mirrors the actual driving pattern, as emphasized by (Nguyen et al., 2019). Researchers have employed various parameters, totaling more than 58, to compare formulated DCs with collected real-world data and other existing DCs. In the examined literature, many studies employed a set of parameters for cycle assessment, often relying on the precedents of prior research without providing robust justifications for their choices. However, in order to identify key parameters significantly influencing emission levels and FC, (Nguyen et al., 2019) utilized the hierarchical agglomerative clustering (HAC) method. This approach helped them identify a minimal subset of representative variables from an initial pool of 33, ultimately selecting the 14 most indicative variables. Similarly (Ericsson, 2001) employed factorial analysis to reduce the initial 62 parameters to 16, out of which nine were identified as having a notable impact on emissions. Additionally, (Lee & Filipi, 2011) utilized statistical regression analysis to assess the significance of each parameter in representing the response of DCs, discovering that eight out of the 27 variables were significant for evaluating the DC.

The emission levels of CO_2, CO, and NO_X exhibit greater sensitivity to speed and acceleration, decreasing as the absolute value of acceleration increases in low-speed and medium-speed zones, and rising with both speed and acceleration in high-speed zones, as indicated by (Yang et al., 2019). For CO and NO_X, emission rates peak when speed and acceleration reach their maximum, while the highest HC rate is typically observed in the medium-speed and high acceleration zone. In a local DC test, it was found that the highest emission rates of CO_2, CO, and NO_X occurred during acceleration, with the lowest values observed during idling (Yang et al., 2019). However, it is worth noting that with modern vehicles and advanced after-treatment devices, a direct correlation is not always evident (Valverde, et al., 2021). Table 2.4 provides a simplified representation of the most commonly utilized parameters.

Table 2.4: DC characteristic parameters

Category	Parameters	Units	Yugendar et al., 2020	Azman et al., 2018	Nguyen et al., 2019	Najem et al., 2018	Anida et al., 2019	Peng et al., 2020	Huertas et al., 2019	Nguyen & Bui, 2020	Mahayadin et al., 2018	Liu et al., 2021	Lipar et al., 2016
			LuDC	MUDC	HB DC	BCC DC	KT DC	ZDC	TMC	HDC	MURDC	TDC	LJDC
Cycle distance & time related	C_L	km		5.86	18.32	6.27	10.07	4.92		18.32	13.29	10.31	10.19
	C_T	s		1138	3936	1041	1089	1184		3936	1500	1800	1587
	% of t_{driv}	%		63.18									77.5
	P_c	%	2.39		14.1		4.68	14.49	29.3	3.6	61.73		22.55
	P_a	%	51	32.43	34.17		45.78	33.32	27.2	46.90	10.13		27.73
	P_d	%	41.17	30.76	32.70		42.84	28.78	23.7	48.79	8.73		28.23
	P_i	%	5.40	36.82	7.62		6.7	22.93	19.3	3.37	19.4	26.7	22.5
Driving Mode related	P_{cr}	%			11.41								
	t_{acc}	s			1345								440
	t_{dec}	s			1287								448
	t_{cru}	s			555								342
	t_{cre}	s			449								
	t_{idl}	s		419	300								357
	t_{driv}	s											1230
	V_{trip}	km/h		20.6	16.76		36.27			17.38	37.17		29
	V_{avg}	km/h	24.83	21	18.14	21.63	33.27	14.96	11.2	16.67	31.89	20.62	22.5
	SD of V	km/h		21.4	10.52			13.56	9.7	10.71		0.78	18.57
Vehicle Speed related	75^{th}-25^{th} % of V	km/h											35
	95^{th} % of V	km/h			33					36.4			
	V_{max}	km/h		91	44	63.62		49.63	28.4	46.3		83.4	70
	a_{avg}	m/s^2		0.53	0.5		0.53		0.4	0.46	0.75	0.47	0.83
	d_{avg}	m/s^2			-0.52		0.56		-0.5	-0.44	-0.89		-0.77
	a_{SD}	m/s^2			0.49			0.7	0.2	0.06		0.02	0.61
	d_{SD}								0.4	0.05			
Acceleration related	a_{95th}	m/s^2			1.11								
	d_{95th}	m/s^2			-1.11								
	No. of a			79									151
	No. of 'a' per km	/km		13.48					7.4				14.82
	a_{max}	m/s^2			3.06	2.66		4.031	1.6	3.85		2.43	
	d_{max}	m/s^2			-2.78	-3.09		-5.4	-2.1	-3.39			
	No. of stops			18	21	7							21
	Stops per km	/km		3.07	1.15	0.87							2.08
Stop related	Avg. distance between stops	m											485.19
	PKE	m/s^2			0.34				241.3				0.51
	RMSA	m/s^2			0.49		0.72		0.4				
Slope related	i_{max}	deg						4.79					
	i_{min}	deg						-3.4					
	i_{avg}	deg						-0.23					

LuDC is the Ludhiana DC, HBDC is the Hanoi DC, KTDC is the Kuala Terengganu DC, ZDC is the Zhengzhou DC, TMC is the Toluca-Mexico city DC, HDC is the Hanoi DC, MURDC is the Malaysia's urban road DC, TDC is the Tianjin DC, LJDC is the LJURBAN DC, C_L is the DC length, C_T is the DC duration, t_{driv} is the driving time, P_a is the percentage of acceleration time, P_d is the percentage of deceleration time, P_i is the percentage of idle time, P_c is the percentage of cruise time, P_{cr} is the percentage of creeping mode, t_{acc} is the acceleration time, t_{dec} is the deceleration time, t_{cru} is the cruising time, t_{cre} is creeping time, t_{idl} is the idling time, V_{trip} is average trip speed, SD is the standard deviation, V is the vehicle speed, V_{avg} is the average driving/vehicle speed, V_{max} is the maximum vehicle speed, a_{avg} is the average acceleration, d_{avg} is the average deceleration, a_{95th} is the 95th percentage of acceleration, d_{95th} is the 95th percentage of deceleration, PKE is the positive kinetic energy, RMSA is the root mean square of acceleration, VSP_{max} is the maximum specific power, i_{max} is the maximum slope, i_{min} is the minimum slope, and i_{avg} is the average slope.

2.3.9. Comparison of driving cycles

Table 2.5 presents a comparison of the cycle parameters of various DCs. Table 2.5 shows that regular traffic circumstances are present in Ludhiana and Kuala Terengganu DCs, which have lower idle ratios of 5.4% and 6.7%, respectively. Vadodara DC and MUDC, on the other hand, have greater idle percentage than other DCs—39.2% and 36.82%, respectively—which may indicate more traffic congestion, particularly in cities with a large concentration of nearby signalised intersections. In comparison to other cycles, MUDC has a lesser acceleration ratio of 10.13%, whereas Ludhiana and Baqubah have greater acceleration ratios of 50.99% and 50.33%, respectively. The mean proportions of idle, cruising, acceleration, and deceleration are 19.77±7.89%, 17.35±16.07%, 33.25±9.74%, and 30.22±9.27%, respectively, according to statistical analysis of the comparable local DCs. When comparing local DCs with standard DCs, it is noteworthy that the percentages of acceleration and deceleration are typically larger in the local DCs which result in higher emissions. In contrast, it was found that the majority of the time, the percentages of cruise and idle were smaller.

Table 2.5: Comparison of local and standard DCs

Name of DC	Year	V_{avg} (km/h)	V_{max} (km/h)	% of P_i	% of P_C	% of P_a	% of P_d	C_L (Km)	C_T (Sec)	Considered routes
TDC (Liu et al., 2021)	2021	20.62	83.4	26.7				10.31	1800	Expressways, main roads, secondary roads, and branch road
CLTC (Liu et al., 2020)	2020	28.96	114	22.11	22.83	28.61	26.4	14.48	1800	Urban, rural and motorway
HDC (Nguyen & Bui, 2020)	2020	16.67	46.97	7.62	14.1	34.17	32.7	18.32	3936	Urban area
ZDC (Peng et al., 2020)	2020	14.96	49.63	22.93	14.97	33.32	28.8	4.92	1184	Not clear but heterogeneous traffic condition was considered
HBDC (Nguyen et al., 2019)	2019	18.14	44	7.62	14.1	34.17	32.7	18.32	3936	Inner-city (circular, radial, and straight route types)
KTDC (Anida et al., 2019)	2019	33.27	65	6.7	4.68	45.78	42.8	10.07	1089	Not clear
Nanjing (Yang et al., 2019)	2019	30.73	85.65	20	30	27	23	10	1172	Expressways, arterial roads, secondary trunk roads, and branch roads
TMC (Huertas et al., 2019)	2019	11.2	28.4	19.3	29.7	27.2	23.7	18.67	6000	Urban, extra-urban, and mixed urban and extra-urban of medium traffic flow
Bangalore (Kiran & Verma, 2018)	2018	20.71	65.17	21.75	13.56	34.74	30	9.4	2088	Not included motorways.
MURDC (Mahayadin et al., 2018)	2018	31.89	90	19.4	61.73	10.13	8.73	13.29	1500	Urban, highway
MDC (Amin et al., 2018)	2018	20.41	60	21.75	3.22	37.34	37.69	5.78	1020	Arterial road
MUDC (Azman et al., 2018)	2018	21	91	36.82	-	32.43	30.8	5.86	1138	Standstill, slow, smooth, & highway driving
Baqubah (Al-samari, 2017)	2017	21.63	68	25.56	0	50.33	48.5	6.33	1052	Not clear
Colombo (Galgamuwa et al., 2016)	2016	20.3	58	20.5	12.75	36.1	30.7	6.77	1200	Considered different routes based on daily traffic conditions
LJDC (Lipar et al., 2016)	2016	22.5	70	22.5	21.55	27.73	28.2	10.19	1587	Not considered motor way
TWFA (Amirjamshidi & Roorda, 2015)	2015	18.4		17.1	3	43.8	36.1	9.2	1800	Major arterials
WLTC* (Liu et al., 2020)	2014	46.42	131	12.7	27.8	30.9	28.6	23.21	1800	Urban, rural and motorway
FTP 75* (Liu et al., 2020)		33.9	90.16	17.2	24.7	31.1	27.1	17.68	1874	Cold, stabilisation, and hot phase
JC 08* (Giakoumis, 2017)		24.4	81.6	28.74	1.5	36.13	33.64	8.16	1204	Included motorway but it is shorter (154 sec)
ARTEMIS (Amin et al., 2018)		59.2	150.4	9.64	16.19	38.84	35.32	51.69	3143	URM 150 (urban, rural and motorway)
NIER-09* (Kim et al., 2018)		34.1	70.9	11.7	0	43.4	44.9	8.74	926	
CUEDC Petrol*(Giakoumis, 2017)		38.95	94	20.42	25.26	26.82	27.49	19.44	1797	Congested, residential, arterial, and freeway

Table 2.5 shows that the WLTC has a maximum speed of 131 km/h and an average speed of 46.42 km/h, respectively, which are much faster than other local DCs. Among local DCs, the CLTC has the greatest Vmax (114 km/h), indicating better road infrastructure in China. On the other hand, several local DCs show lower maximum speeds, frequently less than 100 km/h, suggesting that either there were no highways consideration when the data were collected, or maybe there were no highway in the city under consideration. With the Vavg of 33.27 km/h the KTDC has highest average velocity among the local DCs, and it is followed by the MURC at 31.89 km/h, indicating comparatively less traffic congestion. Statistical analysis of the compared local DCs reveals means of Vavg and Vmax as 22.06±6.43 km/h and 68.40±23.66 km/h, respectively. The mean average speed of local DCs is generally observed to be lower than that of standard DCs, except for JC08.

Table 2.5 illustrates that ARTEMIS, WLTC, and TMC have longer lengths compared to other cycles, with 51.687 km, 23.21 km, and 18.667 km, respectively, while the MUDC stands out as the shortest cycle at 5.86 km. In terms of cycle duration, as indicated in Table 2.5, the Toluca-Mexico City and Hanoi cycles have the lengthiest cycle times at 100 minutes and 65.6 minutes, respectively. The mean cycle length for the compared local DCs is 11.07±4.59 km, which is shorter than WLTC, FTP-75, ARTEMIS, and CUEDC. This suggests that, on average, local DCs have shorter lengths compared to standard DCs.

2.4. Comparison of RDE tests with laboratory-based and real-world emissions

Since 2017, EU emission regulations have incorporated a component of legal homologation (Czerwinski et al., 2018), mandating new PVs to undergo emission testing on public roads as part of the certification process (Bodisco & Zare, 2019). The EC has sanctioned RDE tests to narrow the discrepancy between emissions reported by manufacturers and those actually emitted on the road (Bodisco & Zare, 2019; Tzamkiozis et al., 2017). PEMS are employed for real-time measurement of CO/CO_2, NO/NO_2, and PN concentrations in the exhaust gas of vehicles operating under genuine driving conditions (Luján et al., 2018; Williams et al., 2018; Noralm, 2018). Simultaneously, PEMS records vehicle-related parameters and environmental conditions such as location, velocity, and temperature (Bodisco & Zare, 2019). The RDE, introduced in EU legislation, comprises four successive regulatory packages: RDE 1 (EU Regulation

2016/427), RDE 2 (EU Regulation 2016/646), RDE 3 (EU Regulation 2017/1154), and RDE 4 (EU Regulation 2018/1832) (Suarez-bertoa et al., 2019).

Conducting emissions assessments on a CD is a standard procedure for comparing a vehicle's emissions and confirming compliance with established emission limits. However, CD tests have limitations due to their inability to accurately represent actual on-road driving conditions. Table 2.6 presents a comparison of RDE with laboratory-based cycles (WLTC, FTP-75, and CADC).

As outlined in Table 2.6, RDE results for CO_2 are 3-41% higher than WLTC, with exceptions noted in the results reported by (Thomas et al., 2017; Triantafyllopoulos et al., 2019). RDE for NO_X is 10-326% higher than laboratory-based DCs, except for tests conducted in Beijing and Xiamen. Similarly, real-world emissions of CO and HC also demonstrate an increasing trend compared to laboratory-based emission measurements. The reviewed articles highlight that on-road emissions and FC tend to be significantly higher than values derived from laboratory tests, primarily due to factors like driver behavior, diverse weather conditions, traffic variations, and gradients. One notable limitation of RDE tests is their lower repeatability compared to laboratory tests. Additionally, it is mentioned that the EU RDE test procedure does not cover congested traffic conditions.

Table 2.6: Comparison of RDE with laboratory-based cycles

DC	Year	Methods applied or source of sample data	Country/city of RDE data	Vehicle category	Laboratory-based emissions level (g/km)	On-road emissions level (g/km)	Difference	FC	References
WLTC	2020	WLTP and RDE	Gothenburg, Sweden	Diesel and gasoline vehicles	143 for CO_2 136 for CO_2	148 for CO_2 151 for CO_2	↑3 %CO_2 for CI vehicles ↑11 % CO_2 for SI vehicles		Debbie et al., 2020
WLTC	2020	WLTP and RDE	NM	Euro 6b diesel			-	↑18.03 %	Pavlovic et al., 2020
WLTC	2020	Real-world data from the consumer	German	WLTP type approved vehicle (2018)	NM	NM	↑14 % CO_2	↑14 %	Dornoff et al., 2020
FTP-75, HWFET	2020	FTP, HWFET, and US06, and Canadian 5-mode on-road driving	Canada	Gasoline and Diesel LDVs	< 0.0435 FTP limit of NO_X	0.061-0.326 for NO_X	1.4-7.5 times FTP NO_X limit	↑22%	Debbie et al., 2020
WLTC	2019	WLTP, and RDE	Lombardy, Italy	Euro 6d-temp diesel (DOC + DPF + SCR)	146.31 for CO_2	165.33 for CO_2 0.282 for NO_X 0.0197 for CO	↑13 % CO_2		Suarez-bertoa et al., 2019
WLTC	2019	WLTP, and on-road testing	Thessaloniki, Greece	Euro 6b diesel (DOC + DPF + EGR)	CO_2 close enough to the RDE CO_2 levels	NOX are 3 times higher than WLTP level	↓50%-100% CO_2 and ↑300 for NOx		Triantafyllopoulos et al., 2019
Standard road speed	2019	On-road, and CD tests	Warsaw	Ford focus PV	229 for CO_2 6.9 for CO 1.23 for NO_X 1.04 for HC	242 for CO_2 7.9 for CO 1.17 for NO_X 0.68 for HC	↑5.4 % CO_2 ↑12.6 % CO ↓5.12 % NO_X ↓50.72 % HC		Wiśniowski et al., 2019
CADC	2019	CADC, and on-road testing	Thessaloniki, Greece	Euro 6b diesel (DOC + DPF + EGR)	NOX levels are close to the levels of the RDE test		NOx levels are close to the levels of the RDE test		Triantafyllopoulos et al., 2019
MIDC	2018	MIDC and the average real-world emissions of the three routes	Dehradun city, India	Gasoline (TWC)	216.83 for CO_2 0.977 for CO 0.008 for THC 0.011 for NO_X	263.35 for CO_2 2.03 for CO 0.021 for THC 0.025 for NO_X	↑1.12-1.39 times for CO_2 ↑1.35-2.39 times for CO, ↑2.17-5.0 times for THC ↑2.04-2.32 times for NOx	↑18.4 %	Lairenlakpam et al., 2018
WLTC	2018	WLTP and pre-recorded RDE cycle under lab-RDE cycle	Italy	Euro 6 gasoline (TWC) and diesel (DOC + DPF + NS)	NC	NC	↑10 % CO_2 ↑15 %NOx		Varella & Giechaskiel, 2018
WLTC	2018	Powertrain Road Performance Simulator (PRoPS) within the Matlab-Simulink	Lombardy	Euro 5 diesel	180 for CO_2 ≈0.31 for NO_X 1.21 for CO 0.05 for HC 0.013 for PM_{10}	400 for CO_2 ≈0.84 for NO_X 1.82 for CO 0.28 for HC 0.015 for PM_{10}	↑≈ 122 %CO_2, ↑≈ 1.71 times for NO_X, ↑≈ 350.4 % CO, ↑≈ 4.6 times for HC, ↑≈ 14.5% PM10		Chindamo & Gadola, 2018
CADC	2018	PRoPS within the Matlab-Simulink	Lombardy	Euro 5 diesel	380 for CO_2 ≈0.08 for NO_X 0.095 for CO 0.045 for HC 0.0065 for PM_{10}	400 for CO_2 ≈0.84 for NO_X 1.82 for CO 0.28 for HC 0.015 for PM_{10}	↑ 5.26 %CO_2, ↑≈ 9.5% times for NO_X, ↑≈ 18 times for CO, ↑≈ 5.2 times for HC ↑≈ 13.77 times for PM10		
WLTC	2017	WLTP and simulation of real-world driving	NC	Euro 5 gasoline and diesel	143.9 for CO_2	162.6 for CO_2	↑13 % CO_2		Tsiakmakis et al., 2017
WLTC	2017	Real-world data from the consumer website Spritmonitor.de	German	Gasoline and diesel	NM	NM	↑37 % CO_2 (gasoline) ↑41 % CO_2 (diesel)		Tietge et al., 2019
WLTC	2017	WLTP and RDE	Beijing and Xiamen	Euro 5 gasoline LDV (TWC)	182 for CO_2 0.62 for CO 0.028 for NO_X	175 for CO_2 0.248 for CO 0.0185 for NO_X	↓4 % CO_2, ↓60 % CO, and ↓34 % NO_X		Thomas et al., 2017
WLTC	2016	WLTC simulated on IVE model and on-road testing	Deharsun, India	Euro 4 gasoline LDV (TWC)	111.23 for CO_2 0.953 for CO 0.08 for HC 0.086 for NO_X	145.7 for CO_2 1.4 for CO 0.1304 for HC 0.141 for NO_X	↑31 %CO_2, ↑46.9 %CO, ↑63 %HC, and ↑64 % NO_X		Kumar et al., 2016
WLTC	2016	WLTP and on road data	NM	Euro 5 vehicles	130.25 for CO_2 0.409 for NO_X	143.687 for CO_2 0.498 for NO_X	↑10.% for CO_2 ↑21.83 % NO_X	↑10.55 %	Duarte et al., 2016

2.5. Factors influencing real driving emissions(RDE)

RDE tests face challenges related to testing boundary conditions, uncertainties in PEMS, and methods of data analysis. Achieving reproducibility in RDE tests is difficult, as dynamic and environmental conditions are specific to each geographical location, making a set of conditions representative for one location but not necessarily applicable to another test site. This review emphasizes key factors influencing RDE results, outlined below.

2.5.1. Influence of road grade on the RDE

Neglecting to account for road grade can lead to significantly inaccurate estimations of vehicle emissions. According to findings by (Costagliola et al., 2018), a route with a 5% road grade resulted in an almost 100% increase in both CO_2 and FC compared to a flat road. Conversely, a grade of -4% exhibited a nearly 70% decrease in CO_2 relative to the flat road, and road grades of 4-5% increased NO_X emissions between two and five times compared to flat terrain. (Gallus et al., 2017) noted that road grades from 0-5% contributed to a 65-81% increase in CO_2 and an 85-115% increase in NO_X. Furthermore, dynamic driving on uphill roads was found to result in three times greater CO_2 and eight times higher NO_X emissions (Triantafyllopoulos et al., 2019). The comparison by (Pavlovic et al., 2020) shows that when comparing roads with grades below -1% to those above +1%, the average impact of road grade on the FC gap is approximately 56%.

2.5.2. Influence of cold temperature on the RDE

In urban environments, the phenomenon of cold starts can substantially contribute to overall vehicle emissions and FC due to frequent short trips (Weiss et al., 2017). When the atmospheric temperature drops from 25°C to 8°C during a cold start within a considered period of 300 seconds, the result is a 16% increase in CO_2 (FC), a 195% increase in CO, a 280% increase in PN, and an 11% decrease in NO_X (Pielecha et al., 2021). Exclusions of cold starts and idling in the EU RDE regulations lead to an 8% reduction in CO_2 emissions in urban drive mode, along with an 18% reduction in CO emissions (Thomas et al., 2017). For diesel vehicles undergoing an RDE test, trips conducted in temperatures ranging from 5°C to 10°C exhibit up to a 30% difference in NO_X emissions. In contrast, gasoline vehicles show less significant differences in NO_X emissions compared to diesel vehicles (Varella et al., 2017). CO_2 emissions are highest during a cold start, with a factor of 1.6 and 1.3 at temperatures of -7°C and +23°C, respectively.

In the case of a gasoline direct-injection vehicle equipped with a particulate filter, PN emissions at -7°C are 2.6 times higher than those at the ambient temperature of 23°C during a warm start (Nakamura et al., 2019).

2.5.3. Influence of route selection on RDE

In numerous urban centers, traffic congestion is on the rise, with a majority of PVs in developing nations predominantly operating through congested traffic and signalized intersections. While the EU's RDE legislation allocates a nearly equal share to urban roads, rural roads, and motorways, each category contributes different emission levels and FC.

As per a study conducted by (Suarez-bertoa et al., 2019), an examination was carried out on the on-road emissions of 6d-Temp vehicles across various routes, including those aligned with EU procedures, a city motorway route for extended motorway driving, and a hill route exclusively involving urban operations. The median NO_X emissions factor varied from 34 mg/km on the city route to 318 mg/km during RDE dynamic tests featuring more acceleration. Median particulate number (PN) emissions were twice as high during dynamic routes (2 x 10^{12} #/km) compared to RDE routes (1 x 10^{12} #/km). PN median emissions were 3.5 times lower on the city motorway route compared to RDE routes. Gasoline vehicles exhibited median CO emissions of 167 mg/km during the hill route test and 2850 mg/km during the RDE dynamic test.

A study by conducted (Williams et al., 2018) RDEs performance tests on three distinct routes. Route 1 predominantly featured urban driving sections, lacking a motorway segment. Route 2 primarily resembled driving on rural roads. Route 3 conformed to the specifications outlined in the European Union's RDE legislation. The study revealed that the emission of CO increased proportionally with the test duration, irrespective of the test route type. The tests yielded higher CO and HC emissions compared to the EU RDE test, particularly when the tests were shorter and urban and rural segments constituted a larger proportion of the entire test. The authors affirmed that it is feasible to reduce the test distance by approximately 20% without a significant impact on the results of specific distance exhaust emissions.

Furthermore, a study by (Triantafyllopoulos et al., 2019) involved on-road testing with CI vehicles on two routes within the Thessaloniki region, Greece. The first route adhered to the specifications of the RDE regulation, while the second route was configured to simulate a more dynamic driving profile referred to as DYN. In the DYN scenario, CO_2 levels were 50% to

100% higher than those in RDE, and NO_X emissions were two to eight times greater than RDE, surpassing the emission limit by 25-40 times.

2.5.4. Influence of PEMS uncertainty on RDE

Several PEMS devices are available, including Horiba, AVL, OBM, and the Semtech DS analyzer. PEMS are prone to increased measurement uncertainty caused by potential drift in analyzers over time and variations in exhaust flow rate (Giechaskiel et al., 2018).

The investigation conducted by (Czerwinski et al., 2016) examined the outcomes of three PEMS, namely Horiba OBS ONE, AVL M.O.V.E, and OBM Mark IV/TU Wien. These PEMS devices were installed on the same vehicle, which underwent testing on the CD following the NEDC, WLTC, and CADC. The obtained results were compared with those from the CVS, specifically the Horiba MEXA 7100. The disparities between PEMS 1, 2, and 3 and CVS values across all cycles were approximately -12%, 35%, and -3% for NO_X, and around 25%, 3%, and 55% for CO, respectively. The average deviation across all cycles between PEMS and CVS values was 37% for NO_X and 67% for CO. All PEMS devices indicated higher CO_2 levels compared to CVS, confirming elevated readings by PEMS relative to CVS. The authors suggested that insufficient synchronization of transient parameters, including exhaust gas mass flow, concentration, and density of the measured parameter, was the primary reason for the observed differences. Additionally, the study compared on-road trip results (38 km) for PEMS 1, 2, and 3, revealing average FC values of approximately 5.7, 5.4, and 5.5 l/100km, respectively. CO_2 emissions were approximately 135, 138, and 130 g/km, CO emissions were around 400, 150, and 170 mg/km, and NO_X emissions were approximately 26, 30, and 20 mg/km, respectively. The differences between PEMS devices were more pronounced for NO_X and CO emissions.

The study conducted by (Casadei, et al., 2021) compared PEMS to bags in Italian laboratories, utilizing a diesel vehicle as a reference over two consecutive years. The results indicated that, on average, PEMS values for CO were 5-20 mg/km higher than those obtained from bags, with deviations of approximately ±5 g/km for CO_2, ±10 mg/km for NO_X, and $\pm 1x10^{11}$ p/km for PN. The authors concluded that PEMS demonstrate accuracy under controlled laboratory conditions, and the differences between PEMS and the bag readings were well within the tolerances specified by EU regulations. They recommended a reduction in these tolerances.

In the study by (Varella & Giechaskiel, 2018), at the Vehicle Emissions Laboratory (VELA) of the Joint Research Centre (JRC) in Italy, tests were performed after the WLTC and a pre-recorded RDE cycle on the CD. PEMS and laboratory equipment (bags) were compared. CI vehicles were tested using PEMS #2 and PEMS #3 (M.O.V.E. and AVL), while SI vehicles were tested using PEMS #1 (Horiba OBS-ONE) and PEMS #2 (M.O.V.E. AVL). Based on the study's findings, NO_X emissions variances between the instruments were found to be within 5% at mean values of 20 PPM or more, while they rose to 15% at 7 PPM and 30% at 1 PPM. The authors concluded that the measurement of exhaust flow was the main cause of the differences between PEMS and bag measurements.

According to a study by (Pavlovic et al., 2020), the average FC of vehicle travels that took place in the real world was 60% greater than the average FC recorded during an RDE compliant travel using PEMS.

2.5.5. Influence of data analysis methodology on RDE

The EU RDE framework has identified two approaches for analyzing RDE data: the moving average window (MAW) and power binning (PB) methods. Presently, some researchers are adopting the vehicle-specific power (VSP) method. In a study conducted by (Varella & Villafuerte, 2017) in Lisbon, Portugal, the on-road data analyzed using the MAW, PB, and VSP methods were evaluated. The MAW method exhibited an overall difference of approximately 7% for CO_2 and 10% for NO_X compared to the VSP method. In a study conducted in Beijing and Xiamen (Thomas et al., 2017), it was observed that the application of the MAW method had a minimal impact on overall CO_2 emissions but resulted in a decrease of 12% for CO and 21% for NO_X. These differences in results are believed to stem from the use of different analysis methods or the development of a new analysis tool.

RDE offer a more realistic representation of actual emissions compared to laboratory-based DCs. However, there is no assurance that the outcomes will align precisely with those outlined in the RDE report. This discrepancy arises due to variations in drivers' styles, uncertainties in PEMS, and fluctuations in traffic congestion, geographical factors, and environmental conditions across different locations. The implementation of EU RDE faces challenges in developing countries, and it does not encompass congested urban traffic conditions. In essence, further investigation is necessary to improve the reproducibility of RDE tests, minimize PEMS uncertainties, and regulate geographical and environmental factors to ensure the most accurate representation of results.

2.6. Vehicular emissions in AA

Ethiopia contributed approximately 0.3% to global emissions, and as of 2017, it ranked as the 22nd most exposed to climate change and the 31st least-prepared nation for enhancing resilience, emphasizing the pressing need for action (Wang et al., 2019). The transportation sector consumed 6.1% of total energy consumption in 2013 (Ministry of Water and Energy, 2013) with a projected 285% increase in FC from 2015 to 2035 (Stephen et al., 2017). According to (USAID, 2015), Ethiopia committed to capping its 2030 GHG emissions at 145 $MtCO_2e$, translating to a 64% (255 $MtCO_2e$) reduction from predicted levels in 2030, with a specific 10 $MtCO_2$ reduction targeted from the transport sector. PC GHG emissions are anticipated to reach 13.1 $MtCO_2e$ in 2030, assuming a 10% improvement in average fuel efficiency (Berhanu, 2017). In 2018, air pollution in AA affected over 800,000 individuals with respiratory issues, as reported by Ethiopia's Ministry of Health (Bikis & Pandey, 2021). The measured air quality indicated levels exceeding 35 $\mu g/m^3$ PM2.5 and 100 Air quality index (AQI), categorizing it as unhealthy (Bikis & Pandey, 2021). In 2017, an estimated 21% (2,700 deaths) of non-accidental deaths in the city were attributed to poor air quality, projected to increase to 32% (6,200 deaths) by 2025 (Bikis & Pandey, 2021).

Elevated levels of air pollution from various motor vehicles, including cars and vans, have been observed at public transportation stations. Nowadays, the escalation of air pollutants in AA stems from public transportation, industrial activities, wood-burning for cooking, and dust production along major roads, posing a growing threat to human health. Individuals residing and working in close proximity to streets experience higher incidences of health issues linked to air pollution from transportation. AA is grappling with a rapid surge in air pollutants due to the escalating number of cars, coupled with a lack of adherence to air pollution regulations established by relevant authorities. The absence of retirement procedures for older vehicles exacerbates the urban environmental condition, as these aged vehicles emit higher levels of pollutants. The concentration of PM2.5 at stations for public transport in AA surpasses the limits set by the WHO (25 $\mu g/m^3$) (Bikis & Pandey, 2021). The deterioration of air quality in AA is primarily driven by the substantial growth in the transportation sector, swift urbanization, inadequately and slowly constructed road infrastructure, and the utilization of high-sulfur-containing fuels, as highlighted by (Tarekegn & Gulilat, 2018). In general, researchers studying vehicle-related emissions in AA include (Jida et al., 2020; Tefera et al., 2020; Embiale et al., 2019; Bikis & Pandey, 2021; Wondifraw, 2018; Tsegaye et al., 2019; Taka et al., 2020).

2.7. Artificial neural network (ANN)

An ANN is a computational framework that draws inspiration from the organization and operations of biological NNs, such as those found in the human brain (Mohammed et al., 2023). It is made up of layers of networked nodes, or neurons (Predić et al., 2016). Every neuron takes in incoming signals, applies activation functions to process them, and then sends the result to other neurons (Zhou et al., 2023). ANNs are used in many different domains, such as natural language processing, pattern identification, predictions, audio and picture recognition, and many more (Abiodun et al., 2019). An ANN generally comprises an input layer, one or more intermediate layers known as hidden layers, and an output layer (Witaszek, 2020). Neurons within each layer are linked to neurons in the following layer via weighted connections. The arrangement and quantity of layers can vary depending on the complexity of the task and the desired level of performance (Predić et al., 2016). ANN acquires knowledge from data via a procedure known as training (Witaszek, 2020). Popular training methods encompass backpropagation, which fine-tunes connection weights to minimize the distinction between real and forecasted results (Azeez et al., 2019). Additionally, widely utilized techniques such as gradient descent, stochastic gradient descent, and variations like the Adam optimizer are prevalent in the field (Abiodun et al., 2019).

According to recent studies, NN-based models may be able to overcome these issues due to their rapid computation and accurate prediction of emissions (Motallebiaraghi et al., 2021). NNs have been used e.g. to predict air quality, vehicle emissions and air pollution (Howlader et al., 2023). Using ANN, (Seo & Park, 2023) developed an approach for predicting CO_2, NO_X and CO exhaust emissions from diesel cars using data on six operating parameters (vehicle speed, engine RPM, torque, coolant temperature, air flow rate, air-fuel ratio) collected by the OBD interface. Using the integrated deep NN method (Howlader et al., 2023) devised an approach in which instantaneous emissions (CO_2, CO, NO_X, HC) from LDVs can be predicted minute by minute. Multiple regression and an ANN model were used by (Hassine et al., 2021) to model vehicle emissions of HC, CO, and NO_X based on experimental speed profiles and acceleration data. They found that multiple linear regression predicted vehicle emissions with an accuracy of 0.723-0.921, whereas the ANN model predicted emissions with an accuracy of 0.95-0.99 (Hassine et al., 2021). Chen et al., 2023 developed a general approach for predicting engine NO_X emissions that uses a new graph NN model based on dimensional embedding algorithms.

2.8. Summary

The DC plays a crucial role in quantifying vehicle emissions and FC, aiming to accurately represent real vehicle driving patterns for reliable estimates of emissions. Growing concerns revolve around the discrepancy between actual driving conditions and the standardized DCs employed for vehicle certifications by regulatory authorities. This study conducted a comprehensive review of recent pertinent research on DCs used for quantifying vehicle emissions and FC. The analysis focuses on local DCs, examining their route selection, data collection methods, cycle formation approaches, and assessment parameters, comparing them to standard DCs. Additionally, the study addressed the gaps between RDE, laboratory conditions, and real-world data. Through a comparative assessment of local DCs and standard DCs, the findings of the reviewed literature studies indicate that:

- for calculating emission levels and FC, it is recommended to use a DC that exhibits the highest alignment with real driving data from on-road vehicles. Consequently, the development of typical or local DCs reflecting regional driving patterns is recommended for the type approval tests of both new and existing vehicles,
- the majority of the examined local DCs failed to differentiate between distinct stages of urban rods, rural roads and highways,
- in comparison to the WLTC, the local DCs exhibit the potential to yield higher emissions and FC. This is attributed to increased acceleration time and a greater representation of local driving characteristics specific to a particular location,
- a notable challenge associated with many developed local DCs is the limited sample size derived from a few vehicles over a short period,
- previous studies commonly employ MT and Markov chain methods for constructing DCs to assess emission levels and FC.

Subsequent investigations into DCs should acknowledge the significance of meticulous route planning, comprehensive data collection, effective data filtration, and the selection of paramount characteristic parameters. Additionally, careful consideration should be given to the timing of data collection, encompassing peak hours, off-peak hours, and weekends. Regarding the comparison between laboratory-based emissions measurements and real-driving emissions, as well as vehicular emissions in AA, and ANN-based vehicle emissions estimation, the findings of the reviewed literature studies lead to the following conclusions:

- PEMS measurements during RDE surpass those obtained through CD-based measurements,
- RDE outcomes lack reproducibility compared to laboratory-based measurements, revealing deviations both within and outside of defined boundaries,
- in controlled laboratory settings, PEMS indicate higher emissions than CVS with low uncertainty. The primary factors contributing to PEMS uncertainty are the drift of the analyzer over time and variations in exhaust flow rate,
- discrepancies between RDE and real-world emissions arise from factors such as cold temperatures, road gradients, diverse route types, dynamic driving conditions, uncertainties in PEMS, and RDE analysis tools,
- ascending terrain significantly amplifies CO_2, FC, and NO_X due to increased energy demands on inclined roads,
- operating in cold temperatures results in increased CO, PN, and CO_2 emissions compared to warmer conditions, attributable to a richer air-fuel mixture in cold environments and the catalytic converter not reaching optimal operating temperatures. However, while the engine is running cold, NO_X emissions show a declining tendency.
- a more dynamic character than the prescribed RDE boundaries leads to elevated CO_2, NO_X, and PN emissions. Extended motorway driving reduces NO_X and PN emissions, while shorter trips on urban routes yield higher CO and HC emissions than the EU RDE.
- the previous emissions inventory for AA utilized the NEDC for estimating vehicle emissions, and air emission levels in AA exceed global guidelines related to human health and environmental well-being due to the increasing number of vehicles on the road and the absence of vehicle emissions standards in the city.

- ANN-driven models can estimate vehicular emissions by addressing obstacles in developing precise vehicle emissions models, due to their swift computational abilities and accurate emissions forecasts.

2.9. Research gaps

- A significant research gap exists in the field of DC analysis, as no established methodology exists for determining the appropriate duration of a DC. This lack of standardization hinders the comparability and generalizability of findings across studies. Additionally, numerous DCs have been created around the world, but the majority of them have not taken gradients into account.
- A significant research gap exists in the clustering of driving data, particularly concerning the identification of the optimal clustering method for application with PCA.
- Existing emission inventories were developed primarily based on vehicle classification and ignored variations in road types.
- In previous studies, the optimal driving speed at which CO, HC, and CO_2 emissions are simultaneously minimized has not been investigated.
- In previous studies, other than the speed, acceleration, and drive modes related variables, DC characteristics such as slope, number of stops, route type, PKE, and RPA have not been considered for their influence on DC development for vehicle emissions and FC determination.

This study addressed critical research gaps in prior DC development and emission modeling. Firstly, it investigated the most optimal clustering method for driving data, enabling effective classification using PCA, aiming to determine the approximate duration of a DC by considering actual driving conditions in AA's urban roads and the AAE. Secondly, it addressed the limitations of existing emission inventories by incorporating road gradients and developing real time models for determining emissions and FC for each route type. Third, it explored the trade-offs between different emission reduction strategies, aiming to minimize the overall environmental impact. By addressing these research gaps, this study contributed significantly to the development of more accurate and reliable DCs and emission models, ultimately leading to more sustainable transportation solutions.

CHAPTER THREE

MATERIALS AND METHODS

3.1. Introduction

This study focuses on examining real-time emissions and FC levels of light-duty vehicles. The first step was to construct a DC that accurately represents the traffic flow characteristics of AA's road conditions including the AAE. In Uppsala, Sweden, FC and exhaust emissions were measured in the laboratory using the DC developed in this study and WLTC. Additionally, on-road emissions tests were conducted in AA city on predetermined routes using a portable emissions tester. The developed DC in this study was also used for emissions and FC simulations with COPERT and Matlab/Simulink.

Generally, to accomplish the stated objectives, the following procedures were followed:

1) Reviewing the literature comprehensively
2) Drive-cycle data collection
3) Data filtration and removing outliers
4) Data clustering based on PCA
5) Developing a local DC for the study area using ANN and micro-trip methods
6) Conducting vehicle emissions and FC tests on the CD setup
7) Performing an inventory of vehicle emissions and FC
8) Conducting on-road vehicle emissions tests in AA
9) Developing an ANN-based real-time emissions and FC simulation model
10) Comparing the results obtained

The overall study workflow and their relation are shown in Figure 3.1.

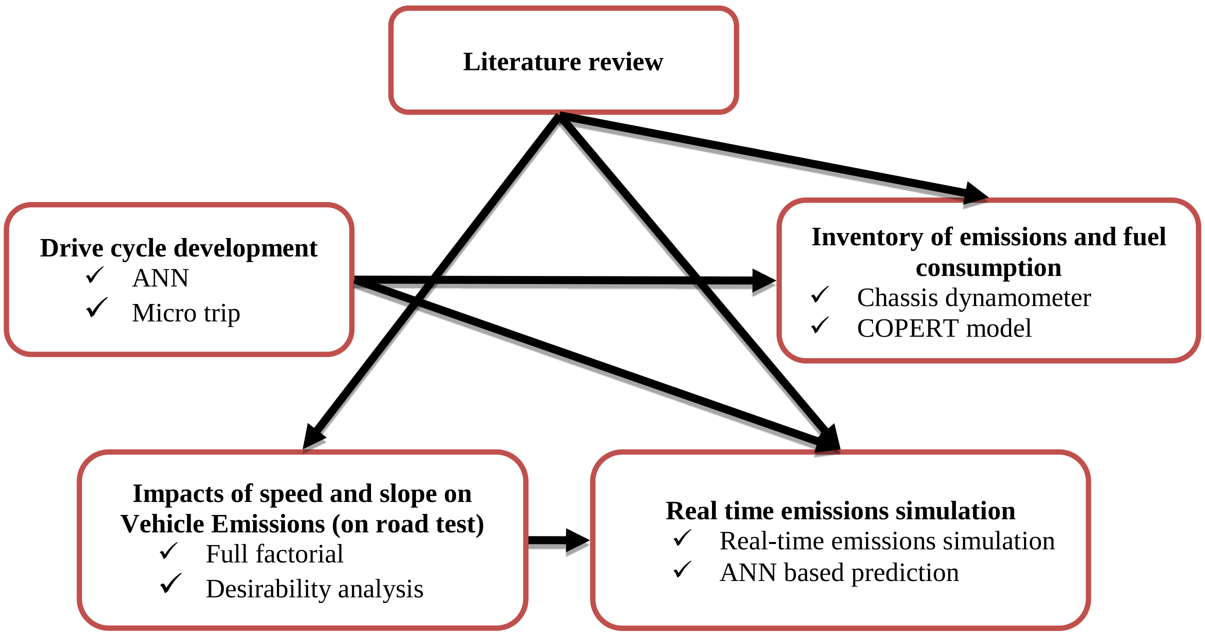

Figure 3.1: Overall study workflow and their relations

3.2. Region of study

The chosen study areas for this study were the AA urban roads and the AAE. AA, with a population of 5,227,794, is experiencing a 4.42% growth rate (World Population Review, 2021). The city has five main entry and exit routes connecting it to neighboring cities such as Akaki, Sendafa, Sululta, Holeta, and Sebeta. In September 2014, AA was connected to the AAE, the first expressway in Ethiopia and East Africa. This expressway has become a crucial part of the regional transportation network, servicing over 20,000 vehicles per day, making it the road with the highest traffic volume in the country. The inclusion of the AAE is particularly important, as the driving characteristics on this expressway differ significantly from the urban roads within AA. Vehicles on the AAE typically maintain high speeds for extended periods, without the frequent stops and starts common in the city's traffic. This unique driving pattern can have a significant impact on the vehicle's emissions and FC profile, which needs to be accurately captured to develop a comprehensive understanding of the environmental impact of transportation in the study area. The main roads connecting AA to various parts of the country, along with real-time traffic data retrieved from Google Maps on September 25, 2021, are illustrated in Figure 3.2. The color scheme in Figure 3.2b indicates the level of traffic congestion: dark red represents highly congested areas, red indicates moderately congested areas, orange indicates low congestion, and green represents free-flowing traffic conditions.

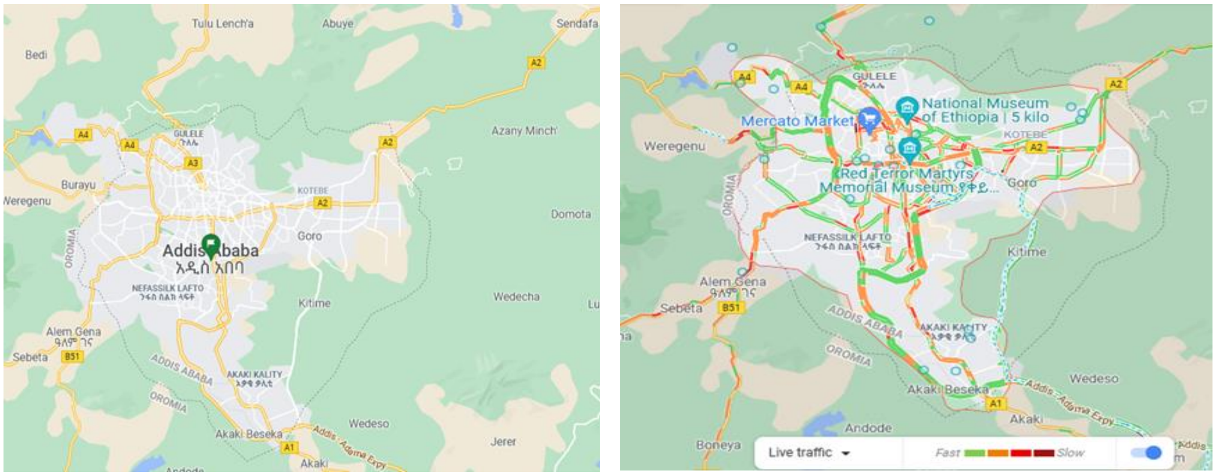

A) Roadways in AA leading to various cities B) Real-time traffic conditions on the main roads of AA

Figure 3.2: Geographical location of the study area map

The city grapples with significant traffic congestion, exacerbating vehicle emissions. According to a study (Baskin, 2018), the annual vehicle growth rate is 9.88%, slightly outpacing the road network expansion rate of 8.22%. The study observed 168 vehicles along a one-kilometer stretch of a single-lane asphalt road. In terms of fuel type, 43.43% of the registered vehicles in the city run on petrol, while 56.57% are diesel-fueled (Baskin, 2018). The city's inadequate transport infrastructure leads to congestion, delays, stress on individuals, and an increased traffic accidents (Bikis & Pandey, 2021). Over half (53.5%) of the vehicles in AA are over 20 years old, with 29.3% surpassing 30 years in age (Fekadu, 2017), indicating that a substantial portion of the vehicle fleet has exceeded its expected service life and is contributing significantly to city pollution. For the majority of citizens, city buses and minibus taxis serve as accessible and economical modes of public transport (Busho & Alemayehu, 2020).

3.3. Materials and Equipment

A description of the equipment used for data collection in this dissertation is provided below.

- OBD II-based GPS
- Test vehicles (gasoline and diesel)
- A CD full set-up with emissions analyzer
- Portable emissions tester

Below is a list of the software that was used in this dissertation for data analysis and simulation. The most recent versions of all the software were in use at the time the study was conducted.

- Matlab R2022b
- IBM SPSS statistics 23
- COPERT 5.6.1
- Minitab 21
- OriginPro 2022

To serve as a model for the development of the DC system, continuous data gathering was carried out using OBD II tracker GPS devices installed on registered vehicles traveling in AA. This research utilized the Acumen and Car-X tracking devices(Figure 3.3), recognized as a global positioning data acquisition system. The GPS device connects to the OBD II and is powered by the vehicle's battery. The data collected, including vehicle speed, latitude, longitude, and time, commenced from the moment the ignition was turned on and continued until it was turned off, adhering to the minimum collection interval specified by the device manufacturer. The specifications of GPS devices employed for this study are shown in Table 3.1.

Acumen Car-X

Figure 3.3: OBD II tracker GPS

Table 3.1: Specifications of the GPS devices employed in this study

Parameters	Acumen	Car-X
Type	OBD II type	OBD II type
Power supply (V)	12V	12V/50mA
Weight of the main unit (g)	300	50
Working temperature (°C)	-20-85 °C	-20-70 °C
Humidity	0-95 %	0-90 %
GSM frequencies (MHz)	1575	900/1800
Position accuracy (m)	≤ 10	< 10
Speed accuracy (m/s)	≤ 0.15	< 0.1
SIM type	2G/3G/4G Micro-Sim	2G/3G/4G Nano sim

Table 3.2 outlines the technical details of the vehicles utilized for the data collection in this investigation. This study looked at vehicle technology and maintenance conditions of the vehicles to minimize their impact on the study results. The emissions and FC of the chosen two vehicles were examined using CDs, considering different engine sizes, fuels, and technological enhancements, as indicated in Table 3.3. The vehicles were selected based on what was commonly available in AA.

Table 3.2: Specifications of vehicles used for data collection and drivers responses

Parameters	Vehicle A	Vehicle B	Vehicle C	Vehicle D	Vehicle E
Driver age	38	43	43	45	39
Vehicle type	PV	Pickup	Van	Mini-bus	Mid-bus
Vehicle Model	Corolla	Tacoma	Starex	5L	Isuzu
Year	2008	2005	2016	2006	2013
Mileage traveled (km)	271,078	413,235	145,698	111,566	351,404
Average daily travel (km)	18	20	40	120	150
Fuel type	Gasoline	Diesel	Diesel	Diesel	Diesel
Engine capacity (lit)	1.5	2.5	2.5	2.8	3.0
Emissions control device	O_2 sensor	EGR	EGR	NA	NA
Maintenance frequency	Regular	Occasional	Regular	Occasional	Regular

Table 3.3: Specifications of tested vehicles on a chassis dynamometer

S/N	Vehicle category	Vehicle Model	Maximum engine power	Accumulated mileage (km)	Technology
1	Passenger car (Euro 4 gasoline)	Toyota Corolla (2010)	96 kW	468,927	Port fuel injection system
2	Passenger car (Euro 6 diesel)	Hyundai (2015)	101 kW	159,370	Particulate filter and SCR

This study utilized COPERT 5.6.1 to assess the emissions and FC of gasoline, diesel, and hybrid vehicles to demonstrate to policymakers how hybrid vehicles contributed to the reduced emissions and FC.

Table 3.4: Specifications of selected vehicles and collected activity data

Selected vehicles	Gasoline vehicle	Diesel vehicle	Petrol-hybrid vehicle
Euro category	Euro 4	Euro 6	Euro 6
Vehicle Model	Toyota Corolla	Hyundai StarX	
Maximum engine power (kW)	96	101	
Accumulated mileage (km)	671,086	211,568	0
Mean activity (km/year)	28,800	43,200	28,800
Technology	Port fuel injection system	Common rail diesel	Gasoline direct injection

Table 3.5 provides details on the portable emissions analyzer, which was used to measure the real-time concentrations of CO, CO_2, and HC on the AA road. Table 3.6 provides details about both vehicles that were used for on-road emissions testing. The vehicles were fuelled with fuel that is sold commercially from nearby stations.

Table 3.5: A portable emissions tester used in this study

Measured parameters	Instrument	Measurement type	Accuracy
CO_2	GA5000 portable gas analyzer	By dual wavelength infrared sensor with reference channel	±0.5% (vol)
CO		Internal electrochemical sensor	±2% (vol)
HC		Internal electrochemical sensor	±2% (vol)

Table 3.6: Technical details of the vehicles employed for on-road emissions testing

Parameters	Gasoline vehicle	Diesel vehicle
Vehicle manufacturer	Sokon Group	Toyota
Vehicle Model	DFSK Glory	Land cruiser
Model year	2016	2019
Engine capacity	1300 CC	4164 CC
Maximum power	112kW	96 kW @3800 rpm
Gross weight	2035 kg	2720 kg
Transmission	Manual	Manual
Mileage	71446 km	90277 km
Fuel control strategy	Electronic fuel injection	Conventional type
Emission control	NA	NA

3.4. Drive cycle development methods

The methodological aspects of DC development for this study are covered in this section. After clustering trips based on PCA, an NN-based prediction method was employed to generate the developed DCs using the trip-based approach. To further illustrate the significance of the methods offered in this study, a DC using the MT method from the same data used for the NN prediction method was created. Figure 3.4 illustrates the steps taken in this study to develop a representative local DC for the study areas. Lastly, it was determined whether or not the acquired DCs could accurately depict the driving patterns in AA and AAE using characteristic parameters shown in Table 3.7.

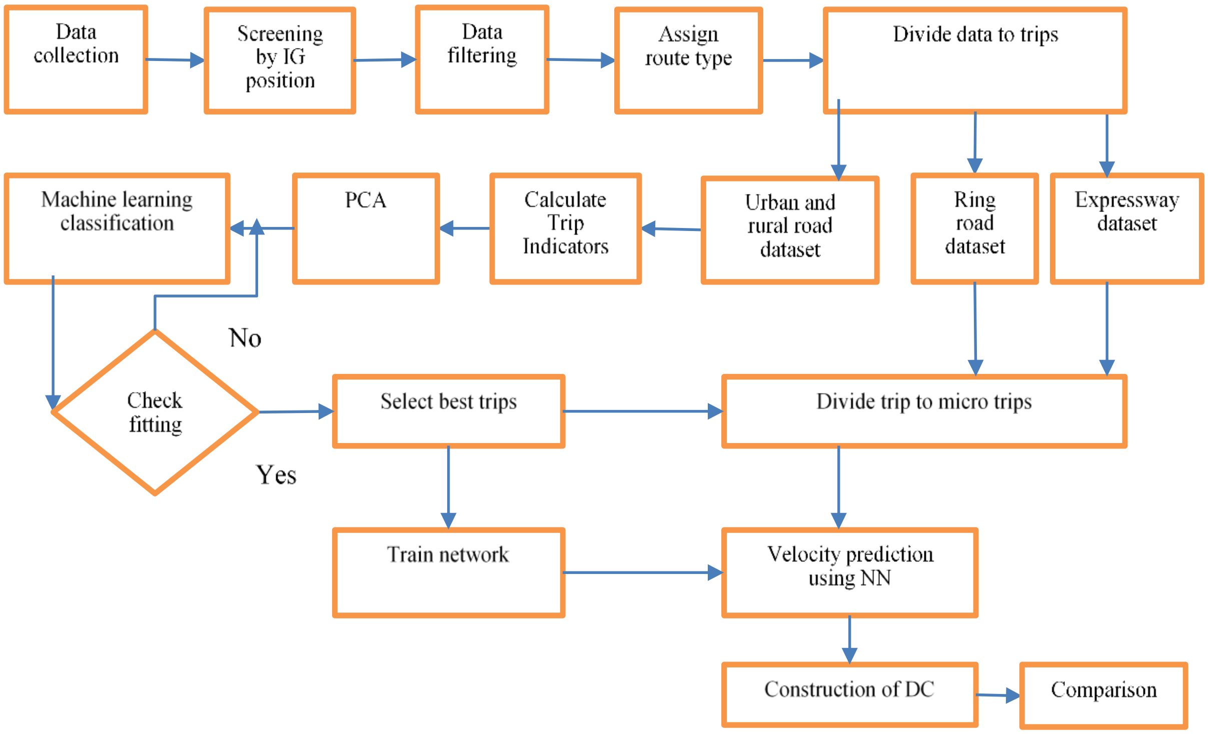

Figure 3.4: Framework for developing a representative local DC for the study areas

3.4.1. Data collection and setup

To establish a model for the development of DC, primary driving data was gathered in AA's urban roads (Figure B1) and AAE (Figure B2). Over a period from October 1, 2021, to the end of December of the same year, cleaned data covering a distance of 7,442.203 km was collected. The data collection involved the use of OBD II-based GPS devices installed on Toyota Corollas, Tacomas, and Hyundai vehicles, as shown in Figure 3.5. Additionally, traditional GPS devices were installed on mini-buses and Isuzu mid-buses that were registered and operational within AA. The total data collected for modeling consisted of 1,893,256 seconds of speed-time points. The real-time driving data recorded by the installed GPS devices included timestamps, latitude and longitude coordinates, vehicle speed, the number of satellites used for data collection, location names at each timestamp, and the ignition switch position. The data collection periods encompassed both working days and weekends, allowing drivers to travel in their usual day-to-day patterns. The minimum and maximum elevations recorded during the driving data collection for this study are 1810 m and 2600 m, respectively.

Figure 3.5: OBD II port for GPS installation

The data collection devices utilized in this research gathered geographical locations with their local names based on Google Maps naming, and the accuracy of location names was verified through Google Maps. By utilizing identified location names and drawing upon experience, data from the AAE and ring roads within AA city were effectively distinguished. Although nearly every trip included segments on urban, extra-urban, and rural roads, data points for ring roads and expressways were available only for some trips. Consequently, data points related to ring roads and expressways were excluded from the trip analysis. Following the removal of outliers, noise reduction in data points, and the exclusion of driving data outside AA and AAE, the analysis covered 4,895.43 km on urban roads, 1,505.14 km on rural roads, 475.28 km on ring roads, and 566.35 km on the expressway. Figure 3.6 illustrates the percentage of distance traveled on each road type.

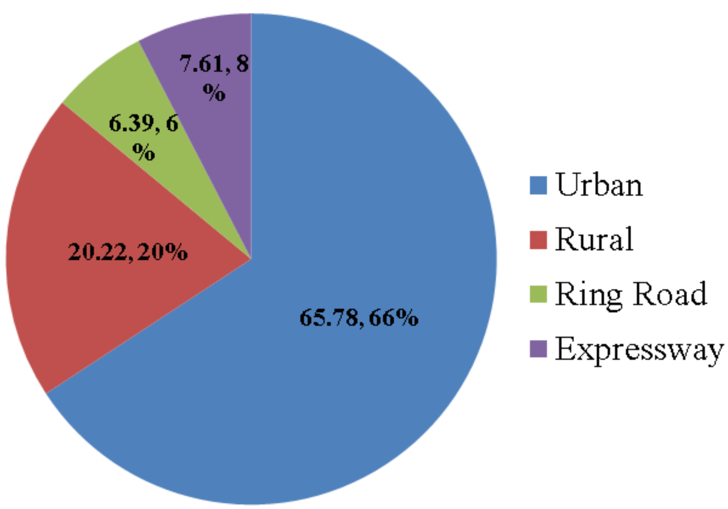

Figure 3.6: Proportion of distance covered on each category of route

3.4.2. Data filtration

Accounting for potential GPS errors induced by vibration, data points exhibiting acceleration beyond 4.5 m/s² and below -4.5 m/s² were excluded during the initial stages of data processing, adhering to the WLTC standard. The distribution of speed, acceleration, and road slope in the original data is depicted in Figure 3.7.

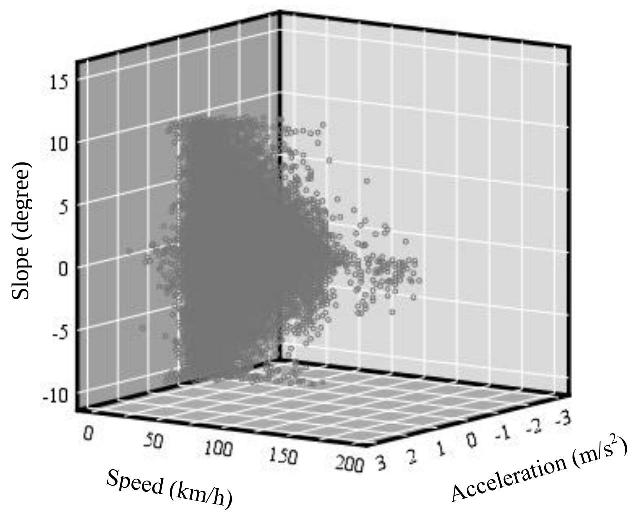

Figure 3.7: Speed, acceleration, and slope distribution

Before refining the speed, road grade, and distance data collected, timestamps were converted to serial time using MATLAB. Outliers were detected through shape-preserving cubic interpolation (PCHIP) employing the moving mean window-centered method. Following the replacement of outliers, the next step involved eliminating noise from the raw data through the application of the Bayes wavelet signal denoise method.

Subsequently, any speed value below 3.6 km/h was adjusted to 0 km/h to address errors originating from the data collection device. Additionally, speeds exceeding 120 km/h were adjusted to 120 km/h, aligning with the maximum speed limit permissible in AAE. Data points indicating road grades exceeding 10 degrees (974 instances) were adjusted to 10 degrees, and those below -10 degrees (1078 instances) were modified to -10 degrees. To finalize the data denoising process, acceleration values were computed for each point in the filtered speed data, and these were scrutinized for adherence to maximum and minimum limits, which were determined as 2.486 m/s² and -2.45 m/s², respectively. Instances of excessive idle time were adjusted to a duration of three minutes, as outlined by (Zhao et al., 2021).

3.4.3. Neural Network based DC development method

3.4.3.1. Approach for constructing the trip-based model

In this context, a trip is defined as a driving journey from the starting point to the destination, encompassing a short stop duration. This could involve commuting from home to the workplace with a preceding short period of parking. Real-world driving trips can feature varying durations of both long and short stops, involving multiple starts and stops between the origin and the final destination for various reasons, such as users planning multiple activities within a single trip or encountering traffic accidents, etc. The gathered driving data were segmented into numerous trips based on parking (stop) durations longer than 30 minutes, although the parking duration itself was not utilized in the subsequent analysis. Figure 3.8 illustrates the speed and time plot for a sample trip from the collected data.

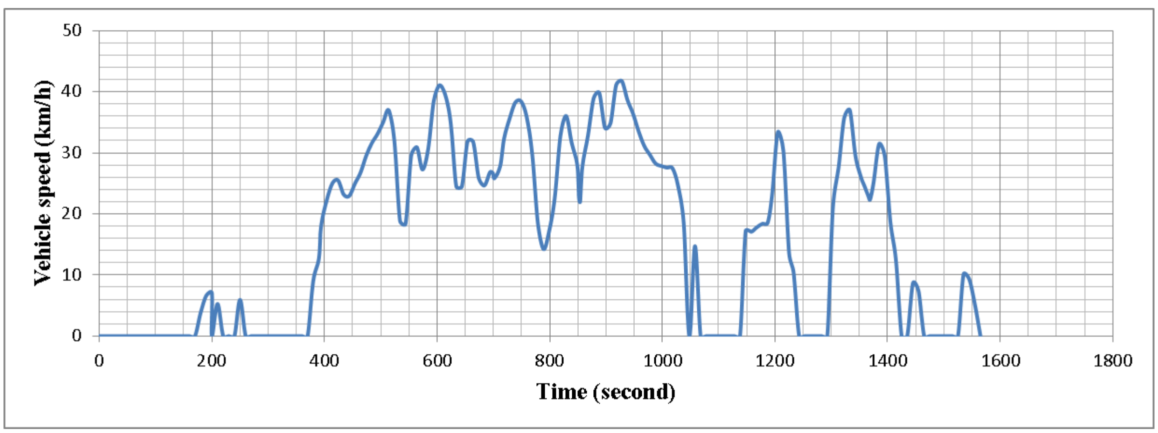

Figure 3.8: Speed vs time of sample trip

A stop duration exceeding 30 minutes was identified as the threshold to delineate the end of a trip. This implies that if the stop duration is less than 30 minutes, the vehicle has not yet reached its ultimate destination, and such stops might occur due to factors like traffic congestion, road accidents, or shopping, after which the trip would resume. Utilizing this criterion, the filtered data were organized into distinct trips, each receiving a unique trip code for identification.

A MATLAB was employed to segment the experimental data into trips, resulting in a total of 726 trips (comprising data from 273, 126, 134, 86, and 107 trips for Toyota Corollas, Tacomas, 5L mini-buses, Hyundai, and Isuzu mid-buses, respectively). In line with established practices for DC development, 17 trip indicators or assessment parameters were chosen for this study. In contrast to average speed, which encompasses idling phases, average driving speed represents the mean of the vehicle's running speed, excluding idle periods. Both a vehicle's speed and acceleration have a direct correlation with the amount of power required by the engine to propel it forward. Describing the load on the engine adequately necessitates a combination of these variables. Consequently, two trip indicators, namely RPA and PKE, were incorporated. RPA involves the integral of the instantaneous speed and positive acceleration product across a specific trip section, while PKE is the summation of differences between the squares of the final and initial speeds during successive acceleration, divided by the distance traveled. These indicators are presented in Table 3.7.

Table 3.7: Trip indicators

S/N	Trip indicators	Abbreviation	Unit
1	Driving time	T_{total}	s
2	Distance travelled	S_{sum}	m
3	Average driving speed	V_{davg}	km/h
4	Average speed	V_{avg_all}	km/h
5	Maximum speed	V_{max}	km/h
6	The standard deviation of speed	V_{sd}	
7	Average acceleration	a_{avg}	m/s^2
8	Maximum deceleration	dec_{max}	m/s^2
9	Maximum acceleration	a_{max}	m/s^2
10	The standard deviation of acceleration	a_{sd}	m/s^2
11	Stop per kilometre	N_{spkm}	/km
12	Relative positive acceleration	RPA	m/s^2
13	Positive kinetic energy	PKE	m/s^2
14	Percentage of idle mode	P_{idl}	%
15	Percentage of acceleration mode	P_{acc}	%
16	Percentage of cruising mode	P_{cru}	%
17	Percentage of deceleration mode	P_{dec}	%

Seventeen trip indicators or evaluative metrics were subsequently calculated for the data obtained from each of the 726 trips. While vehicle speed, time, and distance traveled were directly recorded, the acceleration value for each time point was determined in accordance with the WLTP standard. Subsequently, based on the acceleration value, the following driving modes were identified: idle (velocity is zero), acceleration (greater than 0.1 m/s^2), deceleration (less than -0.1 m/s^2), and cruising state (between -0.1 and 0.1 m/s^2) (Tong & Ng, 2020). For any given time point, the acceleration value can be determined using the following equation (3.1):

$$a_i = \frac{V_{i+1} - V_i}{t_{i+1} - t_i}, \; i = 1, 2, 3 \; ..... \; n, \qquad 3.1$$

Where a_i is the acceleration from the i^{th} second to the $(i+1)^{th}$ in m/s^2, V_i is the speed at the i^{th} second in m/s, and t_i is the time point of the i^{th} second.

Speed-related indicators such as V_{max}, V_{dmean}, V_{mean}, and V_{std} can be calculated by using the equations 3.2 to 3.4.

$$V_{max} = max\{V_1, V_2, \ldots, V_i\}, \qquad 3.2$$

$$V_{mean} = mean\{V_1, V_2, \ldots, V_k\} = S/T, \qquad 3.3$$

$$V_{std} = std\{V_1, V_2, \ldots, V_k\} \qquad 3.4$$

Acceleration-related indicators such as a_{max}, d_{max}, a_{mean}, and a_{std} can be calculated by using the equations 3.5 to 3.7.

$$a_{max} = max\{a_1, a_2, \ldots, a_{k-1}\}, \qquad 3.5$$

$$dec_{max} = min\{a_1, a_2, \ldots, a_{k-1}\}, \qquad 3.6$$

$$a_{std} = std\{a_1, a_2, \ldots, a_{k-1}\}, \qquad 3.7$$

Indicators including P_{acc}, P_{dec}, P_{idl}, P_{cru}, and can be calculated by equations 3.8 to 3.11:

$$P_{acc} = \frac{T_{acc}}{T_{total}}, \qquad 3.8$$

$$P_{dec} = \frac{T_{dec}}{T_{total}}, \qquad 3.9$$

$$P_{idl} = \frac{T_{idle}}{T_{total}}, \qquad 3.10$$

$$P_{cru} = \frac{T_{cr}}{T_{total}}, \qquad 3.11$$

Following the cleanup of the dataset, computations were performed for 17 trip indicators or evaluative metrics for each of the 726 trip records, and a sample is presented in Table 3.8. In the process of selecting the most valuable data points, frequency, and cumulative frequency were established for all 726 trips to exclude very short trips from further analysis. Trips lasting less than 540 seconds or covering a distance of less than 500 meters were eliminated. Data from 199 short trips were excluded from subsequent analysis due to their limited information, which could potentially lead to inaccurate interpretations. As previously mentioned, the collected datasets should encompass diverse characteristics for various route types, considering different times of day, days of the week, and districts served. Therefore, a cluster analysis technique was applied to categorize the 527 remaining trips based on the 17 trip indicators. The large number of variables in the data could compromise computational efficiency and diminish the clustering effect (Zhao et al., 2021). Consequently, since 17 trip indicators were deemed too numerous, their dimensions were reduced using PCA.

Table 3.8: Trip indicators result of sample trips

Trip code	1	3	4	5	…	FT272	FT273
S_{sum}	7519.82	14192.06	12389.96	11269.07	…	8244.18	10875.87
T_{total}	1595	2999	3040	2346	…	2160	3409
V_{davg}	7.094	7.392	6.661	7.463	…	5.507	4.751
V_{max}	11.605	16.084	12.584	15.846	…	11.479	13.725
V_{sd}	2.635	3.366	2.570	2.843	…	2.708	3.646
V_{avg_all}	4.715	4.732	4.076	4.804	…	3.817	3.190
a_{avg}	-0.002	0.000	0.005	0.001	…	-0.010	0.004
dec_{max}	-0.498	-1.421	-0.762	-0.565	…	-0.754	-0.511
a_{max}	0.401	1.310	0.614	0.848	…	0.612	0.819
a_{sd}	0.148	0.233	0.170	0.171	…	0.208	0.116
N_{spkm}	1	1	3	2	…	3	2
RPA	0.005	0.006	0.005	0.005	…	0.004	0.003
PKE	0.102	0.120	0.116	0.108	…	0.130	0.070
P_{idl}	0.601	0.611	0.620	0.608	…	0.329	0.378
P_{acc}	0.072	0.092	0.065	0.080	…	0.083	0.023
P_{cru}	0.256	0.214	0.245	0.228	…	0.435	0.531
P_{dec}	0.072	0.084	0.069	0.083	…	0.079	0.026

3.4.3.2. Principal component analysis (PCA)

PCA is a technique that transforms a set of intricate variables into a few principal components (Guo et al., 2020; Zhou et al., 2017). The essence of PCA lies in amalgamating original parameters into a novel set of uncorrelated comprehensive parameters for analysis, rather than relying on the original parameters themselves (Liu et al., 2014; Peng et al., 2015). As outlined in (Zhao et al., 2021), PCA simplifies data, providing results with more effective information. When applying PCA for decomposition, common factors ($F = F_1, F_2, \ldots F_n$) and the original variables are modeled as linear combinations of these common factors. Typically, a transformation method such as Varimax rotation is employed to enhance the interpretability of results by rotating factors in multidimensional space, aiming to achieve the most simplified structure (George, 2016). In this study, Eigen decomposition and Varimax rotation were employed along with the Kaiser Normalization methods. Following the reduction of dimensions, trips were categorized using the clustering method.

3.4.3.3. Trip clustering

The formation of groups aims to maximize statistical differences between groups and ensure statistical homogeneity within each group (Tong & Ng, 2020). Different clustering methods may yield distinct solutions; hence, to determine the most suitable clustering method, a classification learner was implemented using MATLAB. For this, supervised machine learning methods are used to train models for data classification. The algorithms use all available classification learning approaches to the input dataset and use the observations to calculate accuracy ratings. Based on these observations, forecasts are also produced, which results in the ROC curve and confusion matrix calculations. A model's performance or validation accuracy score is compared with the trained data after it has been trained in the classification learner, aiding in the choice of a suitable clustering technique. Choosing the approach with the highest validation accuracy, the trip clustering method was selected based on the classification learner's findings. NN clustering performed better than the other approaches in this investigation.

By training a NN on patterns, NN clustering uses a self-organizing map to help the network identify and categorize objects according to their relative topology and similarity. A self-organizing map is made up of a competitive layer that may divide a dataset of vectors with any number of dimensions into as many classes as the neurons in the layer, as shown in Figure 3.9. Due to the 2D topology of these neurons, the layer may approximate the topology of the dataset in 2Ds and reflect its distribution. The self-organizing map batch technique was utilized to train the network (trainbu, learnsomb). Following the application of the clustering technique, which effectively categorized the trips into distinct groups, the selection of the best trip followed.

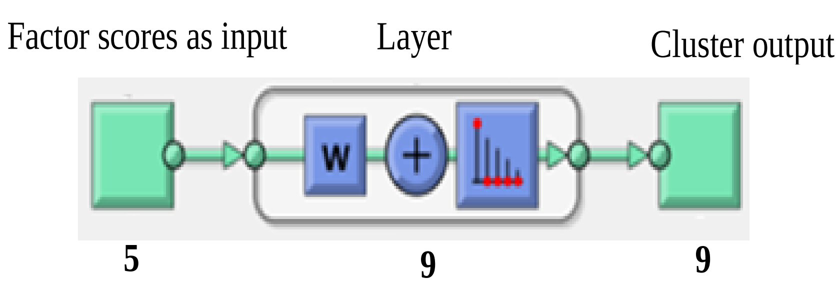

Figure 3.9: Neural network clustering diagram

3.4.3.4. Selection of the best trip

With the input information available, suitable trips were chosen based on a computed similarity score for each cluster. This similarity score was derived from the summation of relative errors between the indicators of the candidate trips and the target DC. Considering the values of the target cycle indicators, the relative error for each indicator of the candidate trip was calculated for each group, following equation 3.12.

$$\varepsilon_{\beta k} = \left|\frac{(M_{\beta k} - \overline{M_k})}{\overline{M_k}}\right| \times 100 \qquad 3.12$$

Where

$\varepsilon\beta k$ = the relative error for the kth parameter of the candidate trips β, β is the number of candidate trips, and k = 1, 2,…, N, N is the total number of trip indicators

$M\beta k$ = the magnitude of the kth trip indicator of the candidate trip β and

$\bar{M}k$ = the magnitude of the kth trip indicator of a target trip.

Subsequently, the similarity score for a candidate trip could be computed using equation 3.13.

$$S_\beta = 100 - \frac{\sum_{k=1}^{N} \epsilon_{\beta k}}{N} \qquad 3.13$$

Where $S\beta$ is the similarity score for candidate trip β.

The similarity score was determined using 100 minus the average relative errors derived from the parameters of candidate trip β. The resulting score ranges from zero to 100%, where 100% signifies no errors and a complete alignment with the target cycle. The candidate trip possessing the highest score is considered the optimal choice, representing the closest match to the provided input information. It is important to emphasize that all trip indicators were accorded equal treatment in the calculation. The best trip was chosen based on the closest alignment with the trip-level indicators.

The optimal trips from each cluster were segmented into MTs. A MT is defined as a driving sequence between two idling events. The division of the driving sequence into MTs for the selected best trips adhered to WLTC standards, encompassing ring road and expressway data points. Each MT was then assigned a code name. Ultimately, based on relative error considerations, the two most representative MTs were chosen for each cluster. Furthermore, to incorporate ring road and expressway data points in the final DC, one micro trip from each was selected. The chosen MTs were organized in a sequential time series, encompassing urban, extra-urban, rural, ring road, and expressway segments.

3.4.3.5. NN-based vehicle speed prediction

Prediction involves dynamic filtering, utilizing historical values from one or more time series to forecast future values. Nonlinear filtering and prediction make use of dynamic NNs, incorporating delay-line taps. In a research effort focused on developing a DC for light-duty vehicles in Beijing, a RNN approach was employed (Qiu et al., 2018). A study by (Chen et al., 2020) employed a convolutional NN for DC prediction, while (Wang et al., 2015; Xu, 2013) utilized a NN algorithm to establish a DC recognizer. The target time steps are divided into training, validation, and testing sets by the NN model, which allots 70%, 15%, and 15% of the time steps at random to each set. In this study, the nonlinear autoregressive with external input (NARX) model was applied to predict the output y(t). This model forecasts y(t) based on d past values of y(t) and another series x(t), as depicted in equation 3.14 and Figure 3.10.

$$y(t) = f(x(t-1), \ldots x(t-d), y(t-1), \ldots, y(t-d)) \tag{3.14}$$

Where y(t) is the predicted vehicle speed at time 't' (output speed), d is past speed value of y(t), x(t) is speed series of MTs of respective route (input speed) and target speed is the speed of best selected MT.

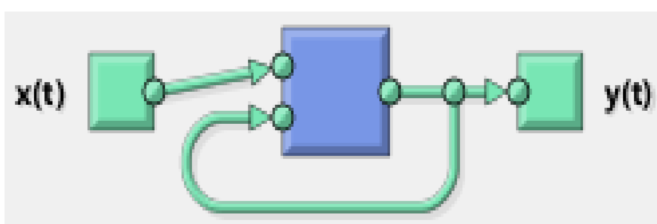

Figure 3.10: NARX diagram

All data from MTs data transformed into time series and employed as the training data (input data) specific to their respective routes. The chosen MTs from each route were then utilized as test data (target) during the implementation of the NN. A visual representation of the employed NN model is illustrated in Figure 3.11.

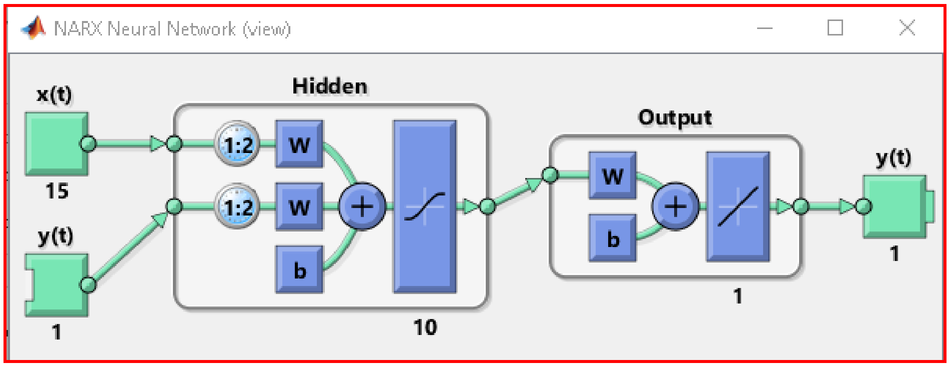

Figure 3.11: Neural network diagram

The network underwent training using Bayesian regularization coupled with a back-propagation training algorithm. Despite its longer duration, this technique is capable of offering robust generalization, particularly for intricate, small, or noisy datasets. The cessation of training was determined by adaptive weight minimization (regularization). In this study, when the error estimation is significant, it was addressed by retraining the model and/or by adding hidden neurons. These steps were repeated multiple times until an acceptable result was achieved. The NN predicted speed values for each road category, which were then aggregated to create a representative local DC. Finally, a comparison was made between the DCs developed using the NN method, the micro-trip (MT) method, collected data, and standard DCs.

3.4.4. Micro trip method of DC construction

The most effective approach for constructing DC is the MT method, as highlighted by (Huertas et al., 2019). To validate the methodology proposed in this study, we employed the MT approach to create a DC using the same dataset utilized for the NN prediction method. After denoising and segmenting the speed-time data into MTs, driving characteristic parameters were computed. Utilizing MATLAB, we derived 9451 MTs from the data, excluding very lengthy ones exceeding 1000 seconds and extremely short ones with driving points less than 30 seconds. Employing the K-means clustering algorithm, the remaining 6680 MTs were classified into six clusters. The MTs closest to each cluster's center were selected as the representative MTs to form a DC for that cluster. The MT selection process persisted until a sufficient number of MTs were chosen from each cluster, ensuring proportional representation based on the duration of each traffic condition in the collected data. In alignment with the WLTC and the current DC durations, we opted for a DC duration ranging between 1500 seconds (Mahayadin et al., 2018) and 1800 s (Liu et al., 2021).

The assessment of the driving pattern's representativeness within the potential DC is conducted by evaluating its alignment with a set of characteristic parameters (CPs), referred to as target parameters. The driving patterns extracted from the collected driving data and those belonging to the clustered group are delineated through these target parameters. Subsequently, the candidate DC is characterized by its own set of characteristic parameters (CP*). The determination of a DC representing a specific driving pattern is established on the premise that the characteristic parameters of the candidate DC closely resemble the target parameters. Therefore, the level of representativeness for a candidate DC is determined by the relative difference between paired CPs, as outlined in equation 3.15 (Huertas et al., 2019).

$$RD_i = \frac{|CP_i - CP_i^*|}{CP_i} \qquad 3.15$$

Throughout the cycle development, a maximum permissible disparity among the paired CPs is set at 15% (Arun et al., 2017). The iteration of obtaining candidate DCs is reiterated multiple times until the established threshold of acceptability is achieved. The candidate DCs that meet this threshold are deemed representative. Employing this method results in the generation of various candidate DCs, and the optimal one, exhibiting the least difference among paired CPs, is selected for comparison with processed experimental data and the DC developed through the NN prediction method.

3.5. Methods for determination of emissions and FC

Emission inventories play a crucial role in air quality studies by supplying data for air quality models, often applied in estimating emissions across annual timeframes. The outlined approach involves the generation of emission inventories utilizing the Computer Program to Calculate Emissions from Road Transportation (COPERT). This method is employed to compute air emissions from PVs based on routes, and the results are verified through an experimental CD setup. Notably, this type of investigation has not been previously undertaken in the studied area. To carry out this study, vehicle exhaust emissions and FC were measured and determined using the framework showed in Figure 3.12.

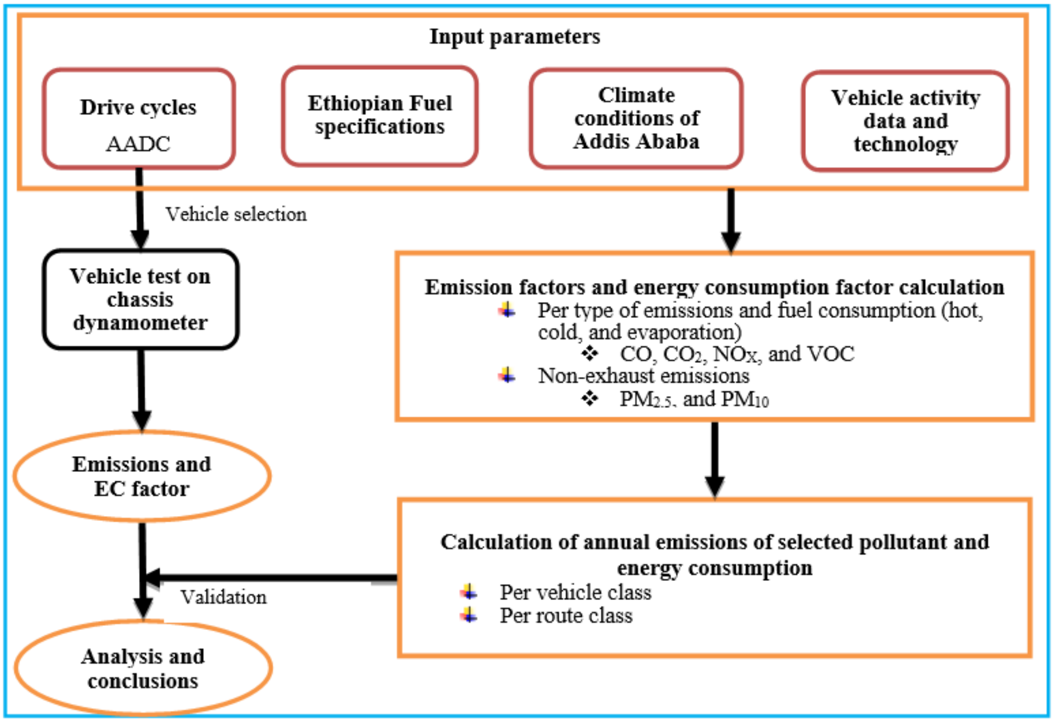

Figure 3.12: Framework for measuring and determining emissions and FC

Fuel standards for gasoline and diesel obtained from the Ethiopian Petroleum Enterprise for AA, Ethiopia, for 2022 are depicted in Table 3.9.

Table 3.9: Available fuel specifications

Parameters	Petrol	Diesel
Energy Content [MJ/kg]	43.774	42.695
Density [kg/m^3]	720-740	820-860.
S Content [% wt]	Max 0.05	Max 0.05
Pb Content [g/l]	Max 0.013	Not specified
Cd Content [ppm wt]	0.0002	0.00005
Cu Content [ppm wt]	0.0045	0.0057
Cr Content [ppm wt]	0.0063	0.0085
Ni Content [ppm wt]	0.0023	0.0002
Se Content [ppm wt]	0.0002	0.0001
Zn Content [ppm wt]	0.033	0.018
Ash Content [% wt]	Not specified	Max 0.01
RON/ Cetane index	Min 92	Min 48

3.5.1. Experimental setup

During a CD test, exhaust samples were collected from the test vehicle while it was driven on the dynamometer platform, both under the WLTC and the developed DC for this study area. The experimental setup of the CD system depicted in Figure 3.13 and Figure A1 in Appendix A was conducted under controlled conditions in a laboratory in Uppsala, Sweden. On the CD, both a gasoline and diesel car was tested using the entire set of chosen driving cycles. A driver assistance system with tolerance levels was used to assist the driver in adhering to selected cycles. The measurement system includes an emissions analyzer that can analyze the concentrations of CO_2, CO, and NOx from the vehicles. Then, based on the distance of cycles, the FC and pollutant concentrations were changed to emission factors (g/km).

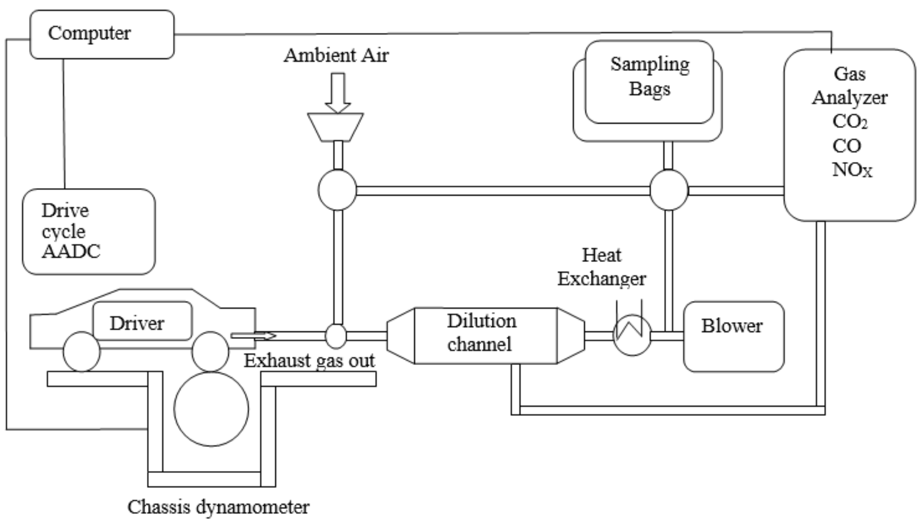

Figure 3.13: Set-up of CD for emission and FC measurements

3.5.2. COPERT based emissions and FC inventory

In this investigation, the COPERT methodology was employed for the computation of emissions originating from PVs. The emissions considered encompassed those arising from operational phases, including hot operation, cold start, and evaporation. Information on annual mileage was provided by the driver or vehicle owner and subsequently input into COPERT, taking into account the relevant AA climate data and the distance covered by vehicles in each category. COPERT generated quantified results for the five most significant pollutant emissions such as CO_2, CO, NO_X, PM, and VOC associated with road transport during the specified period, categorized by route. These top five emissions pose environmental and public health risks. To examine the impact of congested urban, urban, rural, and highway driving patterns on emissions and FC were employed in this study.

With the use of Equations 3.16 to 3.19, the emissions inventory for a variety of vehicle types was determined in tonnes annually per vehicle (Ntziachristos et al., 2009). Cold start emissions (E_{cold}) were determined following the equations 3.16 and 3.17

$$E_{cold} = \beta \times bc \times N \times M \times e_{hot} \times \left(\frac{e_{cold}}{e_{hot}} - 1\right) \tag{3.16}$$

$$\frac{e_{cold}}{e_{hot}} = A \times V + B \times T + C \tag{3.17}$$

Where, β represents the proportion of mileage covered under cold engine conditions, bc is the beta reduction factor, N denotes the number of vehicles in stock, M is the mileage per vehicle, e_{hot} stands for the hot emission factor, e_{cold}/e_{hot} indicates the over-emission level relative to hot emissions, V corresponds to vehicle speed in kilometers per hour, T represents the temperature in degrees Celsius, A represents the coefficient that modifies the ratio based on the vehicle's speed (V), while B adjusts the ratio based on the ambient temperature (T), and C represents the constant term that accounts for baseline effects not captured by the speed or temperature.

The calculation of hot emissions (E_{hot}) was carried out using Equation 3.18 and expressed as the total vehicle kilometers driven during the considered time for a given activity level (NM).

$$E_{hot} = NM \times e_{hot} \tag{3.18}$$

Equation 3.19 indicates that COPERT considers evaporation encompassing diurnal fuel losses ($E_{diurnal}$), after-use (E_{soak}), and running losses ($E_{running}$).

$$E_{evap} = E_{diurnal} + E_{soak} + R_{running} \tag{3.19}$$

3.6. Method for testing on-road emissions

The investigation utilized GPS, portable emissions testers, and petrol and diesel-powered vehicles to collect data. The study employed an experimental approach involving the selection of vehicles, route determination, emission measurements, and the application of full factorial and desirability analysis for data analysis. A portable emissions tester, installed on the selected vehicles, was employed to measure tailpipe emissions released into the atmosphere while the vehicles were traveling on-road. MINITAB 21 was used to analyze and interpret the collected on-road emissions data, while OriginPro 2022 was used to plot the results.

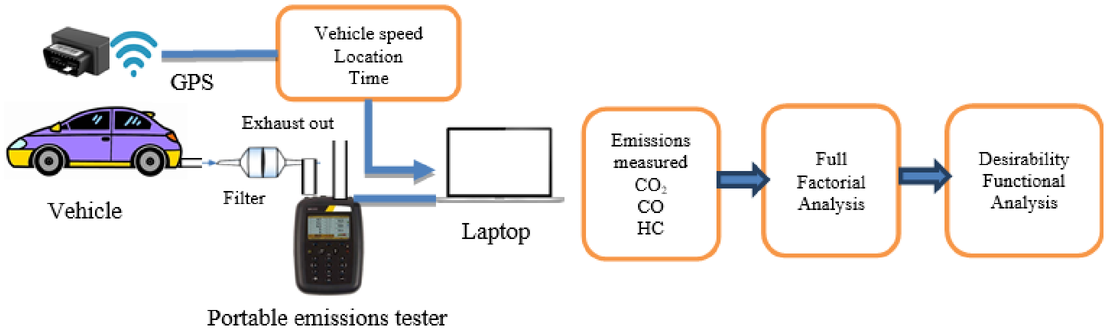

Figure 3.14: Followed methods for on-road emissions test

3.6.1. Route selection

On-road data collection took place in AA, Ethiopia, utilizing different road slope sections as outlined in the experimental design. Figure 3.15 (a – d) depicts four routes chosen as study sites in AA, Ethiopia.

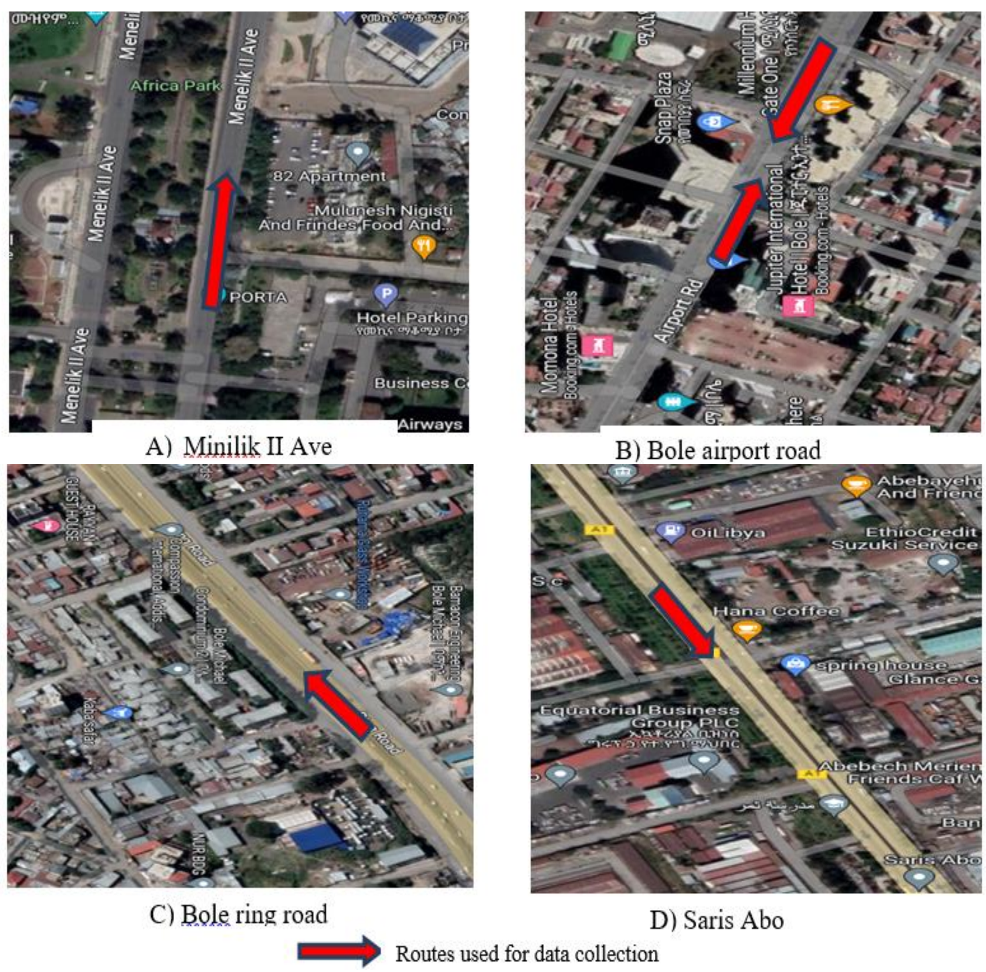

Figure 3.15: Selected routes for data collection

3.6.2. Design of the experiment

In the experimental design of this study, a full factorial design is employed as a method to assess how different levels of inputs impact outputs through the careful designing and executing of the experiment. This approach allows for the testing of all input combinations while thoroughly controlling for other variables. It enables the identification of the optimal input/output combination for achieving the most effective output. The factors were vehicle speed (10 km/h, 20 km/h, 30 km/h, 40 km/h, and 50 km/h) and road slope (-2^o, 0^o, 2^o, 4^o, and 6^o) with three repetitions (25 x 3 = 75 runs) at constant vehicle load. The number of vehicles used in data collection was two, with mileages of 71,446 km and 90,277 km for the petrol and diesel vehicles, respectively. In the city of AA, the selection of road slope and vehicle speed levels for this study took into consideration the road slope and vehicle speed limit. The levels of each factor were deliberately changed to assess their influence on tailpipe emissions, encompassing CO_2, CO, and HC.

3.6.3. Data collection

The GA5000 model of portable emissions tester, manufactured by GeoTech, was utilized in this study to measure the tailpipe emissions of selected vehicles. Additionally, a GPS based on OBD-II was installed in the selected vehicles for detecting road slopes and location information. The number of vehicles used for data collection was two, one powered by petrol and the other by diesel. Throughout the entire data collection process, each vehicle was loaded with four passengers (275 kg). Figure 3.16 shows a central unit featuring integrated sensors and a system designed for real-time data acquisition, processing, recording, and display. The gas analyzer utilized measured the concentrations of CO, CO_2, O_2, HC, and H_2S. However, for this study's purposes, the GA5000 was used to measure only CO_2, CO, and HC emissions. Sampling of tailpipe emissions was conducted using 3 mm outer diameter stainless steel probes equipped with clamps. An 8 m tube connected the probe to the portable emissions tester located inside the vehicle. This study assumed that the fractional volume of a specific gas entering the data collection probe of the tester is equal to the fraction of that particular gas considered out of the total volume. The steps described in Figure 3.17 were followed when experimenting.

a) Exhaust sampling line b) Measuring device during the experiment

Figure 3.16: GA5000 portable gas analyzer used during the experiment

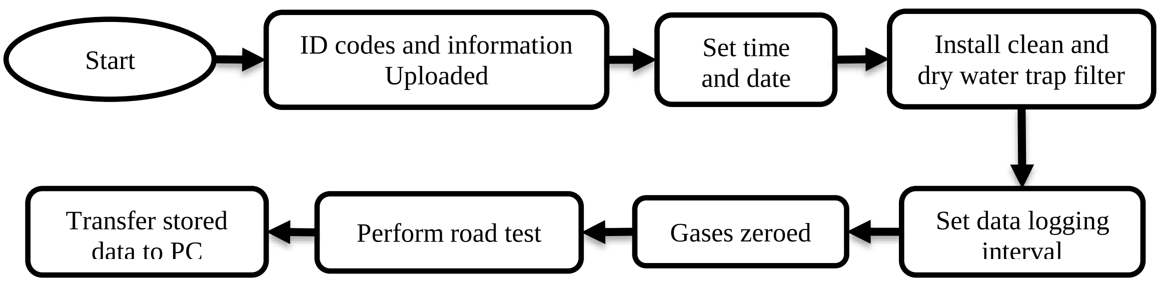

Figure 3.17: Procedures of experimental data collection

At the start of each test, the portable gas analyzer was positioned on the rear passenger seat, powered on, and allowed to warm up for 10 minutes. It operated on an internal battery, which could be recharged using a 220 V alternative current power supply. When fully charged, the battery could provide the portable emissions analyzer for 8 continuous hours. Additionally, GPS was utilized to gather data on the vehicle's speed and location. The portable gas analyzer captured and stored the raw data internally. Following the installation of its data logging software, the data was transferred to the laptop via a USB cable. A web-based portal was used to access the GPS data that was gathered. The position and speed of the vehicles were then correlated with the emissions data that had been gathered. To process the experimental data further in Minitab 21, it was finally saved as an Excel file.

Experiments were carried out between June 7th and June 11th, 2023, with ambient temperatures ranging from 12 ^{o}C to 25 ^{o}C. The raw emissions data for HC, CO_2, and CO were captured by the portable gas analyzer in percentage volume. The correlation adopted by (Pilusa et al., 2012) was used to convert tailpipe emissions in percentage form to g/km. Equations 3.20 to 3.22 provide the formulas used for the unit conversion of CO, CO_2, and HC tailpipe emissions.

$$CO_2\left(\frac{g}{km}\right) = 166.3 \times CO_2\ (\%vol) \qquad 3.20$$

$$CO\ \left(\frac{g}{km}\right) = 9.66\ \times 10^{-3} \times CO\ (\%vol) \qquad 3.21$$

$$HC\ \left(\frac{g}{km}\right) = 5.71 \times 10^{-3} \times HC\ (\%vol) \qquad 3.22$$

3.6.4. Full factorial analysis (FFA)

Following the conversion of the measured emissions unit to grams per kilometer (g/km), a comprehensive analysis was conducted through a full factorial approach. This involved main effect analysis, interaction analysis, a Pareto chart depicting standardized effects and residuals, and regression analysis. This methodology facilitated the identification of crucial variables influencing emissions levels and their interactions, while also providing a means to assess the model's accuracy.

In the context of the conventional regression approach, predictive models were developed to establish the correlation between input factors and output responses within a system. In this study, regression analysis was employed to model and evaluate the relationship between variables such as vehicle speed and road slope, and three performance attributes: CO_2, CO, and HC. Equation 3.23 presents a general linear regression model incorporating multiple predictors.

$$Y = c + c_1\chi_1 + c_2\chi_2 + \ldots + c_{12}\chi_1\chi_2 + c_{13}\chi_1\chi_3 + \ldots + c_{11}\chi^2_1 + c_{22}\chi^2_2 + \ldots \qquad 3.23$$

Where: Y is the response , χ_1, χ_2, χ_3 … are the independent factors, c_1, c_2, c_{12}, c_{22}… are the cofficients of regression.

3.6.5. Desirability function analysis (DFA)

In this investigation, we employed DFA to simultaneously optimize CO_2, CO, and HC emissions. DFA, a widely utilized optimization technique, evaluates a set of responses and selects variables that optimize these responses (Ali et al., 2022). To concurrently optimize multiple responses, both academia and industry commonly employ the DFA method (Devarajaiah & Muthumari, 2018; Thorisingam & Mustafa, 2022). Notably, (Ali et al., 2022) utilized DFA to identify risk factors associated with the lowest CO_2 emissions in Africa, while (Perec, 2022) applied DFA to optimize machining settings for high-pressure abrasive water jet cutting of Hardox 500 steel. The objective of the optimization procedure is to minimize, maximize, or attain a target value for the responses (y_i) through the use of the desirability function d_i (y_i). Each yi value is assigned a score between 0 and 1, with 1 representing the most desirable value and 0 indicating the least desirable value (Devarajaiah & Muthumari, 2018). DFA relies on a composite desirability function to amalgamate various response qualities into a single response function (Perec, 2022). In this study, the analysis proceeded through distinct steps to arrive at the solution.

1. Calculate desirability index:

Since one of the aims of this study is to minimize CO_2, CO, and HC, the preference is for the smallest achievable values. Consequently, the findings from this study should guide the identification of the most efficient operational range for emission reduction. When the output response attains its minimum, the factor d_i is computed as outlined in previous studies (Ali et al., 2022; Devarajaiah & Muthumari, 2018; Perec, 2022):

$$d_i = \begin{cases} 1, y_i \leq y_{min} \\ \left(\frac{y_i - y_{max}}{y_{min} - y_{max}}\right)^r, y_{min} \leq y_i \leq y_{max}, r \geq 0 \\ 0, y_i \geq y_{min} \end{cases} \qquad 3.24$$

Where: d_i is the individual desirability, y_i is the expected value, y_{min} is the lower tolerance limit, y_{max} is the upper tolerance limit, and r is the weight.

When the y_i is less than a certain criteria value, the desirability value equals 1. If the y_i oversteps the specific value, the desirability value equals 0.

2. Calculate composite desirability

The individual desirability indices for all responses were combined into a unified value using equation 3.25, resulting in the overall desirability function (D).

$$D = \sqrt[w]{d_1^{w1} \times d_2^{w2} \dots d_i^{wi}} \qquad 3.25$$

Where: D is the overall desirability, d_i is individual desirability, w_i is the weight of the response y_i, and w is the sum of the individual weights.

3. Choose the optimum level responses and their combination

Ultimately, identify the optimal configuration for level control settings, with a high composite desirability value indicating a recommendation for low emissions levels.

3.7. Methods for real-time simulation of tailpipe emissions

One of the key tasks in sustainable development is modeling vehicle emissions to assess the impacts of various parameters on the amount of pollutants emitted by vehicles and the transport sector as a whole. To enable the modeling of real-time PV emissions in this study, experimental data on speed, acceleration, road slope, number of stops, drive modes, route types, PKE, RPA, and technical characteristics of selected vehicles were used to develop a representative local DC for this study areas. This local DC is considered representative of the traffic flow characteristics of the AA including AAE. It provides a means to model light-duty vehicles FC and exhaust emissions under real-time conditions. The ANN method was used for modeling vehicle emissions, in a four-step procedure (Figure 3.18):

Step 1: Selection of study site, driving cycles, and vehicles.
Step 2: Collection of data on selected DCs characteristics related to vehicular emissions.
Step 3: Development of a Matlab/Simulink-based emissions model using selected DCs.
Step 4: Modelling of vehicular emissions (HC, CO, NO_X, PM) using an ANN method, and comparing the results with those from a COPERT model and an experimental CD test.

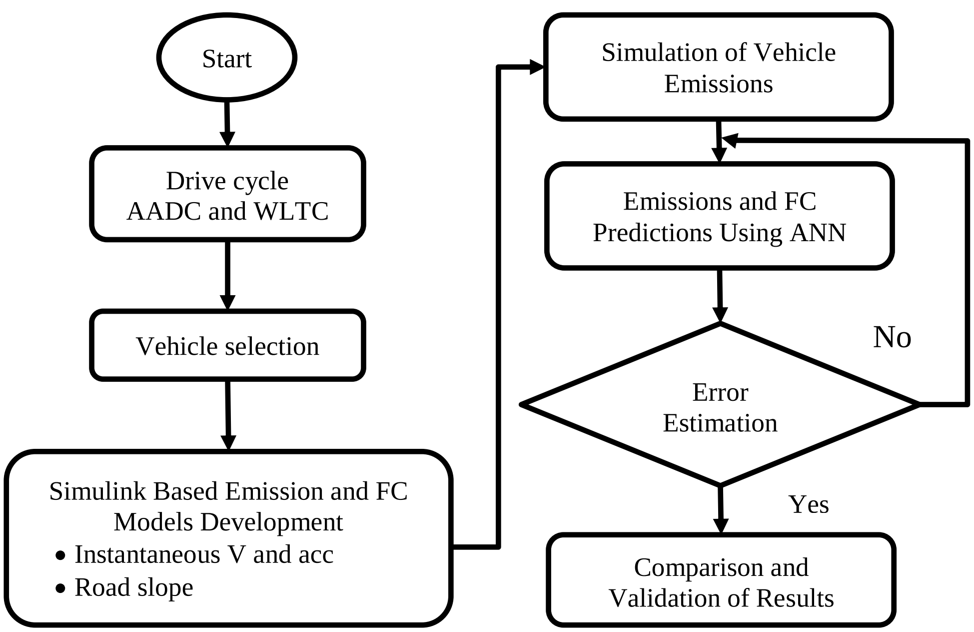

Figure 3.18: The proposed approach for real-time emissions prediction

Table 3.10 details vehicle specifications used in Simulink to simulate real-time exhaust emissions and FC. The selection of vehicles was based on types commonly available in AA.

Table 3.10: Technical details of the selected vehicles for the real-time simulation

Vehicle parameters	Vehicle 1	Vehicle 2
Fuel type	Gasoline	Diesel
Vehicle name and model	Toyota Corolla	Hyundai minivan
Maximum power (kW)	91	101
Vehicle weight (kg)	1760	1972
Transmission	5-speed manual	5-speed manual
Coefficient of drag	0.335	0.34
Emission technology	NA	Catalytic convertor

3.7.1. Real-time tailpipe emissions and FC simulation

Simulation models must reflect real-world situations sufficiently well to produce valid emissions estimates and can be programmed to contain whatever data are required for emissions modeling. To ensure that predicted emissions are reliable and consistent, the models must be evaluated, while to keep up with changes in real-world conditions, the models must be continuously reviewed and updated.

Through block diagrams, codes, and programming, Matlab/Simulink can be used to model and simulate vehicles using vehicle dynamics concepts and a variety of DCs. In this study, real-time emissions and FC were simulated using both the local DC developed for this study area and the WLTC. A high-level need is linearly propagated backward through several systems, such as a vehicle, wheels, transmission, and engine in a purely backward-facing simulation. Real-time vehicle performance was simulated using equation 3.26 for vehicle dynamics (Hassine et al., 2021).

$$F = M_v g C_u + \frac{1}{2}\rho C_d A_{VEH} V^2 + m_v a + m_v g sin(\theta) \qquad 3.26$$

Where: F is the tractive force required at the wheel in N, m_v is the mass of the vehicle in kg, C_u is the coefficient of rolling resistance, and A_{VEH} is the frontal area of the vehicle in m^2.

Equation 3.27 is used to get the total power at the wheel (P_T) (Donateo & Filomena, 2020; Aksoy et al., 2014)

$$P_T = F\ V \qquad 3.27$$

Before creating emissions models, it is crucial to determine the variables influencing emissions and how they interact. One way to measure emissions is as a percentage of the fuel that cars use (U.S. Environmental Protection Agency, 2016). The Energy Demand Module determines how much engine energy is required to maintain a preset velocity profile by using longitudinal vehicle dynamics. The depiction of the instantaneous drivetrain energy balance is given in Equation 3.28 (Tsiakmakis et al., 2019). The numerator represents the power required at the wheels to propel the vehicle along the specified velocity profile, while the denominator displays the efficiency of the complete drivetrain.

$$P_{dtr} = \frac{\left(F_0 \times cos(\phi) + F_1 \times V + F_2 \times V^2 + m \times a + m \times g \times sin(\phi)\right) \times V}{\eta_{dtr}} \qquad 3.28$$

Where the η_{dtr} and the road load coefficients for the vehicle are denoted by the factors F_0, F_1, and F_2.

Equation 3.29 presents the fuel usage computed using an equation from (Tsiakmakis et al., 2019). FC is normalized by engine capacity and measured using the fuel mean effective pressure (FMEP).

$$FMEP(t) = \frac{-\left(a + b*Cm(t) + c*Cm(t)^2\right) + \sqrt{\left(a + b*Cm(t) + c*Cm(t)^2\right)^2 - 4*a2*\left(\left(T(t)/Ttrg\right)^{-k}*\left(l + l2*Cm(t)^2\right) - BMEP(t)\right)}}{2*a2} \qquad 3.29$$

Where, BMEP is denoted as the engine brake mean effective pressure. The average piston velocity is represented by Cm, the engine coolant temperature is denoted by T, and the engine's target operating temperature is indicated by Ttrg. The engine's thermodynamic efficiency is defined by the empirical parameters a, b, c, and a2, while the engine losses from friction and pumping are represented by the values l and l2. The calculated generic values for these parameters are then inputted into the corresponding model based on specific engine categories.

Where total power is converted into FC by multiplying by a consumption factor b (equation 3.30) based on the technical specifications of the vehicle (Aksoy et al., 2014). FC amount is then converted into emissions as equation 3.31.

$$Fuel\ consumption = bP_T \qquad 3.30$$

$$Emissions = C_e\ x\ fuel\ consumption \qquad 3.31$$

Where C_e is a vehicle emissions constant, the value of which can be obtained from vehicle technical specifications.

As depicted in Figure 3.19, each vehicle model in Simulink is organized into four main components: driver controller, vehicle powertrain controller, powertrain architecture, and environmental conditions. The detailed simulation blocks are shown in Figures F1 and F2 in Appendix F.

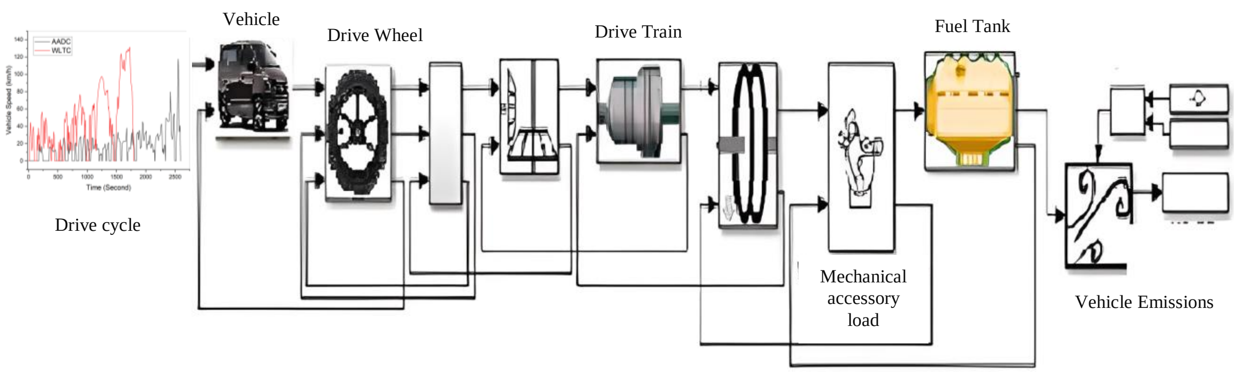

Figure 3.19: The developed Simulink block for vehicle emissions simulation

3.7.2. Artificial neural network prediction methods

In an ANN, each node is referred to as an artificial neuron, and the arcs are referred to as synaptic weights (Donateo & Filomena, 2020). The multilayer perceptron NNs model has a greater capacity for prediction than conventional multi-regression models (Cabaneros et al., 2019). In this study, an ANN predictive modeling technique was used to predict real-time tailpipe emissions and FC for two selected PV types (Table 3.10). The procedures followed in model development are briefly explained in this section, where ‘epochs’ refers to the frequency with which the bias terms and network weights were modified to produce the optimal model. Multiple trial-and-error runs were conducted while adjusting all parameters, to accurately reflect the influence of these parameters on model performance.

The ANN model was used to anticipate real-time exhaust emissions and FC from on-road PVs given a specific set of inputs. The simulated real-time exhaust emissions and FC values obtained from the Simulink were employed to train the developed ANN. Figure 3.20 depicts the ANN architecture developed in Matlab, with 13 independent predictors (inputs) to the network and a hidden layer with 10 neurons to predict response at any given time. The dataset collected was split into two segments, for training and testing, with 70% of the data used for training and 30% for testing. The ANN model was trained by adjusting its weights and biases to maximize the performance of the network. The network was trained using a Bayesian regularisation algorithm since this is the most commonly used method in the field of NNs for building nonlinear models of complex relationships and finding optimal solutions (Zhou et al., 2023). The selection of data for ANN training and the subsequent pre-processing phase are critical for successful ANN training.

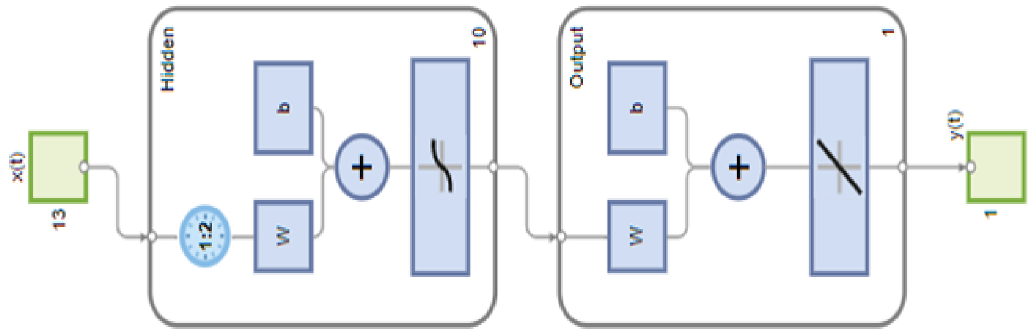

Figure 3.20: ANN model used for predicting vehicle exhaust emissions

The variables chosen as predictors and outputs in this study are shown in Figure 3.21, where x(t) represents input variables or predictors (vehicle speed, road slope, acceleration, deceleration, distance traveled, idle time, drive time, number of stops, drive mode, RPA, PKE, and route type at one-second intervals) and y(t) represents output variables (CO, HC, NO_X, and PM emissions at one-second intervals).

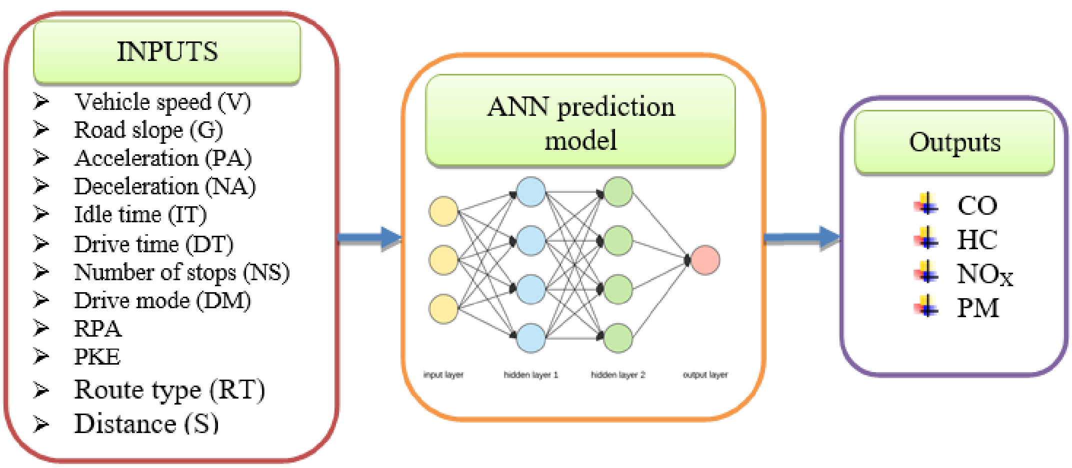

Figure 3.21: Inputs and outputs or targets of the ANN model

In this study, the goodness-of-fit of the ANN model was evaluated using Mean Square Error (MSE) and the coefficient of determination (R^2), which are standard performance measures in ANN models (Donateo & Filomena, 2020). The MSE is calculated using Equation 3.32, while the R^2 is calculated using Equation 3.33 (Tang et al., 2023).

$$MSE = \frac{1}{N}\sum_{i=0}^{N}(y_i - x_i)^2 \quad 3.32$$

$$Rsquare = \frac{\sum_{i=1}^{n}(\hat{y}_i - \bar{y})^2}{\sum_{i=1}^{n}(y_i - \bar{y})^2} \quad 3.33$$

Where N is the total number of data points, y_i is the model output, x_i is the observed value $\hat{y}_i$ is the predicted value of emissions, and $\bar{y}$ is the average value of emissions.

CHAPTER FOUR

RESULTS AND DISCUSSION

4.1. Results and discussion of the developed DCs

After employing the two previously described approaches, we developed local DCs and evaluated how well they matched the real-time acquired data.

4.1.1. Results of NN-based DC

4.1.1.1. Principal component analysis

This study used PCA with SPSS 26 on all trip indicators data from 527 trips in order to minimise the dimension of the trip indicators. Prior to conducting PCA analysis, a correlation test was conducted. The results, which are displayed in Table 4.1, demonstrate that the sample size was adequate for PCA analysis since KMO, a measure of sampling adequacy, was found to be more than 0.7 and significance was zero.

Table 4.1: KMO and Bartlett's test

Kaiser-Meyer-Olkin Measure of Sampling Adequacy		0.709
Bartlett's Test of Sphericity	Approx. Chi-Square	9288.26
	df	136
	Sig.	.000

With eigenvalues over one for components 1, 2, 3, 4, and 5, and a cumulative percentage of variance of 80.247 percent, significant information was present. A cumulative value of more than 80% is considered acceptable, as stated in (Peng et al., 2019). Due to insufficient information, components with an eigenvalue of less than one were disregarded. The resultant component matrix is presented in Table 4.2, and Figure 4.1 shows the eigenvalue scree plot.

Table 4.2: Total variance explained

Component	Initial eigenvalues			Extraction sums of squared loadings			Rotation sums of squared loadings		
	Total	% of variance	Cumulative %	Total	% of variance	Cumulative %	Total	% of variance	Cumulative %
1	5.652	33.249	33.249	5.652	33.249	33.249	3.648	21.459	21.459
2	3.187	18.748	51.997	3.187	18.748	51.997	3.48	20.469	41.928
3	2.13	12.531	64.528	2.13	12.531	64.528	2.861	16.828	58.756
4	1.51	8.88	73.408	1.51	8.88	73.408	2.143	12.608	71.364
5	1.163	6.839	80.247	1.163	6.839	80.247	1.51	8.883	80.247
6	0.934	5.495	85.742						
7	0.588	3.46	89.202						
8	0.422	2.484	91.686						
9	0.347	2.039	93.724						
10	0.339	1.993	95.717						
11	0.252	1.482	97.199						
12	0.187	1.098	98.297						
13	0.126	0.743	99.04						
14	0.062	0.364	99.404						
15	0.053	0.311	99.716						
16	0.034	0.202	99.918						
17	0.014	0.082	100						

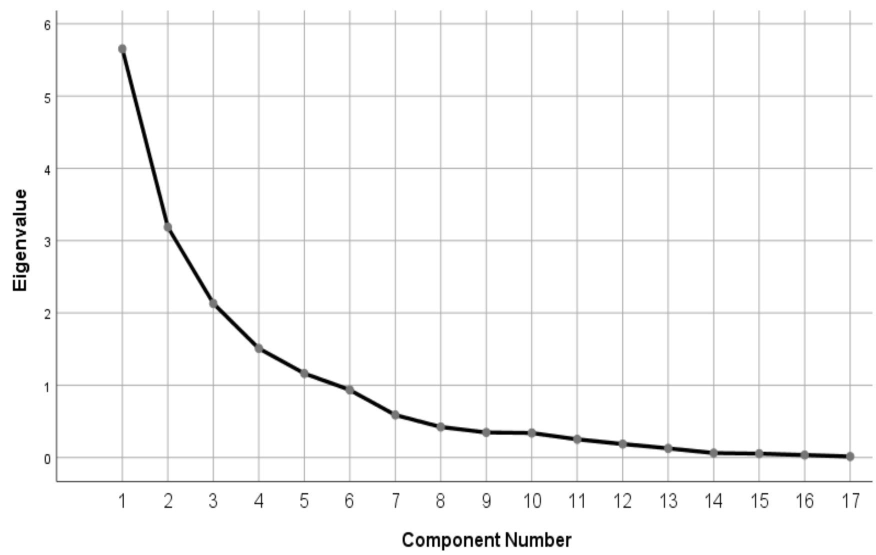

Figure 4.1: Scree plot

The trip indications are clearly clustered based on their similarities, as seen by the scores of the five rotational component matrices shown in Table 4.3. In addition, the component plot in the rotated space is shown in Figure 10 and Table 4.3. Factor one (F_1) comprises indicators related to velocity and distance; Factor two (F_2) comprises the percentage of acceleration and deceleration time, PKE and average, and standard deviation of acceleration; Factor three (F_3) comprises indicators related to stops and the percentage of cruising mode; Factor four (F_4)

comprises maximum acceleration and deceleration; and Factor five (F_5) comprises RPA and trip duration. Principal component score matrices were generated for each trip by multiplying the trip data matrix by the principal component matrix, as shown in the sample Table 4.4. Scores of the five principal components were taken as the research object for clustering.

Table 4.3: Rotated component matrix

Indicators	F_1	F_2	F_3	F_4	F_5
V_{davg}	0.888				
V_{max}	0.869				
V_{sd}	0.833				
V_{avg_all}	0.754				
S_{sum}	0.673				
P_{dec}		0.941			
P_{acc}		0.82			
a_{avg}		-0.766			
PKE		0.673			
a_{sd}		0.579			
P_{idl}			0.947		
P_{cru}			-0.852		
N_{spkm}			0.723		
a_{max}				0.904	
dec_{max}				-0.781	
T_{total}					0.785
RPA					0.539

Extraction Method: Principal Component Analysis.
Rotation method: Varimax with Kaiser normalisation[a]

Table 4.4: Sample calculated factor score

Trip code	FAC1_1	FAC2_1	FAC3_1	FAC4_1	FAC5_1
FT189	-1.836	-1.185	-1.183	-0.933	0.18
FT245	-0.383	-0.729	-0.812	-0.259	-0.82
FT94	-0.681	-0.509	-1.204	-0.298	-0.584
FT98	-1.152	-0.547	-1.783	-0.236	-0.366
FT179	-0.757	-0.755	-2.085	-0.548	-0.314
FT35	-1.421	-1.030	-1.063	-0.468	-0.157
FT1000	-0.358	-0.148	-1.519	0.168	-0.878
FT193	-0.829	-0.882	-1.373	-0.247	-0.397
FT124	0.560	-0.144	1.349	0.278	-1.638
FT134	-1.166	-0.949	-1.806	-0.651	-0.150

4.1.1.2. Clustering result analysis

To determine the best model, the validation accuracy score of the model's performance was compared to the trained data after the model was trained using a classification learner. The accuracy score of the classification learning approaches was computed using MATLAB software. The accuracy score is represented as the proportion of true results (true positives and negatives) divided by the total number of cases examined (true positives, false positives, true negatives and false negatives). Table 4.5 summarizes the accuracy score results for each classification learner method applied. The NN classifier approach performed the best, as indicated by the accuracy score; therefore, the NN clustering method was applied to devide the trips into different groups.

Table 4.5: Accuracy score of classification learner methods

S/N	Methods	Accuracy (validation)
1	Decision trees	63.9-71.3 %
2	Discriminant analysis	65.0-82.0 %
3	Naïve Bayes classifiers	61.3-71.2 %
4	Support vector machines	68.5-85.2 %
5	Nearest neighbour classifiers	71.3-74.4 %
6	Neural network classifier	82.9 - 86.5 %

A confusion matrix plot was utilised in order to illustrate the performance of the chosen classifier in each class. True positive rates (TPR) and false negative rates (FNR) were used to determine how well the classifier performed in each class. The proportion of correctly identified observations per true class is referred to as TPR. FNR is the percentage of observations that are erroneously categorised in each class. In Figure 4.2, scattered plots are displayed. Figure 4.3 shows that 94.7%, 84.6%, 87.4%, and 72.9% of the TPR for extra-long trips (ELT), long trips (LT), medium trips (MT), and short trips (ST), respectively, were appropriately identified.

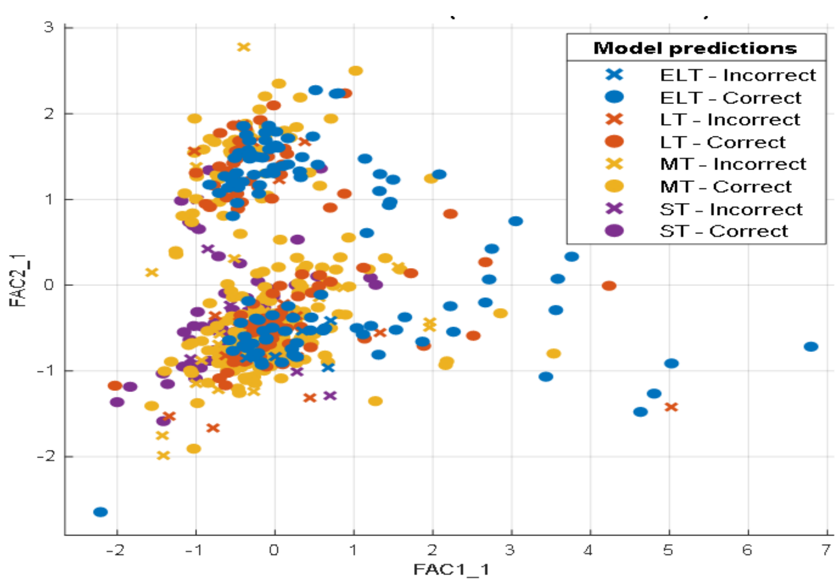

Figure 4.2: Scattered plot of narrow NN

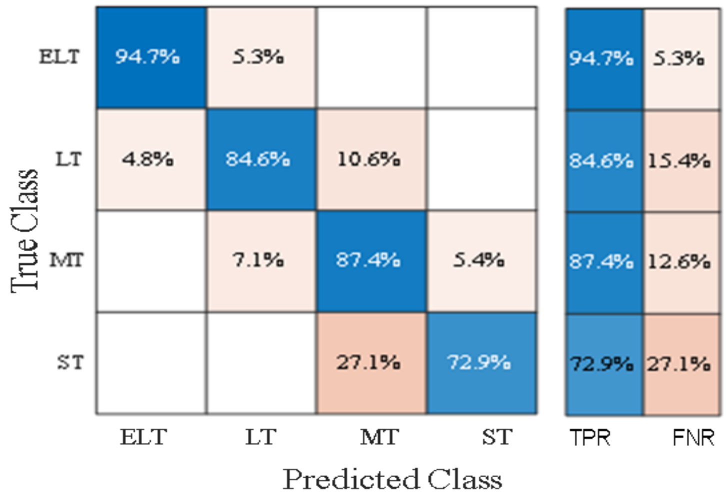

Figure 4.3: Validation confusion matrix of NN classifier

Figure 4.4 displays the true and false positive rates for the receiver operating characteristics (ROC) curve of the NN-trained classifier, with the classifier's overall quality indicated by the area under the curve. The false positive rate (FPR) of the selected method was 0.01; this means that 1% of the observations are mistakenly assigned to the positive class by the classifier. In this study, the classifier correctly assigned the data to the positive class at a TPR of 95%; the area under the curve (AUC) was 0.97, indicating the best classifier performance.

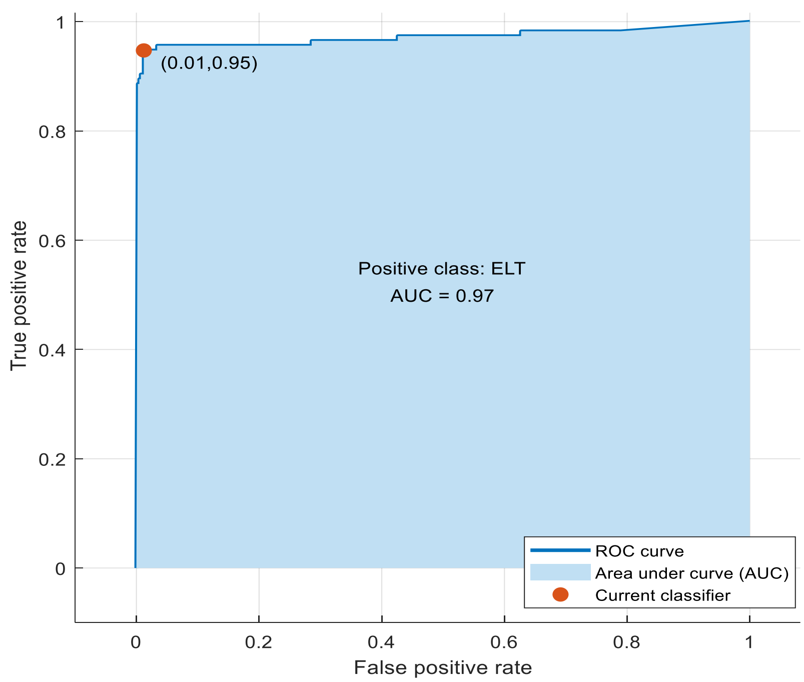

Figure 4.4: ROC curve of NN classifier

To cluster the trips based on the computed five PCA score values, the NN clustering approach was used, setting the 3x3 matrix dimension. Using this method, nine clusters were created from the 527 trips. Neighbor weight distances, neighbor connections, and weight placements on self-organizing maps showed the highest clustering performance, as demonstrated in Figures 4.5 to 4.7. For clusters 1 to 9, the corresponding numbers of trips were 77, 58, 75, 25, 31, 136, 15, 68, and 42, respectively.

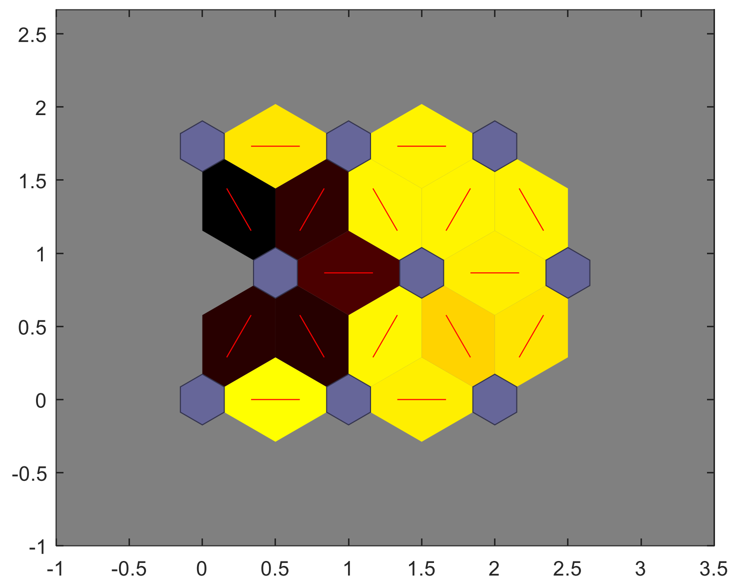

Figure 4.5: Self-organizing map neighbor weight distances

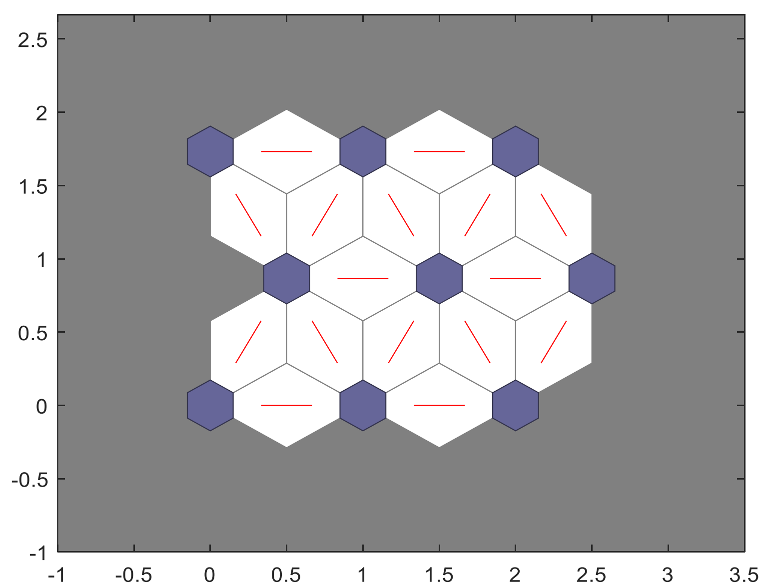

Figure 4.6: Self-organizing map neighbor connections

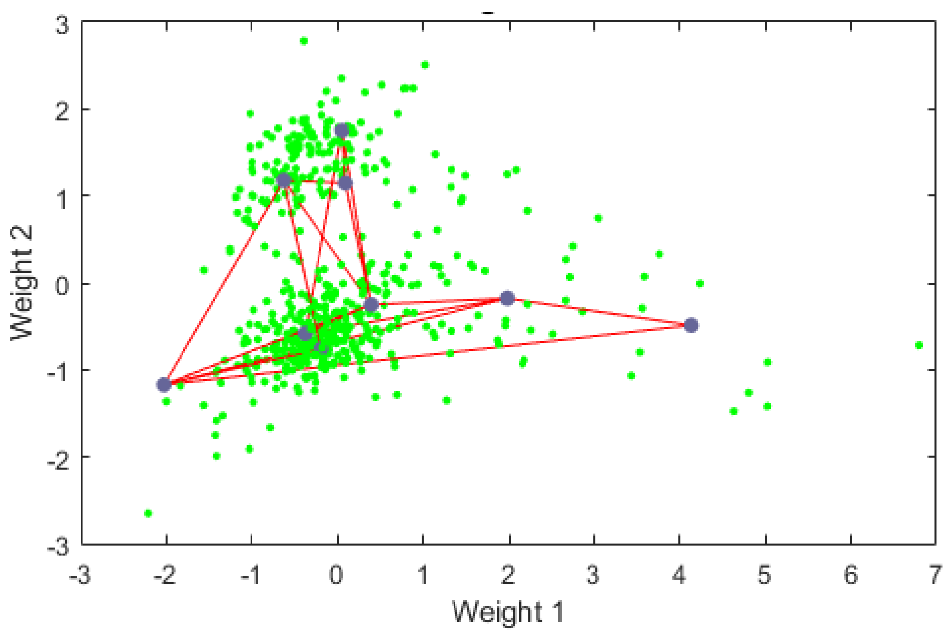

Figure 4.7: Self-organizing map weight positions

4.1.1.3. Selected trips and micro trips

The trips which most correctly reflected their cluster were chosen as the best trip after each cluster's relative error and similarity score were calculated. This was used to select the top nine trips. Among the best trips, nine had similarity scores of 0.97, 0.95, 0.96, 0.87, 0.92, 0.98, 0.86, 0.99, and 0.98 for clusters 1 to 9, respectively. In this study, equal weight was given to each of the trip indications during computation.

The nine best trips that were chosen were divided into MTs, and characteristic parameters for each MT were computed. Based on similarity scores, the top MTs that best represent their group were selected. Based on this, eighteen MTs were chosen from the nine clusters. Sequence numbers 1–12, 13–16, and 17–18 represnts the chosen MTs for urban, extra-urban, and rural road segments, respectively, as indicated in Table 4.6. Additionally, all driving data on the ring road and the AAE were split into MTs. Then best MT was selected for both the ring road (sequence number 19 in Table 4.6) and the AAE segment (sequence number 20 in Table 4.6).

Table 4.6: Selected MTs

Sequence number	MT code	T_{total}	T_{idle}	T_{drive}	S	Route
1	EMT1	245	174	71	245.766	Urban
2	DMT7	229	107	122	430.225	Urban
3	CMT12	154	101	53	300.688	Urban
4	IMT8	119	45	74	332.236	Urban
5	EMT6	72	41	31	130.299	Urban
6	CMT2	82	37	45	281.14	Urban
7	HMT26	70	19	51	288.133	Urban
8	HMT10	72	19	53	240.567	Urban
9	FMT4	160	17	143	664.625	Urban
10	DMT11	50	10	40	79.368	Urban
11	FMT12	70	8	62	244.875	Urban
12	BMT6	51	7	44	183.937	Urban
13	AMTC29	90	35	55	434.186	Extra-urban
14	AMTC2	110	35	75	491.025	Extra-urban
15	BMT7	111	15	96	609.743	Extra-urban
16	GMT90	130	9	121	643.646	Extra-urban
17	IMT4	339	25	314	2098.639	Rural
18	GMT33	180	5	175	1210.502	Rural
19	RRMT3	160	3	157	1918.478	Ring road
20	EWMTC18	100	24	76	820.486	Expressway
Total		2594	736	1858	11648.57	

4.1.1.4. NN-based speed prediction

The nonlinear autoregressive with external input (NARX) model was used for predicting a series of vehicle speeds y(t) for each route type based on historical values d of y(t) and another series of data x(t) using the NN. A back-propagation training approach combined with Bayesian regularisation was employed to train the network. For urban, extra-urban, rural, ring road, and expressway, the best training performance was attained at 177, 431, 554, 676, and 214 epochs, respectively. For each route category, Figure 4.8 displays the speed output element's response using both the training and test datasets.

In Figure 4.8, the term 'training target' refers to the desired output for each input pattern of vehicle speed in the particular time series computed from the training dataset. During the training process, the NN generates predicted outputs, referred to as 'training outputs', for each input pattern in the training dataset. Initially, these output values are random or arbitrary, but as the training progresses, they converge towards the actual training targets.

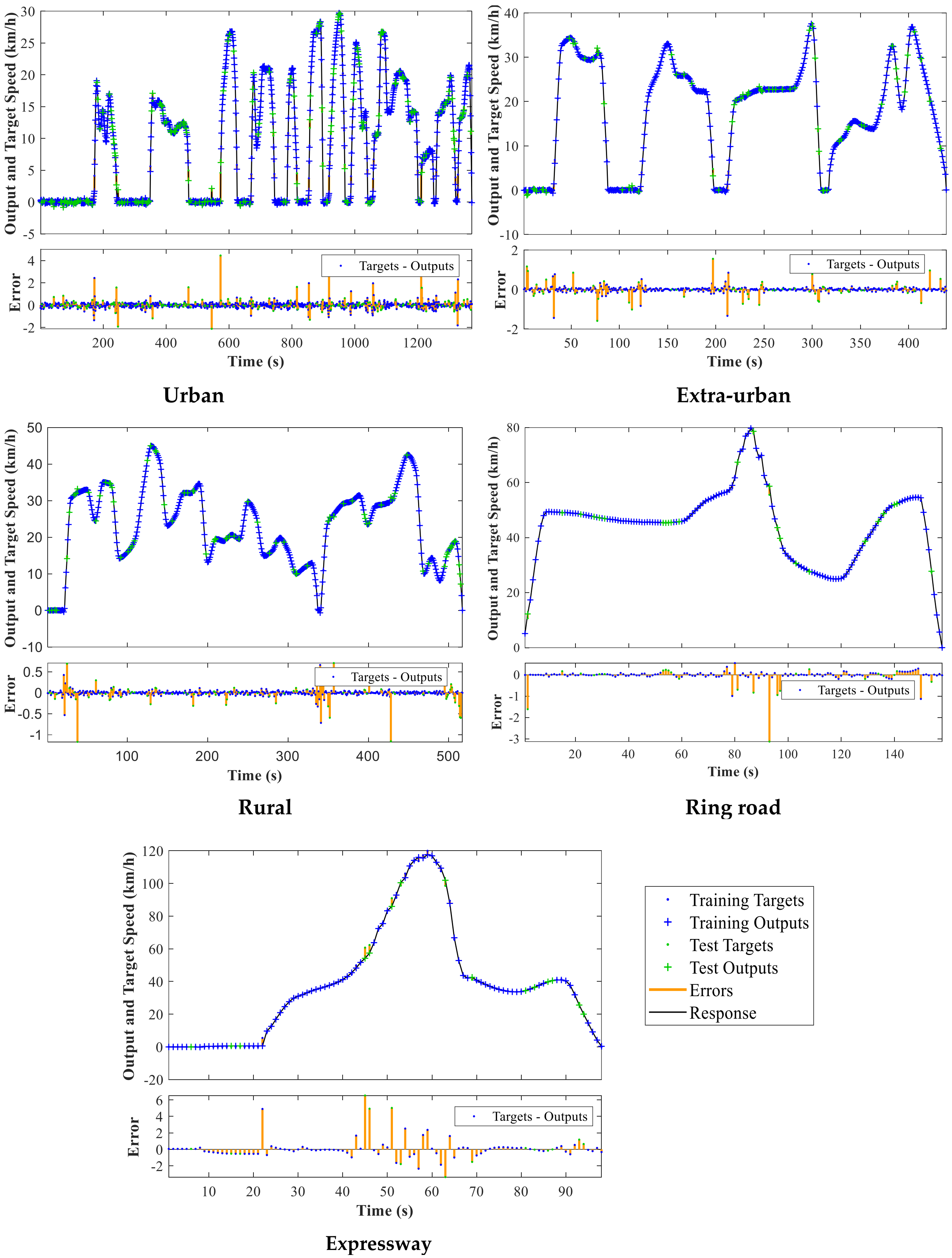

Figure 4.8: Response of time series predicted vehicle speed

Figure 4.9 displays the regression fit of the training, test, and combined data. Appendix E (Figure E1) displays the regression fit of the training and test data separately. The best fit was indicated by the R-value for each route, which was greater than 0.99. Consequently, the predicted speed values for the given time series were incorporated into the final developed DC.

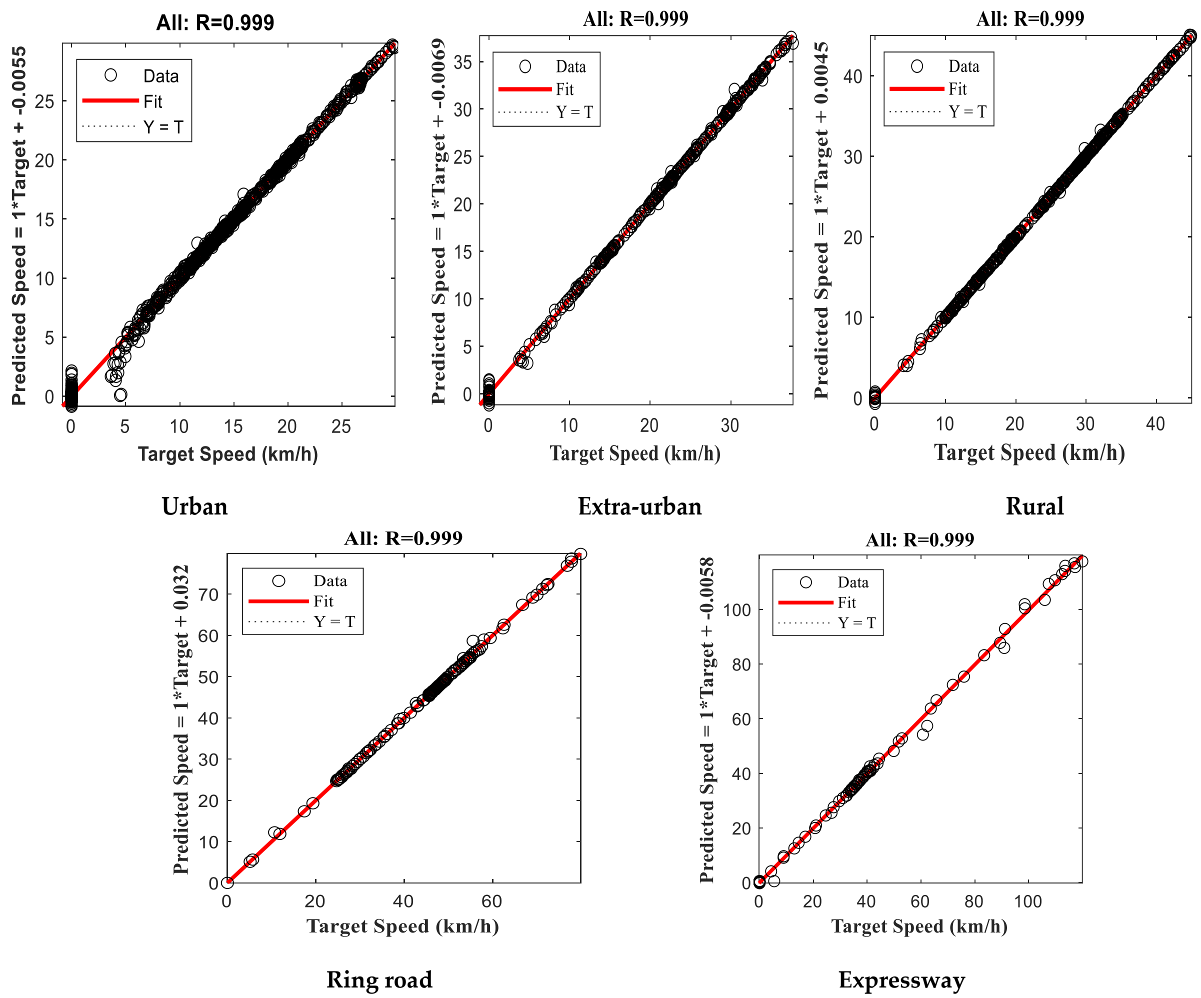

Figure 4.9: Regression fit of all training and test data

The DCs developed was derived by combining the predicted vehicle velocity of the urban, extra-urban, rural, ring road and expressway sections, as discussed in the section on NN-based prediction. The urban, extra-urban, rural, ring road and expressway sections had durations of 1374 s, 441 s, 519 s, 160 s and 100 s respectively, as shown in Table 4.7.

Table 4.7: AADC characteristic parameters of each route section

Indicators	Urban	Extra-urban	Rural	Ring road	Expressway
S_{sum}	3400.659	2176.239	3306.434	1946.877	1055.271
T_{total}	1374	441	519	160	100
V_{davg}	15.797	22.644	24.39	44.64	50.652
V_{max}	29.847	37.919	45.10	79.762	117.67
V_{sd}	2.497	3.212	2.95	4.057	9.525
V_{avg_all}	8.91	17.766	22.936	43.805	38
dec_{max}	-2.133	-1.824	-1.198	-3.584	-4.5
a_{max}	1.975	1.876	2.147	2.705	3.44
a_{sd}	0.291	0.393	0.333	0.73	1.205
N_{spkm}	3.529	1.838	0.605	0.514	0.948
RPA	0.079	0.1	0.091	0.173	0.507
PKE	0.175	0.215	0.191	0.365	1.06
P_{idl}	0.436	0.215	0.06	0.019	0.25
P_{acc}	0.146	0.215	0.249	0.331	0.43
P_{cru}	0.272	0.37	0.451	0.45	0.05
P_{dec}	0.146	0.2	0.241	0.2	0.27

Figure 4.10 shows the final speed-time profile of the developed DC based on the NN development approach for AA urban road conditions including the AAE. Table 4.8 presents its characteristic parameters. This dynamic DC comprises 20 MTs. It lasted for a total of 2594 seconds, covering a distance of 11.885 km, and its average and maximum speed were 16.495 km/h and 117.67 km/h respectively.

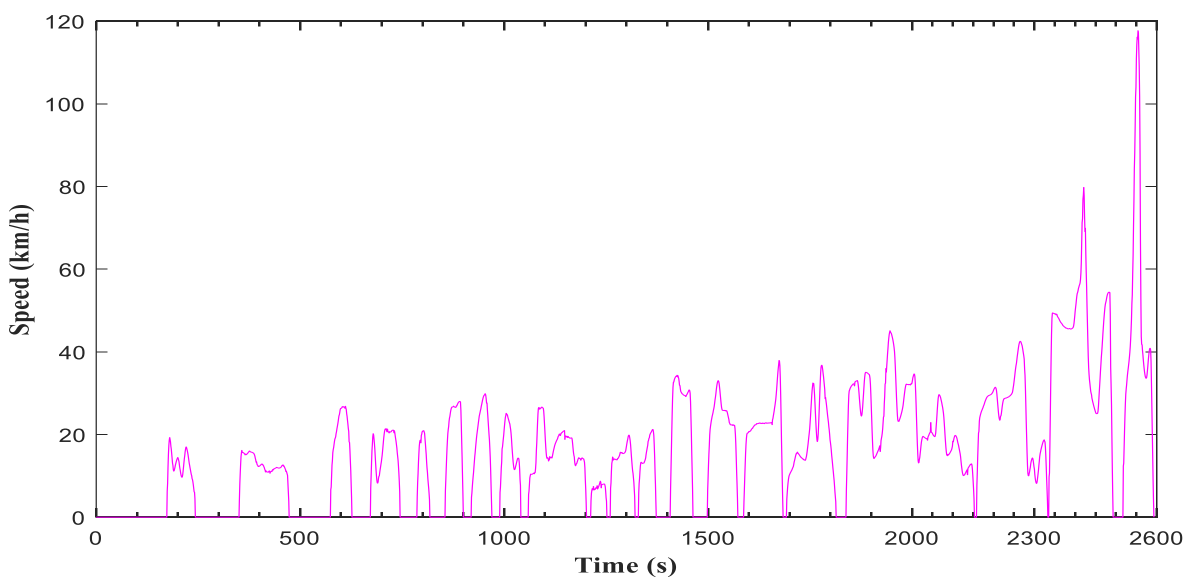

Figure 4.10: Candidate DC developed for this study area using the NN method

To classify the driving sequences into distinct groups, previous research by (Guo et al., 2020; Peng et al., 2015; Ji et al., 2018; Zhou et al., 2017) used the k-means clustering approach to the computed principal component score results. However, in the methodology proposed in this study, a machine learning classification algorithm was utilized to categorize trips based on the computed principal component score results, with the NN clustering method demonstrating superior accuracy compared to alternative approaches.

The DC length was determined using the approach suggested in this study, rather than relying on previous studies. The DC duration of this study best fits the real-time data gathered. This approach yielded a DC duration of 2594 seconds with a deviation of 0.14 from the daily average trip duration, indicating that this DC duration is reasonably similar to the driving data collected in real time from AA. However, (Zhao et al., 2021) initially decided to apply a DC duration of between 1200 s and 1300 s, and two DCs were developed that have a duration of 1216 s and 1261 s. (Peng et al., 2015) defined the duration of the designed DC as 1200 s. Similarly, reference (Guo et al., 2020) decided on a DC duration of 1200 s, while reference (Tong & Ng, 2020) randomly constituted a DC until the required cycle duration was achieved. Additionally, the distance covered by this DC is 11.885 km and relative difference of 0.13 which is close to average daily trip distance of 13.667 km.

4.1.2. Results of Micro trip based DC

Following MATLAB's denoising and segmentation of the speed time data into MTs, the driving characteristic parameters listed in Table 4.8 were computed. The K-means clustering algorithm was then used to group the 6680 MTs into six clusters. The distribution of composite characteristic indicators in clusters 1, 2, 3, 4, 5, and 6 is regarded as expressway, extra-urban, rural, ring road, congested (urban low speed phase), and urban (medium speed phase) circumstances respectively, as Table 4.8 and Figure 4.11 demonstrate. There are 1296, 1495, 1754, 1438, 593, and 104 MTs in the congested, urban, extra-urban, rural, ring roads and expressways respectively.

Table 4.8: Composite characteristic parameters in each cluster

Parameters	Cluster					
	1	2	3	4	5	6
Number of MTs	104	1754	1438	593	1296	1495
Share of T_{total}	0.049	0.191	0.32	0.091	0.064	0.284
V_{max}	120	40	50.2	80	9.2	30
V_{avg}	50.035	16.471	23.11	42.083	4.972	8.561
V_{davg}	55.068	21.345	25.02	46.522	6.871	15.478
Acc_{max}	3.556	2.066	2.384	2.919	1.106	1.868
Dec_{max}	-4.399	-2.004	-1.238	-3.272	-1.278	-2.5
$PAcc_{avg}$	0.732	0.25	0.188	0.297	0.15	0.222
Dec_{avg}	-1.287	-0.273	-0.272	-0.394	-0.201	-0.261
P_{acc}	0.249	0.247	0.286	0.312	0.142	0.155
P_{cru}	0.464	0.285	0.309	0.333	0.388	0.239
P_{dec}	0.24	0.239	0.27	0.288	0.192	0.167
P_{idl}	0.097	0.228	0.136	0.067	0.278	0.439
Route type	Expressway	Extra-urban	Rural	Ring road	Congested	Urban

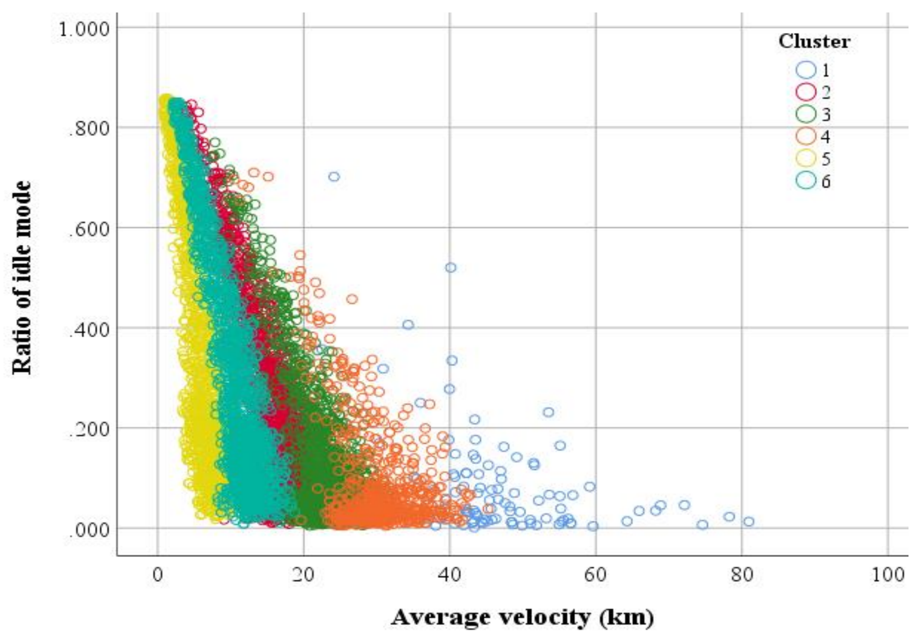

Figure 4.11: Clustering of MTs in the two dimensional feature space

In Figure 4.11, the colors correspond to the following road conditions: yellow (cluster 5) indicates congested urban roads, light blue (cluster 6) represents urban road, red (cluster 2) denotes extra-urban road conditions, green (cluster 3) represents rural road conditions, orange (cluster 4) indicates ring roads, and blue (cluster 1) represents expressways. Several candidate

DCs were generated in this study using the MT approach; the best one, with the fewest paired CPs, was chosen, and its characteristic parameters are displayed in Table 4.9. The candidate DC generated with the MT method is displayed in Figure 4.12. The complete duration (T_{total}) of this cycle amounts to 1539 seconds, during which the urban, extra-urban, rural, ring road, and expressway sections comprised 553, 299, 434, 144, and 109 seconds respectively. The cycle's overall length is 8.73 km, of which 1.24, 1.35, 2.65, 1.69, and 1.79 km were covered by urban, extra-urban, rural, ring road, and expressway sections, respectively. In total, ten MTs, collectively spanning 1539 seconds and covering a distance of 8.732 km, constitute the DC formed using the MT method. These MTs are distributed as follows: two in the congested area, three in the urban area, two in the extra-urban area, one in the rural area, one on the ring road, and one on the expressway. The cycle's maximum speed of 109 km/h, average speed of 20.426 km/h, driving average speed of 27.287 km/h, and idle ratio of 0.252 are all illustrated in the speed profile presented in Figure 4.12.

Table 4.9: Characteristic parameters of the candidate DC based on MT method

CPs	V_{max}	V_{avg}	Vd_{avg}	Acc_{max}	Dec_{max}	$PAcc_{avg}$	Dec_{avg}	P_{acc}	P_{cru}	P_{dec}	P_{idl}
Urban	30	8.102	14.178	1.3279	-1.4	0.194	-0.251	0.16	0.242	0.17	0.428
Extra urban	40	16.25	21.408	1.776	-1.662	0.25	-0.277	0.22	0.341	0.194	0.241
Rural	51.8	22.008	25.47	1.2526	-1.332	0.263	-0.263	0.26	0.325	0.279	0.136
Ring road	69.1	42.285	45.44	2.8559	-2.749	0.345	-0.465	0.39	0.306	0.236	0.069
Expressway	109	59.222	64.552	3.0556	-4.469	0.601	-0.786	0.36	0.303	0.257	0.082
Overall DC	109	20.426	27.287	3.0556	-4.469	0.281	-0.325	0.24	0.293	0.218	0.252

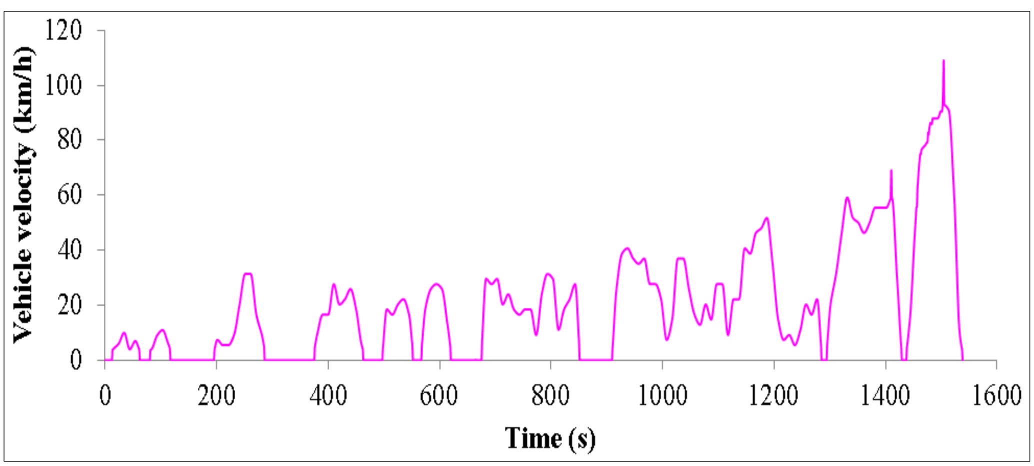

Figure 4.12: Candidate DC developed using MT method

4.1.3. Discussion

After using the two previously mentioned approaches, this study identified the appropriate DC for each approach and assessed how well the DCs matched the driving conditions in AA and AAE. Figure 4.13 displays the values acquired for each route's CPs in relation to the target. This study assessed the generated DCs' representativeness using each of the CPs listed in Table 4.10. With the exception of expressways, the DC generated by the NN prediction approach precisely matches every CP that describes a route, significantly better than the MT method. This study observed that the paired CPs for the NN approach closely approach the maximum allowable deviation, mainly due to the longer travel distances on the expressway without interruptions. Moreover, the NN was trained on a smaller dataset for the expressway compared to the training data used for other routes. A comparison was conducted between the duration characteristics of DCs generated with NN prediction and MT approaches. When comparing the durations, the DC generated by the NN approach is longer (2594 s), whereas the DC generated using the MT method is comparatively shorter (1539 s). The DC duration obtained using NN prediction is extremely close to the daily trip average of 3051 s. The MT-based cycle distance (8.732 km) is comparatively shorter than the DC distance generated using the NN method (11.885 km). With a relative difference of 0.13, the daily average trip distance of the gathered data is 13.667 km, which is quite close to the DC distance generated using NN prediction.

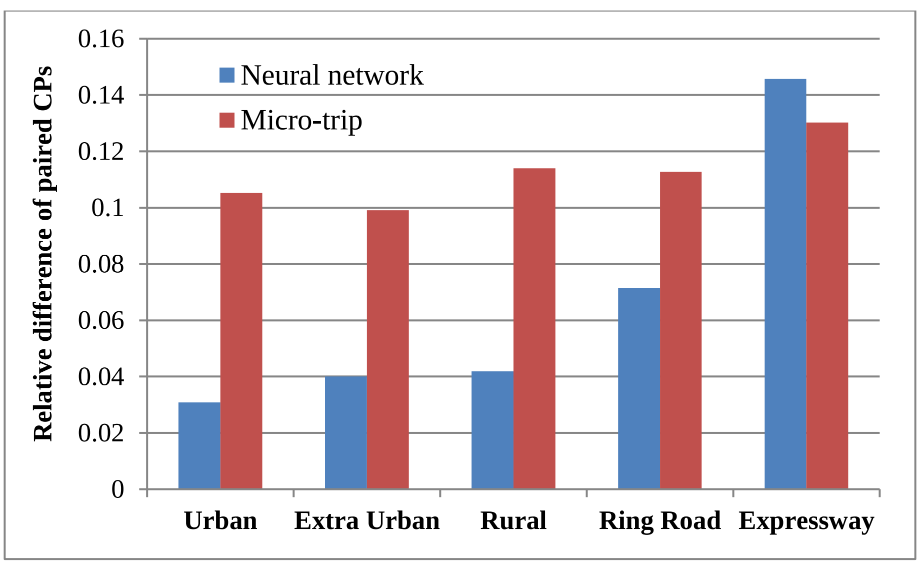

Figure 4.13: Route based relative difference of paired CPs compared with target

The vehicle velocity characteristics of processed experimental data and DCs generated by the two different approaches were compared in Figure 4.14. When considering the maximum, average, and average driving velocities, the NN approach outperforms the MT method in terms of accuracy. This indicates that the NN method's speed distribution is reliable and accurate in capturing the real driving circumstances in AA road conditions including the AAE.

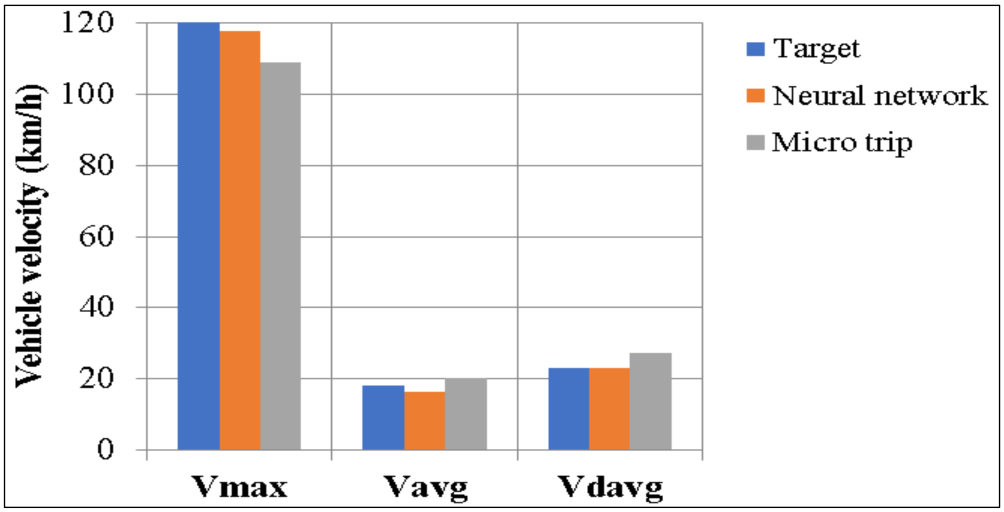

Figure 4.14: Comparison of vehicle velocity characteristics

Regarding the maximum acceleration and deceleration, the NN-based DC exhibits a relative deviation of 0.005 and 0.023, whereas the MT technique yields a deviation of 0.116 and 0.016 from the target, respectively. The NN based DC is found to be closer to the target data than the MT based DC on the basis of the average acceleration and deceleration comparison. Furthermore, the DC cycle generated by NN exhibits higher values for acceleration-related parameters compared to the MT-based cycle, suggesting that the NN method's acceleration and deceleration activities are more aggressive.

The driving mode distribution, encompassing idle time, acceleration, deceleration, and cruising, in the developed DCs closely resembles the processed experimental data for both approaches, as depicted in Figure 4.15. However, the deviation in driving modes between the MT-based cycle and the NN method is smaller.

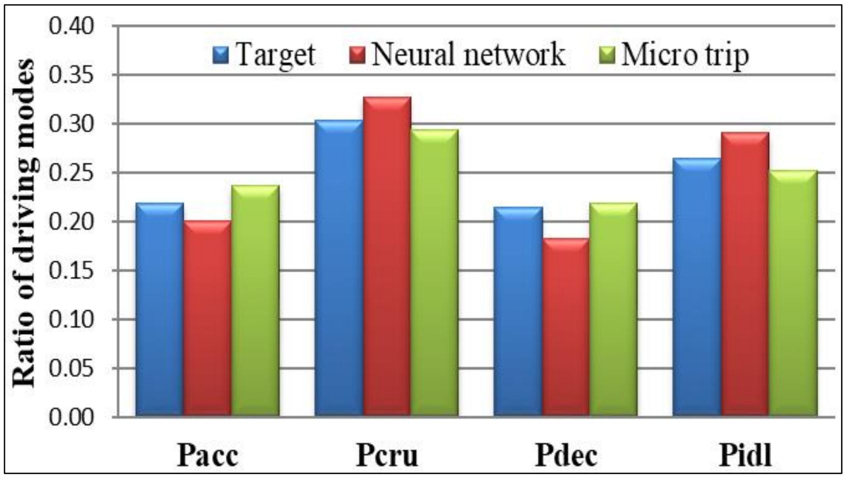

Figure 4.15: Comparison of driving modes characteristics

In terms of all characteristic parameters, the DC generated by NN prediction generally aligns more closely with the experimental data than the DC developed using the MT approach. Additionally, with the exception of the average deceleration (Dec_{avg}) of the MT approach, all CPs of DCs generated by NN and MT were within the threshold. The DC generated by NN prediction exhibits lower deviations than the DC generated with the MT approach, as indicated in Table 4.10; the relative differences (RD) are 0.056 and 0.111 respectively.

Table 4.10: The relative difference of CPs between the target and developed DCs

CPi	Target	NN		MT	
		AADC	RDi	DC	RDi
V_{max}	120	117.67	0.019	109	0.092
V_{avg}	18.064	16.495	0.087	21.247	0.131
Vd_{avg}	23.241	23.242	0.001	27.476	0.141
Acc_{max}	3.456	3.44	0.005	3.056	0.116
Dec_{max}	-4.399	-4.5	0.023	-4.469	0.016
$PAcc_{avg}$	0.338	0.355	0.05	0.304	0.15
Dec_{avg}	-0.491	-0.47	0.043	-0.398	0.338
P_{acc}	0.218	0.2	0.084	0.236	0.083
P_{cru}	0.303	0.327	0.078	0.295	0.033
P_{dec}	0.214	0.182	0.128	0.218	0.018
P_{idl}	0.264	0.29	0.099	0.251	0.045
	RD		0.056		0.111

As the results indicate, the NN prediction approach proposed in this study significantly enhances the representativeness of DCs and addresses the issues regarding the determination of DC duration and the limited representativeness of the MT method. However, (Zhao et al., 2021) initially decided to have a DC duration of between 1200 s and 1300 s, and two DCs were developed that have a duration of 1216 s and 1261 s. (Peng et al., 2015) defined the duration of the designed DC as 1200 s. Similarly, a study by (Guo et al., 2020) decided on a DC duration of 1200 s, while (Tong & Ng, 2020) randomly constituted a DC until the required cycle duration was achieved.The trip method proposed in this study served as the foundation for determining the DC duration. In this study, a machine classification learner was applied to classify trips, and the NN clustering method had better performance accuracy than the other approaches. However, the studies by (Guo et al., 2020; Ji et al., 2018; Peng et al., 2015; Zhou et al., 2017) applied the k-means clustering algorithm to the principal component score to classify the driving sequences into different clusters.

After comparing the DC developed using NN method with the DC developed using the MT method and the collected driving data, it was determined that the NN-based DC best represents the driving patterns of AA urban road conditions including the AAE. Therefore, this NN-based DC shown in Figure 4.10 was chosen for the subsequent sections of this study and is referred to as the Addis Ababa driving cycle including Addis-Adama Expressway (AADC).

4.1.4. Comparison of AADC with standard DCs

An analysis was conducted to compare the characteristic parameters of the FTP-75, WLTC, CLTC, and collected data with the AADC produced in this study (Table 4.11). The results demonstrate that the DC duration problem was resolved by the approach proposed in this study. AADC, WLTC, FTP-75, and CLTC had relative differences of -0.056, 0.528, 0.398, and 0.344, respectively, compared to the collected data in this study. This indicates that, in terms of all distinctive criteria considered in this study, the AADC generated in this study better fits the actual road and traffic conditions in AA and AAE when compared to current standard DCs used by other countries. Furthermore, the generated AADC's characteristic parameters are more representative since they are closer to the data sources. Compared to standard DCs, the AADC developed in this study exhibited significantly longer idle times and much higher acceleration and deceleration rates. Prolonged periods of idle time were observed in the AADC due to frequent vehicle stops and movements caused by traffic congestion and closer traffic light signals. In comparison to the WLTC, FTP-75, and CLTC, the developed AADC has a shorter trip length (11.885 km) but a comparatively longer duration (2594 s).

Table 4.11: Comparison of the developed AADC with standard DCs

CPi	Target	AADC	RDi	WLTC	RDi	FTP-75	RDi	CLTC	RDi
V_{max}	120	117.67	0.019	131.31	0.094	91.25	0.240	114	0.050
V_{avg}	18.064	16.495	0.087	46.5	1.574	33.89	0.876	28.96	0.603
V_{davg}	23.241	23.242	0.001	53.15	1.287	25.82	0.111	37.15	0.599
Acc_{max}	3.456	3.44	0.005	1.75	0.494	1.48	0.572	1.47	0.575
Dec_{max}	-4.399	-4.5	0.023	-1.5	0.659	-1.48	0.664	-1.47	0.666
$PAcc_{avg}$	0.338	0.355	0.05	0.42	0.243	0.51	0.509	0.45	0.331
Dec_{avg}	-0.491	-0.47	0.043	-0.44	0.104	-0.58	0.181	-0.49	0.002
P_{acc}	0.218	0.2	0.084	0.309	0.417	0.311	0.427	0.286	0.312
P_{cru}	0.303	0.327	0.078	0.278	0.083	0.247	0.185	0.228	0.248
P_{dec}	0.214	0.182	0.128	0.286	0.336	0.271	0.266	0.264	0.234
P_{idl}	0.264	0.29	0.099	0.127	0.519	0.172	0.348	0.221	0.163
RD			0.056		0.528		0.398		0.344

4.2. Emissions inventory and FC results

4.2.1. The chassis dynamometer's emissions and FC test results

Comparing the test to on-road emission testing, the CD offers a reproducible method for emission testing while also being quicker and less expensive. Moreover, testing on a CD is a common procedure with good accuracy that can be useful for comparing the performance of various automobiles.

The AADC and the WLTC were both used in this study to measure the FC, CO_2, CO, and NOx for PCs on a CD in Uppsala, Sweden. WLTC and AADC were used as comparison DCs for the Gasoline (Toyota corolla) and diesel (Hyundai) vehicle types. The selection of vehicles was based on what was commonly available in AA, Ethiopia. The obtained emission factors are shown in Table 4.12 for the average of three trial measurements. Additionally, the results of emissions and FC from CD tests, including error bars, are shown in Figure A2 under Appendix A. The CO emissions for gasoline vehicles were overestimated by 41.17% when using the WLTC compared to the AADC. In contrast, the CO emissions for diesel vehicles were underestimated by 30.43% when using the WLTC compared to the AADC. Regarding CO_2 emissions, the WLTC method underestimated the values by 21.84% for gasoline vehicles and

18.89% for diesel vehicles, compared to the AADC. The WLTC underestimated FC by 21.78% for gasoline vehicles and 17.5% for diesel vehicles, compared to the AADC. The WLTC method also underestimates NO_X emissions by 9% for gasoline vehicles and 19.79% for diesel vehicles. For understudied PCs, WLTC underestimates CO_2, EC, and NO_X by 20.43%, 19.84%, and 18.76%, respectively, and CO is overestimated by 34.54% compared to AADC.

The AADC more accurately the driving conditions of AA and the AAE compared to the WLTC, as evidenced by the emissions and FC results from experimental findings. Consequently, considering the local weather and fuel specifications of AA, we chose to use the AADC to simulate the annual emissions level and FC of PVs in the study area.

Table 4.12: Emission factors results from chassis dynamometer

Measured parameters	Fuel type	AADC	WLTC
CO (g/km)	Petrol	0.68	0.96
	Diesel	0.069	0.048
	Total	0.375	0.504
CO_2 (g/km)	Petrol	213.68	167.01
	Diesel	195.43	158.5
	Total	204.55	162.75
FC (litters/100km)	Petrol	8.72	6.82
	Diesel	6.74	5.56
	Total	7.74	6.19
NO_X (g/km)	Petrol	0.066	0.06
	Diesel	0.586	0.47
	Total	0.326	0.265

4.2.2. Emissions level and FC results from different routes

This study utilized COPERT to assess the emissions and energy consumption of hybrid vehicles along with gasoline and diesel PVs to demonstrate to policymakers how the hybrid car reduces emissions and energy consumption compared to conventional cars. Additionally, this study determined the amounts of FC and emissions for various road types under the AADC and WLTC for comparison. According to the AADC, the shares of congested urban, urban, rural, and highway distances were 28.61%, 18.31%, 44.2%, and 8.88%, respectively. The FC and emission levels derived from AADC were significantly dissimilar from those of WLTC, as indicated in Figures 4.16 to 4.22.

Figure 4.16 illustrates the COPERT estimation of annual CO emissions from vehicles for the year 2022 in metric tons per year per vehicle. In the AADC, congested urban (56.97%) was associated with the highest total CO emission levels, followed by urban (36.38%), rural (5.54%), and finally, highway routes (1.12%). However, in the WLTC scenario, urban driving (52.29%) was where a significant amount of CO was discovered, followed by congested urban (34.18%), highway (8.65%), and then the rural route (4.89%). When the entire route is considered, diesel and hybrid vehicles release more emissions under AADC than WLTC, while gasoline vehicles release more emissions under WLTC. In urban areas, a cold start can affect a vehicle's overall CO emissions (Weiss et al., 2017) and it is also more susceptible to high speeds (Alves et al., 2015).

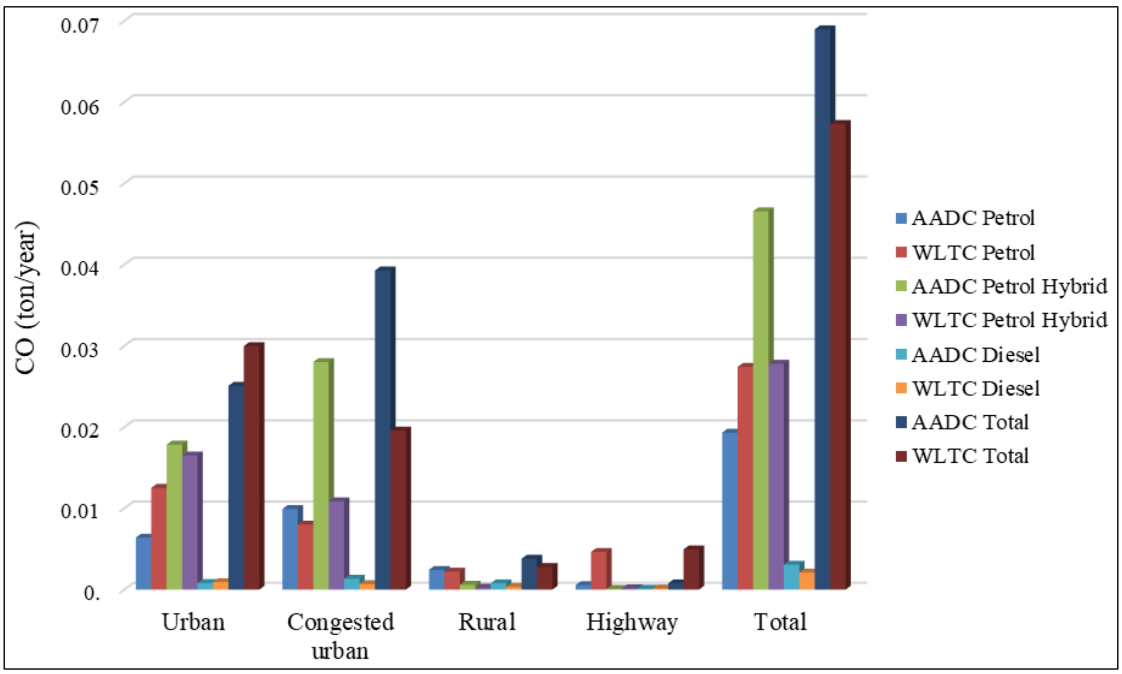

Figure 4.16: Annual CO emission levels for various routes

Figure 4.17 displays the COPERT estimation of CO_2 emissions from vehicles for the year 2022 in metric tons per year per vehicle. In the AADC, petrol vehicles release the most CO_2 at 2.44 metric tons per year per vehicle, followed by rural areas with emissions of 2.06 metric tons per year per vehicle, urban areas at 1.35 metric tons per year per vehicle, and highways at 0.37 metric tons per year per vehicle. Under the WLTC, petrol vehicles emit the greatest CO_2 on highways at 1.52 metric tons per year per vehicle, followed by rural areas at 1.24 metric tons per year per vehicle, urban areas at 1.16 metric tons per year per vehicle, and congested urban areas at 0.94 metric tons per year per vehicle.

For diesel vehicles, the highest CO_2 emissions occur in congested urban areas at 3.09 metric tons per year per vehicle, followed by rural areas at 3.01 metric tons per year per vehicle, urban areas at 1.73 metric tons per year per vehicle, and highways at 0.56 metric tons per year per vehicle. In the WLTC drive cycle, the greatest CO_2 emissions from diesel vehicles are observed on highways at 2.17 metric tons per year per vehicle, followed by rural areas at 1.86 metric tons per year per vehicle, urban areas at 1.59 metric tons per year per vehicle, and congested urban areas at 1.22 metric tons per year per vehicle.

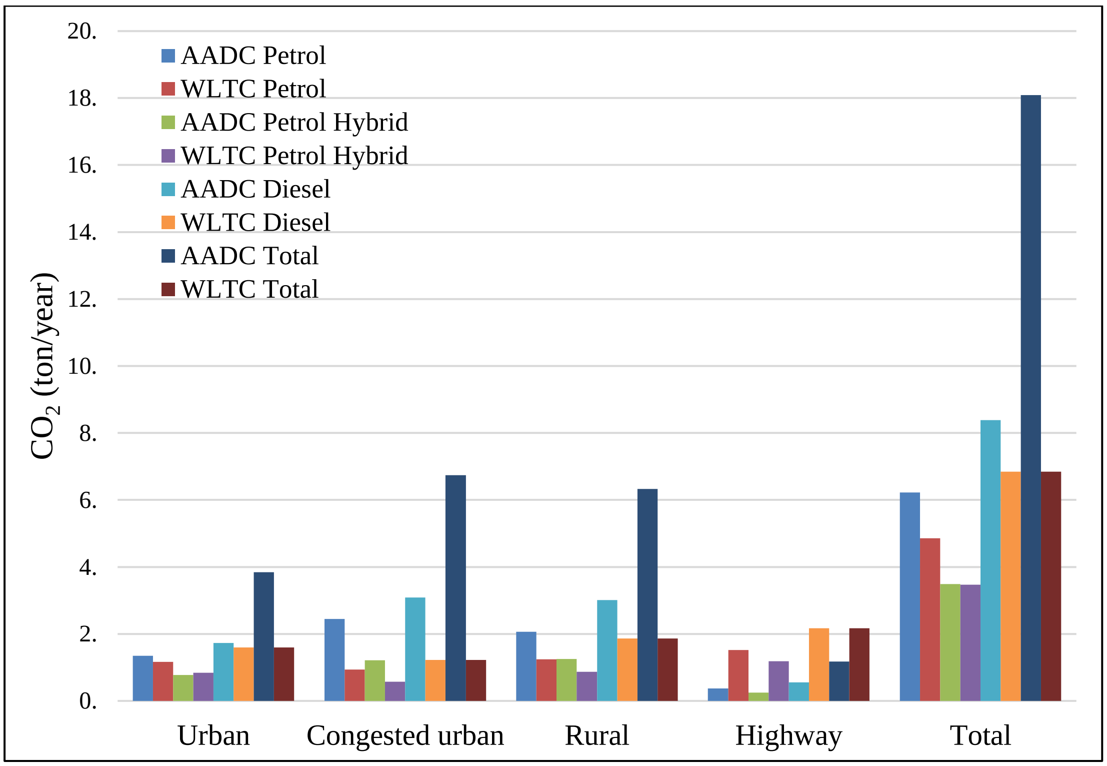

Figure 4.17: Annual CO_2 emission levels for various routes

In the AADC, petrol hybrid vehicles release the most CO_2 in congested urban areas, with 1.21 metric tons per year per vehicle. Rural areas release 1.25 metric tons per year, followed by urban areas at 0.77 metric tons per year per vehicle and highways at 0.25 metric tons per year. In the WLTC, the highest CO_2 emissions are in rural areas at 0.87 metric tons per year per vehicle, followed by urban areas at 0.84 metric tons per year per vehicle, highways at 0.57 metric tons per year per vehicle, and congested urban areas at 0.57 metric tons per year per vehicle. Under both WLTC and AADC, hybrid vehicles emit roughly the same amount of CO_2 when considering the entire route, but gasoline and diesel vehicles emit more CO_2 under AADC than WLTC. In comparison to a gasoline-powered vehicle, a hybrid vehicle reduces CO_2 gas by 43.95% for the AADC. This indicates a highly significant impact on GHG reduction. The predominant factor contributing to the highest CO_2 emissions share in congested urban areas under the AADC was primarily attributed to frequent stops at traffic lights, slow driving speeds, rapid acceleration at low speeds, and frequent driving within congested traffic zones. This finding is consistent with the study conducted by (Alves et al., 2015 which also identified frequent stops and high accelerations as factors contributing to increased CO_2 emissions.

Figure 4.18 illustrates the COPERT estimation of annual FC from vehicles for the year 2022 in liters per year per vehicle. Driving on rural (34.95%), urban (21.27%), and highway (6.5%) routes were associated with lower FC levels for AADC while driving in congested urban areas (37.29%) was associated with the highest FC levels. In the WLTC scenario, highway driving (31.66%) had the highest FC, followed by rural areas (27.2%), urban areas (23.29%), and finally congested urban areas (17.85%). When considering the entire route, hybrid vehicles consume roughly the same amounts of energy under both WLTC and AADC. The FC of diesel and gasoline vehicles decreased by 21.83% and 18.38%, respectively, under WLTC as compared to AADC. In comparison to AADC, WLTC underestimated FC by 22.34% when considering the entire route and all vehicles. The energy consumption of the hybrid vehicle was also 44% lower than that of a gasoline-powered vehicle. Despite covering less distance than rural routes, congested urban routes in AA tend to consume more fuel than other routes. This is primarily caused by frequent stops, slow average driving speeds, and fast acceleration at low speeds. FC can also be considerably influenced by a cold start in urban areas (Weiss et al., 2017).

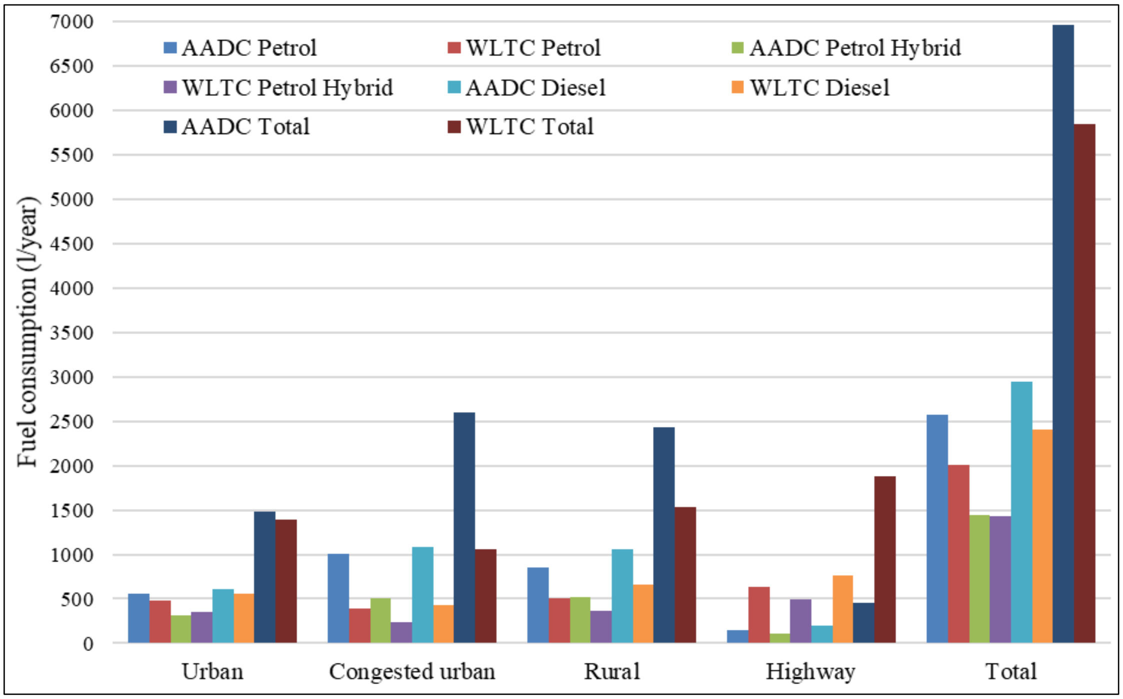

Figure 4.18: Annual FC for various routes

Figure 4.19 depicts the COPERT-based estimation results of annual NO_X emissions for the year 2022 in metric tons per year per vehicle. Driving in congested urban peak hours (38.19%) was found to be associated with the highest NO_X gas levels, while driving on rural (33.72%), urban (22.13%), and highway (5.96%) routes were found to be associated with the lowest NO_X gas levels, for AADC. In the WLTC scenario, the concentration of NO_X was highest along the highway (31.63%), followed by rural areas (26.59%), urban areas (23.17%), and finally congested urban areas (18.61%). When considering the entire route, hybrid vehicles emit 11.39% more NO_X under WLTC than AADC. Diesel and gasoline vehicles emit 15.33% and 21.34% less NO_X under WLTC than under AADC, respectively. WLTC underestimated NO_X emissions by 33.4% compared to the AADC when considering the entire route and all vehicles. As a result of frequent stops and high acceleration in congested urban areas, the engine temperature increases, which is one of the main reasons for the highest share of NO_X emissions in congested urban areas of AA. Studies by (Alves et al., 2015) indicated that frequent stops and high acceleration cause NO_X emissions to increase.

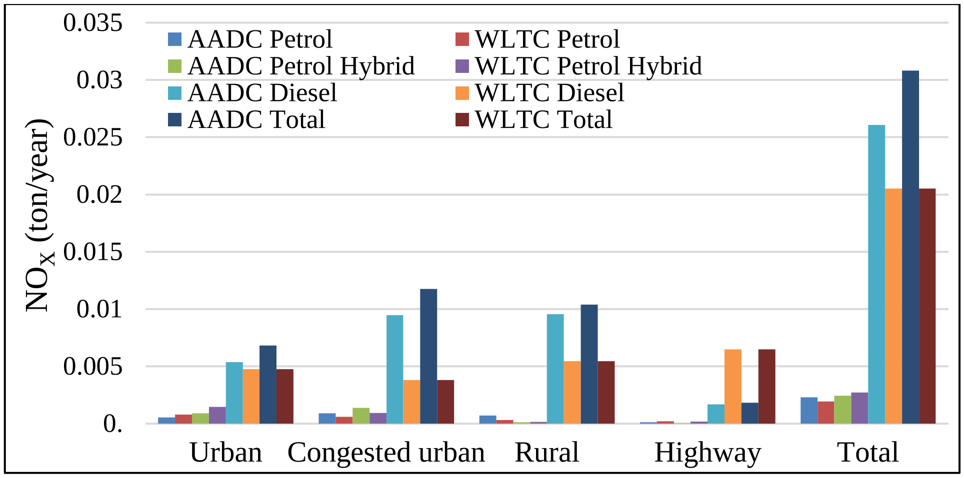

Figure 4.19: Annual NO_X emission levels for various routes

In this study, road, brake, and tire wear were considered in non-exhaust PM estimation. Figures 4.20 and 4.21 displays the COPERT-based annual PM2.5 and PM10 emissions for 2022 in kilograms per year per vehicle. The AADC cycle results in higher PM2.5 and PM10 emissions than the WLTC cycle for all vehicles under consideration. In comparison to the AADC, the WLTC underestimated PM10 emissions by 26% and PM2.5 emissions by 67% when considering the entire route and all vehicles. The highest contributions of PM2.5 and PM10, 44.27% and 44.47%, respectively, came from rural areas.

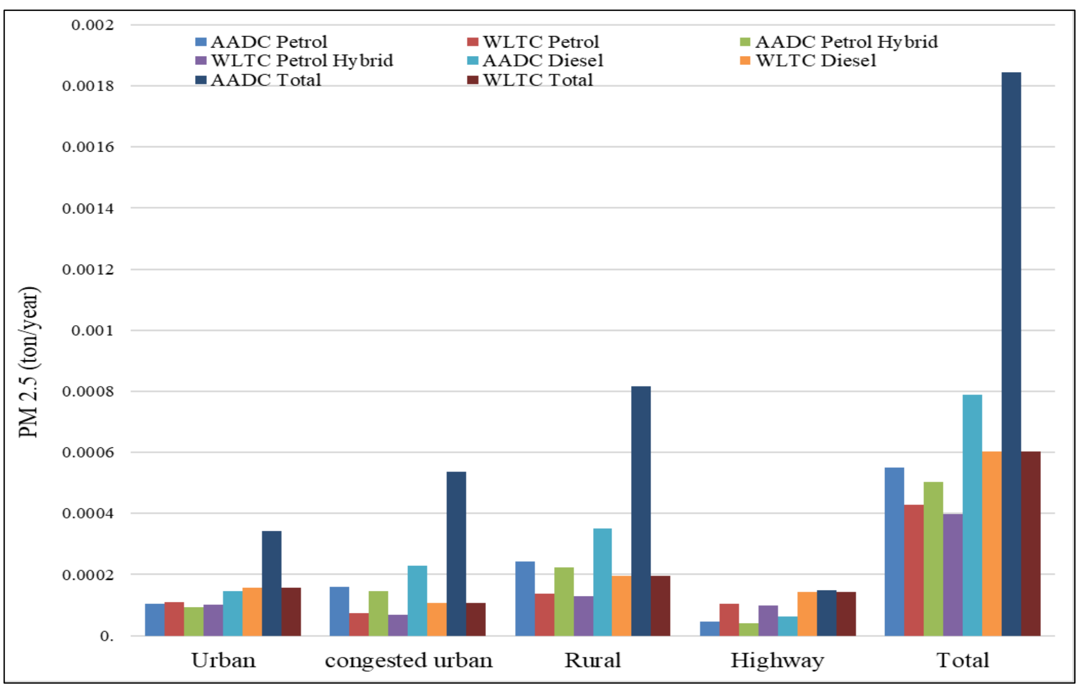

Figure 4.20: Annual PM2.5 emission levels for various routes

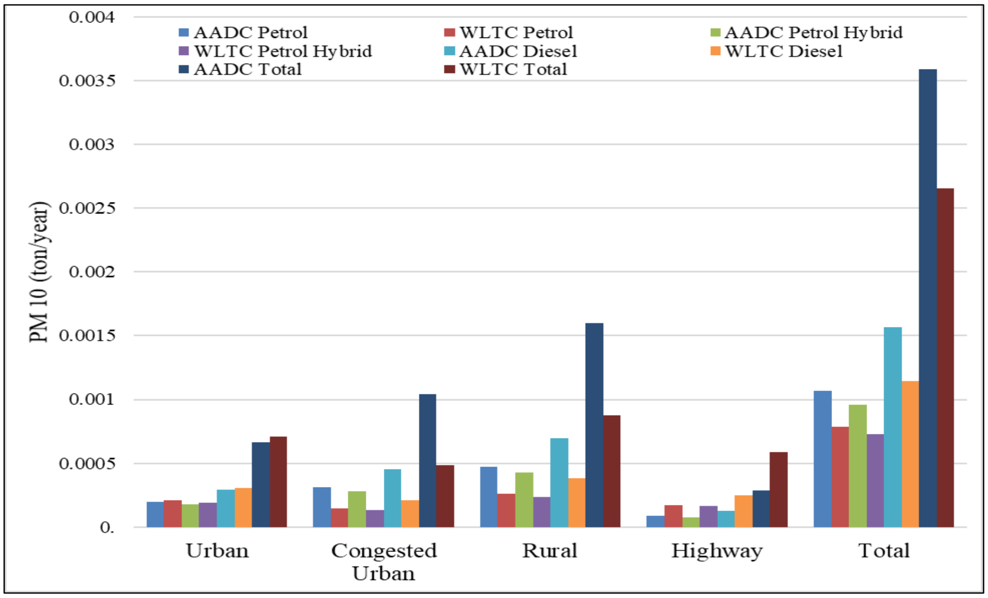

Figure 4.21: Annual PM10 emission levels for various routes

Estimation of volatile organic compounds (VOCs) takes into account hot, cold, and evaporative emissions, with diesel vehicles not included in this analysis. Determining the trend in VOC emissions becomes challenging when diesel engines are considered, and the amount is also negligible (Alves et al., 2015). Figure 4.22 shows VOC emissions in tons per year per vehicle for each route and DC. When considering the entire route for gasoline, and hybrid vehicles, the WLTC underestimated VOC emissions by 18.9% compared to the AADC. Under AADC, 96.94% of the total VOC was concentrated in urban and congested urban areas, while the contribution of rural and highway areas to the total VOC was insignificant.

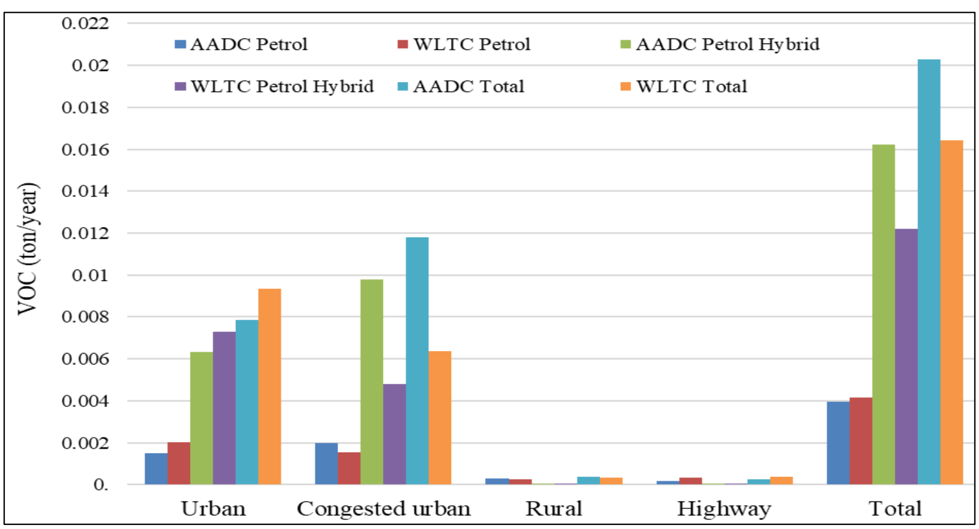

Figure 4.22: Annual VOC emission levels for various routes

To assess the representativeness of the DC developed in this study, we employed the COPERT model to compare the FC and emissions of vehicles under two different DCs configurations: the WLTC and the AADC developed in this study. This comparative analysis aimed to determine how well the standardized WLTC and the locally-developed AADC reflect the actual driving emissions and FC observed in AA urban roads and on the AAE. The results of this comparison are presented in Table 4.13. Based on these findings, the study recommends that when estimating the road transportation emissions of passenger vehicles in this study sites, the emission and FC factors derived from this analysis shall be utilized.

Table 4.13: A comparison of emissions and FC factors based on the COPERT model

Estimated parameters	Fuel type	AADC	WLTC
CO (g/km)	Petrol	0.6712	0.9518
	Petrol Hybrid	1.6169	0.9653
	Diesel	0.0711	0.0487
	Total	0.6842	0.5686
CO2 (g/km)	Petrol	215.9289	168.755
	Petrol Hybrid	121.0153	120.489
	Diesel	194.1663	158.4736
	Total	179.4839	150.5584
EC (liter/100km)	Petrol	8.93	6.98
	Petrol Hybrid	5.00	4.98
	Diesel	6.82	5.57
	Total	6.93	5.85
NOX (g/km)	Petrol	0.0796	0.0674
	Petrol Hybrid	0.0846	0.0943
	Diesel	0.6037	0.4748
	Total	0.3056	0.2497
PM 2.5 (g/km)	Petrol	0.0192	0.0149
	Petrol Hybrid	0.0175	0.0138
	Diesel	0.0183	0.0139
	Total	0.0183	0.0142
PM 10 (g/km)	Petrol	0.0371	0.0274
	Petrol Hybrid	0.0333	0.0252
	Diesel	0.0362	0.0265
	Total	0.0356	0.0264
VOC (g/km)	Petrol	0.1375	0.1451
	Petrol Hybrid	0.5633	0.4238
	Total	0.2011	0.1631

4.2.3. Discussions of emissions inventory and FC

Previous studies also revealed that standard DCs tended to underestimate emissions and FC when compared to local DCs, this study supports these findings. The study by (Zhang et al., 2021) found that the Guangzhou drive cycle's FC, NOx, and CO were, respectively, 1.34, 1.24, and 1.32 times greater than those of the WLTC. Local DC-based simulations of HC, CO, and NOx emissions were, respectively, 155%, 63%, and 64% larger than WLTC-based simulations, according to a study done in India by (Pathak et al., 2016). In comparison to the European DC, Singapore's DC had 5, 5, 8, 22, and 47% higher FC, CO_2, CO, HC, and NO_X emissions (Ho et al., 2014). In general, due to its high average velocity, the WLTC had the lowest overall emissions (Zhang et al., 2021) due to better road infrastructure and less traffic congestion. Emissions and FC rates rose due to the vehicle's low speed, frequent stops, and high instantaneous speed variability (Tamsanya & Chungpaibulpatana, 2009). The emissions factor findings from the COPERT model and the CD showed a significant difference. We believe that the absence of cold start operation in the CD is the main cause of this discrepancy; this explanation is consistent with (Alves et al., 2015) findings who found that the absence of cold start emissions could lead emission inventories to understate emissions.

According to the AADC, the shares of congested urban, urban, rural, and highway distances were 28.61%, 18.31%, 44.2%, and 8.88%, respectively. Congested urban routes have higher FC and CO, CO_2, NO_X, and VOC emissions than other routes, regardless of covering less distance than rural ones. In our opinion, frequent stops, slow average driving speeds, and higher acceleration at low speeds were the main causes of this. NO_X and CO_2 emissions are sensitive to frequent stops and high accelerations, whereas CO emissions are more vulnerable to high speeds, according to (Alves et al., 2015). A cold start can have a substantial influence on a vehicle's overall emissions and fuel usage in urban areas (Weiss et al., 2017). In the congested urban areas of AA, driving results in emissions of 56.25% CO, 37.28% CO_2, 38.19% NO_X, 58.25% VOC, 29% $PM_{2.5}$, and PM_{10}, and 37.29% energy consumption. In the case of AA, traffic congestion occurs due to several factors, including the driving culture of the drivers, the absence of proper stations for passengers to board and disembark, drivers stopping abruptly to drop off or pick up passengers without regard for the vehicles behind them, the presence of unnecessary turning points, and a lack of knowledge among some traffic police officers on how to manage crossroads effectively. To reduce road vehicle emissions in congested urban areas, the AA city administration must take corrective actions which reduce traffic congestion. These measures may include installing a smart traffic lighting system, improving access to public transportation, enhancing road infrastructure, imposing road use fees for private vehicles, scheduling shifts for even and odd license plate numbers, introducing bridges and flyovers for crossroads, and providing pedestrian underpasses beneath bridges or flyovers. The second area that needs more attention in terms of total emissions and FC is driving in rural areas. This accounts for 34.95% of fuel use, 34.97% of CO_2, 33.72% of NO_X, and 44% of $PM_{2.5}$ and PM_{10} emissions. Based on our observations in the area, we believe that raising the speed limit here would reduce emissions. In general, driving in congested urban and rural areas contributes to 60% to 73% of all emissions and FC. Focusing efforts on these areas would be crucial for the city administrator of AA to effectively decrease air pollution from PVs.

4.3. On-road emissions test results

4.3.1. General Factorial Regression for CO_2

The main effect and interaction plot of CO_2 emissions for petrol and diesel vehicles at different road grades are shown in Figures 4.23 and 4.24. The average CO_2 on-road emissions test results for gasoline and diesel vehicles, including the standard error, are presented in Table G1 under Appendix G, and this data is based on three trial measurements. In Figure 4.23, a main effect plot is depicted, showing the mean response of CO_2 emissions on the y-axis. This mean is calculated by averaging the responses for each level of the speed factor across all levels of the slope factor. Conversely, the mean response for each level of the slope factor is determined by averaging across all levels of the speed factor. Usually, a road's gradient increases the average CO_2 emissions drastically. Road gradients of 2°, 4°, and 6° resulted in CO_2 emissions rates for gasoline-powered vehicles were 16.25%, 28.58%, and 43.36% greater, respectively, than the flat road. According to the results shown in Figure 4.23a, a gasoline-powered vehicle traveling at 40 km/h produced the least amount of CO_2. At this speed, the engine operates at its most efficient point. The throttle position is relatively low, and the engine is able to maintain a consistent speed with minimal effort. This results in lower fuel consumption and, consequently, lower CO_2 emissions. Whereas for diesel vehicles the CO_2 emissions rate for road gradients of 2°, 4°, and 6° were 53.7%, 91.08%, and 245.85% respectively higher than the emission rates of level road, and 36% reduction in CO_2 was observed in downhill of -2°. According to this study, a diesel vehicle travelling between 20 and 30 km/h produced the least amount of CO_2. This is due to the diesel engine's increased efficiency at these speeds, which results in reduced CO_2 and FC. These changes were observed due to the CO_2 emissions rate having a strong correlation with FC (Meng et al., 2023). On routes with positive road grades, the vehicle requires more power, which results in increasing FC and CO_2 emissions. An engine's CO_2 emissions are influenced by the oxygen in the combustion chamber and its temperature (Gopal et al., 2014).

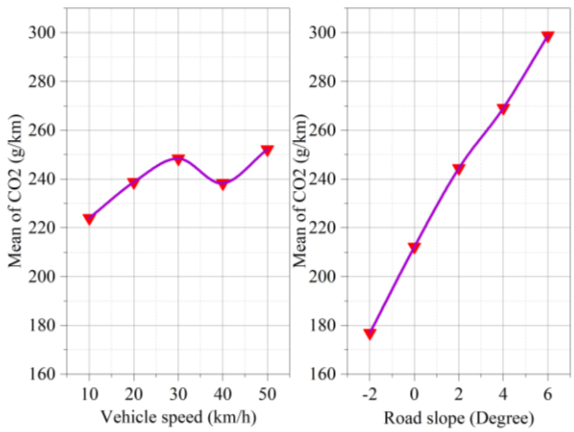

a. SI engine operated vehicle

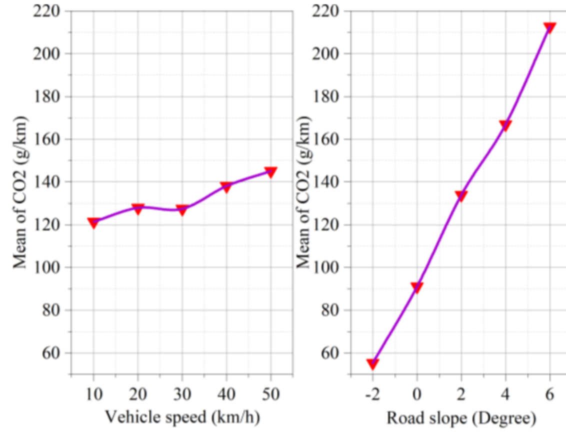

b. Diesel engine operated vehicle

Figure 4.23: Main effect plot for CO_2

This study demonstrates that gasoline-powered vehicles emit the highest amount of CO_2 when traveling at 30 km/h, as compared to speeds of 10, 20, 40, and 50 km/h on both level and downhill roads with a gradient of -2° (Figure 4.24a). This indicates that during downhill driving at 30 km/h on a -2° slope or on level roads, the engine operates at a lower gear with higher engine RPM, resulting in higher CO_2 output. Nevertheless, when the vehicle speed is less than 30 km, the engine RPM should be near idle, lowering CO_2 and FC at lower speeds. With increasing vehicle speed beyond 30 km/h on -2° slopes and on level roads, CO_2 production decreases due to increased engine RPM, resulting in the engine operating within a lower efficiency range. Furthermore, for gasoline vehicles on road slopes of 2 and 4 degrees, the peak CO_2 emission occurred at 50 km/h, in contrast to speeds ranging from 10 km/h to 40 km/h. On a 6-degree road slope, the peak CO_2 emission was observed at 20 km/h, comparing to speeds of 10, 30, 40, and 50 km/h. The study found that CO_2 emissions of diesel vehicles (Figure 4.24 B) on a -2 degree road slope remained relatively constant across speeds from 10 to 50 km/h. The lowest emissions were recorded at 20 km/h on level roads, while the lowest were at 30 km/h on a 2-degree road slope. Higher driving speeds increased CO_2 emissions on a 4-degree road slope, while inconsistencies were observed on a 6-degree road slope.

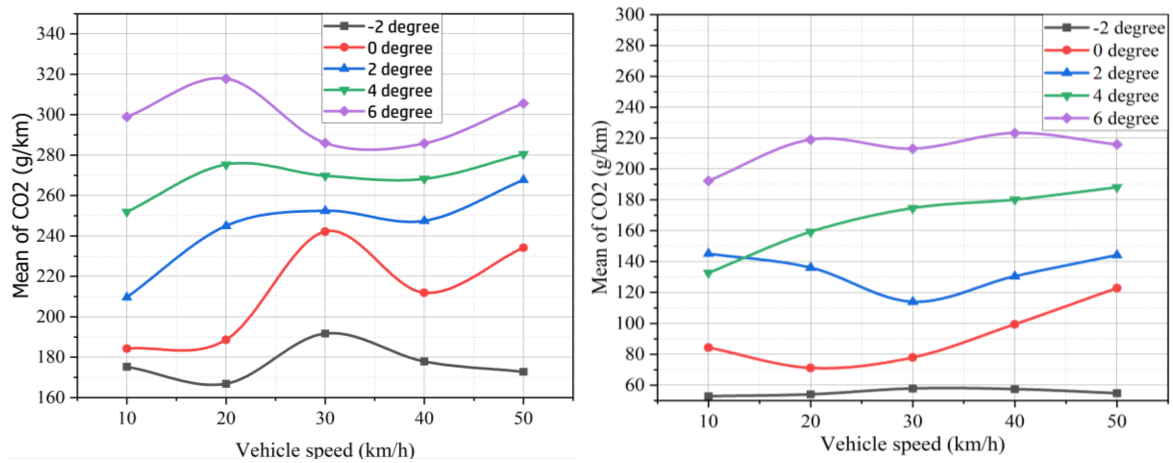

a. SI engine operated vehicle b. Diesel engine operated vehicle

Figure 4.24: Interaction plot for CO_2

Minitab 21 was utilized to conduct regression analysis with a 95% confidence level. Equations 4.1 and 4.2 present the fitted regression equations for CO_2 emissions of petrol and diesel vehicles, respectively.

$$CO_2(g/km) = 189.77 + 0.682 \times V + 16.89 \times G - 0.0615 \times V \times G \quad 4.1$$

$$CO_2(g/km) = 79.1 + 0.461 \times V + 17.82 \times G - 0.0571 \times V \times G \quad 4.2$$

Where V is vehicle speed in km/h, and G is road slope in degree (°)

The R-square (R-sq) shows how much the regression model contributes to the explanation of variability. R-sq values close to 1 suggest that most of the dependent variables are sufficiently explained by the regression model. Table 4.14 displays the values of R-sq and adjusted R-sq, indicating that the model findings for both petrol and diesel vehicles had the highest levels of accuracy and precision. From these findings, it can be observed that the regression models formulated for gasoline and diesel vehicles are dependable approaches for predicting CO_2.

Table 4.14: Model Summary for CO_2, CO, and HC

Emissions	Vehicle	R-sq (%)	R-sq (adj) (%)	R-sq (pred) (%)
CO_2	Gasoline	99.98	99.97	99.96
	Diesel	96.03	95.47	94.48
CO	Gasoline	99.89	99.84	99.76
	Diesel	85.91	83.9	76.15
HC	Gasoline	96.65	95.04	92.46
	Diesel	73.12	72.57	70.63

For both petrol and diesel vehicles, the Pareto chart in Figure 4.25 shows that both vehicle speed and road slope passed the red dotted line at a 95% confidence interval, suggesting that both variables are relevant for influencing CO_2 emissions. Furthermore, the Pareto chart demonstrated that road slope has a bigger impact on CO_2 formation than vehicle speed. Therefore, neglecting the effect of road slope during the determination of CO_2 emissions from vehicles will lead to incorrect estimations.

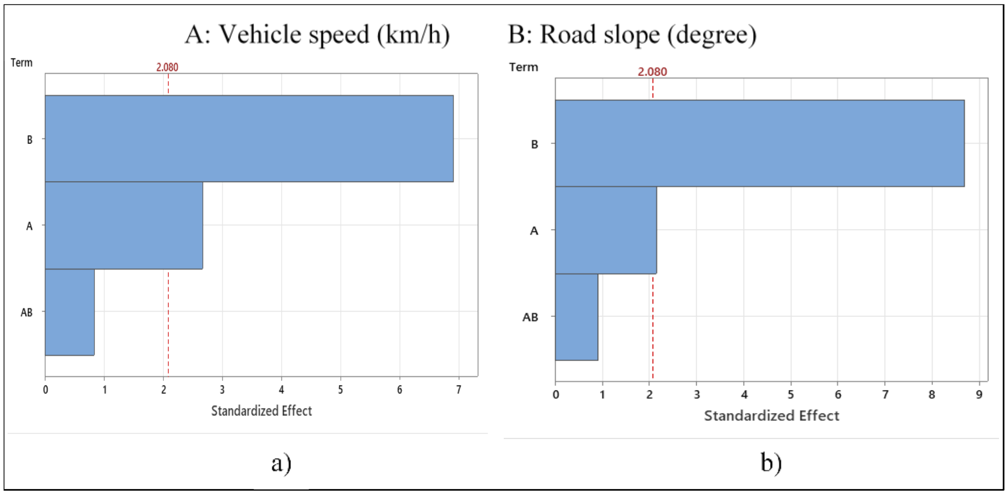

Figure 4.25: Pareto chart of the standardized effects of CO_2 for a) SI vehicle b) CI vehicles

As depicted in Figure 4.26, surface plots generated by Minitab 21 are utilized to examine the variations in CO_2 levels with road slope and vehicle speed for both petrol and diesel vehicles.

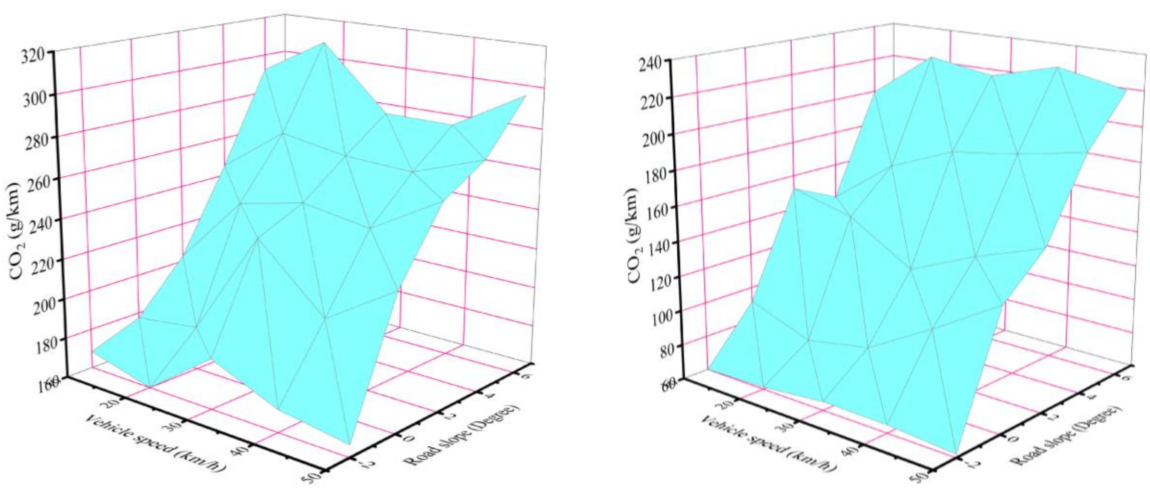

Figure 4.26: Surface plot of CO_2 emissions

4.3.2. General Factorial Regression for CO

Figures 4.27 and 4.28 illustrate the main and interaction effects of CO emissions levels for various road grades of the tested vehicles in this study. The average CO on-road emissions test results for gasoline and diesel vehicles, including the standard error, are presented in Table G1 in Appendix G. This data is based on three trial measurements. Figure 4.27 shows a main effect plot displaying the mean response of CO emissions across all speed factor levels and slope factor levels. Generally, the average CO emissions increase significantly as the road gradient increases and decrease as the vehicle speed increases. For petrol vehicles, the CO emissions level for roads with gradients of 2°, 4°, and 6° were respectively 37.76%, 168.47%, and 177.1% higher than the emission rates for roads with a level road, and a reduction of 10.27% was seen when driving downhill at a -2°. Whereas for diesel vehicles, the CO emissions level for roads with gradients of 2°, 4°, and 6° were 42.84%, 76.48%, and 104%, respectively, higher than the emissions level of a level road, and an 8.9% CO reduction was seen on downhill roads of -2°.

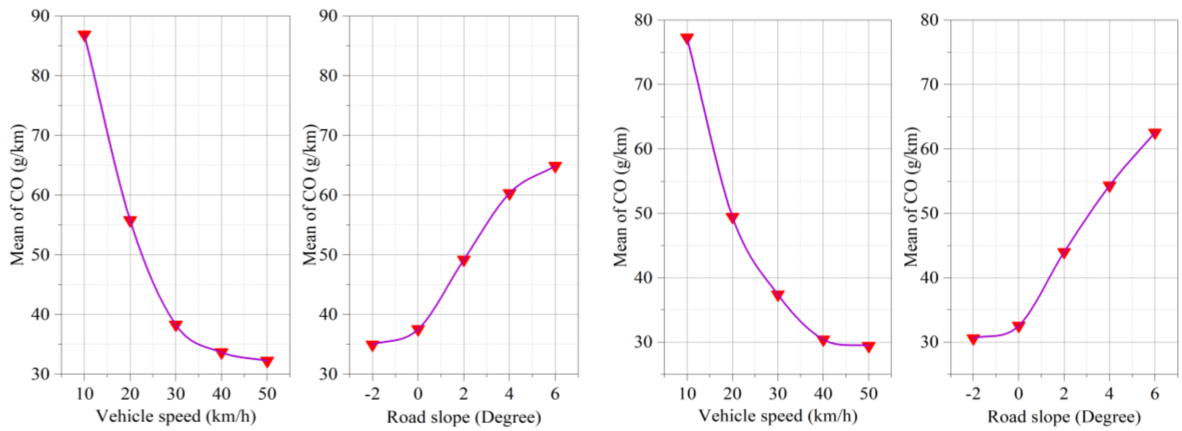

a. SI vehicle b. CI vehicle

Figure 4.27: Main effect plot for CO

The fitted regression analyses for CO emissions from petrol and diesel vehicles are presented in equations 4.3 and 4.4, respectively. Both the petrol and diesel vehicle regression equations exhibited the highest levels of accuracy and precision in the outcomes, as shown by the values of R-sq and adjusted R-sq in Table 4.14.

$$CO\ (g/km) = 77.83 + 1.224 \times V + 5.49 \times G - 0.0453 \times V \times G \qquad 4.3$$

$$CO\ (g/km) = 68.48 + 1.075 \times V + 5.38 \times G - 0.0367 \times V \times G \qquad 4.4$$

Where V is vehicle speed in km/h, and G is road slope in degree (°)

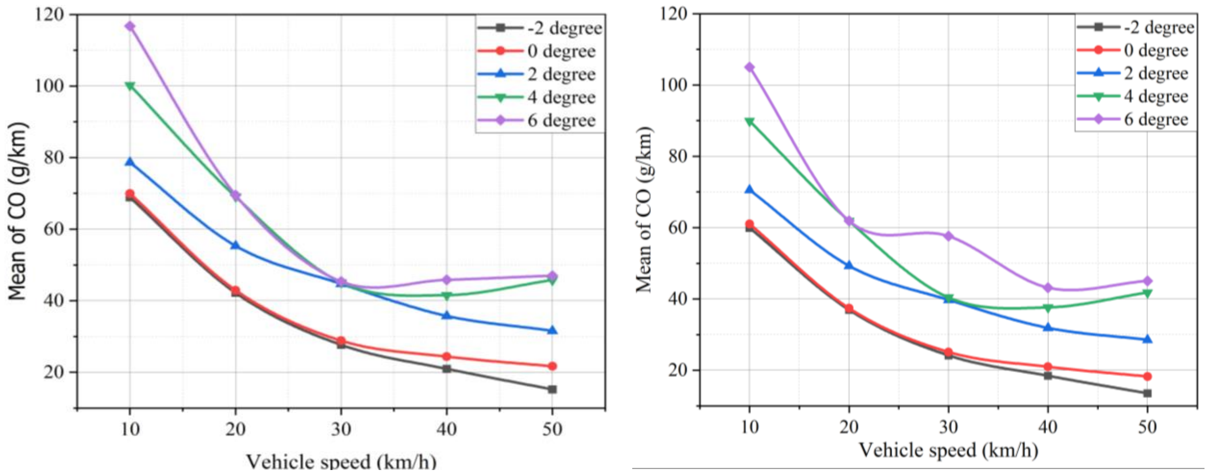

a. SI vehicle b. CI vehicle

Figure 4.28: Interaction plot for CO

The Pareto chart in Figure 4.29, for both petrol and diesel vehicles, indicates that road slope and vehicle speed have both surpassed the red dotted line at a 95% confidence interval, suggesting their significant relevance for estimating CO emissions. Therefore, ignoring the road gradient when estimating a vehicle's CO emissions would lead to inaccuracies. Additionally, Figure 4.30 displays the generated surface plots, illustrating the variation of CO with vehicle speed and road gradient. Thus, it can be stated that the established regression models are reliable methods for accurately determining CO emissions from vehicles operating on petrol and diesel fuel.

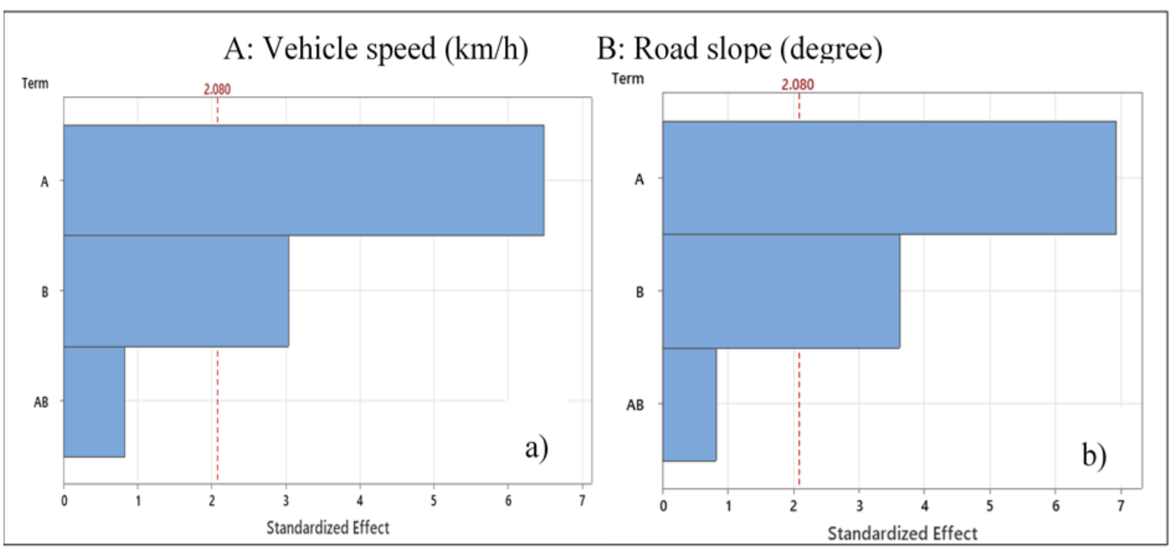

Figure 4.29: Pareto chart of the standardized effects of CO a) SI vehicle b) CI vehicles

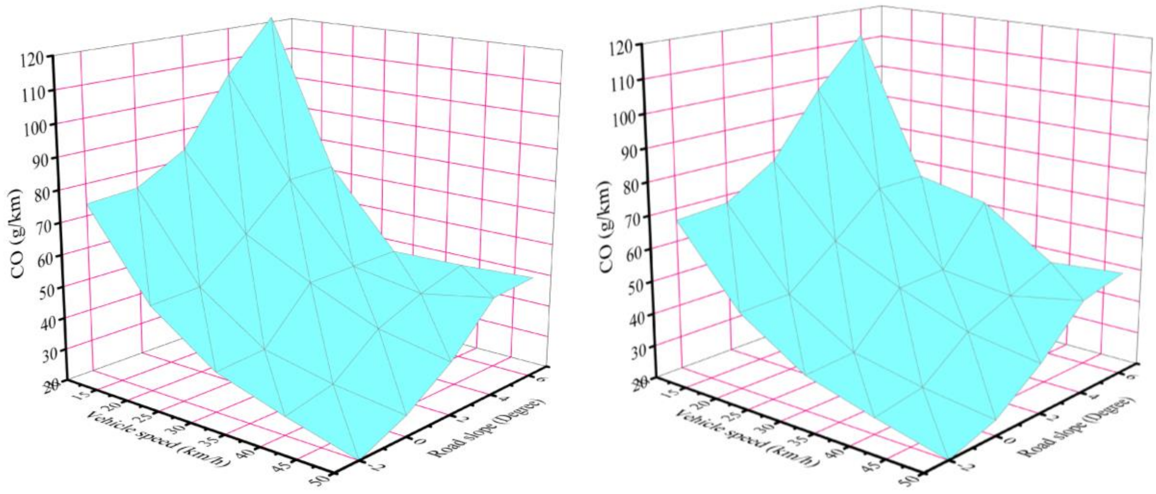

a. SI vehicle b. CI vehicle

Figure 4.30: Surface plot of CO emissions

4.3.3. General Factorial Regression for HC

Figures 4.31 and 4.32 display the HC emissions rate for petrol and diesel vehicles on various road slopes. The average HC on-road emissions test results for gasoline and diesel vehicles, including the standard error, are presented in Table G1 of Appendix G. This data is based on three trial measurements. Figure 4.31 shows a main effect plot displaying the mean response of HC emissions across all speed factor levels and slope factor levels. Lower HC emissions were observed for both petrol and diesel vehicles at 30 km/h. For petrol vehicles, the rate of HC emissions exhibited a declining pattern as the road slope ascended from level to 4° angles, with peak HC emissions noted at a 6° road slope. Conversely, for diesel vehicles, an increase in HC emissions rate was observed as the road slope rose from -2° to 4°, followed by a decrease as the slope increased further. The reduction in HC emissions rate for petrol vehicles at higher throttle angles is likely attributed to increased engine load, which decreases the amount of HC emissions (Xing et al., 2017). On the contrary, for diesel vehicles, the initial rise in HC emissions rate at a lower angle is likely due to reduced engine load (Liu et al., 2018), preventing the engine from reaching its optimal combustion temperature, and resulting in incomplete combustion and increased HC emissions (Wu et al., 2019). On a level road, the HC emissions rates for petrol vehicles on roads with slopes of -2 degrees, 2 degrees, and 4 degrees did not significantly differ, whereas traveling uphill at a 6° caused the HC emissions to increase by 27%. Similarly, for diesel vehicles' HC emissions rate on roads with gradients of -2° and 2° did not differ significantly compared with level roads, HC increased by 20.83% and 13.44% on 4° and 6° uphill routes, respectively. Figure 4.32 indicates that there is no consistent relationship between HC emissions and speed. A similar observation was noted by (Bokare & Maurya, 2013). However, unique characteristics were observed for HC emissions at 20 km/h on a 6° slope. This phenomenon occurred due to increased incomplete combustion processes and the utilization of a lower gear at this particular driving speed and road slope.

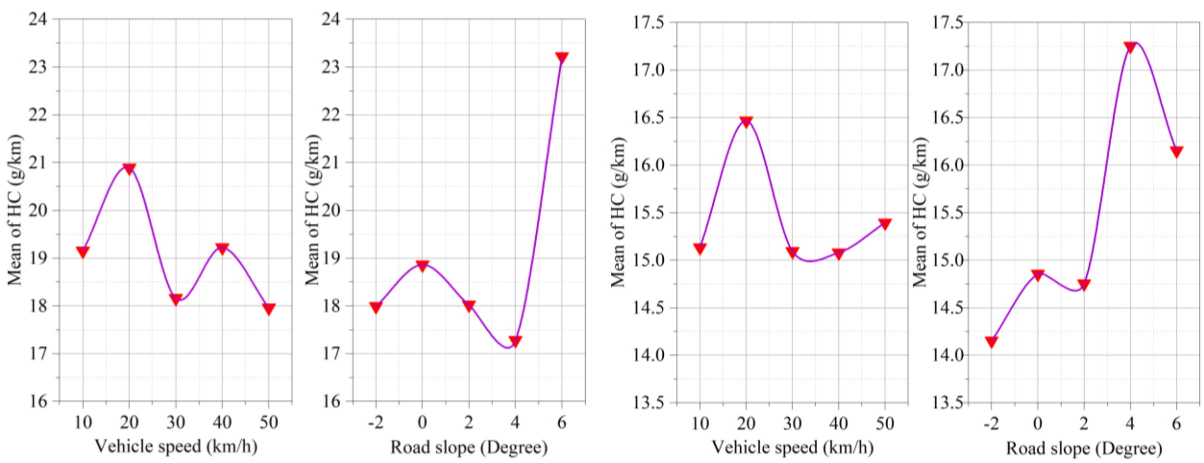

a. SI vehicle

b. CI vehicle

Figure 4.31: Main effect plot for HC

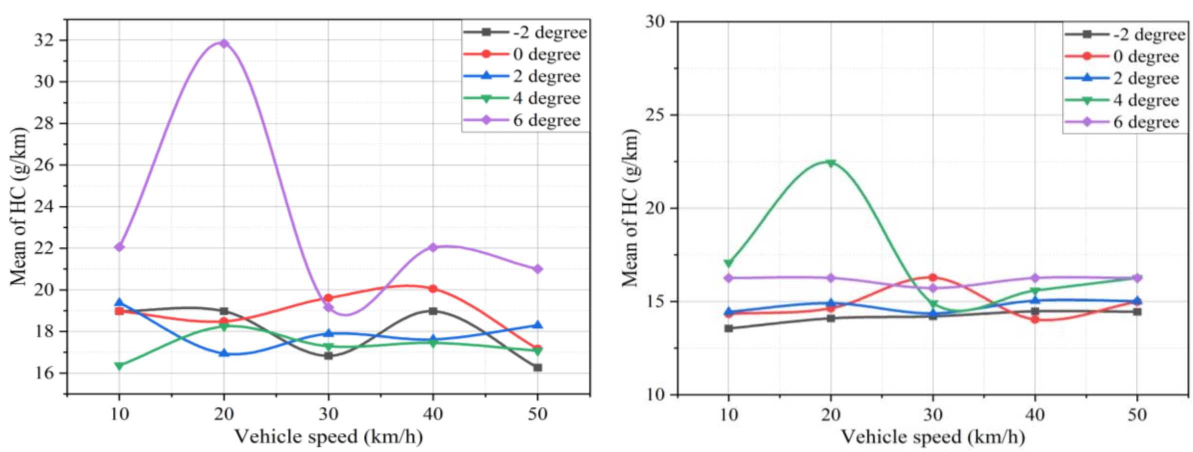

a. SI vehicle

b. CI vehicle

Figure 4.32: Interaction plot for HC

The regression models fitted for HC emissions for petrol and diesel vehicles are presented in equations 4.5 and 4.6, respectively. Table 4.14 demonstrates that the R-squared and adjusted

R-squared values for petrol and diesel vehicles indicated the highest levels of accuracy and precision.

$$HC\ (g/km) = 19.09 + 0.0302 \times V + 0.598 \times G - 0.00052 \times V \times G \qquad 4.5$$

$$HC\ (g/km) = 14.647 + 0.0049 \times V + 0.523 \times G - 0.00676 \times V \times G \qquad 4.6$$

Where V is vehicle speed in km/h, and G is road slope in degree (°)

4.3.4. Desirability functionality analysis (DFA)

In this study, following the full factorial analysis, the DFA was applied to the experimentally collected on-road data using Minitab 21 to determine the optimal driving speeds for urban roads to simultaneously reduce the formation of CO, HC, and CO_2. The solutions were derived from various tests carried out on different road gradients and vehicle velocities of the vehicles examined in this study. Table 4.15 presents the top three solutions obtained.

Table 4.15: Solutions of DFA

S/N	Speed (km/h)	Slope (°)	Average HC (g/km)	Average CO (g/km)	Average CO_2 (g/km)	Composite Desirability
1	40	-2	15.445	23.549	117.892	0.948
2	50	-2	15.973	17.734	118.134	0.948
3	30	-2	15.497	16.518	128.587	0.948
4	40	0	16.753	19.999	153.677	0.831
5	30	0	16.225	25.815	153.436	0.827
6	50	0	16.276	18.784	164.13	0.821
7	30	2	15.757	33.765	191.143	0.72
8	40	2	16.285	31.55	191.224	0.709
9	50	2	15.808	30.334	201.678	0.694
10	40	4	17.165	42.283	220.085	0.556
11	30	4	16.638	48.098	219.844	0.555
12	50	4	16.689	41.067	230.538	0.528
13	30	6	19.055	54.492	257.58	0.285
14	40	6	19.583	48.676	257.821	0.281
15	20	6	21.111	69.268	252.954	0.243

As depicted in Table 3.4 and Figure 4.33 (A), at road slopes of -2°, speeds of 40 km/h, 50 km/h, and 30 km/h exhibit nearly equal composite desirability indexes of 0.948. This suggests that the composite desirability is unaffected by vehicle speed on the downslope of the road. As shown in Table 4.4 and Figure 4.33 (B), on level roads, speeds of 40 km/h, 30 km/h, and 50 km/h have composite desirability indexes of 0.831, 0.827, and 0.821, respectively. The peak composite desirability index on level roads was observed at 40 km/h, representing the optimal speed for minimizing CO, HC, and CO_2 emissions. At this speed, vehicles traverse the level road at an optimal pace that is neither too fast nor too slow, thereby maximizing fuel efficiency and leading to a simultaneous reduction in CO_2, CO, and HC emissions. The composite desirability indexes for 30 km/h, 40 km/h, and 50 km/h at 2° road slopes are 0.72, 0.709, and 0.694, respectively. According to this study, 30 km/h is the optimal speed to minimise CO, HC, and CO_2 emissions on 2° road slopes. This result indicates that on roads with a 2° road slope, a speed of 30 km/h was preferred for reducing emissions. Additionally, it confirms the effectiveness of speed limits in mitigating environmental damage. The top three composite desirability indexes for roads with 4° and 6° road slopes were all less than 0.7. When compared to other road slopes, the outcome was not significant. Consequently, these road slopes were deemed unsuitable for determining the optimal vehicle speed for operation. Therefore, it is advisable to limit the driving speed of vehicles on such slopes, in order to reduce emissions.

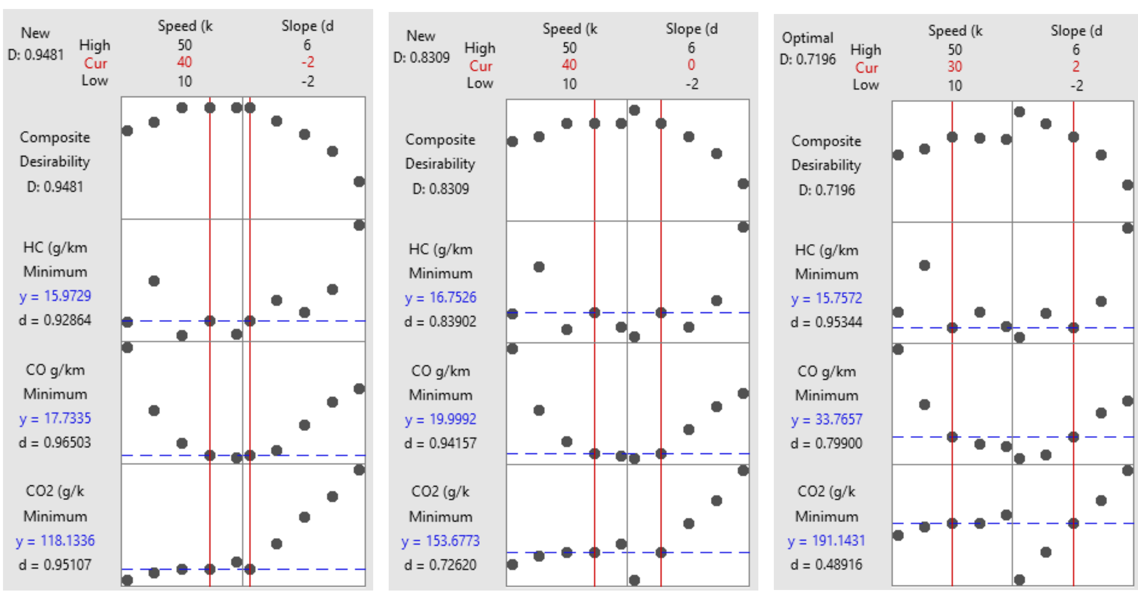

A) -2 degree road slopes B) Level road C) +2 degree road slopes

Figure 4.33: Plots illustrating DFA's responses

General, the implementation of DFA in this study revealed that, on a level road, traveling at a speed of 30 km/h resulted in a 2.82% increase in CO_2, an 18.97% increase in CO, and a 5.28% increase in HC emissions compared to the optimized speed of 40 km/h for vehicles. Additionally, when comparing the optimized vehicle speed of 30 km/h on a 2° road, operating at a speed of 20 km/h on the same gradient led to a 4% increase in CO_2 emissions, a 23.92% increase in CO emissions, and a 1.26% decrease in HC emissions. The uncertainty of the portable emissions tester used in this study is 3.82% for CO_2, 5.12% for CO, and 2.91% for HC.

4.4. Real-time emissions simulation results

4.4.1. Overall cycle-based emissions simulation results

4.4.1.1. Hydrocarbon emissions

Simulated real-time HC emissions from the selected petrol and diesel vehicles in WLTC and AADC are shown in Figure 4.34. In AADC, the maximum HC (0.045 g/s) was found in idle mode for the petrol vehicle when road slope was not considered. In WLTC, the maximum HC observed was 2.57 g/km, at 0.2 km/h. The maximum HC in AADC for the diesel vehicle was found at 11.63 km/h, while in WLTC it was found at 39 km/h. For the petrol vehicle, the results showed that WLTC generated more HC emissions at the beginning of the cycle (up to 170 s) than AADC. On average, AADC produced 87.47% and 237.66% higher HC emissions than WLTC for the petrol and diesel vehicle, respectively. When road slope was considered in AADC, the petrol vehicle had 4.54% higher HC emissions, while the diesel vehicle had 15.09% higher HC emissions. Thus AADC resulted in higher emissions than WLTC, meaning that it is essential to consider AADC when evaluating a vehicle's HC emissions. Road slope in AADC should also be considered when estimating HC emissions from vehicles.

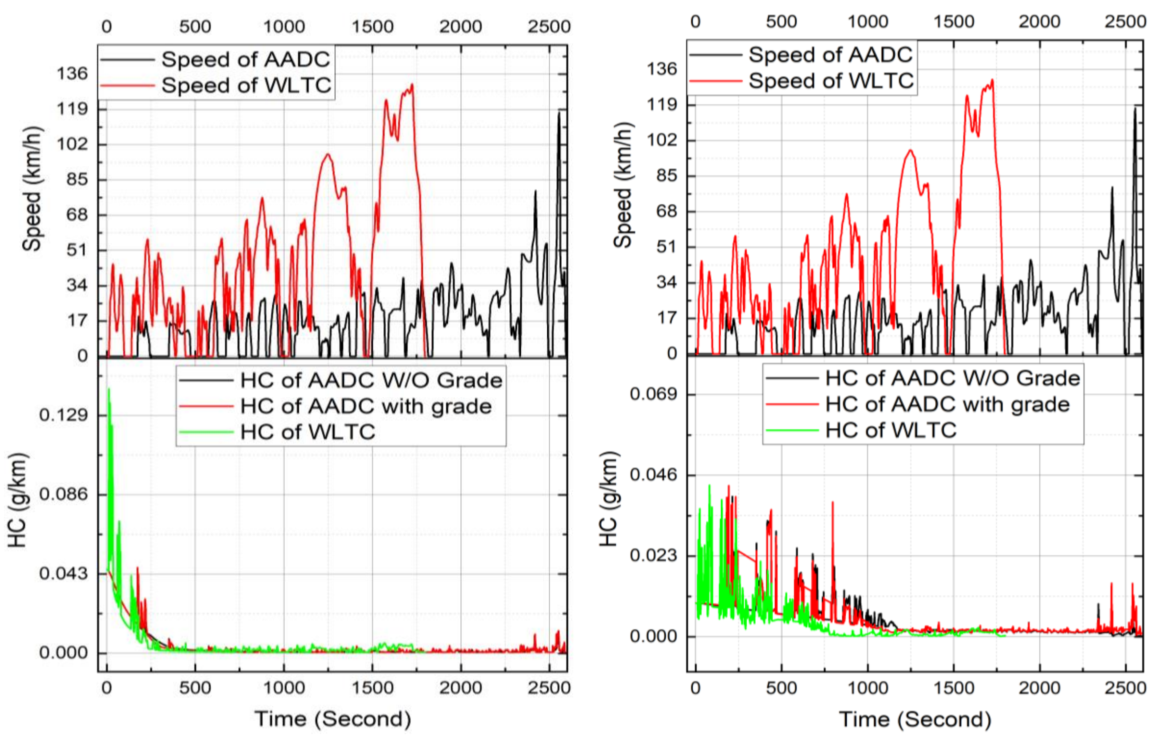

Figure 4.34: HC emissions from (left) the petrol vehicle and (right) the diesel vehicle

4.4.1.2. Carbon monoxide emissions

Simulated real-time CO emissions from the petrol and diesel vehicles in WLTC and AADC are shown in Figure 4.35. In AADC, maximum CO was 0.00895 g/km at 114.2 km/h for the petrol vehicle when road slope was not taken into account, while it was 0.0107 g/km at 116.11 km/h with a -0.754 degree road slope. In WLTC, maximum CO was 0.0336 g/km at 41.3 km/h. The maximum CO (0.0326 g/km) in AADC for the diesel vehicle was found at 12.15 km/h, while in WLTC the maximum CO (0.0093 g/km) was found at 38.5 km/h. For the petrol vehicle, it was found that WLTC generated more CO emissions at the beginning of the cycle than AADC. On average, for the petrol and diesel vehicles the AADC generated 84.54% and 409.42% more CO emissions, respectively, than WLTC. In addition, the petrol vehicle's CO emissions were 10.10% higher and the diesel vehicle's CO emissions were 22.57% higher when road slope was taken into account. For both vehicle types, the AADC emissions were much greater than the WLTC emissions. A previous study also found that higher road slope generally resulted in higher CO emissions (Engelmann et al., 2021). The sharp peaks in CO emissions shown in Figure 4.35 were attributed to dynamic driving events and higher slope power demands. In a previous study, most CO emissions were found to occur within the first 500 s of the cycle, followed by very low emissions afterwards (Chenna & Jathar, 2019).

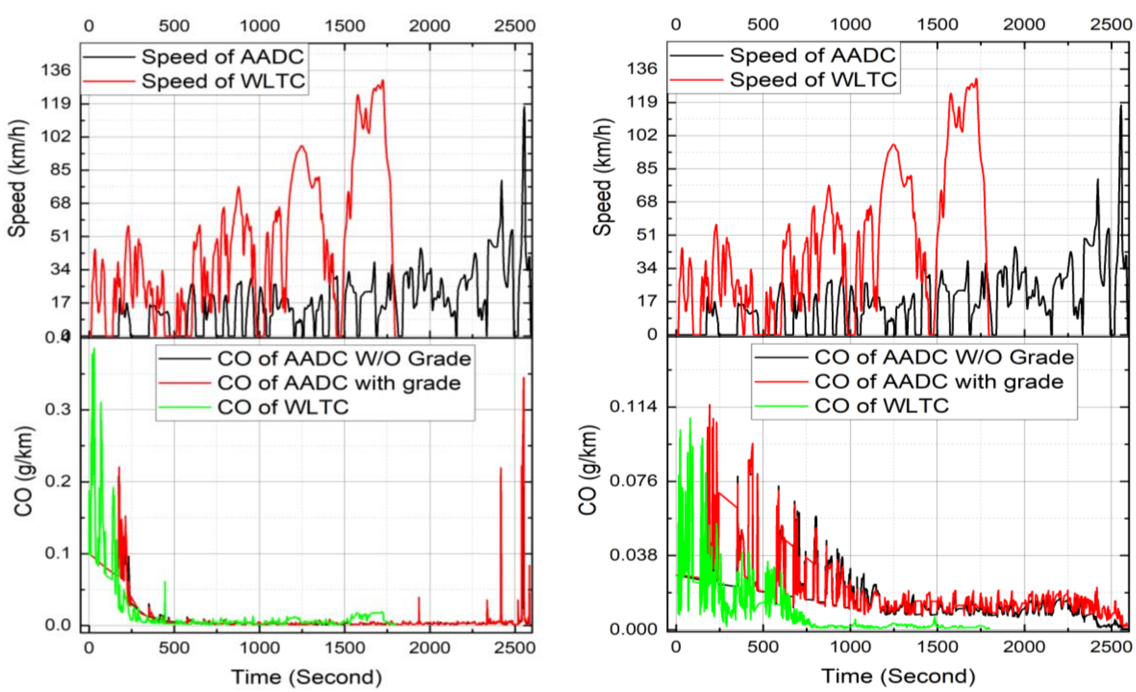

Figure 4.35: CO emissions from (left) the petrol vehicle and (right) the diesel vehicle

4.4.1.3. Nitrogen oxide emissions

Simulated real-time NO_X emissions from the petrol and diesel vehicles in WLTC and AADC are shown in Figure 4.36. In AADC, maximum NO_X for the petrol vehicle was 0.0178 g/km at 6.27 km/h when road slope was not considered, while with a -2.34 degree slope maximum NO_X was 0.0061 g/s at 27.1 km/h. In WLTC, maximum NO_X for the petrol vehicle was 1.0252 g/km at 0.2 km/h. The maximum NO_X in AADC for the diesel vehicle was 0.0086 g/km at 104.03 km/h when road slope was not considered, while it was 0.0104 g/km at 51.68 km/h with a -0.25 degree slope. In WLTC, it was 0.0057 g/km at 81.8 km/h. Compared with WLTC, the petrol vehicle produced 4.21% more NO_X and the diesel vehicle produced 22.31% less NO_X than in AADC. When road slope was considered in AADC, the petrol vehicle had 33.18% higher NO_X and the diesel vehicle had 8.93% lower NO_X emissions than in WLTC.

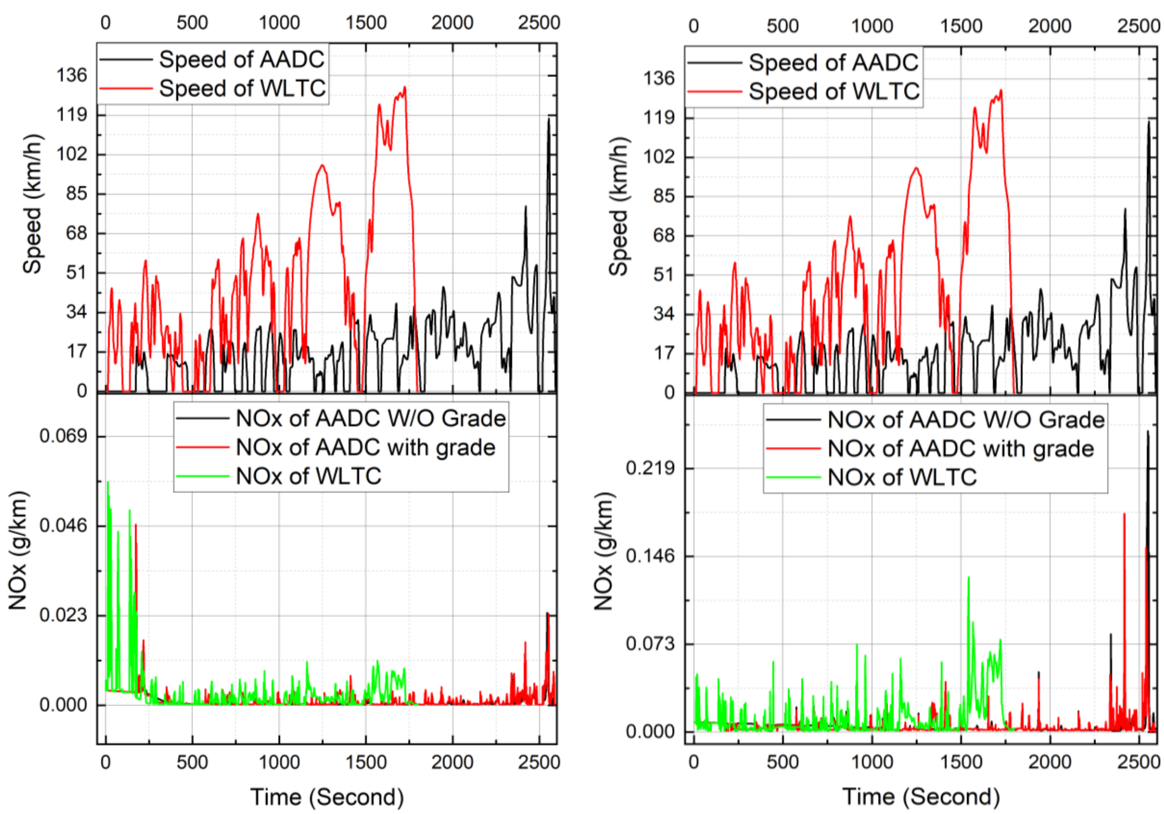

Figure 4.36: NOx emissions from (left) the petrol vehicle and (right) the diesel vehicle

4.4.1.4. Particulate matter emissions

Simulated real-time PM emissions from the diesel vehicle in WLTC and AADC are shown in Figure 4.37. In AADC, maximum PM was 0.0008 g/km at 101.63 km/h when slope was not considered, while it was 0.0013 g/km at 101.63 km/h with a -1.93 degree slope. In WLTC, maximum PM was 0.0001 g/km at 130.1 km/h. Emissions of PM from the diesel vehicle were 21.3 % higher in AADC than in WLTC. When slope was taken into account, PM emissions were 42.68% higher in AADC.

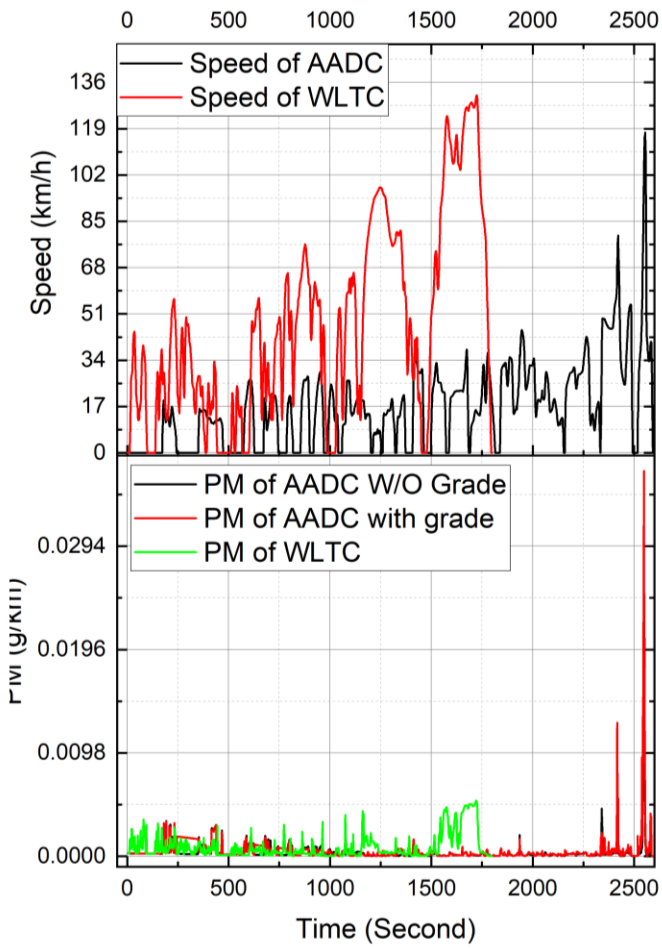

Figure 4.37: PM emissions from the diesel vehicle

4.4.2. Route-based emissions simulation analysis

4.4.2.1. Hydrocarbon emissions

Hydrocarbon emissions were not significantly affected by slope in congested urban road conditions, according to the route-based emissions simulation analysis (Figure 4.38). However, when road slope was considered, HC emissions from the petrol vehicle increased by 22.57%, 17.31% and 17.3% in extra-urban, rural and motorway conditions, respectively. The HC emissions from the diesel vehicle were unaffected by road slope in extra-urban conditions, but increased by 13.5%, 8.14% and 8% in urban, rural and motorway conditions, respectively (Figure 4.38). The highest HC emissions were observed in urban areas, followed by extra-urban, rural and motorways.

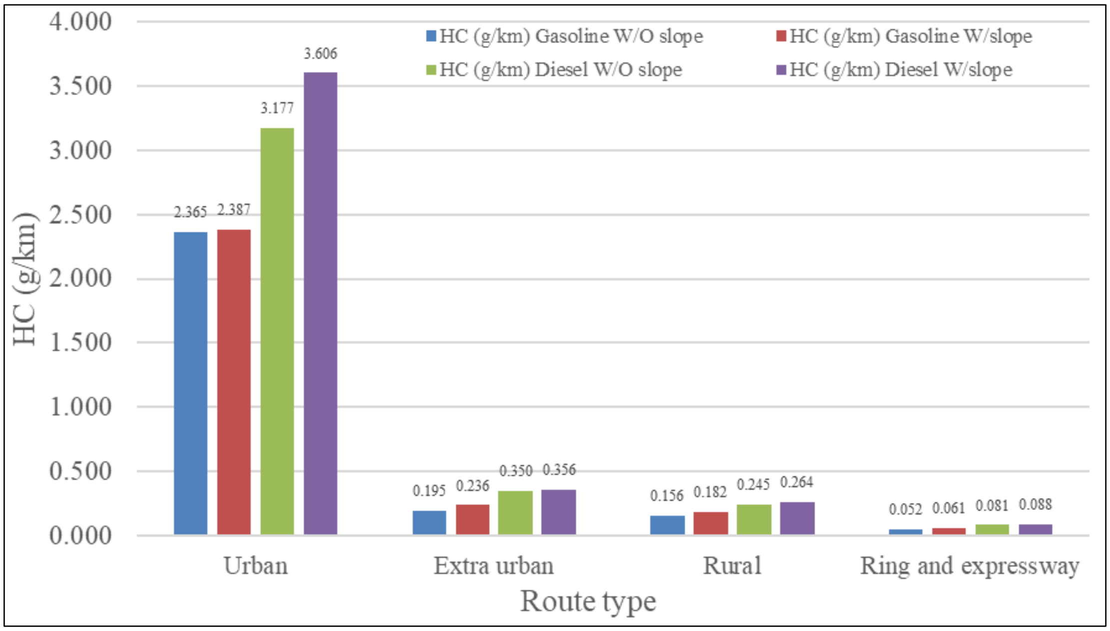

Figure 4.38: Route-based HC emissions

4.4.2.2. Carbon monoxide emissions

The CO emissions from the petrol vehicle did not differ significantly for congested urban road conditions when road slope was taken into consideration, but increased by 24.3%, 14.07% and 14% in extra-urban, rural and motorway conditions, respectively (Figure 4.39). For the diesel vehicle, CO emissions in congested urban, extra-urban, rural and motorway conditions increased by 18.13%, 26.77%, 24.5% and 24%, respectively, when road slope was considered. Urban areas emitted more CO than extra-urban areas, followed by rural areas and then motorways (Figure 4.39). This difference in emissions was due to factors such as traffic density and lower engine efficiency at low vehicle speeds. Road slopes possibly also influenced emissions from the vehicles, as the steeper the slope, the greater the acceleration required.

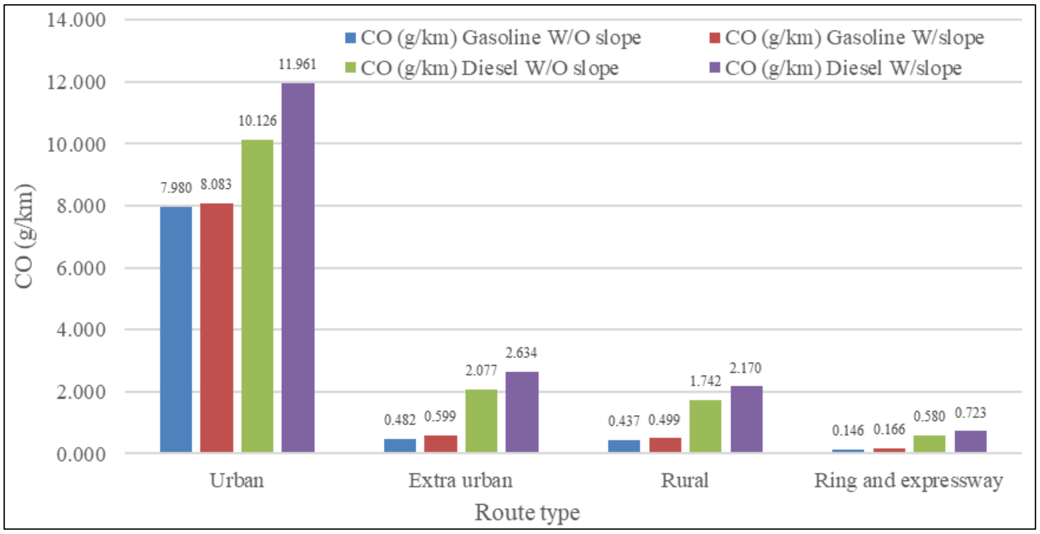

Figure 4.39: Route-based CO emissions

4.4.2.3. Nitrogen oxide emissions

There were significant effects of road slope on NO_X emissions from the petrol vehicle in congested urban, extra-urban, rural and motorway road conditions, with an increase of 23.18%, 58.61%, 41% and 41.07%, respectively (Figure 4.40). The NO_X emissions from the diesel vehicle increased by 7.56%, 9.94% and 8.9% in extra-urban, rural and motorway conditions, respectively, when road slope was taken into account, but decreased by 6.7% in congested urban conditions. The highest NO_X emissions from the diesel vehicle were observed in urban areas, followed by extra-urban, rural and motorways areas. A previous study also found higher NO_X emissions in urban areas, as a result of higher driving dynamics (Engelmann et al., 2021).

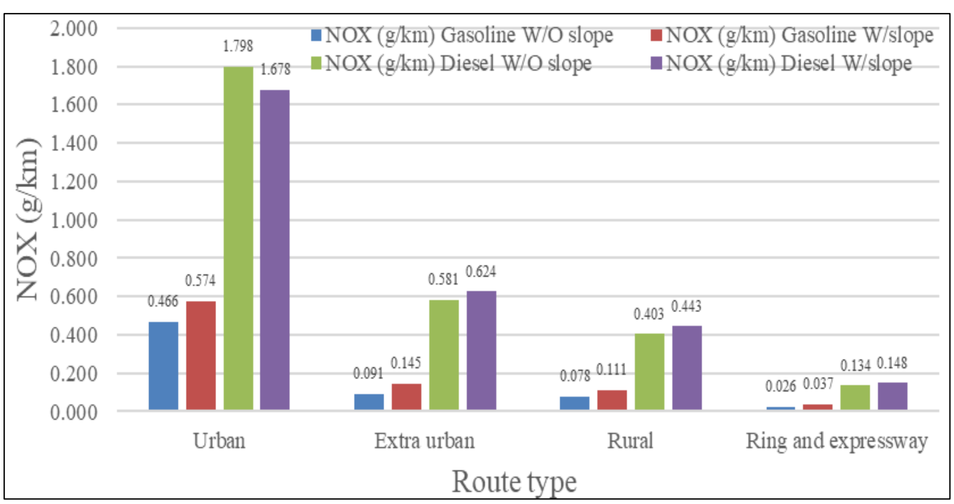

Figure 4.40: Route-based NO_X emissions

4.4.2.4. Particulate matter emissions

Emissions of PM from the diesel vehicle were highly affected by road slope, with an increase for congested urban, extra-urban, rural and motorway road conditions of 35.16%, 42.17%, 13.5% and 11.5%, respectively (Figure 4.41). Urban areas had the highest PM emissions, followed by extra-urban, rural and motorway areas.

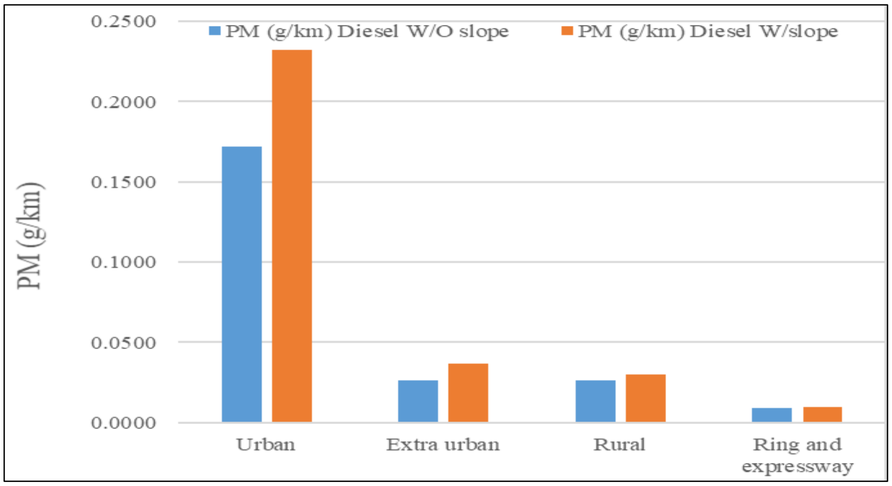

Figure 4.41: Route-based PM emissions

4.4.2.5. Fuel consumption

Simulated real-time FC per 100 km for the petrol vehicle was 8.5, 12.5 and 15.5 L for WLTC, AADC, and AADC with slope, respectively, while for the diesel vehicle it was 8.5, 10.8, and 12.2 L, respectively. In AADC and AADC with slope, petrol consumption increased by 47% and 82%, respectively, while diesel consumption increased by 27% and 43%, respectively, compared with WLTC.

4.4.3. Emissions results predicted by ANN

An ANN model was utilized to predict tailpipe emissions from PVs based on the driving patterns of AA's road conditions and the AAE. The predicted emissions of HC, CO, NOx, PM and FC using the ANN model are presented below.

4.4.3.1. Hydrocarbon emissions

With 13 DC features, a double array of 2594 time steps was input at one-second intervals. The target consisted of a double array of 2594 time steps with one feature. Using 10 and 12 hidden layer sizes resulted in the best ANN model performance for the petrol and diesel vehicle, respectively (Table 4.16). The models predicted emissions accurately for both vehicle types (R^2 = 0.854-0.999). A previous study using an ANN model for predicting HC emissions achieved an R^2 value of 0.953 (Hassine et al., 2021).

Table 4.16: Performance value of the ANN model in prediction of emissions

Vehicle type	Emissions	MSE		R square	
		Training	Test	Training	Test
Gasoline	HC	1.346×10^{-7}	1.392×10^{-5}	0.999	0.922
	CO	5.122×10^{-7}	4.928×10^{-4}	0.999	0.883
	NO_X	2.033×10^{-7}	1.249×10^{-6}	0.982	0.887
Diesel	HC	6.489×10^{-6}	1.446×10^{-5}	0.92	0.854
	CO	2.438×10^{-5}	3.692×10^{-5}	0.956	0.943
	NO_X	3.581×10^{-7}	2.077×10^{-5}	0.962	0.894
	PM	9.422×10^{-8}	4.95×10^{-7}	0.982	0.921

During training, as long as the training and test error kept declining the ANN was trained for as many epochs as weight changes made in the NN, and the boundary changed from under-fitting to optimal. The best training performance was observed for prediction of HC emissions from the petrol and diesel vehicles at 271 and 200 epochs, respectively, after which there was no further reduction in mean square error (Figure 4.42).

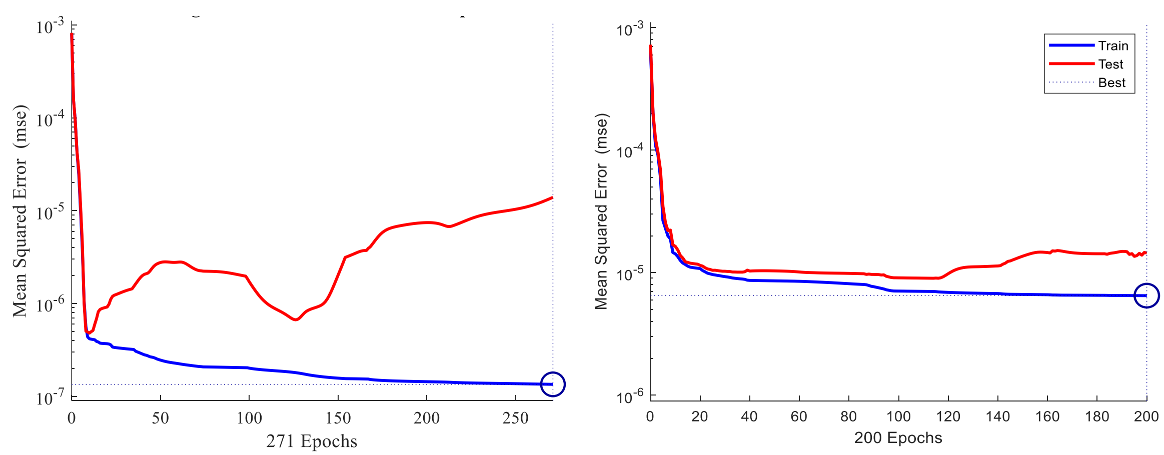

Figure 4.42: HC prediction epochs for (left) the petrol vehicle and (right) the diesel vehicle

Figure 4.43 shows the trajectory of predicted HC emissions based on the training and test data. Targets minus outputs were very close to zero, indicating that HC emissions were very accurately predicted by the ANN model, except for some points.

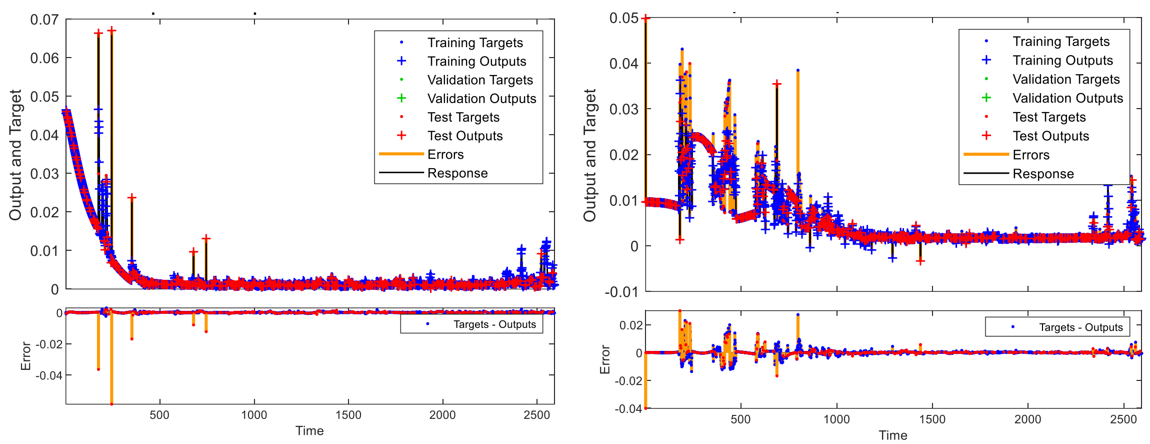

Figure 4.43: Response of the output element in prediction of HC emissions for (left) the petrol vehicle and (right) the diesel vehicle by the ANN model

For the petrol vehicle, route type (RT), drive mode (DM), idle time (IT), drive time (DT), vehicle speed (V) and distance (S) were the most significant predictors of HC emissions, followed by deceleration (NA) and road slope (G), while RPA, PKE, drive time (DT) and number of stops (NS) were the least significant (Figure 4.44). For the diesel vehicle, the most significant predictor of HC emissions was RT, followed by V, S, IT, DT, DM, and G, then NA, PA and PKE, while the least significant predictors were RPA and NS.

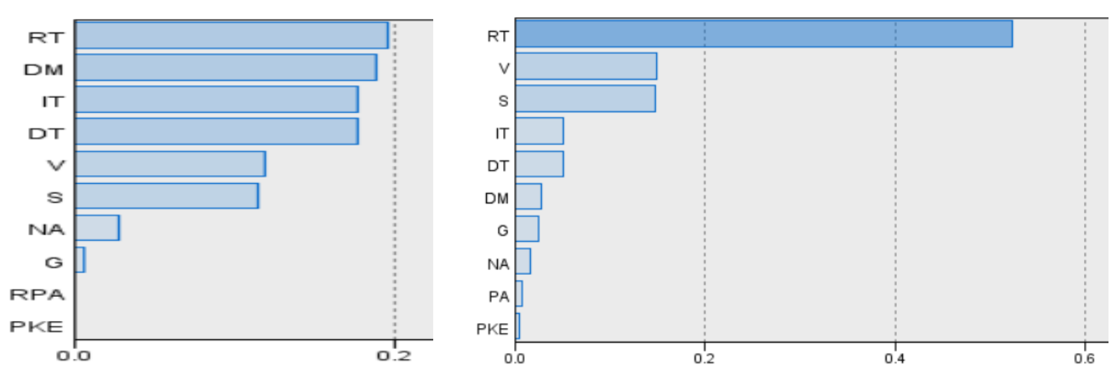

Figure 4.44: Importance of different variables as predictors of HC emissions from (left) the petrol vehicle and (right) the diesel vehicle

4.4.3.2. Carbon monoxide emissions

Using 15 and 10 hidden layer sizes resulted in the best performance in predicting CO emissions from the petrol and diesel vehicle, respectively (for MSE and R^2 values, see Table 4.16). The CO emissions from the petrol and diesel vehicle were best predicted at 271 and 200 epochs, respectively (MSE 5.122 x 10^{-7} and 2.43 x 10^{-5}, respectively; R^2 0.999 and 0.956, respectively) (Figure 4.45). Previous studies using an ANN model for predicting CO emissions achieved R^2 of 0.962 (Hassine et al., 2021), or R^2 of 0.72 for predicted CO concentrations in Tehran city (Shams et al., 2020).

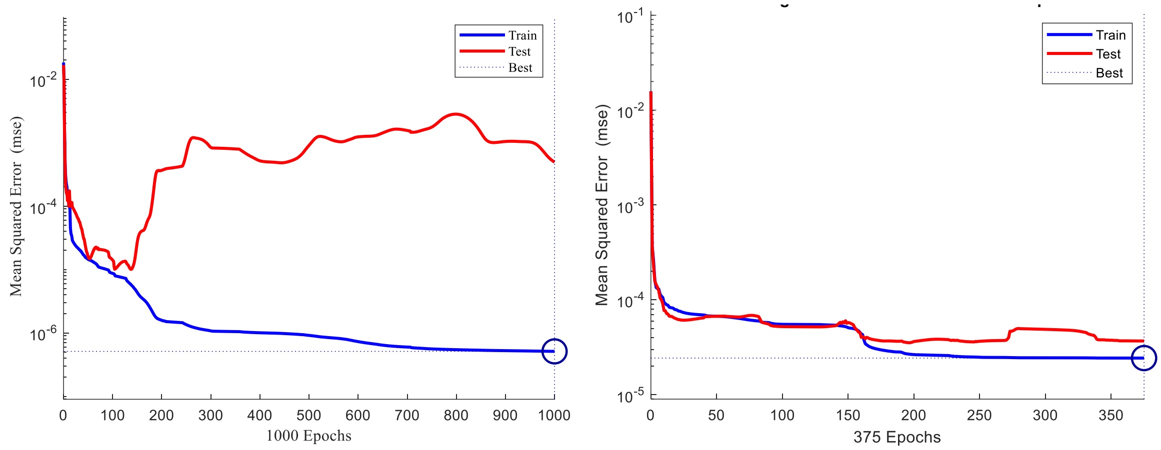

Figure 4.45: CO prediction epochs for (left) the petrol vehicle and (right) the diesel vehicle

Figure 4.46 shows the projected CO emissions trajectory based on the training and test data. Targets minus outputs were very close to zero, with a few exceptions, indicating that ANN model predictions of CO emissions were remarkably accurate.

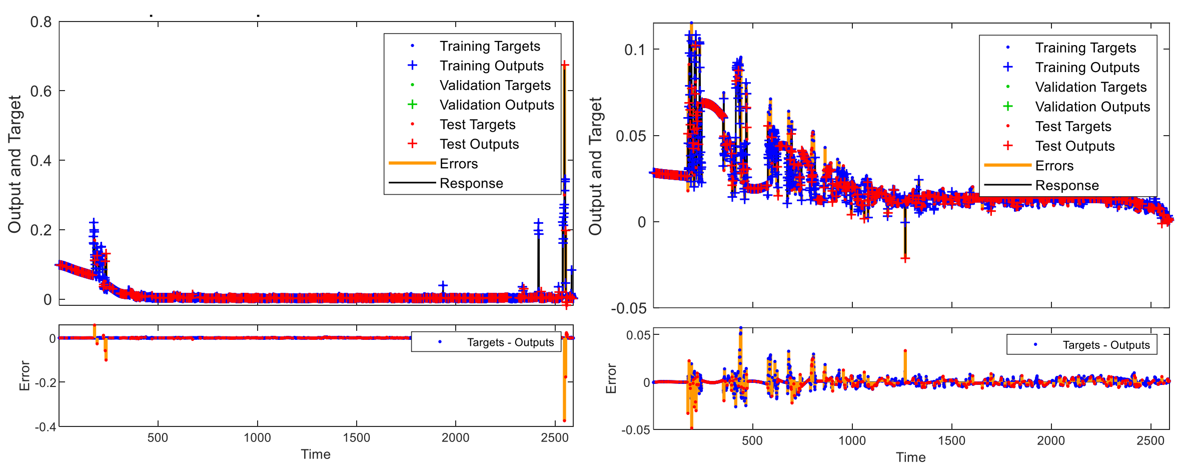

Figure 4.46: Response of the output element in prediction of CO emissions for (left) the petrol vehicle and (right) the diesel vehicle by the ANN model

For the petrol vehicle, the most significant predictors of CO emissions in the ANN model were RPA and PKE, followed by DM, RT and PA, and then IT, DT and NA, while G, NS, S and V had the least significance (Figure 4.47). For the diesel vehicle, RT was the most significant predictor of CO emissions, followed by V, S, IT, DT and DM, and then NA, G, PA and PKE, while RPA and NS were least significant.

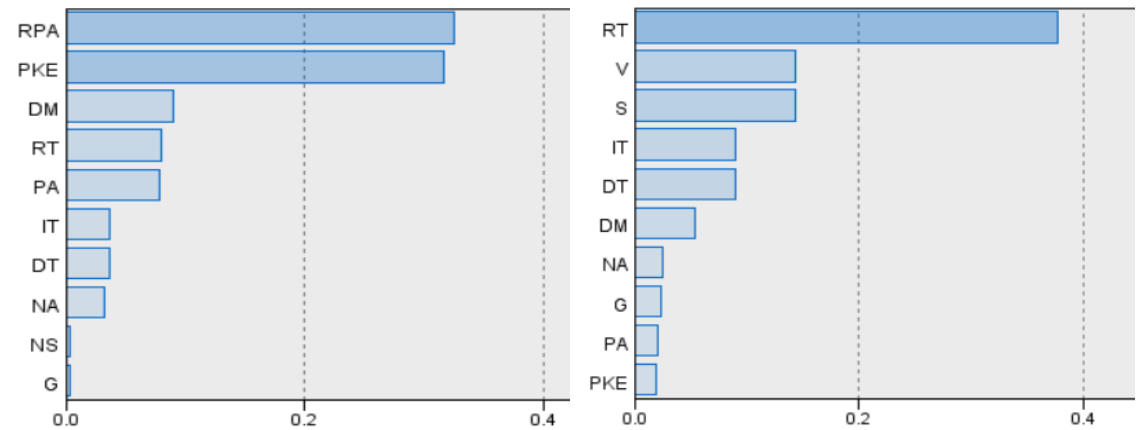

Figure 4.47: Importance of different variables as predictors of CO emissions from (left) the petrol vehicle and (right) the diesel vehicle

4.4.3.3. Nitrogen oxide emissions

Using 20 and 15 hidden layer sizes resulted in the best performance in model prediction of NO_X emissions from the petrol and diesel vehicle, respectively (for MSE and R^2 values, see Table 4.16). The NO_x emissions from the petrol and diesel vehicle were best predicted at 441 and 218 epochs, respectively (MSE 2.03×10^{-7} and 3.58×10^{-7} respectively; R^2 0.982 and 0.962, respectively) (Figure 4.48). Previous studies achieved R^2 values of 0.98 (Hassine et al., 2021) and 0.85 when using an ANN model for predicting NO_X emissions (Donateo & Filomena, 2020).

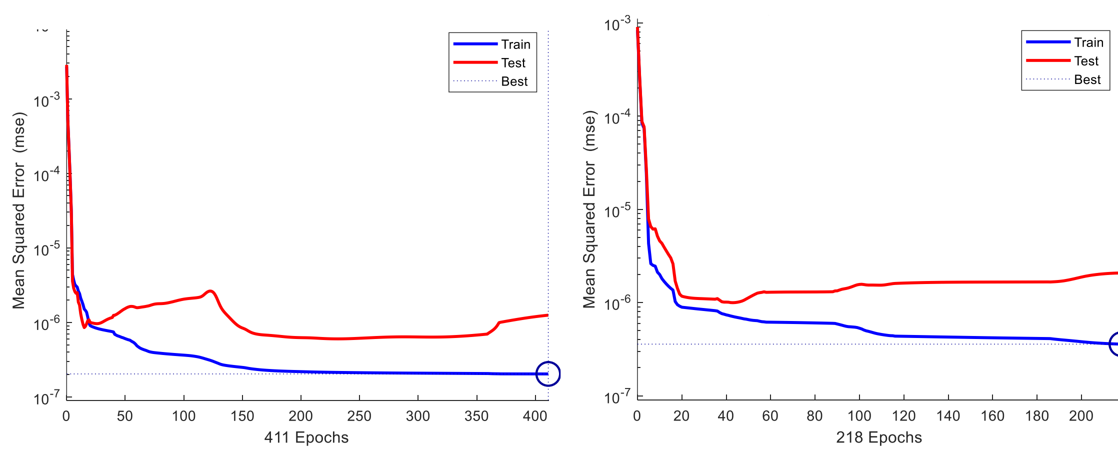

Figure 4.48: NOx prediction epochs for (left) the petrol vehicle and (right) the diesel vehicle

Figure 4.49 shows projected the NO_X emissions trajectory based on the training and test data. With a few exceptions, the ANN model prediction of NO_X was remarkably accurate.

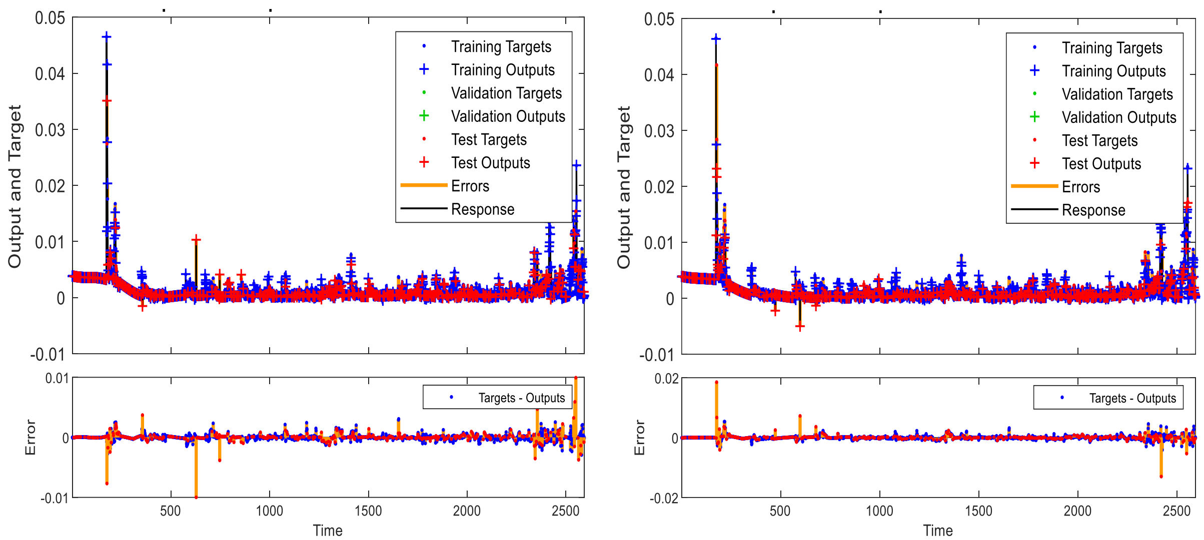

Figure 4.49: Response of the output element in prediction of NOx emissions for (left) the petrol vehicle and (right) the diesel vehicle by the ANN model

For both the petrol and diesel vehicles, RPA, PKE, PA, S and V were the most significant predictors of NO_X emissions, followed by NA, RT, DM, IT and DT, while G and NS were the least significant (Figure 4.50).

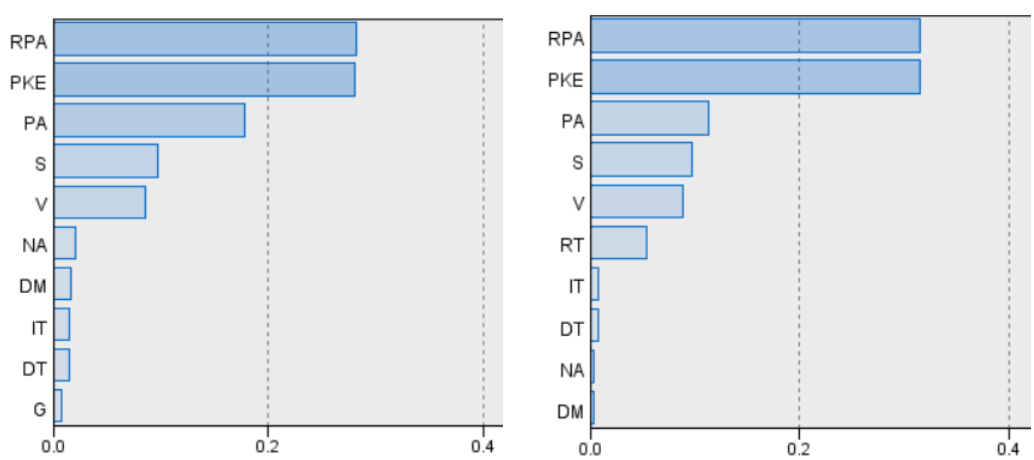

Figure 4.50: Key predictors of NOx emissions from (left) the petrol vehicle and (right) the diesel vehicle

4.4.3.4. Particulate matter

Using 10 hidden layers resulted in the best performance in prediction of PM emissions from the diesel vehicle (for MSE and R^2 values, see Table 4.16). The PM predictions were best at 77 epochs (MSE $9.42x10^{-8}$) (Figure 4.51 a). Figure 4.51 b shows the projected PM emissions based on the training and test data. With a few exceptions, ANN prediction of PM was remarkably accurate. A previous study using an ANN model to predict PM emissions, validating the model against trained experimental datasets achieved R^2 of 0.86 (Chenna & Jathar, 2019).

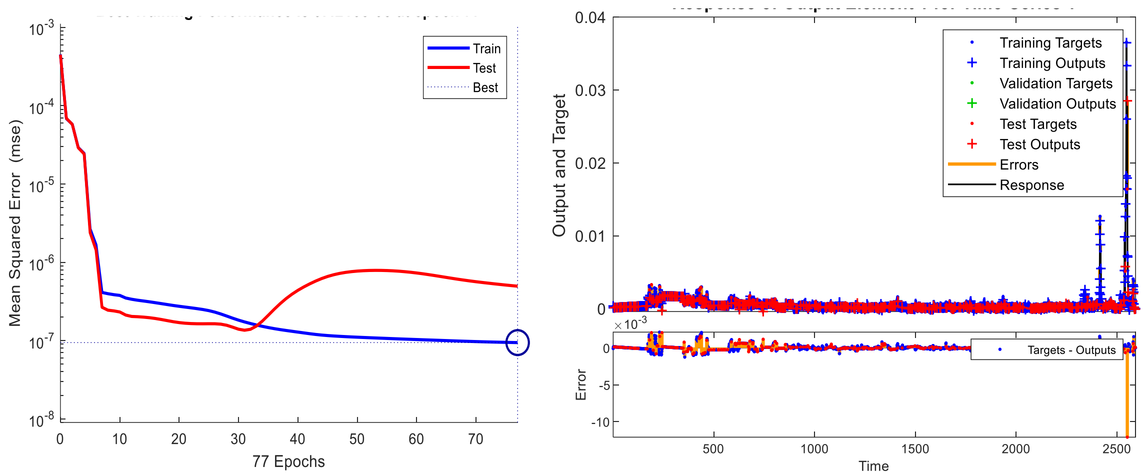

Figure 4.51: (Left) PM prediction epochs and (right) response of the output element in prediction of PM for the diesel vehicle

The variables RPA, PKE, S, V, PA and RT were the most significant predictors of PM emissions of the diesel vehicle, while, IT, DT, G, NA, NS and DM were the least significant (Figure 4.52).

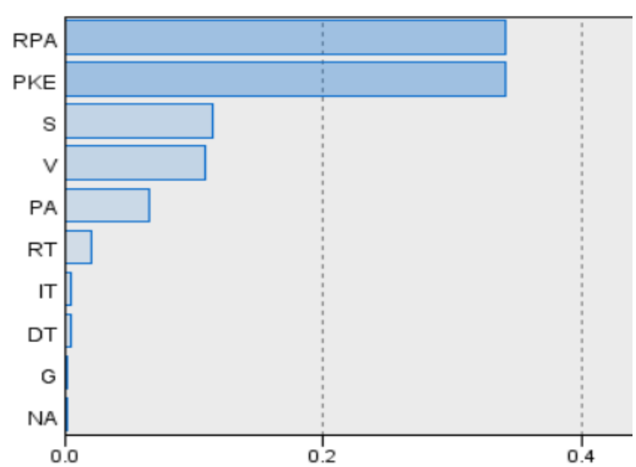

Figure 4.52: Importance of variables in predicting PM emissions from diesel vehicles

4.5. Comparison of emissions and FC results

There were significant differences in the CO, NO_X, and FC values produced by the ANN prediction model, the COPERT model and an experimental CD, with higher values of all predicted by the ANN model (Table 4.17). Despite this, the ANN prediction model underestimated diesel vehicle NO_X emissions. The ANN predictions were more accurate than those of the COPERT model, due to the fact that COPERT ignores road slope and is based on average vehicle speed (Lejri et al., 2018; Wondifraw, 2018). The ANN prediction model also performed well compared with the experimental CD, as a result of the absence of cold start operation in the latter. It has been reported previously that excluding cold start operation can lead emission inventories to understate emissions (Alves et al., 2015). Similar findings were reported by (Triantafyllopoulos et al., 2019), discovered that dynamic driving combined with an uphill route increased NO_X emissions eight-fold. The accuracy of the ANN predictions obtained in this study was very promising, suggesting that ANNs can be used to predict tailpipe emissions in e.g. situations where PEMS are not available or practical. The ANN mode predictions can be important decision support for policymakers tasked with making decisions about lowering emissions from vehicular traffic. However, the performance of the ANN model is highly dependent on the input data used for training. It is specifically tailored to the conditions and characteristics of the provided dataset, which limits its applicability to other contexts or datasets.

Table 4.17: Comparison of emissions results obtained using the ANN prediction model, the COPERT model and an experimental CD

Measured parameters	Fuel type	ANN predicted	Chassis dynamometer	COPERT Model
	Petrol	3.07	0.68	0.671
CO (g/km)	Diesel	3.03	0.069	0.071
	Total	3.05	0.375	0.371
	Petrol	0.24	0.066	0.08
NO_X (g/km)	Diesel	0.28	0.586	0.604
	Total	0.26	0.326	0.342
	Petrol	15.5	8.72	8.93
FC (litters/100km)	Diesel	12.2	6.74	6.82
	Total	13.85	7.74	7.875

5. CONCLUSIONS AND RECOMMENDATION

5.1. Conclusions

This study focus on developing real-time exhaust emissions and FC models for light-duty vehicles in the study area. It involved developing a representative DC, conducting experimental testing on the CD, computing annual emissions and FC using the COPERT model, examining the effects of vehicle velocity and road gradient on tailpipe emissions, and developing an ANN simulation model using Matlab/Simulink. From the results of this study, the following conclusions were derived:

By implementing a trip-based approach, machine classification, and NN based speed prediction, the results show that the DC developed using the NN method more accurately represents the real-time driving conditions in AA urban roads including the AAE compared to the MT method. With collected data, a comparative analysis of the NN and MT approach revealed a relative difference of 0.056 and 0.111, respectively. Furthermore, the NN method yielded the DC duration and distance with the smallest deviations, 0.14 and 0.13, respectively, when compared to the daily average trip length. Also, when compared to standard DCs, it also more closely represents actual driving conditions than WLTC, FTP-75, and CLTC.

The emission factors for the vehicles tested on a CD revealed that the WLTC overestimates CO emissions by 34.54% and underestimates CO_2, EC, and NO_X by 20.43%, 19.84%, and 18.76%, respectively, compared to the AADC. Congested urban routes consumes more fuel and produce more CO, CO_2, NO_X, and VOCs than other routes, even though they cover a shorter distance than rural routes. Emissions from driving in AA's congested urban areas include 56.25% CO, 37.28% CO_2, 38.19% NO_X, 58.25% VOC, 29% $PM_{2.5}$ and PM_{10}, and 37.29% FC for the entire cycle. There was a significant difference between the emissions factor results from the CD and the COPERT model.

The increase in road slopes of 2°, 4°, and 6° led to a rise in CO_2 emissions for gasoline-powered vehicles by 16.25%, 28.58%, and 43.36%, respectively, compared to level roads. In contrast, diesel vehicles produced 53.7%, 91.08%, and 245.85% more CO_2 than on level roads for gradients of 2°, 4°, and 6°, while showing a 36% decrease in CO_2 emissions on slopes of -2°. Generally, CO emissions rise with an increase in road slope and decline as vehicle speed increases. Both petrol and diesel cars released less CO at 30 km/h. The optimal speed to simultaneously minimize CO, HC, and CO_2 emissions was determined to be 40 km/h for level roads and 30 km/h for roads with a 2° incline, based on the composite desirability index. Consequently, with a -2° road slope, the composite desirability indexes for 30 km/h, 40 km/h, and 50 km/h are nearly identical.

The real time simulations of exhaust emissions of HC, CO, NOx and PM and FC were much higher in AADC than in WLTC. When slope was taken into account in AADC, the petrol vehicle studied had 4.54% higher HC emissions, 10.10% higher CO emissions and 33.18% higher NO_x emissions, while the diesel vehicle had 15.09% higher HC emissions, 22.57% higher CO emissions, 8.93% lower NO_x emissions and 42.68% higher PM emissions. Additionally, urban areas had higher HC, CO, NO_X and PM emissions than extra-urban, rural and motorway road conditions, because of the dynamic driving characteristics of the urban environment. Other than number of stops, the predictors used as input to the ANN model were crucial for accurate prediction of real-time exhaust emissions.

Compared with the COPERT model and an experimental CD, the ANN model predicted higher levels of CO, NO_X and FC, but underestimated NO_X emissions from the diesel vehicle. Overall, real-time exhaust emissions from vehicles were successfully predicted using the ANN model, which can overcome the limitations of conventional emissions models.

5.2. Recommendation

As a result of this study, it is recommended that:

- The AA city administration shall adopt the AADC, developed using ANN predictions in this study, as the official legislative driving cycle for determining emissions and FC of light-duty vehicles.
- Emissions monitoring stations shall be placed in the crowded districts of AA, and an emissions reduction plan must be put into action. As part of this strategy, traffic congestion shall be reduced by installing smart traffic lights, introducing bridges and flyovers for crossroads, providing pedestrian underpasses beneath bridges or flyovers, and improving access to public transportation. Additionally, vehicle owners shall be

offered incentives to switch to more fuel-efficient vehicles. Furthermore, stricter standards for vehicle emissions shall be introduced to reduce air pollution.

- When designing roads and establishing speed limits in urban settings, emissions shall be considered because vehicle emissions are sensitive to both speed and road slope to improve public health as well as contribute in the reduction of air pollution.
- Urban regions such as AA should set vehicle speed limitations with the goal of reducing CO_2, HC, and CO emissions simultaneously in addition to accident. This study suggests that the AA city transport authority shall set a speed limit of 30 km/h for two-degree sloped roads and 40 km/h for level roads in order to minimize vehicle emissions simultaneously.
- To estimate current and future real-time exhaust emissions from PVs, we suggest that the AA Environmental Protection Agency shall use the ANN-based simulation model developed in this study, which can overcome the limitations of conventional emissions models.

Future investigations on DCs development shall use weightings for trip indications and evaluate the methodology with big and more diverse driving data sets. In future DC development, researchers must consider driving characteristics such as vehicle speed, road slope, acceleration, deceleration, distance traveled, idle time, drive time, drive mode, route type, PKE, and RPA, as these significantly impact vehicular emissions estimates. This will help improve the representativeness and robustness of the findings. Additionally, further studies shall consider the impacts of various vehicle types, emissions control technologies, mileage, weather conditions, and vehicle loads on vehicle exhaust emissions and FC. This will provide a more comprehensive understanding of the factors influencing real-world vehicle emissions. To further increase the accuracy of real-time vehicle emissions simulation, the inclusion of cold start emissions and evaporative emissions, which contribute a significant portion of pollutant emissions, shall be a focus of future study efforts. Furthermore, to assess vehicle emissions on urban roads in AA, it shall be better to exclude the expressway sub-cycle from the AADC developed in this study. By addressing these areas for future study, researchers can expand the understanding of real-world vehicle emissions, improve the accuracy of emissions simulation models, and support the development of more effective emissions reduction strategies.

REFERENCES

Abdulraheem, K. A., Adeniran, J. A., Aremu, A. S., Yusuf, M. N. O., Yusuf, R. O., Odediran, E. T., Sonibare, J. A., & Du, M. (2023). Quantifications and Predictions of Sectoral Pollutants Emissions in Nigeria from 1980 to 2050. *Environmental Monitoring and Assessment*, *195*(3), 398. https://doi.org/10.1007/s10661-022-108725

Abiodun, O. I., Jantan, A., Omolara, A. E., Dada, K. V., Umar, A. M., Linus, O. U., Arshad, H., Kazaure, A. A., Gana, U., & Kiru, M. U. (2019). Comprehensive Review of Artificial Neural Network Applications to Pattern Recognition. In *IEEE Access* (Vol. 7, pp. 158820–158846). Institute of Electrical and Electronics Engineers Inc. https://doi.org/10.1109/ACCESS.2019.2945545

Adamiak, B., Szczotka, A., Woodburn, J., & Merkisz, J. (2023). Comparison of Exhaust Emission Results Obtained from Portable Emissions Measurement System (PEMS) and a laboratory system. Combustion Engines. https://doi.org/10.19206/CE-172818

Adeyanju A. A., & Manohar K. (2017). Effects of Vehicular Emission on Environmental Pollution in Lagos. Sci-Afric Journal of Scientific Issues, Research and Essays, 4(5), 34–51. http://www.sci-africpublishers.org

Aksoy, A., Küçükoğlu, İ., Ene, S., & Öztürk, N. (2014). Integrated Emission and Fuel Consumption Calculation Model for Green Supply Chain Management. *Procedia Social and Behavioral Sciences*, *109*, 1106–1109. https://doi.org/10.1016/j.sbspro.2013.12.595

Ali, M., Sheha, A., Tsokos, C. P., & Mamudu, L. (2022). Desirability Function Approach to Response Surface Optimization Analysis of Atmospheric Carbon Dioxide CO_2 Emissions in Africa. *Global Journal of Science Frontier Research: H*, *22*(7), 1–10.

Al-samari, A. (2017). Real-World Driving Cycle: Case Study of Baqubah, Iraq. Diyala Journal of Engineering Sciences, 10(2), 39–47.

Alves, C. A., Lopes, D. J., Calvo, A. I., Evtyugina, M., Rocha, S., & Nunes, T. (2015). Emissions from Light-Duty Diesel and Gasoline in Use Vehicles Measured on Chassis Dynamometer Test Cycles. Aerosol and Air Quality Research, 15(1), 99–116. https://doi.org/10.4209/aaqr.2014.01.0006

Amin, M., Aghayan, I., & Ali, S. (2018). Development of Mashhad Driving Cycle for Passenger Car to Model Vehicle Exhaust Emissions Calibrated Using On-Board Measurements. Sustainable Cities and Society, 36 (June 2017), 12–20. https://doi.org/10.1016/j.scs.2017.09.034

Amirjamshidi, G. (2015). Assessment of Commercial Vehicle Emissions and Vehicle Routing of Fleets using Simulated Driving Cycles [PhD Thesis]. University of Toronto.

Amirjamshidi, G., & Roorda, M. J. (2015). Development of Simulated Driving Cycles for Light, Medium, and Heavy Duty Trucks: Case of the Toronto Waterfront Area. Transportation Research Part D: Transport and Environment, 34, 255–266. https://doi.org/10.1016/j.trd.2014.11.010

Andre, M. (2004). The ARTEMIS European Driving Cycles for Measuring Car Pollutant Emissions. Science of the Total Environment, 334–335, 73–84. https://doi.org/10.1016/j.scitotenv.2004.04.070

Anida, I. N., Latiff, N. A. A., & Salisa, A. R. (2019). Driving Cycle Analysis for Fuel Rate and Emissions in Kuala Terengganu City During Go-to-Work Time. Journal of Engineering Science and Technology, 14(6), 3143–3157.

Arsie, I., Pianese, C., & Sorrentino, M. (2010). Development of Recurrent Neural Networks for Virtual Sensing of NOx Emissions in Internal Combustion Engines. International Journal of Fuels and Lubricants, 2(2), 354–361. https://doi.org/10.2307/26271563

Arti, C., Pradeep, K., Kumar, S. S., & Chinmay, P. (2022). Real Time Roadway Pollution in Indian Cities: A Comparative Assessment with Modelled Emission. *Research Journal of Chemistry and Environment*, *26*(5), 97–106.

Arun, N. H., Mahesh, S., Ramadurai, G., Shiva Nagendra, S. M., & Nagendra, S. M. S. (2017). Development of Driving Cycles for Passenger Cars and Motorcycles in Chennai, India. Sustainable Cities and Society, 32(May), 508–512. https://doi.org/10.1016/j.scs.2017.05.001

Ashok, B., Kumar, A. N., Jacob, A., & Vignesh, R. (2021). Emission Formation in IC Engines. In *NOx Emission Control Technologies in Stationary and Automotive*

Internal Combustion Engines: Approaches Toward NOx Free Automobiles (pp. 1-38). Elsevier. https://doi.org/10.1016/B978-0-12-823955-1.00001-2

Aydin, M., Yavuz, A., & Sorusbay, C. (2018). Application of Artificial Neural Network to Predict Exhaust Emissions from Road Transport. In *International Journal of Scientific and Technological Research www.iiste.org ISSN* (Vol. 4, Issue 2). www.iiste.org

Azeez, O. S., Pradhan, B., Shafri, H. Z. M., Shukla, N., Lee, C. W., & Rizeei, H. M. (2019). Modeling of CO Emissions from Traffic Vehicles Using Artificial Neural Networks. *Applied Sciences (Switzerland), 9*(2). https://doi.org/10.3390/app9020313

Azman, M., Rajoo, S., Fadzil, S., & Abidin, Z. (2018). Development of Malaysian Urban Drive Cycle Using Vehicle and Engine Parameters. *Transportation Research Part D*, *63*, 388–403. https://doi.org/10.1016/j.trd.2018.05.015

Baskin, A. (2018). Africa Used Vehicle Report. Proceedings of the Africa Clean Mobility Week, 1–26.

Berry, I. M. (2010). *The Effect of Driving Style and Vehicle Performance on the Real World Fuel Consumption of U.S. Light-duty Vehicles* (Vol. 42, Issue 4) [PhD Thesis]. Massachusetts Institute of Technology https://doi.org/10.1017/CBO9781107415324.004

Bikis, A., & Pandey, D. (2021). Air Quality at Public Transportation Stations/Stops: Contribution of Light Rail Transit to Reduce Air Pollution. Aerosol Science and Engineering, 0123456789. https://doi.org/10.1007/s41810-021-00119-0

Bodisco, T., & Zare, A. (2019). *Emissions (RDE) Euro 6 Regulation Homologation Test*. *X*. https://doi.org/10.3390/en12122306

Boveroux, F., Cassiers, S., De Meyer, P., Buekenhoudt, P., Bergmans, B., Idczak, F., Jeanmart, H., Verhelst, S., & Contino, F. (2021). Impact of Mileage on Particle Number Emission Factors for EURO 5 and EURO 6 Diesel Passenger Cars. *Atmospheric Environment*, *244*. https://doi.org/10.1016/j.atmosenv.2020.117975

Busho, S. W., & Alemayehu, D. (2020). Applying 3D-Eco Routing Model to Reduce Environmental Footprint of Road Transports in Addis Ababa City. *Environmental Systems Research*, *9*(1), 1–22. https://doi.org/10.1186/s40068-020-00179-0

Cardoza Cedillo, L., Montoya, M., Jaldón, M., & Paredes, M. G. (2023). GHG Emission Accounting and Reduction Strategies in the Academic Sector: A Case Study in Mexico. Sustainability (Switzerland), 15(12). https://doi.org/10.3390/su15129745

Chappell, E. (2015). Improving the Precision of Vehicle Fuel Economy Testing on a Chassis Dynamometer [PhD Thesis]. University of Bath.

Chauhan, B. P., Joshi, G. J., & Parida, P. (2020). Development of Candidate Driving Cycles for an Urban Arterial Corridor of Vadodara City. Eur. Transp.-Trasp, 4(75), 1–16.

Chenna, S. T., & Shantanu Jathar. (2019). Artificial Neural Networks for Fuel Consumption and Emissions Modeling in Light-duty Vehicles [PhD Thesis]. Colorado State University.

Chen, Y., Liang, C., Liu, D., Niu, Q., Miao, X., Dong, G., Li, L., Liao, S., Ni, X., & Huang, X. (2023). Embedding-Graph-Neural-Network for Transient NOx Emissions Prediction. Energies, 16(1). https://doi.org/10.3390/en16010003

Chen, Z., Chao, Y., & Shengnan, F. (2020). A Convolutional Neural Network-Based Driving Cycle Prediction Method for Plug-in Hybrid Electric Vehicles with Bus Route. *IEEE Access*, *8*, 3255–3264. https://doi.org/10.1109/ACCESS.2019.2960771

Chindamo, D., & Gadola, M. (2018). What is the Most Representative Standard Driving Cycle to Estimate Diesel Emissions of a Light Commercial Vehicle? *IFAC-Papers OnLine*, *51*(5), 73–78. https://doi.org/10.1016/j.ifacol.2018.06.213

Costagliola, M. A., Costabile, M., & Prati, M. V. (2018). Impact of Road Grade on Real Driving Emissions From Two Euro 5 Diesel Vehicles. Applied Energy, 231, 586–593. https://doi.org/10.1016/j.apenergy.2018.09.108

Crosignani, P., Nanni, A., Pepe, N., Pozzi, C., Silibello, C., Poggio, A., & Conte, M. (2021). The Effect of Non-Compliance of Diesel Vehicle Emissions with Euro Limits on Mortality in the City of Milan. Atmosphere, 12(3). https://doi.org/10.3390/atmos12030342

Cuéllar-Álvarez, Y., Guevara-Luna, M. A., Belalcázar-Cerón, L. C., & Clappier, A. (2023). Well-to-Wheels Emission Inventory for the Passenger Vehicles of Bogotá, Colombia. International Journal of Environmental Science and Technology. https://doi.org/10.1007/s13762-023-04805-z

Czerwinski, J., Zimmerli, Y., Comte, P., & Bütler, T. (2016). Experiences and Results with Different PEMS. *Journal of Earth Sciences and Geotechnical Engineering*, *6*(4), 91-106.

Czerwinski, J., Zimmerli, Y., Hussy, A., Engelmann, D., Bonsack, P., Remmele, E., & Huber, G. (2018). Testing and Evaluating Real Driving Emissions with PEMS. *Combustion Engines*, *174*(3), 17–25. https://doi.org/10.19206/CE-2018-302

Dai, Z., Niemeier, D., & Eisinger, D. (2008). Driving Cycles: A New Cycle-Building Method that Better Represents Real-World Emissions. The U.C. Davis-Caltrans Air Quality Project, 66(66), 37.

Danyo Stephen, Abate Asferachew, Bekhechi Mohammed, & Köhlin Gunnar. (2017). *Realizing Ethiopia's Green Transformation: Country Environmental Analysis, Environment and Natural Resources Global Practice*.

Devarajaiah, D., & Muthumari, C. (2018). Evaluation of Power Consumption and MRR in WEDM of Ti–6Al–4V Alloy and its Simultaneous Optimization for Sustainable Production. Journal of the Brazilian Society of Mechanical Sciences and Engineering, 40(8). https://doi.org/10.1007/s40430-018-1318-y

DieselNet. (2020). *Emission Test Cycles: Worldwide Engine and Vehicle Test Cycles*. https://dieselnet.com/standards/cycles/

Divakarla, K. P., Emadi, A., & Razavi, S. N. (2014). Journey Mapping— A New Approach for Defining Automotive Drive Cycles. IEEE Transactions on Industry Applications, 52(6), 5121–5129. https://doi.org/10.1109/TIA.2016.2593694

Donateo, T., & Filomena, R. (2020). Real Time Estimation of Emissions in a Diesel Vehicle with Neural Networks. E3S Web of Conferences, 197, 06020. https://doi.org/10.1051/e3sconf/202019706020

Dornoff, J., Tietge, U., & Mock, P. (2020). On the Way to" Real-World" CO_2 Values: The European Passenger Car Market in Its First Year After Introducing the WLTP. https://trid.trb.org/view/1708352

Duarte, G. O., Gonçalves, G. A., & Farias, T. L. (2016). Analysis of Fuel Consumption and Pollutant Emissions of Regulated and Alternative Driving Cycles Based on Real-World Measurements. *Transportation Research Part D*, *44*, 43–54. https://doi.org/10.1016/j.trd.2016.02.009

Duran, A., & Earleywine, M. (2018). GPS Data Filtration Method for Drive Cycle Analysis Applications. SAE International, ISSN 0148-7191. https://doi.org/10.4271/2012-01-0743

Embiale, A., Zewge, F., Chandravanshi, B. S., & Sahle-Demessie, E. (2019). Levels of Trace Elements in PM10 Collected at Roadsides of Addis Ababa, Ethiopia, and Exposure Risk Assessment. *Environmental Monitoring and Assessment*, *191*(6). https://doi.org/10.1007/s10661-019-7503-3

Engeljehringer Kurt. (2018). Emission Regulation Trends. AVL. https://www.avl.com/documents/1982862/8084402/01+-+AVL-TechDay+Mattsee+-+Emission+Regulations+-+2018-04-05b.pdf

Engelmann, D., Zimmerli, Y., Czerwinski, J., & Bonsack, P. (2021). Real Driving Emissions in Extended Driving Conditions. Energies, 14(21). https://doi.org/10.3390/en14217310

Ericsson, E. (2001). Independent Driving Pattern Factors and their Infuence on Fuel-Use and Exhaust Emission Factors. *Transportation Research Part D*, *6*(5), 325–345.

Fan, Y. Van, Perry, S., Klemeš, J. J., & Lee, C. T. (2018). A Review on Air Emissions Assessment: Transportation. Journal of Cleaner Production, 194, 673–684. https://doi.org/10.1016/J.JCLEPRO.2018.05.151

Fan, W., Jiang, W., Chen, J., Yang, F., Qian, J., & Ye, H. (2023). Exhaust Emission Inventory of Typical Construction Machinery and its Contribution to Atmospheric Pollutants in Chengdu, China. *Journal of Environmental Sciences (China)*, *125*, 761–773. https://doi.org/10.1016/j.jes.2022.02.018

Farhang Motallebiaraghi, Aaron Rabinowitz, Shantanu Jathar, Alvis Fong, Zachary Asher, & Thomas Bradley. (2021). High-Fidelity Modeling of Light-Duty Vehicle Emission and Fuel Economy Using Deep Neural Networks. SAE Technical Paper, 1–11. https://doi.org/https://doi.org/10.4271/2021-01-0181

Fekadu, Y. (2017). Contribution of Vehicle Exhausts Gas Emissions to the Traffic Air Pollution of Selected Areas of Addis Ababa City [Msc Thesis]. Addis Ababa University.

Fontaras, G., & Ciuffo, N.-G. Z. B. (2017). Fuel Consumption and CO_2 Emissions from Passenger Cars in Europe-Laboratory Versus Real-World Emissions. *Progress in*

Energy and Combustion Science, *60*, 97–131. https://doi.org/10.1016/j.pecs.2016.12.004

Galgamuwa, U., Perera, L., & Bandara, S. (2015). Developing a General Methodology for Driving Cycle Construction: Comparison of Various Established Driving Cycles in the World to Propose a General Approach. *Journal of Transportation Technologies*, *05*(04), 191–203. https://doi.org/10.4236/jtts.2015.54018

Galgamuwa, U., Perera, L., & Bandara, S. (2016). Development of a Driving Cycle for Colombo, Sri Lanka: An Economical Approach for Developing Countries. Advanced Transportation, 50, 1520–1530. https://doi.org/10.1002/atr.1414

Gallus, J., Kirchner, U., Vogt, R., & Benter, T. (2017). Impact of Driving Style and Road Grade on Gaseous Exhaust Emissions of Passenger Vehicles Measured by a Portable Emission Measurement System (PEMS). Transportation Research Part D, 52(2), 215–226. https://doi.org/10.1016/j.trd.2017.03.011

George, B. (2016). Extensions of the General Linear Model into Methods within Partial Least Squares Structural Equation Modeling [PhD Thesis]. University of North Texas.

Ghaffarpasand, O., & Pope, F. D. (2024). Telematics Data for Geospatial and Temporal Mapping of Urban Mobility: New Insights into Travel Characteristics and Vehicle Specific Power. Journal of Transport Geography, 115, 103815. https://doi.org/10.1016/J.JTRANGEO.2024.103815

Giakoumis, E. G. (2017). Driving and Engine Cycles. Springer. https://doi.org/10.1007/978-3-319-49034-2

Giechaskiel, B., Casadei, S., Rossi, T., Forloni, F., & Domenico, A. Di. (2021). Measurements of the Emissions of a “Golden” Vehicle at Seven Laboratories with Portable Emission Measurement Systems (PEMS). Sustainability, 13(8762), 1–13. https://doi.org/https://doi.org/10.3390/su13168762

Giechaskiel, B., Clairotte, M., Valverde-morales, V., Bonnel, P., Kregar, Z., Franco, V., & Dilara, P. (2018). Framework for the Assessment of PEMS (Portable Emissions Measurement Systems) Uncertainty. *Environmental Research*, *166*(June), 251–260. https://doi.org/10.1016/j.envres.2018.06.012

Giechaskiel, B., Valverde, V., Kontses, A., Suarez-Bertoa, R., Selleri, T., Melas, A., Otura, M., Ferrarese, C., Martini, G., Balazs, A., Andersson, J., Samaras, Z., & Dilara, P.

(2021). Effect of Extreme Temperatures and Driving Conditions on Gaseous Pollutants of a Euro 6d-Temp Gasoline Vehicle. *Atmosphere*, *12*(1011), 1–25. https://doi.org/10.3390/atmos12081011

G. Mesay Berhanu. (2017). Ethiopia's Climate-Resilient Green Economy Strategy: A Critical Review. Hankuk University of Foreign Studies.

Gopal, R., Kavandappa Goundar, M., Ramasamy, S., Natarajan, N., & Ramasamy, V. (2014). Experimental and Regression Analysis for Multi Cylinder Diesel Engine Operated with Hybrid Fuel Blends. Thermal Science, 18(1), 193–203. https://doi.org/10.2298/TSCI130130127G

Grüner, J., & Marker, S. (2016). A Tool for Generating Individual Driving Cycles-IDCB. SAE International Journal of Commercial Vehicles, 9, 417–428. https://doi.org/10.4271/2016-01-9019

Guo, S., Wu, K., & Zhang, G. (2020). Application of PCA-K-Means++ Combination Model to Construction of Light Vehicle Driving Conditions in Intelligent Traffic. *Journal of Measurements in Engineering*, *8*(3), 107–121. https://doi.org/10.21595/jme.2020.21433

Hanna Wang-Helmreich, & Florian Mersmann. (2019). Implementation of Nationally Determined Contributions: Ethiopian Country Report. http://www.umweltbundesamt.de/publikationen

Hassine, H., Omrane, F., Barkallah, M., Louati, J., & Haddar, M. (2021). Modelling Vehicle Emissions Using Artificial Neural Network and Multiple Linear Regression Methods. *Journal of Urban and Environmental Engineering*, *15*(1), 58–67. https://doi.org/10.4090/juee.2020.v15n1.058067

He, Y. (2020). Research on the Construction Method of Vehicle Driving Cycle Based on Mean Shift Clustering. *ArXiv Preprint*, 1–26.

Ho, S., Wong, Y., & Chang, V. W. (2014). Developing Singapore Driving Cycle for Passenger Cars to Estimate Fuel Consumption and Vehicular Emissions. *Atmospheric Environment*, *97*, 353–362. https://doi.org/10.1016/j.atmosenv.2014.08.042

Howlader, A. M., Patel, D., & Gammariello, R. (2023). Data-Driven Approach for Instantaneous Vehicle Emission Predicting Using Integrated Deep Neural Network.

Transportation Research Part D: Transport and Environment, *116*. https://doi.org/https://doi.org/10.1016/j.trd.2023.103654

Huertas, I., Quirama, L. F., & Giraldo, M. (2019). Comparison of Three Methods for Constructing Real Driving Cycles. Energies, 12(4), 665. https://doi.org/10.3390/en12040665

Huertas, J. I., Giraldo, M., Quirama, L. F., & Díaz, J. (2018). Driving Cycles Based on Fuel Consumption. *Energies*, *11*(3064), 1–13. https://doi.org/10.3390/en11113064

Huertas, J. I., Quirama, L. F., Giraldo, M. D., & Díaz, J. (2019). Comparison of Driving Cycles Obtained by the Micro-trips, Markov-Chains and MWD-CP Methods. Sustainable Energy Planning and Management, 22, 109–120. https://doi.org/http://dx.doi.org/10.5278/ijsepm.2554

Hui He, & Lingzhi Jin. (2017). *A Historical Review of the US Vehicle Emission Compliance Program and Emission Recall Cases*. https://theicct.org/wp-content/uploads/2021/06/EPA-Compliance-and-Recall_ICCT_White-Paper_12042017_vF.pdf

Hung, W. T., Tong, H. Y., Lee, C. P., Ha, K., & Pao, L. Y. (2007). Development of a Practical Driving Cycle Construction Methodology: A Case Study in Hong Kong. Transportation Research Part D, 12, 115–128. https://doi.org/10.1016/j.trd.2007.01.002

Jaikumar, R., Shiva Nagendra, S. M., & Sivanandan, R. (2017). Modal Analysis of Real Time, Real World Vehicular Exhaust Emissions under Heterogeneous Traffic Conditions. *Transportation Research Part D: Transport and Environment*, *54*, 397–409. https://doi.org/10.1016/j.trd.2017.06.015

Jida, S. N., Hetet, J. F., & Chesse, P. (2020). Estimation of Exhaust and Non-Exhaust Particulate Matter Emissions' Share from On-Road Vehicles in Addis Ababa City. *International Journal of Environmental and Ecological Engineering*, *14*(6), 145–149.

Ji, Y., Li, C., Xie, J., Wang, Y., & Guo, W. (2018). Bus Driving Cycle Construct Based on Principal Component Analysis for Lanzhou City. *14th International Conference on Wireless Communications, Networking and Mobile Computing (WiCOM 2018)*, *137*, 416–425.

Jonson, J. E., Borken-Kleefeld, J., Simpson, D., Nyíri, A., Posch, M., & Heyes, C. (2017). Impact of Excess NOx Emissions from Diesel Cars on Air Quality, Public Health and Eutrophication in Europe. Environmental Research Letters, 12(9). https://doi.org/10.1088/1748-9326/aa8850

Kamble, S. H., Mathew, T. V., & Sharma, G. K. (2009). Development of Real-world Driving Cycle: case Study of Pune, India. *Transportation Research Part D: Transport and Environment*, *14*(2), 132–140. https://doi.org/10.1016/j.trd.2008.11.008

Karimipour, H., Tam, V. W. Y., Le, K. N., & Burnie, H. (2021). Routing on-road Heavy Vehicles for Alleviating Greenhouse Gas Emissions. *Cleaner Engineering and Technology*, *5*. https://doi.org/10.1016/j.clet.2021.100325

Kawsar, S., Biswas, S., Noor, M., & Mamun, M. S. (2023). Investigating the Applicability of COPERT 5.5 Emission Software in Bangladesh and Developing Countrywide Vehicular Emission Inventories. *Environmental Science: Atmospheres*. https://doi.org/10.1039/d3ea00047h

Khalfan, A. M. (2016). Analysis of Tailpipe Emissions, Thermal Efficiency and Fuel Consumption for Urban Real World Driving Using a SI Passenger Car as a Probe [PhD Thesis]. The University of Leeds.

Khumla, P., Radpukdee, T., & Satiennam, T. (2010). Driving Cycle Generation for Emissions and Fuel Consumption Assessment of the Motorcycles in Khon Kaen City. *The First TSME International Conference on Mechanical Engineering*, 1–9.

Kim, W., Kim, C., Lee, J., Yun, C., & Yook, S. (2018). Characteristics of Nanoparticle Emission from a Light-Duty Diesel Vehicle During Test Cycles Simulating Urban Rush-Hour Driving Patterns. *J Nanopart Res*, *20:94*, 1–12. https://doi.org/https://doi.org/10.1007/s11051-018-4197-3

Kiran, S., & Verma, A. (2018). A Novel Methodology for Construction of Driving Cycles for Indian Cities. Transportation Research Part D, 65, 725–735. https://doi.org/10.1016/j.trd.2018.10.013

Kousoulidou, M., Ntziachristos, L., Gkeivanidis, S., & Samaras, Z. (2010). Validation of the COPERT Road Emission Inventory Model with Real-Use Data. *Emissions Inventories—Informing Emerging Issues*, *40*.

Kühlwein, J., German, J., & Bandivadekar, A. (2014). Development of Test Cycle Conversion Factors Among Worldwide Light-Duty Vehicle CO_2 Emission standards. In *The international council on clean transportation* (2014).

Kumar, S., Sood, V., Singh, Y., & Channiwala, S. A. (2016). Real World Vehicle Emissions: Their Correlation with Driving Parameters. *Transportation Research Part D*, *44*, 157–176. https://doi.org/10.1016/j.trd.2016.02.001

Lairenlakpam, R., Jain, A. K., Gupta, P., Kamei, W., & Badola, R. (2018). Effect of Real World Driving and Different Drive Modes on Vehicle Emissions and Fuel Consumption. SAE Technical Paper, 01(5017), 1–10. https://doi.org/10.4271/2018-01-5017

Lee, T., & Filipi, Z. S. (2011). Synthesis of Real-world Driving Cycles Using Stochastic Process and Statistical Methodology. International Journal of Vehicle Design, 57(1), 17–36.

Lejri, D., Can, A., Schiper, N., & Leclercq, L. (2018). Accounting for Traffic Speed Dynamics when Calculating COPERT and PHEM Pollutant Emissions at the Urban Scale. *Transportation Research Part D: Transport and Environment*, *63*, 588–603. https://doi.org/10.1016/j.trd.2018.06.023

Lin, C., Zhou, X., & Wu, D. (2019). Estimation of Emissions at Signalized Intersections Using an Improved MOVES Model with GPS data. International Journal of Environmental Research and Public Health, 16(9), 3647. https://doi.org/https://doi.org/10.3390/ijerph16193647

Lipar, P., Strnad, I., Česnik, M., & Maher, T. (2016). Development of Urban Driving Cycle with GPS Data Post Processing. PROMET-Traffic&Transportation, 28(4), 353–364. https://doi.org/10.7307/ptt.v28i4.1916

Liu, H., Ma, J., Dong, F., Yang, Y., Liu, X., Ma, G., Zheng, Z., & Yao, M. (2018). Experimental Investigation of the Effects of Diesel Fuel Properties on Combustion & Emissions on a Multi-Cylinder Heavy-Duty Diesel Engine. Energy Conversion & Management, 171, 1787–1800. https://doi.org/10.1016/J.ENCONMAN.2018.06.089

Liu, H., Rodgers, M., & Guensler, R. (2019). Impact of Road Grade on Vehicle Speed Acceleration Distribution, Emissions and Dispersion Modeling on Freeways.

Transportation Research Part D: Transport and Environment, *69*, 107–122. https://doi.org/10.1016/j.trd.2019.01.028

Liu, H., Zhao, J., Qing, T., Li, X., & Wang, Z. (2021). Energy Consumption Analysis of a Parallel PHEV with Different Configurations Based on a Typical Driving Cycle. Energy Reports, 7, 254–265. https://doi.org/10.1016/j.egyr.2020.12.036

Liu, X., Ma, J., Zhao, X., Du, J., & Xiong, Y. (2020). Study on Driving Cycle Synthesis Method for City Buses Considering Random Passenger Load. *Journal of Advanced Transportation*, *2020*. https://doi.org/10.1155/2020/3871703

Liu, Y., Liang, Y., Yu, H., An, X., & Li, J. (2021). Comparative Analysis of China Light-duty Vehicle Test cycle for Passenger Car and Other Typical Driving Cycles. *E3S Web of Conferences (Vol. 241, p. 02002). EDP Sciences*, *02002*, 4–8.

Liu, Y., Li, J., & Shen, B. (2014). Research on Driving Cycle of Long-distance Passenger Vehicles Based on Principal Component Analysis and Cluster Algorithm. *International Journal of Control and Automation*, *7*(3), 125–136. https://doi.org/http://dx.doi.org/10.14257/ijca.2014.7.3.13

Liu, Y., Wu, Z. X., Zhou, H., Zheng, H., Yu, N., An, X. P., Li, J. Y., & Li, M. L. (2020). Development of China Light-Duty Vehicle Test cycle. International Journal of Automotive Technology, 21(5), 1233–1246. https://doi.org/10.1007/s12239-020-0117-5

Li, Y., Wang, G., Murphy, C., & Kleeman, M. J. (2023). Modeling Expected Air Quality Impacts of Oregon's Proposed Expanded Clean Fuels Program. *Atmospheric Environment*, *296*, 119582. https://doi.org/10.1016/j.atmosenv.2023.119582

Lozhkina, O. V., & Lozhkin, V. N. (2015). Estimation of Road Transport Related Air Pollution in Saint Petersburg Using European and Russian Calculation Models. *Transportation Research Part D: Transport and Environment*, *36*, 178–189. https://doi.org/10.1016/j.trd.2015.02.013

Luján, J. M., Bermúdez, V., Dolz, V., & Monsalve-serrano, J. (2018). An Assessment of the Real-World Driving Gaseous Emissions from a Euro 6 Light-Duty Diesel Vehicle Using a Portable Emissions Measurement System. *Atmospheric Environment*, *174* (November 2017), 112–121. https://doi.org/10.1016/j.atmosenv.2017.11.056

Mahayadin, A. R., Ibrahim, I., Zunaidi, I., Shahriman, A. B., Faizi, M. K., Sahari, M., Hashim, M. S. M. M., Saad, M. A. M. M., Sarip, M. S., Razlan, Z. M., Rani, M. F. H. H., Isa, Z. M., Kamarrudin, N. S., Harun, A., & Nagaya, Y. (2018). Development of Driving Cycle Construction Methodology in Malaysia's Urban Road System. *International Conference on Computational Approach in Smart Systems Design and Applications (ICASSDA) (Pp. 1-5), 978-1-5386-8369-9/18*, 1–5. https://doi.org/10.1109/ICASSDA.2018.8477619

Mahayadin, A. R., Shahriman, A. B., Hashim, M. S. M., Razlan, Z. M., Faizi, M. K., Harun, A., Kamarrudin, N. S., Ibrahim, I., Saad, M. A. M., Rani, M. F. H., Zunaidi, I., Sahari, M., Sarip, M. S., & Razali, M. Q. H. A. (2017). Efficient Methodology of Route Selection for Driving Cycle Development. *Journal of Physics: Conference Series (Vol. 908, No. 1, p. 012082)*, 1–9. https://doi.org/10.1088/1742-6596/908/1/012082

Marques, K. S. D. S., Palmeira, A. D. S., Moreira, D. M., & Nascimento, E. G. S. (2021). Estimation of Emissions by Road Vehicles in the Metropolitan Region of Salvador, Brazil. Air Pollution XXIX, 252(2021), 105–114. https://doi.org/10.2495/AIR210101

Meena, S., & Singh, S. K. (2022). Assessment of Real Driving Emissions from Vehicles Using Portable Emission Measurement Systems: A Systematic Review. Applied Ecology and Environmental Sciences, 10(5), 273–280. https://doi.org/10.12691/aees-10-5-2

Mei, H., Wang, L., Wang, M., Zhu, R., Wang, Y., Li, Y., Zhang, R., Wang, B., & Bao, X. (2021). Characterization of Exhaust CO, HC and NOx Emissions from Light-Duty Vehicles under Real Driving Conditions. Atmosphere, 12(9). https://doi.org/10.3390/atmos12091125

Meng, X., Pang, K., Di, B., Li, W., Wang, Y., Zhang, J., & Xu, Y. (2023). Road Grade Estimation for Vehicle Emissions Modeling using Electronic Atmospheric Pressure Sensors. *Frontiers in Environmental Science, 10*. https://doi.org/10.3389/fenvs.2022.1051858

Ministry of Water and Energy. (2013). *Ethiopian National Energy Policy (2nd draft).*

Mirsad Trobradović, Boran Pikula, Almir Blažević, D. B. (2020). Investigation of Vehicle Driving Cycles in Urban Traffic Condition. *New Technologies, Development and Application III 6 (Pp. 554-559). Springer International Publishing*, 1–6.

Mohammed, A. S., Atnaw, S. M., Salau, A. O., & Eneh, J. N. (2023). Review of Optimal Sizing and Power Management Strategies for Fuel Cell/Battery/Super Capacitor Hybrid Electric Vehicles. In *Energy Reports* (Vol. 9, pp. 2213–2228). Elsevier Ltd. https://doi.org/10.1016/j.egyr.2023.01.042

Moradi, M. H., Heinz, A., Wagner, U., & Koch, T. (2022). Modeling the Emissions of a Gasoline Engine During High-Transient Operation Using Machine Learning Approaches. *International Journal of Engine Research*, *23*(10), 1708–1716. https://doi.org/10.1177/14680874211032381

Najem, H. S., Jawad, Q. A., Ali, A. K., & Munahi, B. S. (2018). Developing a General Methodology and Construct a Driving Cycle with an Economic Performance Evaluation for Basrah City. *International Journal of Engineering & Technology*, *7*(4.19), 939–944.

Nakamura, K., Dardiotis, C., Kandlhofer, C., & Arndt, M. (2019). Challenges Related to the Measurement of Particle Emissions of Gasoline Direct Injection Engines Under Cold-Start and Low-Temperature Conditions. *International Journal of Automotive Engineering*, *10*(4), 332–339. https://doi.org/https://doi.org/10.20485/jsaeijae.10.4_332

Nandi, B. P., Singh, G., Jain, A., & Tayal, D. K. (2023). Evolution of Neural Network to Deep Learning in Prediction of Air, Water Pollution and its Indian Context. In International Journal of Environmental Science and Technology. Institute for Ionics. https://doi.org/10.1007/s13762-023-04911-y

Nguyen, Y. T., & Bui, N. D. (2020). GPS Data Processing for Driving Cycle Development in Hanoi, Vietnam. *Journal of Engineering Science and Technology*, *15*(2), 1429–1440.

Nguyen, Y. T., Nghiem, T., Le, A., & Bui, N. (2019). Development of the Typical Driving Cycle for Buses in Hanoi, Vietnam. *Journal of the Air & Waste Management Association*, *69*(4), 423–437. https://doi.org/10.1080/10962247.2018.1543736

Noralm, Z. (2018). *Implementing a Method for Conducting Real Driving Emission (RDE)* [KTH]. www.kth.se

Nouri, P., & Morency, C. (2017). Evaluating Microtrip Definitions for Developing Driving Cycles. Transportation Research Board, 2627, 86–92. https://doi.org/http://dx.doi.org/10.3141/2627-10

Ntziachristos, L., Gkatzoflias, D., & Kouridis, C. (2009). COPERT: A European Road Transport Emission Inventory Model. *Information Technologies in Environmental Engineering: Proceedings of the 4th International ICSC Symposium*, *5* (January), 491–504. https://doi.org/10.1007/978-3-540-88351-7

Pavlovic, J., Fontaras, G., Ktistakis, M., Anagnostopoulos, K., Komnos, D., Ciuffo, B., Clairotte, M., & Valverde, V. (2020). Understanding the Origins and Variability of the Fuel Consumption Gap: Lessons Learned from Laboratory Tests and a Real-driving Campaign. *Environmental Sciences Europe*, *32*(53), 1–16. https://doi.org/10.1186/s12302-020-00338-1

Peng, J., Jiang, J., Ding, F., & Tan, H. (2020). Development of Driving Cycle Construction for Hybrid Electric Bus: A Case Study in Zhengzhou, China. *Sustainability (Switzerland)*, *12*(7188), 1–19. https://doi.org/10.3390/su12177188

Peng, J., Pan, D., & He, H. (2015). Study on the Driving Cycle Construction for City Hybrid Bus. *International Conference on Intelligent Systems Research and Mechatronics Engineering*, *(ISRME 2015)*, 1491–1497.

Peng, Y., Zhuang, Y., & Yang, Y. (2019). A Driving Cycle Construction Methodology Combining K-Means Clustering and Markov Model for Urban Mixed Roads. Automobile Engineering, I–II, 1–11. https://doi.org/10.1177/0954407019848873

Perec, A. (2022). Desirability Function Analysis (DFA) in Multiple Responses Optimization of Abrasive Water Jet Cutting Process. Reports in Mechanical Engineering, 3(1), 11–19. https://doi.org/10.31181/rme200103011p

Pielecha, J., Skobiej, K., & Kurtyka, K. (2021). Testing and Evaluation of Cold-Start Emissions From a Gasoline Engine in RDE Test at Two Different Ambient Temperatures. Open Engineering, 11(1), 425–434. https://doi.org/10.1515/eng-2021-0047

Pilusa, T. J., Mollagee, M. M., & Muzenda, E. (2012). Reduction of Vehicle Exhaust Emissions from Diesel Engines using the Whale Concept Filter. Aerosol and Air Quality Research, 12(5), 994–1006. https://doi.org/10.4209/aaqr.2012.04.0100

Piotr Wiśniowski, Ślęzak, M., & Niewczas, A. (2019). Simulation of Road Traffic Conditions on a Chassis. *The Archives of Automotive Engineering*, *84*(2), 171–178.

Predić, B., Madić, M., Roganović, M., Kovačević, M., & Stojanović, D. (2016). Prediction of Passenger Car Fuel Consumption Using Artificial Neural Network: A Case Study in the City of Niš (Vol. 15, Issue 2).

Puchalski, A., Komorska, I., Slezak, M., & Niewczas, A. (2020). Synthesis of Naturalistic Vehicle Driving Cycles using the Markov Chain Monte Carlo Method. *Eksploatacja i Niezawodność, 22(2), 316-322*. https://doi.org/10.17531/ein.2020.2.14

Qiu, D., Li, Y., & Qiao, D. (2018). Recurrent Neural Network Based Driving Cycle Development for Light Duty Vehicles in Beijing. *Transportation Research Procedia*, *34*, 147–154. https://doi.org/10.1016/j.trpro.2018.11.026

Rahman, S. M. A., Fattah, I. M. R., Ong, H. C., Ashik, F. R., Hassan, M. M., Murshed, M. T., Imran, M. A., Rahman, M. H., Rahman, M. A., Hasan, M. A. M., & Mahlia, T. M. I. (2021). State-of-the-art of Establishing Test Procedures For Real Driving Gaseous Emissions From Light and Heavy-Duty Vehicles. Energies, 14(4195), 1–32. https://doi.org/10.3390/en14144195

Ramprasanna, S. R., Ganesh, A. C., Basil Gnanappa, S., & Sutharsan, R. (2020). Comparison Between Artificial Neural Network and SPSS to Predict Vehicle Emission. *AIP Conference Proceedings*, *2204*. https://doi.org/10.1063/1.5141554

Ren, Z., Yang, H., & Lu, T. (2014). Effects of Small-Scale Turbulence on NOx Formation in Premixed Flame Fronts. *Fuel*, *115*, 241–247. https://doi.org/10.1016/J.FUEL.2013.06.037

Ricardo, S., Victor, V., Michael, C., Jelica, P., Barouch, G., Vicente, F., Zlatko, K., Covadonga, A., Suarez-bertoa, R., Valverde, V., Clairotte, M., Pavlovic, J., Giechaskiel, B., Franco, V., Kregar, Z., & Astorga, C. (2019). On-road Emissions of Passenger Cars Beyond the Boundary Conditions of the Real-Driving Emissions Test. *Environmental Research*, *176*(108572), 1–12. https://doi.org/10.1016/j.envres.2019.108572

Romero, C. A., Mejía, L. A., & Acosta, R. (2017). Engine Data Collection and Development of a Pilot Driving Cycle for Pereira City by using Low Cost Diagnostic

Tools. Ingeniería y Competitividad, 19(2), 11–24. https://doi.org/https://doi.org/10.25100/iyc.v19i2.5287

Rosenblatt Debbie, Winther Kim, & Rosenblatt Debbie. (2020). Real Driving Emissions and Fuel Consumption: A Report from the Advanced Motor Fuels Technology Collaboration Programme.

Roychowdhury, A., Chandola, P., & Chattopadhyaya, V. (2016). Urban Air Quality Management in Ethiopia: A Guidance Framework. *Center for Science and Environment (CSE): Delhi, India*.

Sachin Chugh, Prashant Kumar, M Muralidharan, Mukesh Kumar B, M Sithananthan, Anurag Gupta, Biswajit Basu, & Ravinder Kumar Malhotra. (2012). Development of Delhi Driving Cycle: A Tool for Realistic Assessment of Exhaust Emissions from Passenger Cars in Delhi. *SAE International*, *2012-01–0877*. https://doi.org/10.4271/2012-01-0877

Šarkan, B., Loman, M., Synák, F., Skrúcaný, T., & Hanzl, J. (2022). Emissions Production by Exhaust Gases of a Road Vehicle’s Starting Depending on a Road Gradient. Sensors, 22(24). https://doi.org/10.3390/s22249896

Sati, S. A., & Dare, A. J. (2022). An Analysis of the Level of Vehicular Emission in Kaduna Metropolis. *Ghana Journal of Geography*, *14*(1). https://doi.org/10.4314/gjg.v14i1.1

Seo, J., & Park, S. (2023). Optimizing Model Parameters of Artificial Neural Networks to Predict Vehicle Emissions. Atmospheric Environment, 294(119508). https://doi.org/https://doi.org/10.1016/j.atmosenv.2022.119508

Seo, J., Yun, B., Kim, J., Shin, M., & Park, S. (2022). Development of a Cold-Start Emission Model for Diesel Vehicles Using an Artificial Neural Network Trained with Real-World Driving Data. Science of the Total Environment, 806. https://doi.org/10.1016/j.scitotenv.2021.151347

Shafie-Pour, M., & Tavakoli, A. (2013). On-road Vehicle Emissions Forecast Using IVE Simulation Model. Int. J. Environ. Res., 7(2), 367–376. https://www.sid.ir/en/VEWSSID/J_pdf/108220130209.pdf

Shams, S. R., Jahani, A., Moeinaddini, M., & Khorasani, N. (2020). Air Carbon Monoxide Forecasting using an Artificial Neural Network in Comparison with Multiple

Regression. *Modeling Earth Systems and Environment*, *6*(3), 1467–1475. https://doi.org/10.1007/s40808-020-00762-5

Sheen Mclean Cabaneros, John Kaiser Calautit, & Ben Richard Hughes. (2019). A Review of Artificial Neural Network Models for Ambient Air Pollution Prediction. *Environmental Modelling & Software, 119, 285-304., 119,* 285–304. https://doi.org/https://doi.org/10.1016/j.envsoft.2019.06.014

Shepelev, V., Glushkov, A., Slobodin, I., & Cherkassov, Y. (2023). Measuring and Modelling the Concentration of Vehicle-Related PM2.5 and PM10 Emissions Based on Neural Networks. Mathematics, 11(5). https://doi.org/10.3390/math11051144

Shi, J., Yao, Q., Han, X., Wang, Y., Wu, X., Tian, S., Wang, J., Yang, X., Xie, H., Xiang, F., & Ning, P. (2023). Chemical Characteristics of PM2.5 Emitted from Motor Vehicles Exhaust under the Plateau with Low Oxygen Content. *Atmospheric Environment*, *314*, 120053. https://doi.org/10.1016/J.ATMOSENV.2023.120053

Shi, S., Lin, N., Zhang, Y., Cheng, J., Huang, C., Liu, L., & Lu, B. (2016). Research on Markov Property Analysis of Driving Cycles and its Application. *Transportation Research Part D*, *47*, 171–181. https://doi.org/10.1016/j.trd.2016.05.013

Shridhar Bokare, P., & Kumar Maurya, A. (2013). Study of Effect of Speed, Acceleration and Deceleration of Small Petrol Car on its Tail Pipe Emission. *International Journal for Traffic & Transport Engineering*, *3*(4), 465–478. https://doi.org/10.7708/ijtte.2013.3(4).09

Singh, S., Kulshrestha, M. J., Rani, N., Kumar, K., Sharma, C., & Aswal, D. K. (2023). An Overview of Vehicular Emission Standards. *Mapan - Journal of Metrology Society of India*, *38*(1), 241–263. https://doi.org/10.1007/s12647-022-00555-4

Singh, V., Biswal, A., Kesarkar, A. P., Mor, S., & Ravindra, K. (2020). High Resolution Vehicular PM10 Emissions Over Megacity Delhi: Relative Contributions of Exhaust and Non-exhaust Sources. Science of the Total Environment, 699. https://doi.org/10.1016/j.scitotenv.2019.134273

Suarez-bertoa, R., Valverde, V., Clairotte, M., Pavlovic, J., Giechaskiel, B., Franco, V., Kregar, Z., & Astorga, C. (2019). On-road Emissions of Passenger Cars Beyond the Boundary Conditions of the Real-Driving Emissions Test. Environmental Research, 176 (January), 108572. https://doi.org/10.1016/j.envres.2019.108572

Taka, G. N., Huong, T. T., & Shah, I. H. (2020). *Determinants of Energy-Based CO_2 Emissions in Ethiopia: A Decomposition Analysis from 1990 to 2017*. 1–17.

Tamsanya, N., & Chungpaibulpatana, S. (2009). Influence of Driving Cycles on Exhaust Emissions and Fuel Consumption of Gasoline Passenger Car in Bangkok. *Journal of Environmental Sciences*, *21*(5), 604–611. https://doi.org/10.1016/S1001-0742(08)62314-1

Tang, J., Gong, R., Wang, H., & Liu, Y. (2023). Scenario Analysis of Transportation Carbon Emissions in China Based on Machine Learning and Deep Neural Network Models. Environmental Research Letters, 18(6). https://doi.org/10.1088/1748-9326/acd468

Tarekegn, M. M., & Gulilat, T. Y. (2018). Trends of Ambient Air Pollution and the Corresponding Respiratory Diseases in Addis Ababa. Research and Reports on Toxicology, 2(1:5), 1–14. www.imedpub.com

Tefera, W., Kumie, A., Berhane, K., Gilliland, F., Lai, A., Sricharoenvech, P., Samet, J., Patz, J., & Schauer, J. J. (2020). Chemical Characterization and Seasonality of Ambient Particles (PM2.5) in the City Centre of Addis Ababa. *International Journal of Environmental Research and Public Health*, *17*(19), 1–16. https://doi.org/10.3390/ijerph17196998

Teoh, J. X., Stella, M., & Chew, K. W. (2019). Performance Analysis of Electric Vehicle in Worldwide Harmonized Light Vehicles Test Procedure via Vehicle Simulation Models in ADVISOR. *IEEE 9th International Conference on System Engineering and Technology (ICSET)*, *9th*, 215–220.

Thomas, D., Li, H., Wang, X., Song, B., Ge, Y., Yu, W., & Ropkins, K. (2017). A Comparison of Tailpipe Gaseous Emissions for RDE and WLTC Using SI Passenger Cars. *Proceedings of the SAE Powertrain Fuels and Lubricants Meeting 2017*, *01–2391*, 1–14. https://doi.org/10.4271/2017-01-2391

Thorisingam, Y., & Mustafa, M. S. (2022). Augmented Approach to Desirability Function Based on Principal Component Analysis. *International Journal of Academic Research in Progressive Education and Development*, *11*(2). https://doi.org/10.6007/ijarped/v11-i2/13270

Tim Murrells. (2017). *Method for Applying Emission Degradation Correction Factors to The COPERT 5 NOx Emission Factors for Petrol Cars and LGVs*. https://www.gov.uk/government/publications/road-vehicle-emission-factors-2009

Tong, H. Y., & Ng, K. W. (2020). A Bottom-Up Clustering Approach to Identify Bus Driving Patterns and to Develop Bus Driving Cycles for Hong Kong. Environmental Science and Pollution Research, 1–15. https://doi.org/https://doi.org/10.1007/s11356-020-11554-w

Triantafyllopoulos, G., Dimaratos, A., Ntziachristos, L., Bernard, Y., Dornoff, J., & Samaras, Z. (2019). A study on the CO_2 and NOx Emissions Performance of Euro 6 Diesel Vehicles Under Various Chassis Dynamometer and On-road Conditions Including Latest Regulatory Provisions. Science of the Total Environment, 666, 337–346. https://doi.org/10.1016/j.scitotenv.2019.02.144

Tsanakas, N., Ekstr, J., & Olstam, J. (2020). Estimating Emissions from Static Traffic Models: Problems and Solutions. Journal of Advanced Transportation, 1–17. https://doi.org/https://doi.org/10.1155/2020/5401792

Tsegaye, D., Leta, S., & Khan, M. M. (2019). Ambient Air Pollution Status of Addis Ababa City ; The Case of Selected Roadside. 8(2), 39–47. https://doi.org/10.11648/j.ajep.20190802.11

Tsiakmakis, S., Marotta, A., Pavlovic, J., & Anagnostopoulos, K. (2017). The Difference Between Reported and Real-world CO_2 Emissions: How Much Improvement can be Expected by WLTP Introduction? *Transportation Research Procedia*, *25C*, 3937–3947. https://doi.org/10.1016/j.trpro.2017.05.333

Tsokolis, D., Tsiakmakis, S., Dimaratos, A., Fontaras, G., Pistikopoulos, P., Ciuffo, B., & Samaras, Z. (2020). Fuel Consumption and CO_2 Emissions of Passenger Cars over the New Worldwide Harmonized Test Protocol. *Applied Energy*, *179*(443), 1152–1165. https://doi.org/10.1016/j.apenergy.2016.07.091

Tutuianu, M., Marotta, A., Steven, H., Ericsson, E., Haniu, T., Ichikawa, N., & Ishii, H. (2014). Development of a Worldwide Harmonized Light Duty Driving Test Cycle (WLTC) (Vol. 68th, Issue GRPE-68-03).

Tzamkiozis, T., Ntziachristos, L., Merkisz, J., & Lijewski, P. (2017). Assessment of Real Driving Emissions Via Portable Emission Measurement System. *IOP Conference*

Series: Materials Science and Engineering, 1–11. https://doi.org/10.1088/1757-899X/252/1/012084

USAID. (2015). *Greenhouse Gas Emissions in Ethiopia* (Issue 2011).

Uwe Tietge, Sonsoles Díaz, Peter Mock, Anup Bandivadekar, Jan Dornoff, & Norbert Ligterink. (2019). From Laboratory to Road: A 2018 Update of Official and "Real-World" Fuel Consumption and CO_2 Values for Passenger Cars in Europe. www.theicct.org

Varella, R. A., Duarte, G., Patricia, B., Villafuerte, P. M., & Sousa, L. (2017). Analysis of the Influence of Outdoor Temperature in Vehicle Cold-Start Operation Following EU Real Driving Emission Test Procedure. *SAE International*, *10*(2), 596–607. https://doi.org/10.4271/2017-24-0140

Varella, R. A., & Giechaskiel, B. (2018). Comparison of Portable Emissions Measurement Systems (PEMS) with Laboratory Grade Equipment. *MDPI Applied Science*, *1633*, 1–12. https://doi.org/10.3390/app8091633

Varella, R. A., & Villafuerte, P. M. (2017). Comparison of Data Analysis Methods for European Real Driving Emissions Regulation. *SAE International*, *6*(01–0997). https://doi.org/10.4271/2017-01-0997.

Viteri, R., Borge, R., Paredes, M., & Pérez, M. A. (2023). A High Resolution Vehicular Emissions Inventory for Ecuador using the IVE Modelling System. Chemosphere, 315. https://doi.org/10.1016/j.chemosphere.2022.137634

Wang, H., Wu, L., Hou, C., & Ouyang, M. (2013). A GPS-based Research on Driving Range and Patterns of Private Passenger Vehicle in Beijing. International Battery, Hybrid and Fuel Cell Electric Vehicle Symposium, 1–7.

Wang, J., Wang, Q. N., Zeng, X. H., Wang, P. Y., & Wang, J. N. (2015). Driving Cycle Recognition Neural Network Algorithm Based on the Sliding Time Window for Hybrid Electric Vehicles. *International Journal of Automotive Technology*, *16*(4), 685–695. https://doi.org/10.1007/s12239

Wang, T., Cheng, Y., Hu, J., Wan, C., & Zou, B. (2021). Remote NOx Emission Prediction Model based on LSTM Neural Network. E3S Web of Conferences, 268. https://doi.org/10.1051/e3sconf/202126801006

Wang, Y., Szeto, W. Y., Han, K., & Friesz, T. L. (2018). Dynamic Traffic Assignment: A Review of the Methodological Advances for Environmentally Sustainable Road Transportation Applications. Transportation Research Part B: Methodological, 111, 370–394. https://doi.org/10.1016/J.TRB.2018.03.011

Weiss, M., Paffumi, E., Clairotte, M., Drossinos, Y., & Vlachos, T. (2017). Including Cold-Start Emissions in the Real-Driving Emissions (RDE) Test Procedure Effects. https://doi.org/10.2760/70237

Williams, R., Hamje, H., Andersson, J., & Ziman, P. (2018). Comparison of Real Driving Emissions and Chassis Dynamometer Tests on Emissions of Two Fuels in Three Euro 6 Diesel Cars. 7th Transport Research Arena TRA, 1–11.

Witaszek, K. (2020). Modeling of Fuel Consumption using Artificial Neural Networks. *Diagnostyka*, *21*(4), 103–113. https://doi.org/10.29354/diag/130610

Wondifraw, B. (2018). Estimation of Exhaust Emission from Road Transport using COPERT Software: The case of Addis Ababa, Ethiopia. Research Gate, August 2018, 0–15. https://doi.org/10.13140/RG.2.2.14593.71529

World Population Review. (2021). http://worldpopulationreview.com/world-cities/addis-ababa-population/

Wu, Y., Wang, P., Muhammad Farhan, S., Yi, J., & Lei, L. (2019). Effect of Post-Injection on Combustion and Exhaust Emissions in DI Diesel Engine. Fuel, 258, 116131. https://doi.org/10.1016/J.FUEL.2019.116131

Wu, Y., Zhang, W., Zhang, L., Qiao, Y., Yang, J., & Cheng, C. (2020). A Multi-Clustering Algorithm to Solve Driving Cycle Prediction Problems Based on Unbalanced Data Sets : *MDPI Sensors*, *20*(2448), 1–22. https://doi.org/doi:10.3390/s20092448

Wu, Z., Deng, P., & Han, Z. (2022). A Numerical Study on Fuel Film and Emissions Formations During Cold Start in a Diesel Engine using an Improved Spray-Wall Impingement Model. *Fuel*, *320*,123898. https://doi.org/10.1016/J.FUEL.2022.123898

Xing, J., Shao, L., Zheng, R., Peng, J., Wang, W., Guo, Q., Wang, Y., Qin, Y., Shuai, S., & Hu, M. (2017). Individual Particles Emitted from Gasoline Engines: Impact of Engine Types, Engine Loads and Fuel Components. Journal of Cleaner Production, 149, 461–471. https://doi.org/10.1016/J.JCLEPRO.2017.02.056

Xu, S. (2013). LVQ Neural Network based Driving Cycles Recognition for Hybrid Electric Vehicles. *Applied Mechanics and Materials*, *253–255*(2013), 2113–2116. https://doi.org/10.4028/www.scientific.net/AMM.253-255.2113

Yakın, A., & Behçet, R. (2021). Effect of Different Types of Fuels Tested in a Gasoline Engine on Engine Performance and Emissions. International Journal of Hydrogen Energy, 46(66), 33325–33338. https://doi.org/10.1016/J.IJHYDENE.2021.07.133

Yang, Y., Li, T., Hu, H., Zhang, T., Cai, X., & Chen, S. (2019). Development and Emissions Performance Analysis of Local Driving Cycle for Small-Sized Passenger Cars in Nanjing, China. Atmospheric Pollution Research, 10(5), 1514–1523. https://doi.org/10.1016/j.apr.2019.04.009

Yang, Z., Deng, B., Deng, M., & Huang, S. (2018). An Overview of Chassis Dynamometer in the Testing of Vehicle Emission. *MATEC Web of Conferences*, *02015*, 2–5. https://doi.org/https://doi.org/10.1051/matecconf/201817502015

Yugendar, P., Rao, K. R., & Tiwari, G. (2020). Driving Cycle Estimation and Validation for Ludhiana City, India. Traffic and Transport Engineering, 2(10), 229–235. https://doi.org/http://dx.doi.org/10.7708/ijtte.2020.10(2).08

Zégé, L. C., Ámosi, A. V, & Ocsis, I. K. (2020). Review on Construction Procedures of Driving Cycles. International Journal of Engineering and Management Sciences (IJEMS), 5(2), 266–285. https://doi.org/10.21791/IJEMS.2020.2.31.1.

Zhang, L., Huang, Z., Yu, F., Liao, S., Luo, H., Zhong, Z., Zhu, M., Li, Z., Cui, X., Yan, M., & Zheng, J. (2021). Road type-based Driving Cycle Development and Application to Estimate Vehicle Emissions for Passenger Cars in Guangzhou. *Atmospheric Pollution Research*, *12*(8). https://doi.org/10.1016/j.apr.2021.101138

Zhang, S., Wu, Y., Liu, H., Huang, R., Un, P., & Zhou, Y. (2014). Real-World Fuel Consumption and CO_2 (Carbon Dioxide) Emissions By Driving Conditions For Light-Duty Passenger Vehicles in China. Energy, 69, 247–257. https://doi.org/10.1016/j.energy.2014.02.103

Zhao, M., Gao, H., Han, Q., Ge, J., Wang, W., & Qu, J. (2021). Development of a Driving Cycle for Fuzhou Using K-Means and AMPSO. *Journal of Advanced Transportation*, *2021*, 1–15. https://doi.org/10.1155/2021/5430137

Zhao, P., Wang, Y., Chang, N., Zhu, Q., & Lin, X. (2018). A Deep Reinforcement Learning Framework for Optimizing Fuel Economy of Hybrid Electric Vehicles. *IEEE*, 196–202.

Zhao, X., Yu, Q., Ma, J., Wu, Y., Yu, M., & Ye, Y. (2018). Development of a Representative EV Urban Driving Cycle based on a k-Means and SVM Hybrid Clustering Algorithm. *Journal of Advanced Transportation*, *2018*, 22–25. https://doi.org/10.1155/2018/1890753

Zhou, B., Li, Y., Ding, Y., Huang, G., & Shen, Z. (2023). An Input-Output-based Bayesian Neural Network Method for Analyzing Carbon Reduction Potential: A Case Study of Guangdong Province. *Journal of Cleaner Production*, *389*, 135986. https://doi.org/10.1016/J.JCLEPRO.2023.135986

Zhou, W., Xu, K., Yang, Y., & LU, J. (2017). Driving Cycle Development for Electric Vehicle Application Using Principal Component Analysis and K-means Cluster: With the Case of Shenyang, China. The 8th International Conference on Applied Enegy-ICAE2016, 105, 2831–2836. https://doi.org/10.1016/j.egypro.2017.03.620

Zhu, C., Qu, X., Qiu, M., Zhu, C., Wang, C., Wang, B., Sun, L., Yang, N., Yan, G., Xu, C., & Li, L. (2023). High Spatiotemporal Resolution Vehicular Emission Inventory in Beijing-Tianjin-Hebei and its Surrounding Areas (BTHSA) during 2000–2020, China. *Science of the Total Environment*, *873*. https://doi.org/10.1016/j.scitotenv.2023.162389

Zhu, S. (2014). *Development of Vehicle Emissions Models for Australian Conditions*. University of Queensland.

PUBLICATIONS FROM THIS DISSERTATION

In the following papers, parts of this dissertation have been published in peer-reviewed journals.

Published Journal Papers

1. Gebisa, A., Gebresenbet, G., Gopal, R., & Nallamothu, R. B. (2021). Driving Cycles for Estimating Vehicle Emission Levels and Energy Consumption. Future transportation, 1(3), 615-638. https://doi.org/10.3390/futuretransp1030033
2. Gebisa, A., Gebresenbet, G., Gopal, R., & Nallamothu, R. B. (2022). A Neural Network and Principal Component Analysis Approach to Develop a Real-Time Driving Cycle in an Urban Environment: The Case of Addis Ababa, Ethiopia. Sustainability, 14(21), 13772. https://doi.org/10.3390/su142113772
3. Gebisa, A., Gebresenbet, G., Gopal, R., & Nallamothu, R. (2024). Impacts of Vehicle Speed and Slope on Tailpipe Emissions Using Desirability Function Analysis. Ethiopian Journal of Science and Sustainable Development, 11(1), 1-14. https://doi.org/10.20372/ejssdastu:v11.i1.2024.743
4. Gebisa A.; Gebresenbet, G.; Gopal, R.; Nallamothu, R.B. Route-Based Emissions Inventory and Energy Consumption of Passenger Vehicles: Case of Addis Ababa, Ethiopia. ***Under review***
5. Gebisa A.; Gebresenbet, G.; Gopal, R.; Nallamothu, R.B. Real-Time Simulation of Tailpipe Emissions Using Simulink and Artificial Neural Networks. ***Under review***

Conference presentation

1. Gebisa A.; Gebresenbet, G.; Gopal, R.; Nallamothu, R.B. Comparison of Driving Cycles Obtained by the Micro Trip and Neural Network Prediction Methods: The Case of Addis Ababa, Ethiopia. OSST Midterm Conference on January 14, 2023.

APPENDICES

Appendix A: Chassis Dynamometer Experimental Setup

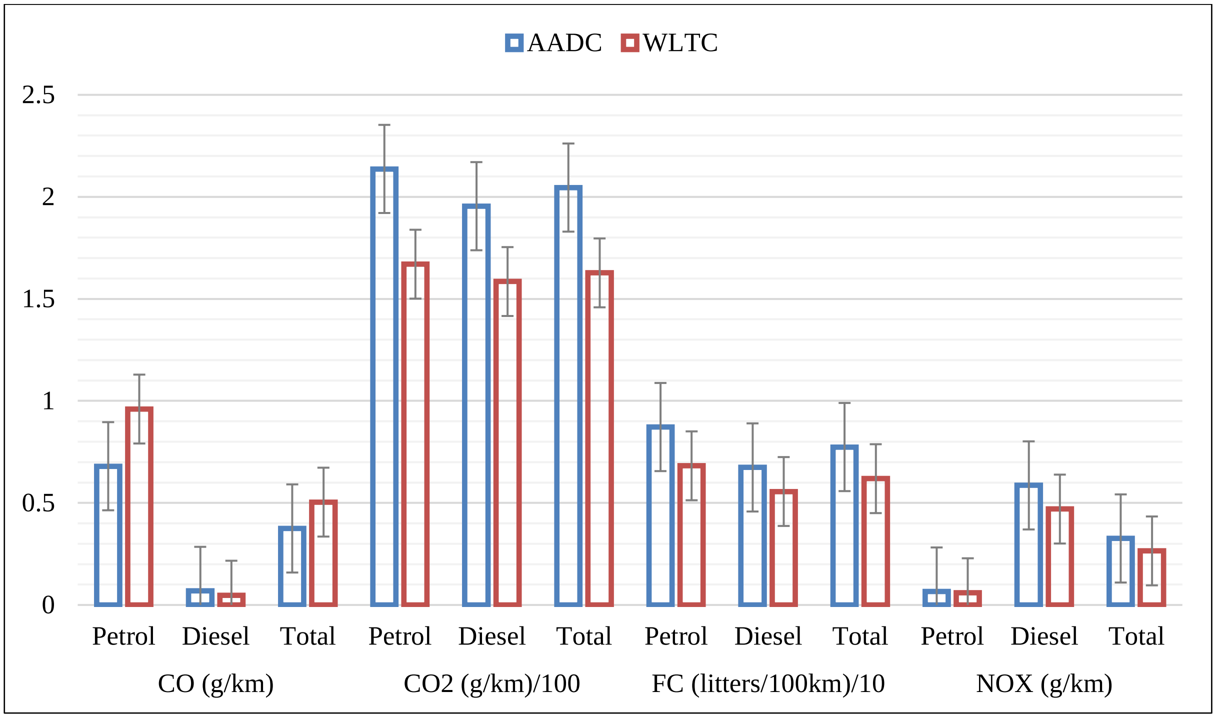

Figure A2: Results of emissions and FC from chassis dynamometer tests, with error bars

Appendix B: The Coverage of Collected Driving Data

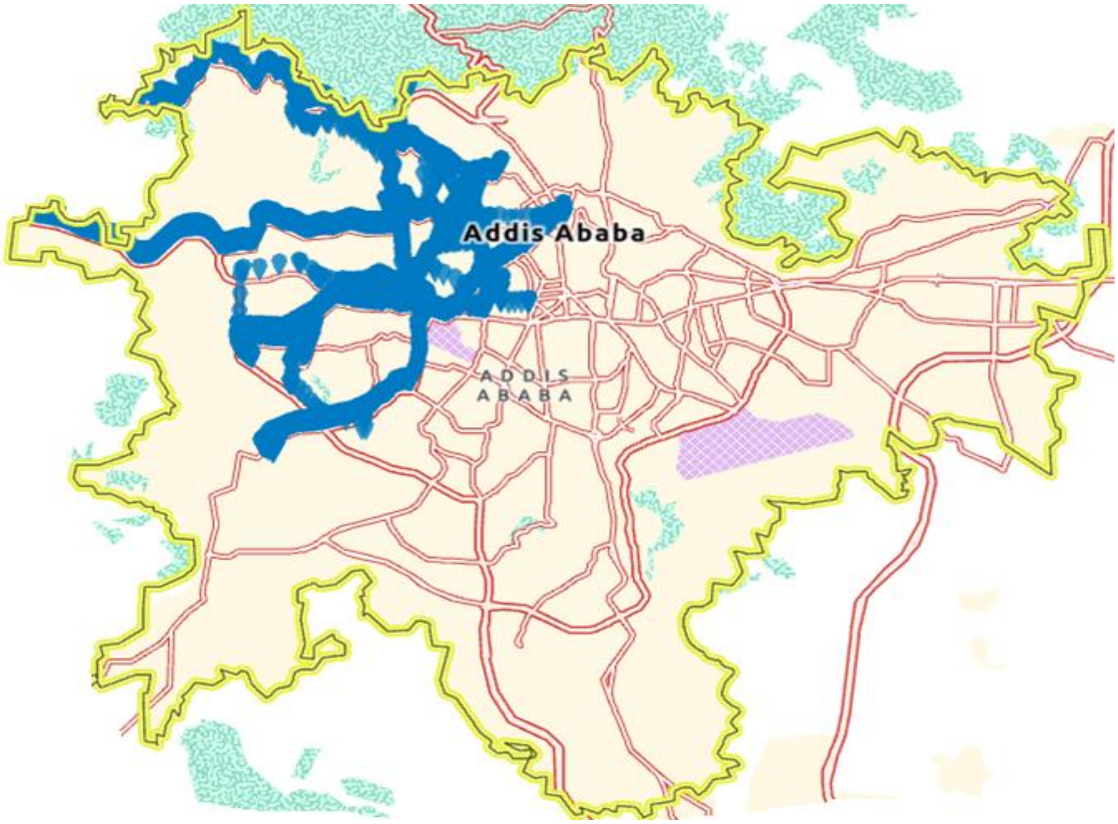

From Vehicle A

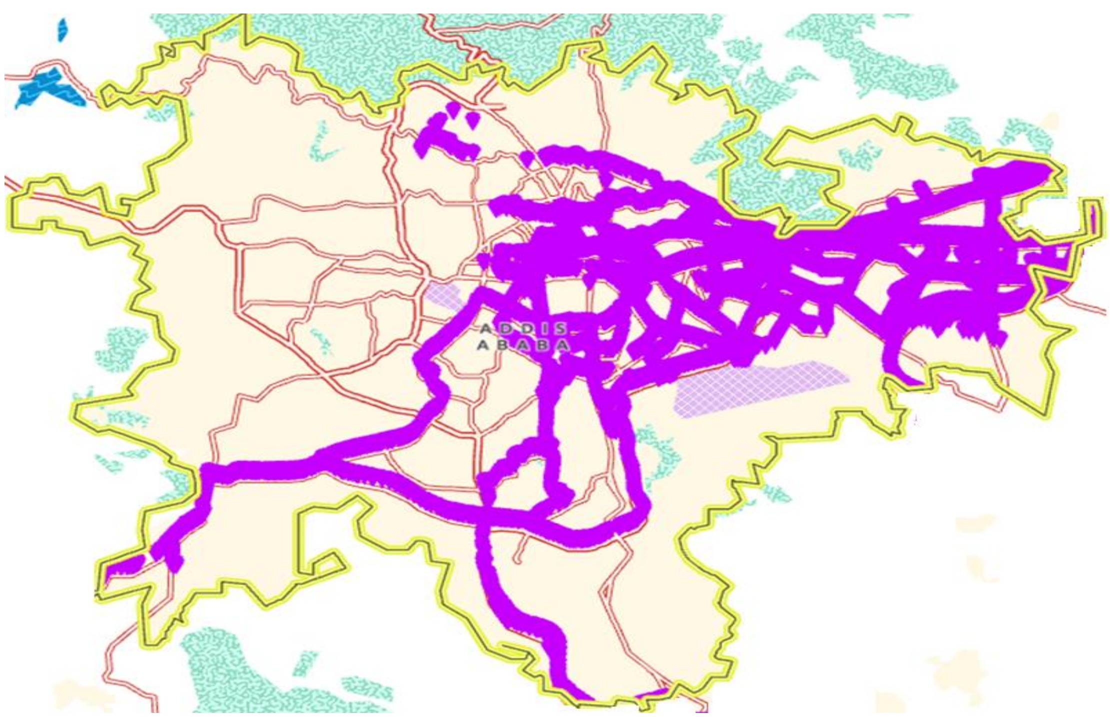

From Vehicle B

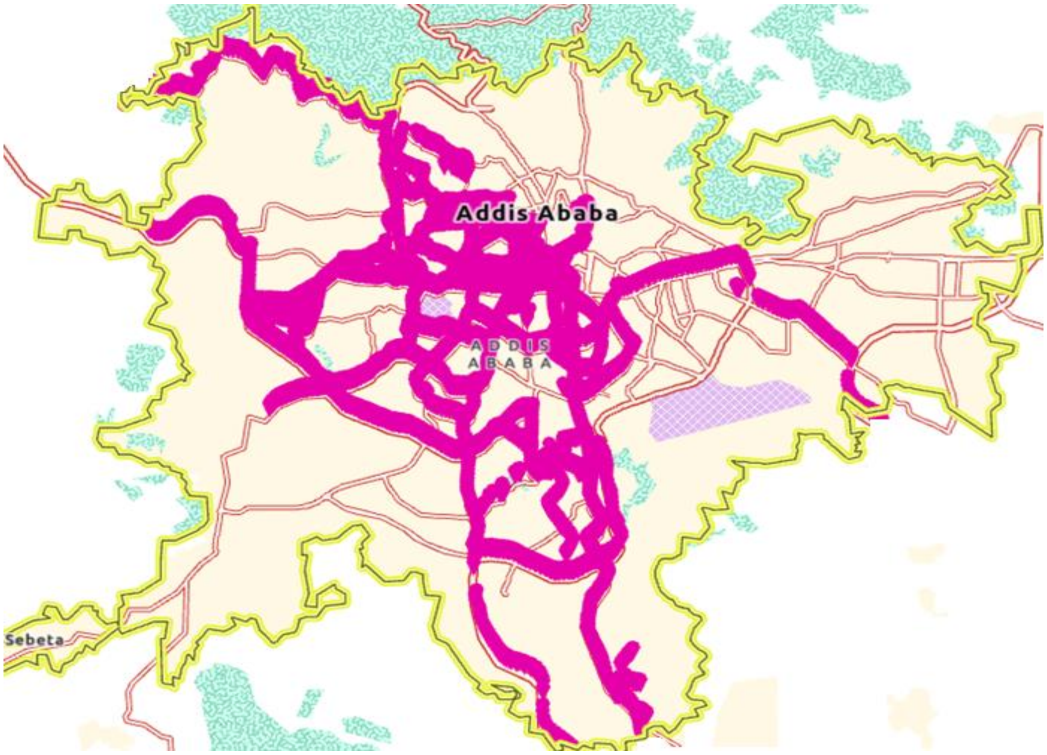

From Vehicle C

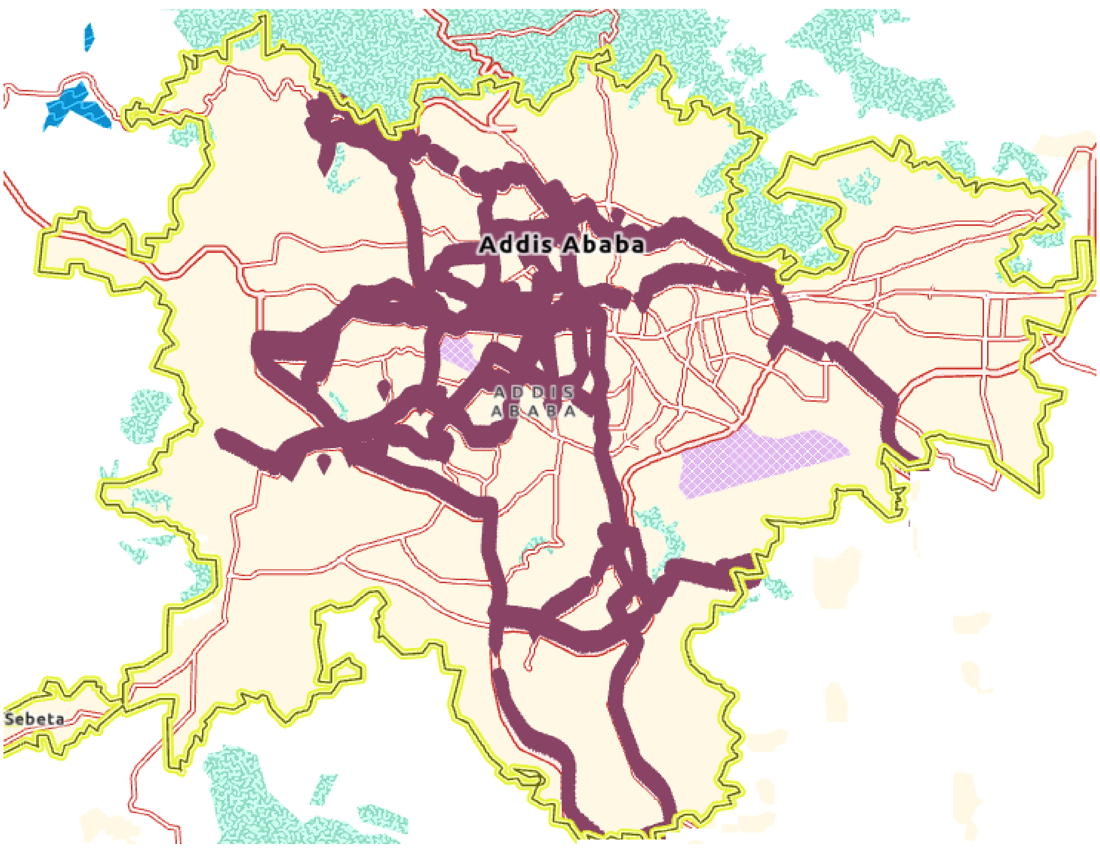

From Vehicle D

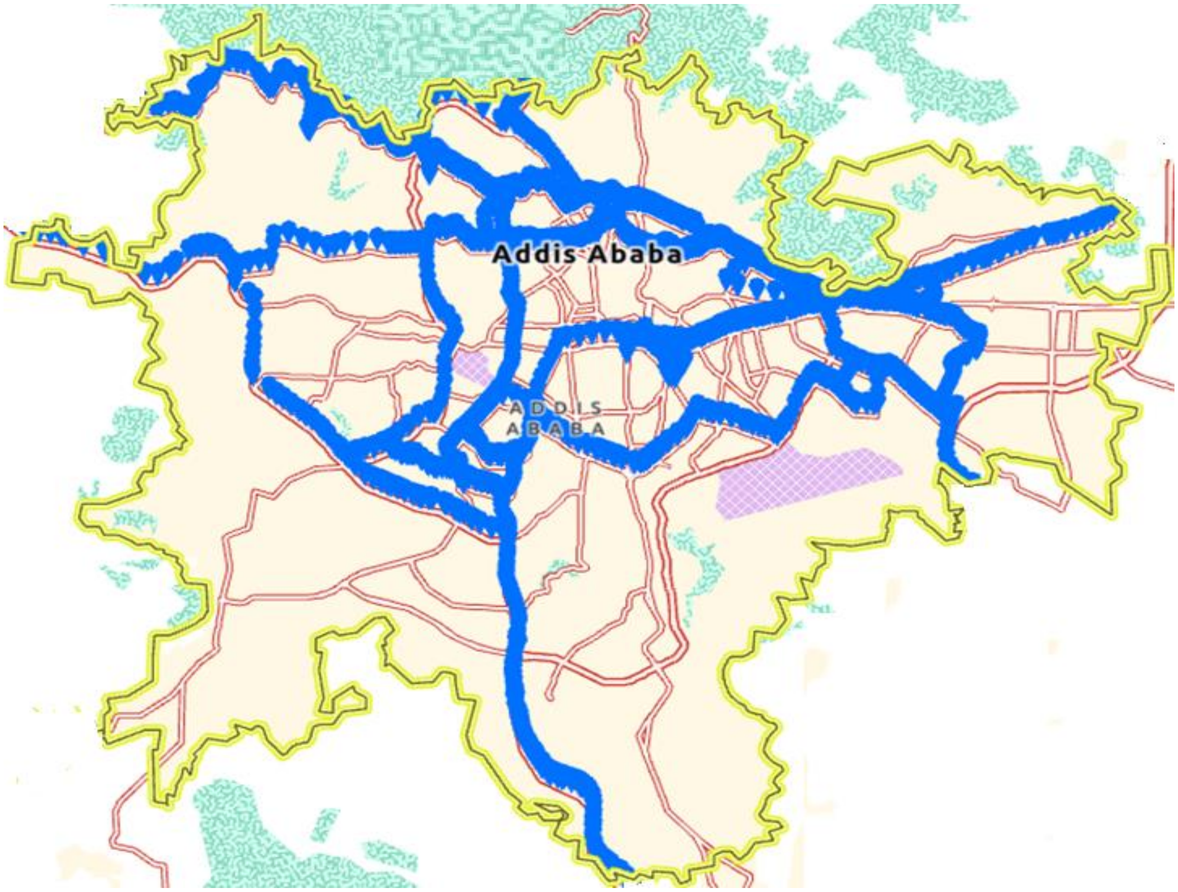

From Vehicle E

Figure B1: A map illustrating the routes used for driving data collection in AA

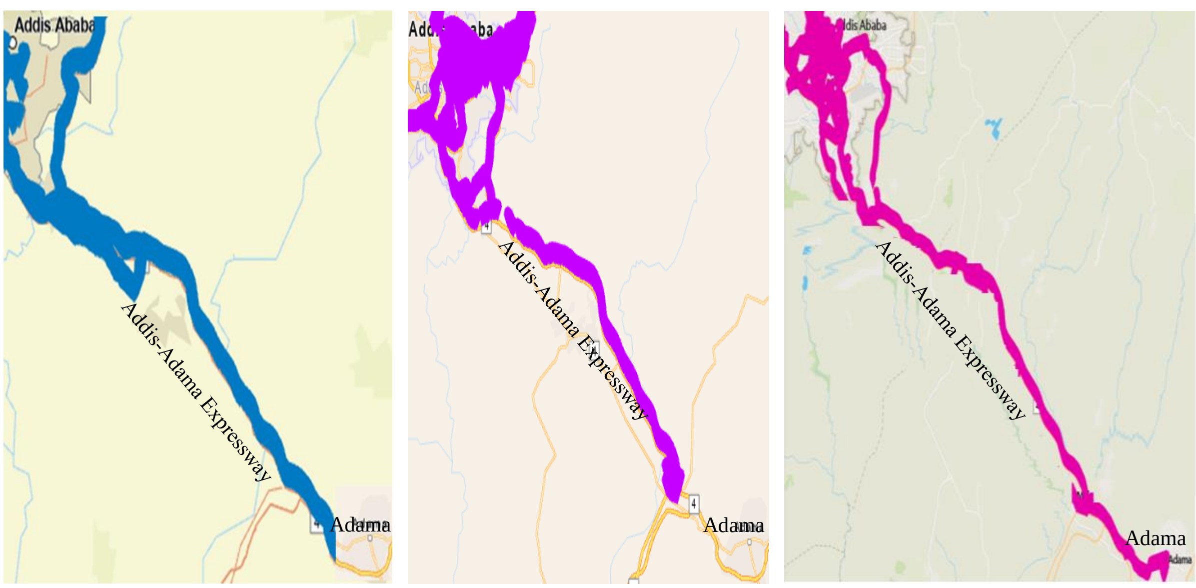

From Vehicle A From Vehicle B From Vehicle C

Figure B2: A map depicting the coverage of the driving data collected from AAE

Appendix C: Removing and Fixing Outliers

Outliers were identified using shape-preserving cubic interpolation (PCHIP) by implementing the moving mean window-centered method. 9 and 105 outliers were identified from data collected by vehicles A, and B respectively, and filled as shown in Figure C1.

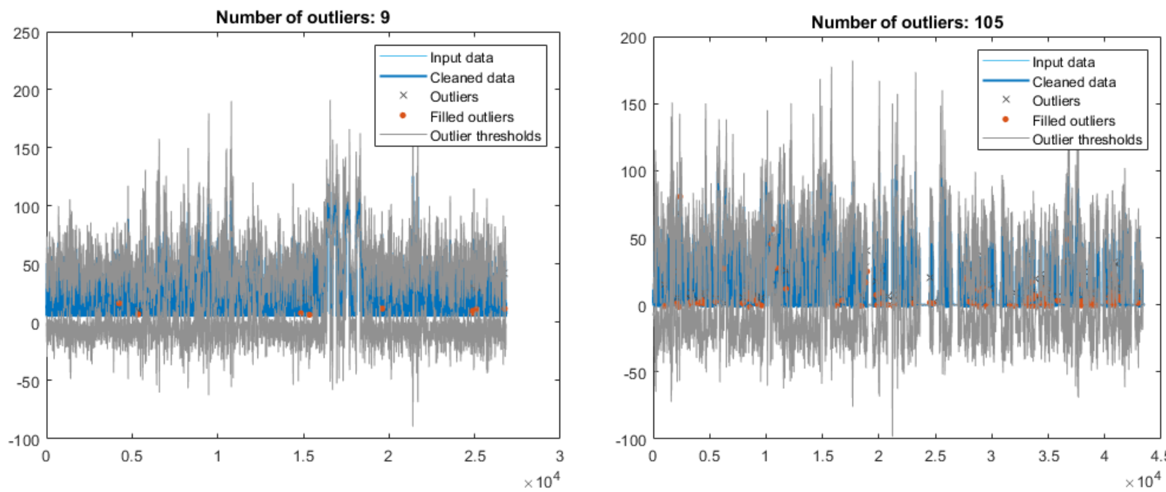

Figure C1: Outliers Vs input data of vehicles A, and B

After filling outliers it is necessary to remove the noise from the collected raw data. Bayes wavelet signal denoise method was implemented to remove noise from the collected data. The screenshot of smoothed data of vehicle A output is shown in Figure C2.

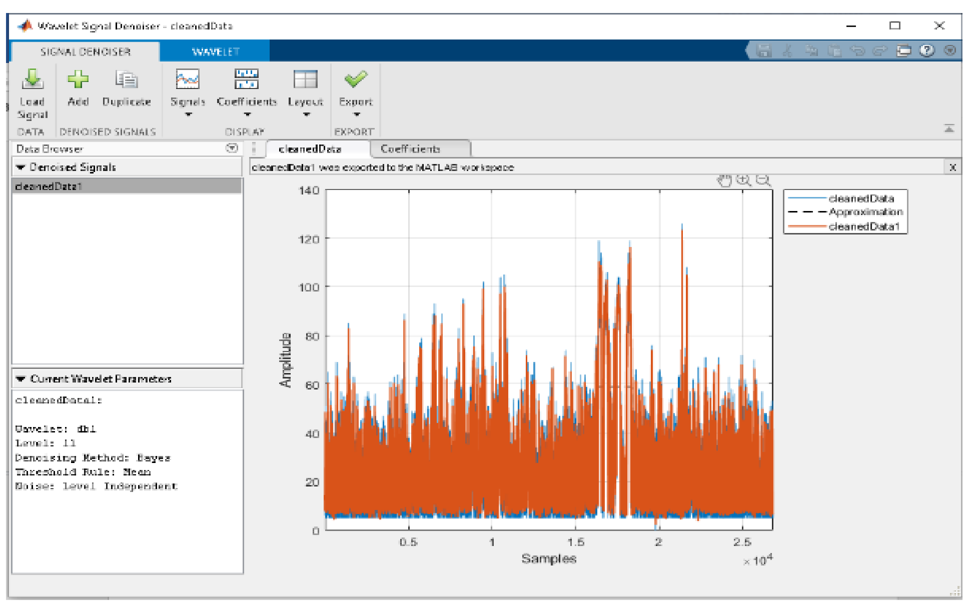

Figure C2: Smoothed collected data Vs raw data of vehicle A

Appendix D: Syntax Used in Matlab

D1: Fill outliers

```
[cleanedData,outlierIndices,thresholdLow,thresholdHigh] = filloutliers(V,..."pchip","movmean",15);
% Display results clf plot(V,"Color",[77 190 238]/255,"DisplayName","Input data")
hold on
plot(cleanedData,"Color",[0 114 189]/255,"LineWidth",1.5,..."DisplayName","Cleaned data")
% Plot outliers
plot(find(outlierIndices),V(outlierIndices),"x","Color",[64 64 64]/255,..."DisplayName","Outliers")
title("Number of outliers: " + nnz(outlierIndices))
% Plot filled outliers
plot(find(outlierIndices),cleanedData(outlierIndices),".","MarkerSize",12,..."Color",[217 83
25]/255,"DisplayName","Filled outliers")
% Plot outlier thresholds
plot([(1:numel(V))'; missing; (1:numel(V))'],...
    [thresholdHigh(:); missing; thresholdLow(:)],"Color",[145 145 145]/255,...
    "DisplayName","Outlier thresholds")
hold off
legend
clear outlierIndices thresholdLow thresholdHigh
cleanedData1 = wdenoise(cleanedData,11, ...
    'Wavelet', 'db1', ...
    'DenoisingMethod', 'Bayes', ...
    'ThresholdRule', 'Mean', ...
    'NoiseEstimate', 'LevelIndependent');
```

D2: Classification learner

```
function [trainedClassifier, validationAccuracy] = trainClassifier(trainingData)
% [trainedClassifier, validationAccuracy] = trainClassifier(trainingData)
inputTable = trainingData;
predictorNames = {'FAC1_1', 'FAC2_1', 'FAC3_1', 'FAC4_1', 'FAC5_1'};
predictors = inputTable(:, predictorNames);
response = inputTable.Length;
isCategoricalPredictor = [false, false, false, false, false];
classificationNeuralNetwork = fitcnet(...
    predictors, ...
    response, ...
    'LayerSizes', 10, ...
    'Activations', 'relu', ...
    'Lambda', 0, ...
    'IterationLimit', 1000, ...
    'Standardize', true, ...
    'ClassNames', categorical({'ELT'; 'LT'; 'MT'; 'ST'}));
```

```
predictorExtractionFcn = @(t) t(:, predictorNames);
neuralNetworkPredictFcn = @(x) predict(classificationNeuralNetwork, x);
trainedClassifier.predictFcn = @(x) neuralNetworkPredictFcn(predictorExtractionFcn(x));
trainedClassifier.RequiredVariables = {'FAC1_1', 'FAC2_1', 'FAC3_1', 'FAC4_1', 'FAC5_1'};
trainedClassifier.ClassificationNeuralNetwork = classificationNeuralNetwork;
inputTable = trainingData;
predictorNames = {'FAC1_1', 'FAC2_1', 'FAC3_1', 'FAC4_1', 'FAC5_1'};
predictors = inputTable(:, predictorNames);
response = inputTable.Length;
isCategoricalPredictor = [false, false, false, false, false];
partitionedModel = crossval(trainedClassifier.ClassificationNeuralNetwork, 'KFold', 5);
 [validationPredictions, validationScores] = kfoldPredict(partitionedModel);
validationAccuracy = 1 - kfoldLoss(partitionedModel, 'LossFun', 'ClassifError');
```

D3: NN Clustering

```
% Solve a Clustering Problem with a Self-Organizing Map
x = LC1';
dimension1 = 3;
dimension2 = 3;
net = selforgmap([dimension1 dimension2]);
net.plotFcns = {'plotsomtop','plotsomnc','plotsomnd', ...
   'plotsomplanes', 'plotsomhits', 'plotsompos'};
 [net,tr] = train(net,x);
y = net(x);
view(net)
%figure, plotsomtop(net)
%figure, plotsomnc(net)
%figure, plotsomnd(net)
%figure, plotsomplanes(net)
%figure, plotsomhits(net,x)
%figure, plotsompos(net,x)
if (false)
        genFunction(net,'myNeuralNetworkFunction');
   y = myNeuralNetworkFunction(x);
end
if (false)
      genFunction(net,'myNeuralNetworkFunction','MatrixOnly','yes');
   y = myNeuralNetworkFunction(x);
end
if (false)
      gensim(net);
end
```

D4: Neural network based speed prediction

```
% Solve an Autoregression Problem with External Input with a NARX Neural Network
X = tonndata(InputEU,false,false);
T = tonndata(TargetEU,false,false);
 trainFcn = 'trainbr';
 inputDelays = 1:2;
feedbackDelays = 1:2;
hiddenLayerSize = 10;
net = narxnet(inputDelays,feedbackDelays,hiddenLayerSize,'open',trainFcn);
net.inputs{1}.processFcns = {'removeconstantrows','mapminmax'};
net.inputs{2}.processFcns = {'removeconstantrows','mapminmax'};
  [x,xi,ai,t] = preparets(net,X,{},T);
net.divideFcn = 'dividerand';
net.divideMode = 'time';
net.divideParam.trainRatio = 70/100;
net.divideParam.valRatio = 15/100;
net.divideParam.testRatio = 15/100;
net.performFcn = 'mse';
net.plotFcns = {'plotperform','plottrainstate', 'ploterrhist', ...
    'plotregression', 'plotresponse', 'ploterrcorr', 'plotinerrcorr'};
 [net,tr] = train(net,x,t,xi,ai);
y = net(x,xi,ai);
e = gsubtract(t,y);
performance = perform(net,t,y)
trainTargets = gmultiply(t,tr.trainMask);
valTargets = gmultiply(t,tr.valMask);
testTargets = gmultiply(t,tr.testMask);
trainPerformance = perform(net,trainTargets,y)
valPerformance = perform(net,valTargets,y)
testPerformance = perform(net,testTargets,y)
view(net)
%figure, plotperform(tr)
%figure, plottrainstate(tr)
%figure, ploterrhist(e)
%figure, plotregression(t,y)
%figure, plotresponse(t,y)
%figure, ploterrcorr(e)
%figure, plotinerrcorr(x,e)
netc = closeloop(net);
netc.name = [net.name ' - Closed Loop'];
view(netc)
[xc,xic,aic,tc] = preparets(netc,X,{},T);
yc = netc(xc,xic,aic);
```

```
closedLoopPerformance = perform(net,tc,yc)
 numTimesteps = size(x,2);
knownOutputTimesteps = 1:(numTimesteps-5);
predictOutputTimesteps = (numTimesteps-4):numTimesteps;
X1 = X(:,knownOutputTimesteps);
T1 = T(:,knownOutputTimesteps);
[x1,xio,aio] = preparets(net,X1,{},T1);
[y1,xfo,afo] = net(x1,xio,aio);
x2 = X(1,predictOutputTimesteps);
[netc,xic,aic] = closeloop(net,xfo,afo);
[y2,xfc,afc] = netc(x2,xic,aic);
multiStepPerformance = perform(net,T(1,predictOutputTimesteps),y2)
nets = removedelay(net);
nets.name = [net.name ' - Predict One Step Ahead'];
view(nets)
[xs,xis,ais,ts] = preparets(nets,X,{},T);
ys = nets(xs,xis,ais);
stepAheadPerformance = perform(nets,ts,ys)
 if (false)
   genFunction(net,'myNeuralNetworkFunction');
   y = myNeuralNetworkFunction(x,xi,ai);
end
if (false)
   genFunction(net,'myNeuralNetworkFunction','MatrixOnly','yes');
   x1 = cell2mat(x(1,:));
   x2 = cell2mat(x(2,:));
   xi1 = cell2mat(xi(1,:));
   xi2 = cell2mat(xi(2,:));
   y = myNeuralNetworkFunction(x1,x2,xi1,xi2);
end
if (false)
      gensim(net);
end
```

Appendix E: Regression Fit of Training and Test Data

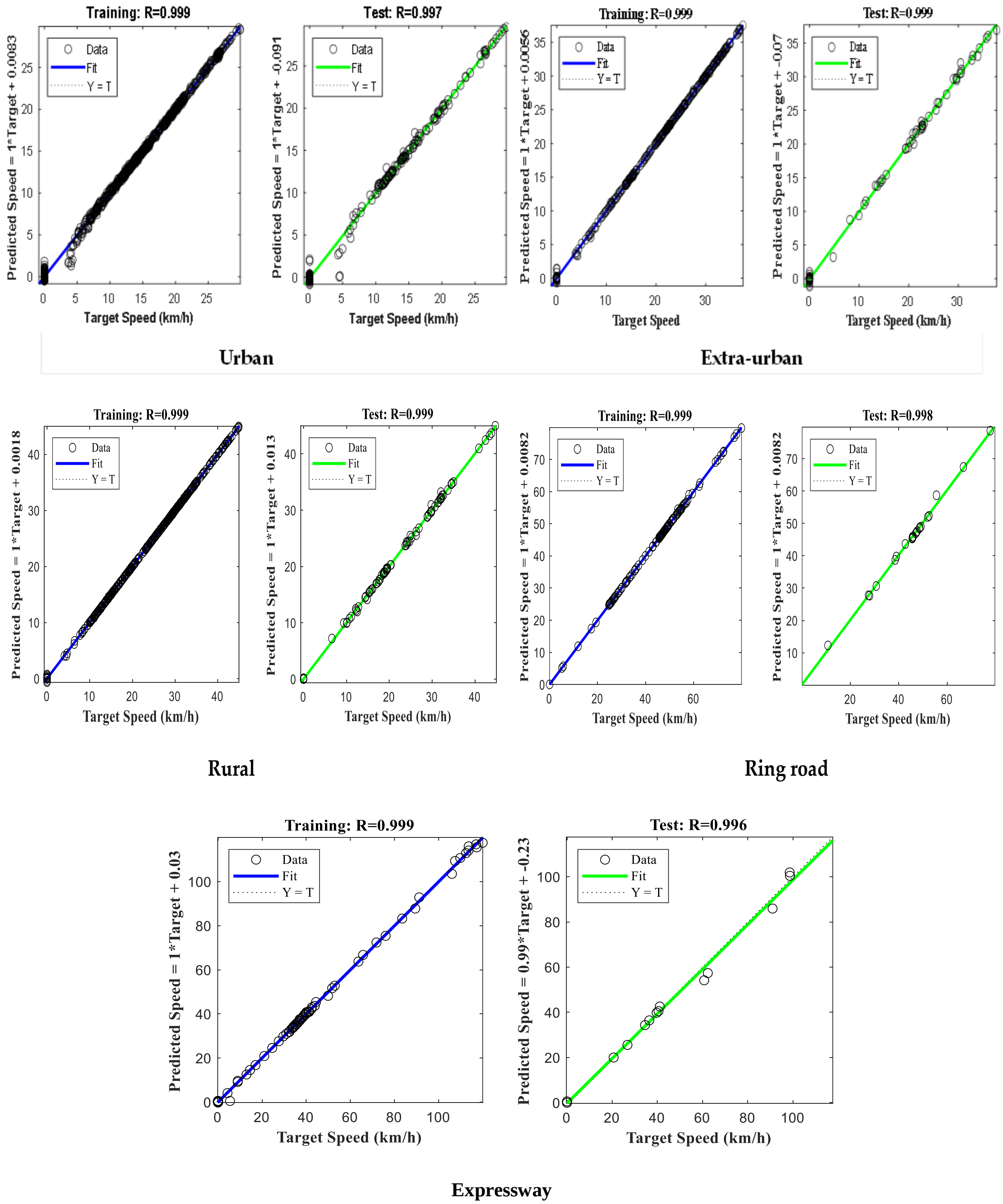

Figure E1: Regression fit of training and test data

Appendix F: Emissions Simulation Model

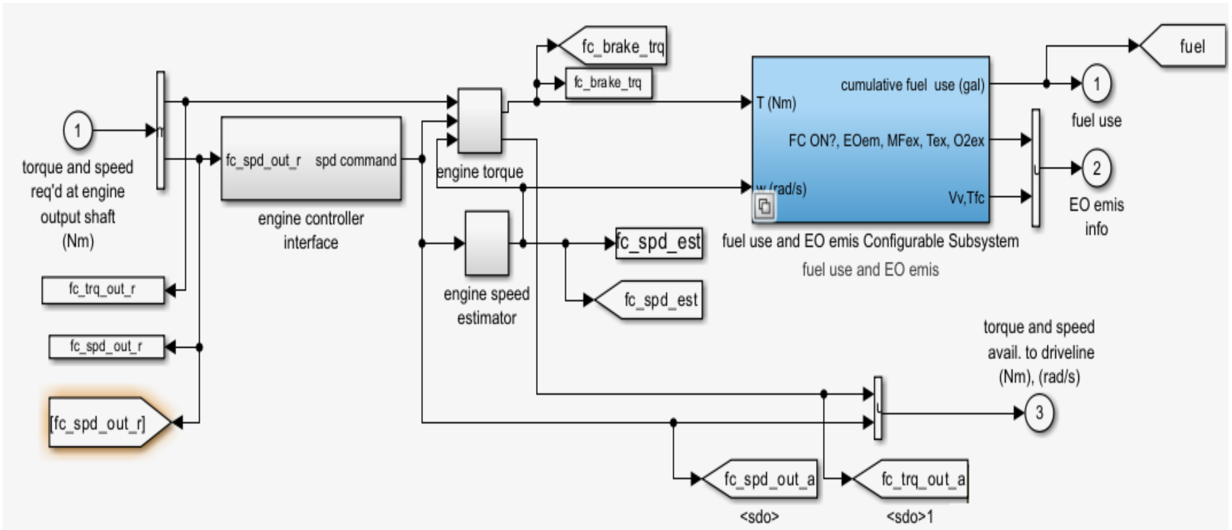

Figure F1: Fuel convertor blocks

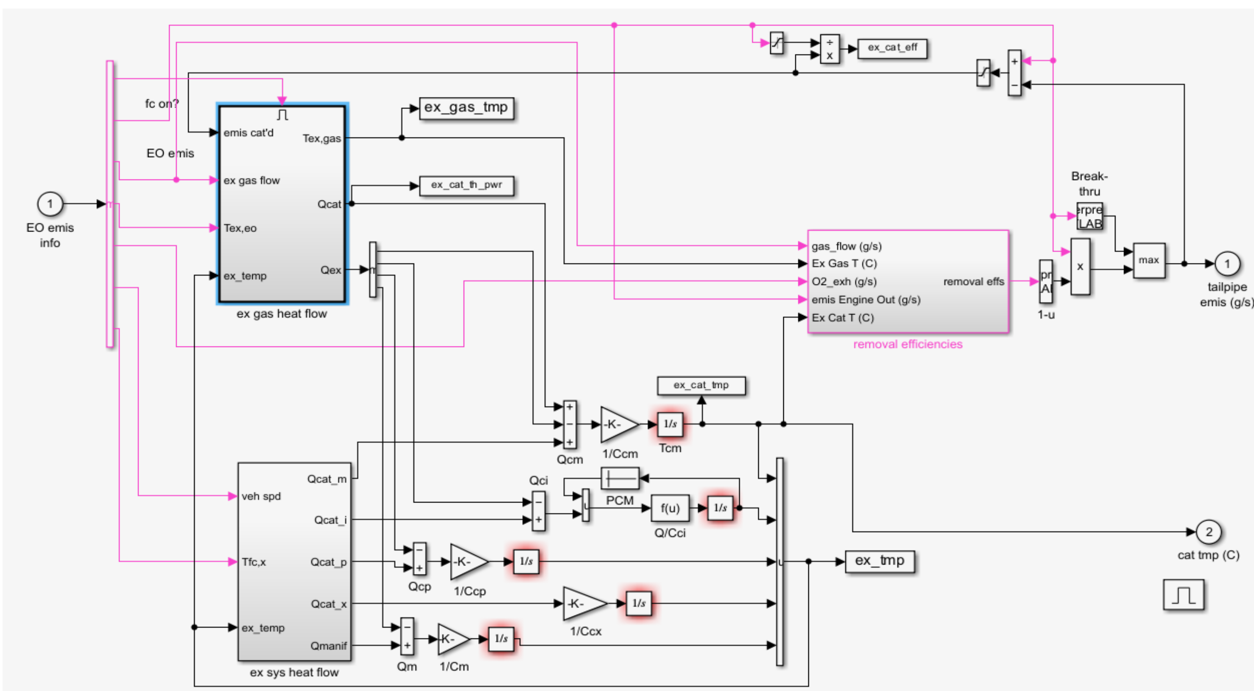

Figure F2: Exhaust emissions simulation blocks

Appendix G: Analysis of Errors in On-Road Emissions Testing

Table G1: On-road emissions test results showing average values from three trials for tested vehicles, with standard error analysis

Slope (Degree)	Speed (km/h)	Gasoline vehicle						Diesel vehicle					
		CO_2 (g/km)	Erro of CO_2	CO (g/km)	Error of CO	HC (g/km)	Error of HC	CO_2 (g/km)	Error of CO_2	CO (g/km)	Error of CO	HC (g/km)	Error of HC
-2	10	175.225	0.232	68.883	1.267	18.970	1.042	52.796	1.456	59.928	0.475	13.550	0.000
0	10	184.190	0.224	69.948	0.734	18.970	0.311	84.287	0.318	61.050	0.577	14.336	0.471
2	10	209.618	0.718	78.623	0.787	19.377	0.358	145.070	1.064	70.571	0.241	14.444	0.264
4	10	251.933	0.482	100.235	0.391	16.368	0.371	132.682	0.247	89.907	0.069	17.073	0.374
6	10	298.942	0.262	116.778	0.653	22.059	0.508	192.340	0.612	105.055	0.222	16.260	0.000
-2	20	166.830	0.908	42.190	0.146	18.970	0.006	53.969	0.838	36.924	0.500	14.092	0.558
0	20	188.624	1.045	42.927	0.417	18.482	0.178	71.150	0.462	37.371	0.320	14.634	0.674
2	20	244.989	0.153	55.323	0.463	16.938	0.398	136.105	0.699	49.298	0.664	14.905	0.422
4	20	275.356	0.440	69.064	0.456	18.238	0.321	159.267	0.611	61.870	0.090	22.439	0.163
6	20	317.850	0.218	69.549	0.693	31.843	0.506	219.072	0.572	61.884	0.730	16.260	0.000
-2	30	191.688	0.062	27.645	0.003	16.829	0.033	57.784	0.260	24.171	0.285	14.200	0.031
0	30	242.165	0.832	28.828	0.881	19.612	0.658	77.845	0.650	25.113	0.284	16.279	1.805
2	30	252.487	0.310	44.712	0.533	17.886	0.156	113.937	0.944	39.716	0.090	14.363	0.632
4	30	269.765	0.053	45.079	0.750	17.290	0.620	174.606	0.401	40.414	1.089	14.905	0.518
6	30	286.000	0.102	45.344	0.660	19.160	0.419	213.204	1.166	57.618	0.162	15.718	0.758
-2	40	177.898	0.031	20.923	0.412	18.970	0.123	57.376	0.217	18.440	0.000	14.471	0.018
0	40	211.900	0.032	24.367	0.176	20.054	0.401	99.349	0.580	20.974	0.562	14.038	0.444
2	40	247.434	0.875	35.744	0.173	17.615	0.307	130.482	0.203	31.884	0.554	15.041	0.067
4	40	268.233	0.117	41.559	0.195	17.452	0.416	180.115	0.347	37.620	0.153	15.583	0.154
6	40	285.788	0.094	45.817	0.268	22.032	0.009	223.310	0.924	43.154	0.457	16.260	0.000
-2	50	172.780	0.012	15.203	0.055	16.260	0.000	54.719	0.104	13.511	0.007	14.444	0.389
0	50	234.182	0.360	21.670	0.495	17.162	0.271	122.821	1.014	18.227	0.640	14.986	0.439
2	50	267.728	0.313	31.585	0.134	18.293	0.349	144.125	0.359	28.526	0.138	15.013	0.195
4	50	280.523	0.012	45.773	0.255	17.073	0.196	188.102	0.217	41.788	0.520	16.260	0.721
6	50	305.625	0.195	46.996	0.806	21.003	0.155	215.812	0.463	45.046	0.508	16.260	0.933